Investigating the pathogenicity of an autism-related CNTNAP2 missense variant in a novel mouse model

Taylor Manett

Sorbonne Université

École Doctorale Complexité du Vivant (ED515)

Institut du Fer à Moulin – "Cortical Development and Pathology" Team

Thèse de doctorat en Neurosciences

Investigating the pathogenicity of an Autism-related *CNTNAP2* missense variant in a novel mouse model

Par **Taylor MANETT**

Dirigée par Laurence GOUTEBROZE et Marta GARCIA

Présentée et soutenue publiquement le 21 septembre 2023

Devant un jury composé de :

Christel Depienne	Rapportrice
Jérôme Honnorat	Rapporteur
Sylvia Soares	Examinatrice
Jérôme Devaux	Examinateur
Marta Garcia	Co-encadrante
Laurence Goutebroze	Directrice de thèse

PhD Project Summary

Autism spectrum disorders (ASD) are neurodevelopmental disorders with genetic and environmental contributing factors, which are characterized by the presence of repetitive/restricted behaviours and deficits in social interaction and communication. In the gene *CNTNAP2*, numerous heterozygous missense variants have been identified in ASD patients, but their potential contribution to the development of the pathology is highly debated, given their presence in the general population. Several of these *CNTNAP2* heterozygous missense variants have been studied *in vitro* to assess their consequences at the cellular level; however, none have been investigated *in vivo*. The overall aim of my PhD project was to better understand whether and how *CNTNAP2* variants could contribute to ASD pathology by characterizing a novel knockin mouse model bearing a *CNTNAP2* heterozygous missense variant identified in an ASD patient.

CNTNAP2 encodes Caspr2, a neuronal cell-adhesion transmembrane glycoprotein identified in the juxtaparanodal regions of the nodes of Ranvier in mature myelinated neurons both in the central (CNS) and peripheral (PNS) nervous system, where it contributes to the formation of axoglial contacts and is required for *Shaker*-type Kv1 channel clustering. Caspr2 also plays multiple functions during brain development, including in axon growth and myelination. Some of the *CNTNAP2* heterozygous missense variants have been shown to lead to Caspr2 misfolding and retention in the endoplasmic reticulum (ER), and to impact mouse cortical neuron axon growth *in vitro*. We generated and thoroughly characterized a mouse model bearing the ER-retained missense variant I236S (KI-I236S mice), assessing whether and how such a variant could alter Caspr2 function in PNS and CNS myelination.

We found that KI-I236S heterozygous mice present sex-dependent behavioral abnormalities, with decreased muscular strength and heat sensitivity in males, and social interaction deficits in females. Brains of mutant mice show no gross morphological differences; however, they do show differential alterations of the two major interhemispheric myelinated tracts, the corpus callosum and the anterior commissure, between males and females. Ultrastructural analyses suggest that the speed or onset of myelin sheath wrapping could be affected in the corpus callosum of mutant males. Myelin defects were also detected in the PNS specifically in males, together with morphological alterations of the node of Ranvier and of unmyelinated sensory C-fibers, possibly accounting for their heat hyposensitivity.

Taken together, my work shows that *CNTNAP2* heterozygous missense variants such as I236S may indeed affect the function of the Caspr2 protein, interestingly in a sex-dependent manner; given this, they may also contribute to the pathogenicity of *CNTNAP2*, with marked effects on myelination in both the CNS and PNS. However, KI-I236S heterozygous mice do not fully recapitulate the phenotypes classically associated with ASD, notably repetitive/restrictive behaviors, suggesting that additional genetic, epigenetic, or environmental factors are required for the development of the ASD pathology.

In this manuscript, I will first introduce relevant topics to the project in the **Introduction**. I will then present my results in **Results I**, which is the main work of my PhD and is in the format of a scientific article which is ready for journal submission; and **Results II**, which includes complementary results and preliminary data relevant to the project. I will discuss my results and consider them in light of what is known in the field, along with proposing some future perspectives on the topic, in the **Discussion**. All work referenced in the manuscript can be found in the section **References**, organized alphabetically. Additional published work from the lab, to which I contributed, can be found in the **Annex.**

Acknowledgements

I would like to extend a massive thank you to the members of the jury for accepting to read and evaluate my PhD dissertation. Thank you so much to **Dr. Christel Depienne** and **Dr. Jérôme Honnorat** for agreeing to be the reviewers of my manuscript, and to **Dr. Sylvia Soares** and **Dr. Jérôme Devaux** for assessing and discussing my work. Thank you all for taking the time to come to Paris for my defense, for sharing your wisdom, and for putting in the energy to evaluate the project.

Thank you to the leaders of the Cortical Development and Pathology Team at the Institut du Fer à Moulin, **Fiona Francis** and **Laurence Goutebroze**, for welcoming me to the IFM and to the team during my M2 internship in 2019 and supporting me until now.

I would like to thank **Laurence Goutebroze** and **Marta Garcia**, my thesis director and co-director, respectively. Laurence, thank you for all of the guidance during the past 3.5 years, for the help in preparing for the doctoral school "concours" and in obtaining a grant from the FRM for the PhD project. Thank you for all of the techniques you've taught me, for all of the help in experiments and organizing the mice, for your understanding when things weren't working out the way we hoped and, most importantly, thank you for helping me to grow as a person. Thank you so much for your efforts in reviewing this manuscript to make it the best it could be. Marta, thank you for all your help with experiments, for your valuable feedback on presentations and writing, and for always reminding me to eat lunch! Your guidance was very appreciated as a professor during my Master and also as a co-director during the PhD.

Thank you to all the people who helped with the work of my PhD. Thanks to **Marika Nosten-Bertrand** and **Gaël Grannec**, who helped me with behavioral experiments and always had good advice for working with mice and analyzing the data. Thank you also to **Alicia François** for your help with the behavioral experiments as well, we've missed you in the lab since you left! A huge thank you to **Carmen Cifuentes-Diaz**, **Mythili Savardijane**, and **Theano Eirinopoulou**, whose work in the microscopy platform at IFM has been such a huge help. Carmen, thank you so much for using your expertise in electronic microscopy to help us with the project. Thanks to **Jérome Devaux** for taking the time to perform the electrophysiology experiments on our mice.

Thank you to the **Cortical Development and Pathology Team** at IFM, and **everyone from the 4th floor**! **Donia Zaidi**, **Valeria Viola**, and **Loïc Angrand** - it was a pleasure to share part of the PhD journey with you! Even though our projects were different, we always supported each other and helped each other however we could! Valeria, we were truly the powerhouses of organization and event planning, and it was so nice to share that with you, despite all the added time and stress. It was so great to be more involved in things outside of benchwork! Thank you also to **Ketakee Ghate** – for all of the chats, the beers, the Indian food, for sharing our love of Germany, for welcoming me into your home in Pune and being the best tour guide and motorbike driver ever! Thank you also to **Richard Belvindrah** for being a great office-mate, for always sharing your cookie stash and for all of the scientific and life advice and discussions. Thank you to all the other **PhD students at the IFM**, it was such a pleasure to support each other during this strenuous time.

Thank you to the IFM Animal Platform, especially **Baptsise Lecomte**, for all of your help managing the mouse lines and maintaining the animals so well, and also helping us with protocols and equipment when necessary.

Thank you to my mentors who have given me career and life advice, as well as reassurance, whenever I needed it: **Brenna Conin, Giorgia Canali,** and **Maxime Saunard**.

Thanks to all of my friends – especially **Kira, Madi, Charlotte, Sarah, Molly, Maia, Alexander, Dylan, Anna, Julia, Dominic, Ruiyi, Auguste, Nefeli, Gina, Hailey, Lauren, Robin** . . . I never would have stayed mentally sane throughout these years without you. I am so lucky to know you all! Thanks to my fellow Michigan transplant, **Claire,** for sharing this international journey with me!

Thanks to my "roommates," even though we haven't lived together in a while – **Ryszard, Alice, Neda,** and **Jacopo**. Jacopo, thank you for being like a big brother to me during my M1 internship at Insitut Curie, for showing me how to dissect and slice a brain, and how to do immunohistochemistry. And of course, for welcoming me into the Picpus lineage! It's been an honor to be a Picpusian with you all.

Thank you to my cousins **Michelle, Chris, and Lily Babu**. Your worldliness and open-mindedness has inspired me since I was young to always strive for more and to see as much of the world as possible. Thank you for adopting me in New York, I love you!

Thank you to the **Bröckelmann / Beier family**, for welcoming me into your family dinners and celebrations, into your homes and your hearts. Thank you for all the small lessons on German culture and family lore. Getting to know you all has been the deepest joy for me during these years!

Thanks to my family, especially **my mom, dad, and brother**. In 2017 I told you I was moving to Paris for 1 (one) year to improve my French and be an au pair, and here we are, six years later! Thank you for your constant support, when I told you I was staying 2 more years to get my Master's degree, and again when I told you I was staying 3 more years to get my doctorate, and again when I told you I was applying for jobs here. Thank you for the plane tickets, the small loans to keep me afloat, and for always trying to keep me in the loop when I'm feeling homesick. Peter, thank you for entertaining my Star Wars universe questions, day and night, without fail. Thank you all for everything during the past 28 years. I love you guys so much.

Finally, thank you to **York**, who has been my true partner in all the ups and downs during these past three years. Thank you for always keeping me positive and encouraging me when I felt like giving up, thank you for always taking care of us, for all of the meals and snacks and cups of coffee when I was analyzing endless EM images and writing my manuscript. Thank you for being the most amazing best friend, for all of the laughs and the music and the adventures. Thank you for coming to the lab with me on the weekends and always listening to me vent about the project when I needed it. Thank you for teaching me shortcuts and sorting hacks in Excel when I had piles of behavioral data to analyze. Thank you for truly everything, for being you and for being my very best friend and for loving me so well.

Table of Contents

Abbreviations **3**

List of Figures **5**

Introduction **7**

1. Neurodevelopmental Disorders and Autism Spectrum Disorders **9**

1. A. Evolution of ASD and DSM Diagnosis 9

1. B. ASD and Brain Morphology 11

1. C. ASD and Brain Connectivity 14

1. D. Genetics of ASD and Risk Factors 16

1. E. Pathways Implicated in ASD 18

1. E. i. Synapse Development 18

1. E. ii. The mTOR Pathway and Axon Development 23

1. E. iii. Myelin Dysregulation 25

2. The *CNTNAP2* Gene in Neurodevelopmental Disorders and ASD **27**

2. A. Genetic Alterations in Neurodevelopmental Disorders 28

2. B. *CNTNAP2* Mutations in ASD patients 30

2. D. *Cntnap2* Mouse Model and ASD 34

3. *CNTNAP2* and Caspr2 Tissue Expression **37**

4. Caspr2 functions in synapse formation and brain connectivity **40**

4. A. Caspr2 and Synaptogenesis 40

4. B. Caspr2 and Connectivity *in vivo* + E/I Balance 41

5. Caspr2 and Cortical Development **45**

5. A. Caspr2 in Cortical Migration and Interneuron Maturation 46

6. Caspr2 and Interhemispheric Myelinated Tracts **48**

6. A. The Corpus Callosum 48

6. B. The Anterior Commissure 50

6. C. Caspr2 in Axon and Myelinated Tract Development 52

7. Myelination and the Node of Ranvier **55**

7. A. General Introduction to Myelination and the Node of Ranvier 55

7. B. Structure of the Node of Ranvier 57

7. B. i. The Node 58

7. B. ii. The Paranode 59
7. B. iii. The Juxtaparanode 59
7. C. Assembly of the Node of Ranvier 60
7. D. Caspr2 and Node of Ranvier Formation 61
7. E. CNS Myelination and the Role of Caspr2 64
7. E. i. Oligodendrocyte Development 64
7. E. ii. CNS Myelination Process 66
7. E. iii. Role of Caspr2 in CNS Myelination 69
7. F. PNS Myelination and the Role of Caspr2 74
7. F. i. Schwann Cell Development 74
7. F. ii. PNS Myelination Process 75
7. F. iii. Role of Caspr2 in PNS Myelination 76
8. Caspr2, Nociception, and Sensitivity 77
8. A. Sensory Fibers of the PNS 77
8. B. Dorsal Root Ganglia and CNS Integration 78
8. C. Caspr2, Temperature / Pain Sensitivity and the mTOR Pathway 80
The PhD Project 83
Results I 87
Results II 143
General Discussion 159
1. How could the I236S *CNTNAP2* variant affect Caspr2 structure and function? 161
2. Effects of I236S variant in myelination and other roles of Caspr2? 162
3. How could *CNTNAP2* variant I236S affect behavioral phenotypes? 165
3. A. Muscular strength and sensory deficits 165
3. B. ASD stereotype behaviors and social deficits 167
4. Sex-dependent effects of the I236S variant? 169
5. Contribution of other *CNTNAP2* variants to ASD? 170
6. *CNTNAP2* variants in other physiological conditions and neurological disorders? 171
References 173
Annex 199

Abbreviations

AC	Anterior Commissure
ADAM22	Disintegrin and metalloproteinase domain-containing protein 22
ADDM	Autism and Developmental Disabilities Monitoring Network
ADHD	Attention deficit hyperactivity disorders
AMPA(R)	α-amino-3-hydroxy-5-methyl-4-isoxazolepropionic acid (receptor)
ASD	Autism spectrum disorders
ATF6	Activating transcription factor 6
BTBR	Black and Tan BRachyury
CAM	Cell adhesion molecule
CC	Corpus callosum
CDC	Center for Disease Control
CDFE	Cortical dysplasia-focal epilepsy
CNP	2’3’-cyclic-nucleotide 3’-phosphodiesterase
CNS	Central nervous system
CNV	Copy number variant
CPN	Cortical projection neuron
CSF	Cerebrospinal Fluid
Cux1	Cut Like Homeobox 1
DIV	Days in vitro
DRG	Dorsal radial glia
DSM-V	Diagnostic and Statistical Manual of Mental Disorders, Fifth Edition
DTI	Diffusion tensor imaging
E(17.5)	Embryonic day (17.5)
E/I	Excitation/inhibition
ECM	Extracellular matrix
EM	Electron microscopy
ER	Endoplasmic reticulum
FA	Fractional anistropy
fMRI	Functional MRI
Foxp2	Forkhead box protein P2
GABA(R)	Gamma-aminobutyric acid (receptor)
GAD65	Glutamic acid decarboxylase 65-kilodalton isoform
HET	Heterozygous
JXP	Juxtaparanode
KI	Knockin
KO	Knockout
Kv1	Voltage-gated potassium channel 1
MAG	Myelin associated glycoprotein
MAGUK	Membrane-associated guanylate kinases
MBP	Myelin basic protein
MECP2	Methyl-CpG Binding Protein 2
mGluR	Metabotropic glutamate receptors
MOG	Mylein oligodendrocyte glycoprotein

MRI	Magnetic resonance imaging
mTOR	Mammalian target of rapamycin
MYRF	Myelin regulatory factor
NaV	Voltage-gated sodium channel
NDD	Neurodevelopmental Disorders
NF	Neurofiliment
NMDA(R)	N-methyl-D-aspartate (receptor)
NMJ	Neuromuscular junction
NOR	Node of Ranvier
OL	Oligodendrocyte
OPC	Oligodendrocyte precursor cell
P(10)	Postnatal day (10)
PI3K	Phosphoinositide 3-kinases
PLP	Proteolipid protein
PN	Paranode
PNS	Peripheral nervous system
PSD	Post-synaptic density
PTEN	Phosphatase and tensin homolog
PV	Parvalbumin protein
PVALB	Parvalbumin gene
SAPAP	Guanylate-kinase-associated-protein
SC	Schwann cell
SHANK	SH3 and multiple ankyrin repeat domains
SNP	Single nucleotide polymorphism
Sox10	SRY-Box Transcription Factor 10
SST	Somatostatin
TAG-1	Transiently expressed Axonal Glycoprotein 1
UPR	Unfolded protein response
WT	Wild type

List of Figures

Fig .1	Graph showing ASD prevalence over time	10
Fig. 2	Graph showing genetic causes of ASD	11
Fig. 3	CC thickness alterations in children	13
Fig. 4	Brain areas affected in ASD patients	14
Fig. 5	Hyperconnectivity in ASD children	16
Fig. 6	Schematic representation of ASD causes	17
Fig. 7	Schematic representation of CAMS and their structures	20
Fig. 8	Schematic representation of the synaptic compartment	20
Fig. 9	Schema of the mTOR signaling pathway	23
Fig. 10	*CNTNAP2* gene and Caspr2 protein diagram	27
Fig. 11	Caspr2 protein structure and conformation predictions	28
Fig. 12	Genetic modifications in *CNTNAP2* gene in NDDs	30
Fig. 13	*CNTNAP2* variants identified in ASD patients	32
Fig. 14	*CNTNAP2* variants identified in ASD patients and healthy individuals	33
Fig. 15	Caspr2 protein tolerance landscape	34
Fig. 16	Caspr2 tissue expression in human and mouse brain during early development	38
Fig. 17	Caspr2 tissue expression in mouse from early development to adulthood	39
Fig. 18	Caspr2 at pre-synapse in excitatory and inhibitory neurons	41
Fig. 19	Altered brain connectivitiy in *Cntnap2* KO mice	43
Fig. 20	Schema illustrating cortical development	45
Fig. 21	Schema showing CC organization in human	48
Fig. 22	Schema showing CC development in mouse	49
Fig. 23	Diagram illustrating CC development in human	50
Fig. 24	Development of AC (ACa and Acp) in mouse brain	51
Fig. 25	Caspr2 modulates axon outgrowth in cortical neurons	52
Fig. 26	CC morphological alterations in *Cntnap2* HET and KO mice	53
Fig. 27	AC morpholigcal alterations in *Cntnap2* HET and KO mice	54
Fig. 28	Schematic representation of a myelinated axon	55
Fig. 29	Schema of myelin protein organization	56
Fig. 30	Differential myelination of PNS vs. CNS	56
Fig. 31	Schematic representation of NOR proteins in the CNS and PNS	57
Fig. 32	Node size and NaV channel density affects conduction speed	58
Fig. 33	Schema showing node formation in the CNS and PNS	61
Fig. 34	Node formation and protein localization in myelinating DRG cultures	63
Fig. 35	Altered node size in *Cntnap2* HET and KO mice	64
Fig. 36	Schema of OL development in mouse	65
Fig. 37	Schema of OL stages of maturation over time	66
Fig. 38	Schema of myelin wrapping in the CNS	67
Fig. 39	Axon diameter determines myelination in CNS	68
Fig. 40	Timeline of myelination in mouse CNS	69
Fig. 41	Delayed myelination of cortex in *Cntanp2* KO mice	70
Fig. 42	CC abnormalities in *Cntnap2* HET and KO mice	71
Fig. 43	ACa and ACp abnormalities in *Cntnap2* HET and KO mice	72
Fig. 44	Myelin protein levels in CC and neocortex of *Cntnap2* KO mice	73
Fig. 45	Caspr2 protein levels in *Cntnap2* HET mice during development	73
Fig. 46	*Cntnap2* HET and KO mice show altered Layer II/III electrophysiology	73

Fig. 47	Schema illustrating Schwann cell development	74
Fig. 48	Electrical stimulation influences PNS myelination	75
Fig. 49	Schema of PNS myelinated fiber architecture	76
Fig. 50	Myelinated fiber anolamies in PNS of *Cntnap2* HET and KO mice	76
Fig. 51	Sensory fiber classifications	78
Fig. 52	Somatosensory circuitry from periphery to brain in mouse	79
Fig. 53	mTOR inhibition rescues heat sensitivity in *Cntnap2* KO mice	81
Fig. 54	Caspr2 expressed in DRG	82
Fig. 55	Caspr2 expressed in C-fibers	82
Fig. 56	*CNTNAP2* variants retained in ER, show delayed clearance from the cell	83
Fig. 57	*CNTNAP2* variants alter Caspr2 function in axon outgrowth	84
Fig. 58	Hypothetical model of how *CNTNAP2* variants impact Caspr2 function	85
Fig. 59	Pedigree of ASD family bearing I236S mutation	86
Fig. 60	Proposed model of Caspr2's role in myelinated fibers throughout development	162
Fig. 61	Cntnap2 expression in proliferating and differentiated OPCs	163
Fig. 62	Altered NMJs in *Cntnap2* KO mice	166
Fig. 63	C-fiber axons altered in *Tsc2* mutant mice	167
Fig. 64	*CNTNAP2* regulated by ERα in the brain	170
Fig. 65	*CNTANP2* variants show continuum of ER-retention	171

Introduction

1. Neurodevelopmental Disorders and Autism Spectrum Disorders

The development of the brain is a highly complex and organized process which must occur in carefully timed and synchronized steps in order to achieve healthy organ development and functioning. There are a multitude of processes which, if perturbed or delayed during critical developmental time periods, could lead to deficits in the morphology and/or functioning of the brain later in life. The group of clinical phenotypes associated with these types of deficits in brain development are referred to as neurodevelopmental disorders (NDD) and include a wide range of symptoms, from mild to extremely severe. Attention Deficit Hyperactivity Disorder (ADHD) and Autism spectrum disorders (ASD) are two of the most common NDDs in the population, with prevalence of 10.2% (children ages 4-17 in the US, 2015-2016) (Xu et al. 2018) and 2.8% (8-year old children in the US, 2020) (Maenner et al. 2023), respectively. Particular interest has been shown in understanding the causes and potential treatments for ASD, as the range of phenotypes is very broad and can range from social problems and hyperactivity to speech or motor deficits and intellectual disability.

1. A. Evolution of ASD and DSM Diagnosis

ASD are defined as "a developmental disability caused by differences in the brain… [leading to] problems with social communication and interaction, and restricted or repetitive behaviors or interests" according to the Center for Disease Control (CDC) (U.S. Department of Health & Human Services 2022). The term "Autism" acquired its modern definition in 1943, when Leo Kanner first used it to describe children with symptoms of social isolation and linguistic disorders, who had problems communicating and exhibited repetitive and restrictive behaviors. In 1944, Hans Asperger described socially-isolated children who displayed normal linguistic abilities; this led to the coining of "Asperger's Syndrome" to describe a new Autism-like disorder (Sharma, Gonda, and Tarazi 2018). It wasn't until 2013 with the publication of the Diagnostic and Statistical Manual of Mental Disorders, Fifth Edition (DSM-V) that these and several other developmental disorders were grouped under the term "Autism Spectrum Disorders," implying a scope of varying disorders with a range of effects and severity (American Psychiatric Association 2013). ASD is complicated to diagnose, and the DSM-V has sought to simplify this process by reducing the exhibited deficits to 1) social communication and 2) repetitive or restricted behaviors. Typically, child psychiatrists would rely on a combination of observed behaviors/development and parental reporting to diagnose a child with ASD.

The prevalence of ASD has been steadily increasing over the past 3 decades (Fig. 1), with an incidence of 1 in 150 children in 2000, which by 2008 reached a incidence of 1 in 88 children, and by 2020 was at an incidence of 1 in 36 children (Maenner et al. 2023). These data have been acquired by the Autism and Developmental Disabilities Monitoring Network (ADDM), a program

funded by the CDC to better understand ASD in the United States. The ADDM has also reported that ASD is nearly 4 times more common among boys than girls. While once thought to be due to 'bad parenting' or problems in one's home life, ASD are now considered to be caused to neurodevelopmental defects occurring during the pre-natal period. However, the onset of ASD are highly variable, with some children showing early onset of symptoms ($\leq$ 18 months of age) while others behave normally until $\geq$ 24 months of age, when they descend into ASD symptoms (Werner et al. 2005).

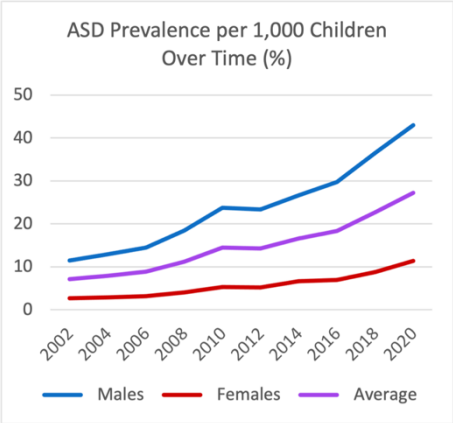

Figure 1: Data from the ADDM Network spanning 2002-2020, collected from 6-14 surveillance sites in the U.S. from 8-year-old children. Created with data from ADDM reports.

It is worth noting that ASD are categorized into two main types: syndromic and idiopathic. Syndromic ASD are associated with known genetic syndromes, such as Fragile X or Tuberous sclerosis. Idiopathic ASD are often attributed to unknown causes. Both types will usually display impaired communication or social skills and highly repetitive stereotypic behaviors (Bishop, Aziz, and Barth 2014). While syndromic ASD have known genetic causes, these genetic variants – including copy number variants (CNVs) and mutations in ASD risk genes – account for variable cases, with some reports ranging from roughly 1% of ASD cases (Fernandez and Scherer 2017) to 7-20% (Schaaf and Zoghbi 2011). Because the genetics of ASD are so complex, some have proposed to subcategorize syndromic ASD into different groups based on genetic contribution. Below is a scheme of genetic contributions to ASD (Fig. 2); the genetics of ASD will be discussed further in section 1.D.

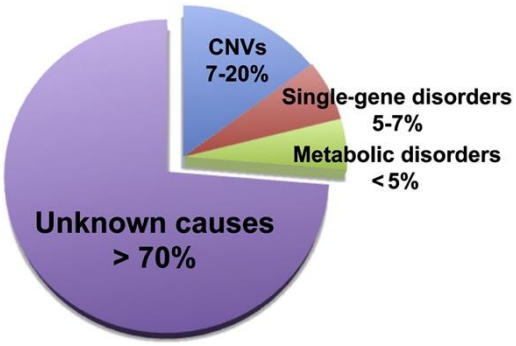

Figure 2: Genetic causes of ASD by type (Schaaf and Zoghbi 2011).

ASD are associated with a wide variety of behavioral phenotypes, as this disorder and its associated comorbid disorders can affect cognitive, somatosensory, and even motor function, as well as social fluency. As it's often difficult to diagnose ASD prenatally, symptoms usually appear slightly later in development, with phenotypes becoming more pronounced as children age. Perhaps the most significant impairment in ASD patients is the social deficit, with the DSM-V requiring that a child display persistent deficits in three different areas of social communication and interaction. These include 1) deficits in social-emotional reciprocity, 2) deficits in non-verbal communicative behaviors used for social interaction, and 3) deficits in developing, maintaining, and understanding relationships (American Psychiatric Association 2013). In addition to these social shortcomings, children must also exhibit at least 2 types of repetitive or restricted behaviors, including 1) stereotyped or repetitive motor movements, use of objects, or speech, 2) insistence on sameness, inflexible adherence to routines, or ritualized patterns of verbal or nonverbal behavior, 3) highly restricted, fixated interests that are abnormal in intensity or focus, and 4) hyper- or hypo-reactivity to sensory input or unusual interest in sensory aspects of the environment (American Psychiatric Association 2013). All these behaviors can be ranked from 1 to 3, with 1 being the mildest and 3 being the most severe. These symptoms may be present from an early developmental period but are sometimes masked and not fully evident until later in childhood. Children with ASD can also be diagnosed with intellectual disability, developmental delay, or language impairment, which can frequently co-occur with ASD.

1. B. ASD and Brain Morphology

Many researchers have sought to better understand the anatomy of ASD by using techniques such as Magnetic Resonance Imaging (MRI) to observe the ASD brain *in vivo* in a non-invasive way. Due to the high soft-tissue contrast, which can easily differentiate white matter, gray matter, and cerebrospinal fluid (CSF), MRI is ideal for volumetric measurements of the brain (Rafiee et al. 2022). Boedhoe and colleagues conducted the largest neuroimaging study on ASD patients to date and observed different patterns of cortical thickness alterations across different age groups; in children, smaller amygdala volume and thicker frontal cortices were detected, while in adults, decreased hippocampal volume was observed (Boedhoe et al. 2020). In adults, Ecker and

colleagues observed no changes in overall brain volume, but an increased gray matter volume in the anterior temporal and dorsolateral prefrontal regions with significant reductions in the occipital and medial parietal regions when compared with controls; they also observed spatially distributed reductions in white matter volume (Ecker et al. 2012).

In a study of adolescents with ASD, it was found that patients showed an increase in gray matter volume in medial and dorsolateral frontal areas, in the lateral and medial parts of the temporal lobes, in the parietal lobes, cerebellum, and claustrum; these patients also showed decreased volume in frontal, parietal, temporal, and occipital white matter (Bonilha et al. 2008). Additionally, children with ASD have been shown to have increased total brain volume and increased amygdala volume (Aylward et al. 2002; R. Chen, Jiao, and Herskovits 2011) and other white matter abnormalities (Yang et al. 2018). These studies and others suggest that altered volumes of specific brain regions in ASD patients could contribute to ASD pathology. Not only this, but they also show that these anatomical differences could change over the course of life or have a temporal component.

White matter structures, such as the corpus callosum (CC), have been particularly implicated in ASD. Many studies have shown that the CC is smaller in adolescents and adults with ASD (R. Chen, Jiao, and Herskovits 2011), but the data has been more difficult to discern in children. A study of adults with ASD showed a decreased CC volume (R. Chen, Jiao, and Herskovits 2011); in other studies, ASD patients were shown to have various CC abnormalities (Aylward et al. 2002; R. Chen, Jiao, and Herskovits 2011). Wolff and colleagues collected MRI images from 270 infants at high-risk for ASD and 108 low-risk controls at 6, 12, and 24 months of age and found that the ASD-risk children had significantly increased CC area and thickness starting from 6 months of age, with particularly robust differences at 6 and 12 months of age (Fig. 3) (Wolff et al. 2015). These results contrast with older studies from ASD adults which show decreased CC volume, suggesting that this structure could change over time. Taken together, the proposed model is one in which the CC is reduced in size during the first year of life, normalizes around age 2, and becomes smaller than normal by age 3, which is maintained into adulthood (Girault and Piven 2020).

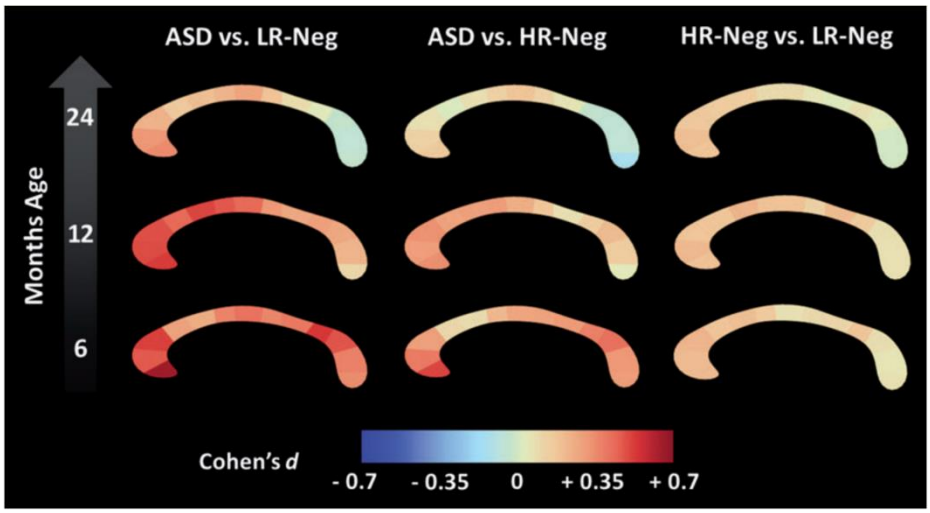

Figure 3: Alterations in CC thickness in young children. Longitudinal effect size data (Cohen's *d*) for pairwise CC thickness differences among high-risk infants who developed ASD, high risk infants without ASD (HR-Neg), and low-risk controls (LR-Neg). Red indicates increased size, blue indicates decreased size, orange indicates regions with little to no differences. CC is represented in sagittal view with rostral end at left and caudal end at right (Wolff et al. 2015).

Furthermore, Wolff's study used data from diffusion tensor imaging to propose that the microstructural properties of callosal white matter, including myelination and axon composition, could explain these differences in CC morphology. Diffusion tensor imaging (DTI) is a type of MRI which uses the diffusion of water molecules to generate higher contrast in magnetic resonance images. It detects molecular diffusion to detect obstacles such as macromolecules, fibers, and membranes, therefore giving a much more detailed picture of microscopic substructures of the tissue than classical MRI techniques. DTI has been used in conjunction with MRI to investigate CC abnormalities in ASD patients in more detail. In a meta-analysis of DTI studies conducted by Zhao and colleagues, they confirmed that white matter abnormalities in the CC are a predominant characteristic of ASD brains (Zhao et al. 2022). In a small study of young children, Bashat and colleagues found higher fractional anisotropy (FA) in the CC of ASD children when compared with healthy children. FA is a measurement which reflects the degree of directed water diffusion in the brain; this measure is indicative of more mature white matter properties, such as myelination, axonal density, and fiber packaging (Ben Bashat et al. 2007; Girault and Piven 2020). Taken together with the results from Wolff et al., the current findings suggest that FA is increased during the first part of life (larger and more mature CC), with a slowing maturation thereafter which could lead to decreased FA in older children and adults (Travers et al. 2012). These DTI studies have been essential for demonstrating that white matter maturation may be affected in ASD individuals. A summary scheme of white matter areas with the most noticeable changes observed in ASD patients is presented in Fig. 4.

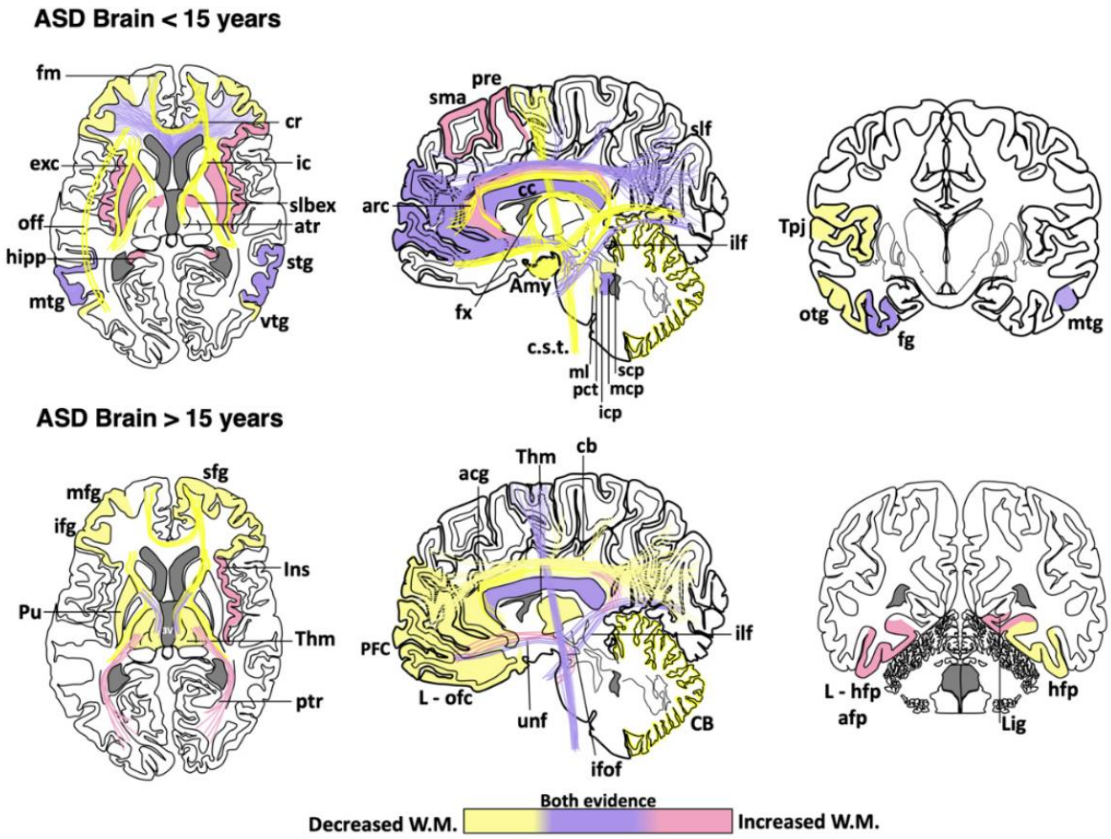

Figure 4: Cortical areas, subcortical areas, and white matter tracts affected in patients with ASD. White matter areas with the most noticeable changes are represented in the three anatomical planes of the human brain: axial, sagittal, and coronal. Brain schemes also indicate the most common myelination changes that are observed in ASD patients during two different stages of development – young (<15 years) and old (>15 years). acg: anterior cingulate gyrus; afp: amygdala-fusiform pathway; Amy: amygdala; atr: anterior thalamic radiation; arc: arcuate fasciculus; CB: cerebellum; cb: cingulum bundle; cc: corpus callosum; c.s.t.: corticospinal tract; cr: corona radiata; exc: external capsule; fm: forceps minor; fx: fornix; fg: fusiform gyrus; hipp: hippocampus; icp: inferior cerebellar peduncle; ifof: inferior fronto-occipital fasciculus; ifg: inferior frontal gyrus; Ins: insula; ic: internal capsule; L-hfp: left hippocampus-fusiform pathway; L-ilf: Left inferior longitudinal fasciculus; L-ofc: left orbitofrontal cortex; lig: lingual gyrus; ml: medial lemniscus; mcp: middle cerebellar peduncle; mtg: middle frontal gyrus; mtg: middle temporal gyrus; off: occipitofrontal fasciculus; otg: occipitotemporal gyrus; pct: pontine crossing tracts; ptr: posterior thalamic radiation; pre: precentral area; PFC: prefrontal cortex; Pu: putamen; slbex: sub-lobar extranuclear area; scp: superior cerebellar peduncle; sfg: superior frontal gyrus; slf: superior longitudinal fasciculus; stg: superior temporal gyrus; sma: supplementary motor area; Tpj: temporoparietal junction; Thm: thalamus; unf: uncinate fasciculus; vtg: ventral temporal gyrus (Galvez-Contreras et al. 2020).

1. C. ASD and Brain Connectivity

While many different morphological abnormalities have been observed in ASD patients, ASD is also thought to be due to problems in connectivity between different brain regions. While DTI allows researchers to detect detailed morphological anomalies, functional MRI (fMRI) is a technology which detects the level of oxygenation of the blood, allowing the brain to be studied on a functional level. It facilitates the study of local- and long-range connectivity in the brain, as well as

the identification of activated regions which are “turned on” in response to certain stimuli. Due to this functional view of the brain, fMRI is now the most used technique in the field. This has been essential in providing evidence that ASD patients may have different activation levels of different brain regions.

Though many agree that brain connectivity in ASD is altered as compared to control individuals, the way in which this connectivity is altered is the subject of debate. One hypothesis in the field is that ASD patients display long-range hypo-connectivity and local hyperconnectivity, while other studies show the opposite. One study in 2013 showed reduced connectivity between the fusiform face area and three separate cortical regions, as well as a decrease in local functional activity in 14-20 year old males with ASD when compared with age-matched controls (Khan et al. 2013). Contrarily, another study in the same year found both local and long-range hyperconnectivity throughout the brain of 110 children aged 7-13 years with ASD (Supekar et al. 2013). In this study, ASD patients with more severe symptoms displayed increased functional connectivity due to elevated hyperconnectivity when compared to other patients with more mild ASD symptoms (Fig. 5) (Supekar et al. 2013). As is the case with brain morphology in ASD patients, variations between studies could be due to ASD patient age of the various samples used. Supekar and colleagues conducted a longitudinal analysis aiming to characterize brain network development in healthy children aged 7-9 years and in healthy young adults aged 19-22 years, which revealed increased long-range connectivity and decreased local connectivity throughout development (Supekar et al. 2013).

fMRI can also be used to monitor brain region activation in response to external stimuli. One recent study investigated face recognition in ASD patients of different ages (older children, teens, and adults) by conducting fMRI while administering the Cambridge Face Memory Test. They found that the ASD group displayed underconnectivity between the fusiform face area and the frontal and primary visual cortices, independent of age, compared to the control group (Lynn et al. 2018). Another study focused on brain areas involved in language which can be associated with communication deficits. Just and colleagues measured brain activity in a group of ASD patients during sentence comprehension and found increased brain activation in Wernicke’s area and decreased in Broca’s area in ASD patients versus controls – two areas heavily involved in language processing (Just et al. 2004). These results are of particular interest given the social impairments and communication problems often observed in ASD patients. Furthermore, another study found that the severity of sensory processing deficits and lower IQ in ASD patients were correlated with reduced interhemispheric connectivity of auditory cortices in ASD; they also found that increased connectivity between the thalamus and auditory cortex was associated with reduced behavioral symptoms of ASD, suggesting that thalamocortical hyperconnectivity could reflect a compensatory mechanism in ASD patients (Linke et al. 2018).

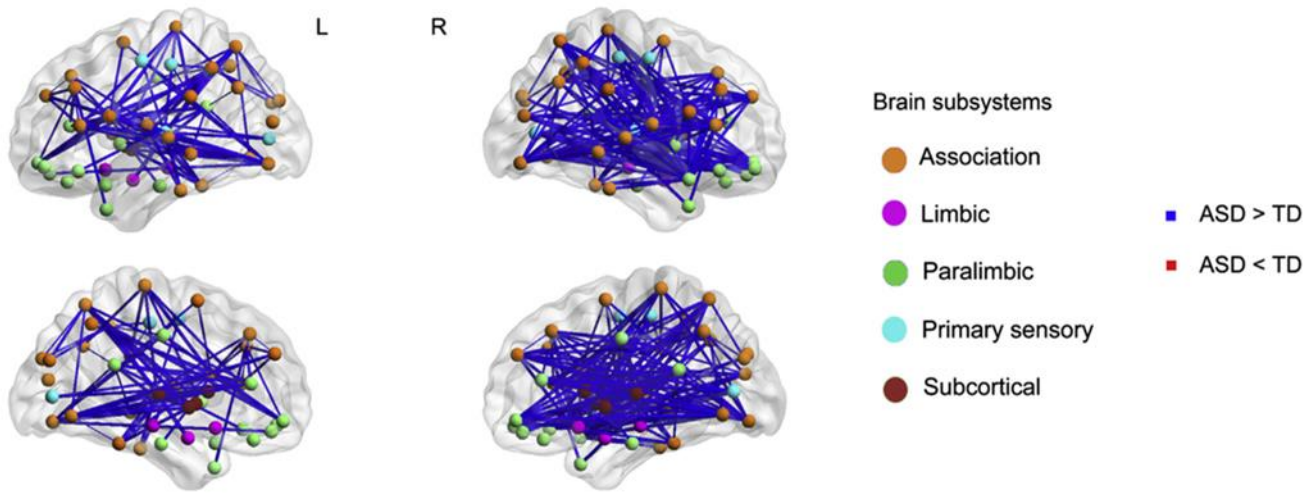

Figure 5: A total of 588 pairs (15%) of anatomical regions showed higher correlations in children with ASD compared to the TD group ($p < 0.05$, corrected for multiple comparisons). No pairs of regions showed higher correlations in the TD compared to the ASD group. Adapted from (Supekar et al. 2013).

1. D. Genetics of ASD and Risk Factors

ASD are considered to have multifactorial causes, including both the pre-natal environment and background genetics (Fig. 6). It has been shown that pregnant women who take certain drugs or are exposed to different immune challenges, such as bacterial or viral infections, could increase the risk that their child develops ASD (Jash and Sharma 2022). In particular, the exposure of the developing fetus to valproic acid (VPA), an anti-seizure drug prescribed to epileptic patients, during pregnancy has been so strongly linked with an ASD phenotype in children that it is commonly used as a rodent model of ASD (Rodier et al. 1996; Nicolini and Fahnestock 2018; Tartaglione et al. 2019) to study the molecular pathways linked to ASD. External environmental factors such as air pollution and environmental chemicals have also been suggested to play a role in developing ASD (Lyall et al. 2017). Other birth complications and deficiencies such as hypoxia, parental age, lack of omega3, and exposure to heavy metals have also been shown to play a role in ASD; these factors can contribute to up to 40-50% of variance in ASD (Modabbernia, Velthorst, and Reichenberg 2017).

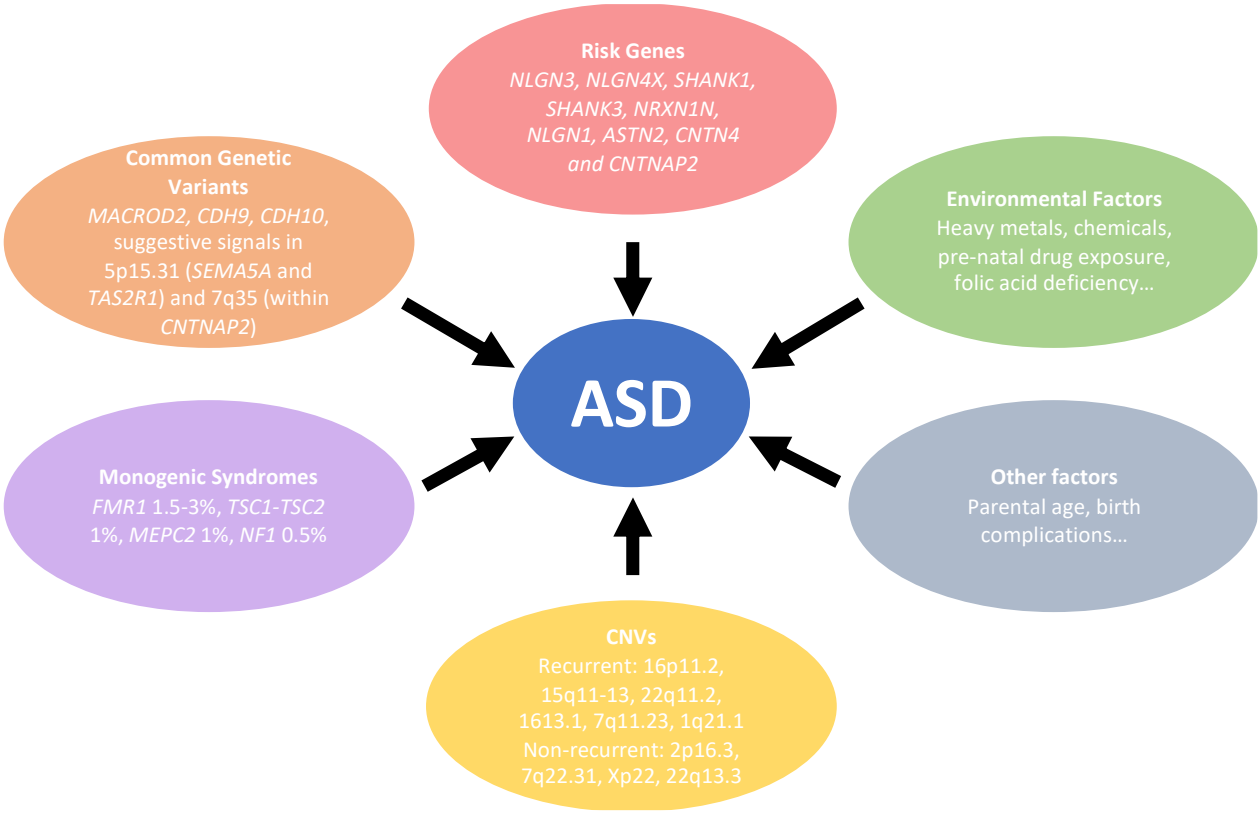

Figure 6: Schematic representation of the multifactorial causes of ASD.

In addition to these environmental contributions, ASD is also now thought to have a genetic component (Fig. 6). In the 1970s, when the role of genetics in human health was beginning to be understood, Folstein and Rutter conducted twin studies on children with Autism phenotypes and found that the incidence among siblings was 50 times higher than the average (S. Folstein and Rutter 1977). What's more, they discovered that monozygotic twins were more likely to share an Autism diagnosis than dizygotic twins, thus suggesting a genetic influence; this theory was proven in 1995 by Bailey and colleagues (Rylaarsdam and Guemez-Gamboa 2019; Bailey et al. 1995). By the early 2000s, it was established that ASD were, at least in part, due to some genetic component. Currently, genetic variation is thought to account of about 50% of the risk for ASD, which could be due to common polymorphisms; however, copy number variants (CNVs) or monogenic disorders have been found in around 30-40% of children with ASD (Glinton and Elsea 2019). To further support the idea that ASD have genetic causes, it's been observed that many children diagnosed with ASD (around 10%) have co-morbid disorders. These include genetic syndromes such as Fragile X syndrome (≈1-2% of ASD cases), tuberous sclerosis (≈1%), Rett syndrome (≈0.5%), and neurofibromatosis (<1%) (Devlin and Scherer 2012). The genes affected in these disorders have all been strongly implicated in intellectual disability, indicating that intellectual disability and ASD likely share common genetic roots.

The genetics of ASD are extremely complex and can include several types of genetic variations, such as single nucleotide polymorphisms (SNP) and CNVs, as well as large chromosomal

rearrangements and duplications that can be either inherited or *de novo*. While some common mutations are also found in the healthy population, it's been suggested that ASD patients present a wider distribution of common CNVs; this insinuates that the accumulation of different polymorphisms may lead to the surpassing of the tolerance threshold and result in a clinical presentation of symptoms (Vicari et al. 2019).

Several "high-risk" genes have been identified, including *NLGN3*, *NLGN4X*, *SHANK1*, *SHANK3*, *NRXN1N*, *NLGN1*, *ASTN2*, *CNTN4*, and *CNTNAP2* (Pinto et al. 2010; Sanders et al. 2012; Vicari et al. 2019; Woodbury-Smith and Scherer 2018). While some genes are shown to have a nearly direct correlation between mutation and ASD diagnoses, others are still debated. One such gene is *CNTNAP2*. There have been several rare mutations found in patients with ASD, intellectual disability, cortical dysplasia focal epilepsy (CDFE) and Epilepsy (Saint-Martin et al. 2018). However, many mutations in the *CNTNAP2* gene have also been discovered in the general population of healthy individuals, leading to some doubt as to its pathogenicity in these disorders (Murdoch et al. 2015); this will be discussed in section 2. B.

As ASD are a spectrum of disorders characterized by social impairments and deficits in language, it is thought that perhaps certain quantitative trait loci (QTLs) related to ASD phenotypes could be linked to the disorder. A study of 152 families from the Autism Genetic Resource Exchange found that language abilities were highly variable among ASD patients, but that there was a strong correlation between language abilities (age at first word) and a loci on chromosome 7q (Maricela Alarcón et al. 2002). The results suggest that there is a language-related susceptibility locus/QTL along the long arm of chromosome 7, specifically on 7q35-36. Later work by the same group found that the locus on 7q35 could contribute to language delay in ASD patients (M. Alarcón et al. 2005). In fact, chromosome 7q has been suggested to be implicated in ASD by several groups (S. E. Folstein and Mankoski 2000; Lamb et al. 2005; Muhle, Trentacoste, and Rapin 2004; Schanen 2006). These findings are very interesting given that some ASD-risk genes are located on chromosome 7q, with *CNTNAP2* being located at 7q35 specifically.

1. E. Pathways Implicated in ASD

ASD has been extensively studied in recent decades due to its large increase in prevalence worldwide. Both genetic studies and mouse/rodent models have been used to identify several major biological mechanisms contributing to brain connectivity that can be disrupted in ASD, including synapse and axon development, and myelination.

1. E. i. Synapse Development

The synapse is a complex cellular compartment where two neurons can exchange essential information. There are two main sides of a synapse: the pre-synaptic side and the post-synaptic side. The pre-synaptic side is the side which sends the message – in this case, produces the

neurotransmitters. The post-synaptic side receives the message/neurotransmitters thanks to specific receptors on the cell surface. Once these receptors have bound their messenger molecules, they can transmit this information via downstream signaling cascades, which are activated by conformational changes in the receptor or altered interactions with its binding partners. Correct synapse formation is critical for accurate communication between cells and different brain areas, as well as for maintaining the excitation/inhibition (E/I) balance within the brain. This E/I balance is also key for fine-tuning connections between brain regions. One of the most crucial parts of synapse formation are the cell adhesion molecules (CAMs). ASD is often referred to as a synaptopathy, as some of the first genes found to be mutated in ASD patients were CAMs, which suggests that development and maintenance of the synapses is an important part of ASD pathophysiology (J. A. Chen et al. 2015). As genetic tools have become more advanced, the implication of CAMs in ASD has only become more pronounced.

Neurexins and Neuroligins

Neurexin proteins are a family of pre-synaptic CAMs that contain a single transmembrane domain with EGF-like domains and laminin-neurexin-sex hormone binding globulin domains in their extracellular arm and a small PDZ-binding domain on their intracellular arm (Fig. 7). The pre-synaptic neurexin proteins interact with their post-synaptic partners, the neuroligins. Neuroligins also possess one transmembrane domain, with a large acetylcholinesterase-like domain in the extracellular part and a short PDZ-binding domain on the intracellular part (Fig. 7). The neurexins and neuroligins interact in a handshake manner across the synapse at both inhibitory and excitatory synapses (Fig. 8). This trans-synaptic bridge links the post-synaptic density with the pre-synaptic protein complex responsible for neurotransmitter release and helps to stabilize both pre- and post-synaptic components. The different types of neuroligins are localized to different subcellular regions, with NLGN1 present in excitatory synapses, NLGN2 present in inhibitory synapses, and NLGN3 present in both types of synapses. The neurexins are encoded by the genes *NRXN1, NRXN2, and NRXN3* in humans, and mutations in *NRXN1* have been observed in ASD patients. Neuroligins are encoded by *NLGN1, NLGN2, NLGN3, NLGN4X* and *NLGN4Y*, and mutations in *NLGN1, NLGN3* and *NLGN4* have also been linked to ASD in humans, though mouse models of the *NRXN* and *NLGN* genes have struggled to encapsulate the social defects seen in human ASD patients (Bemben et al. 2015; J. A. Chen et al. 2015).

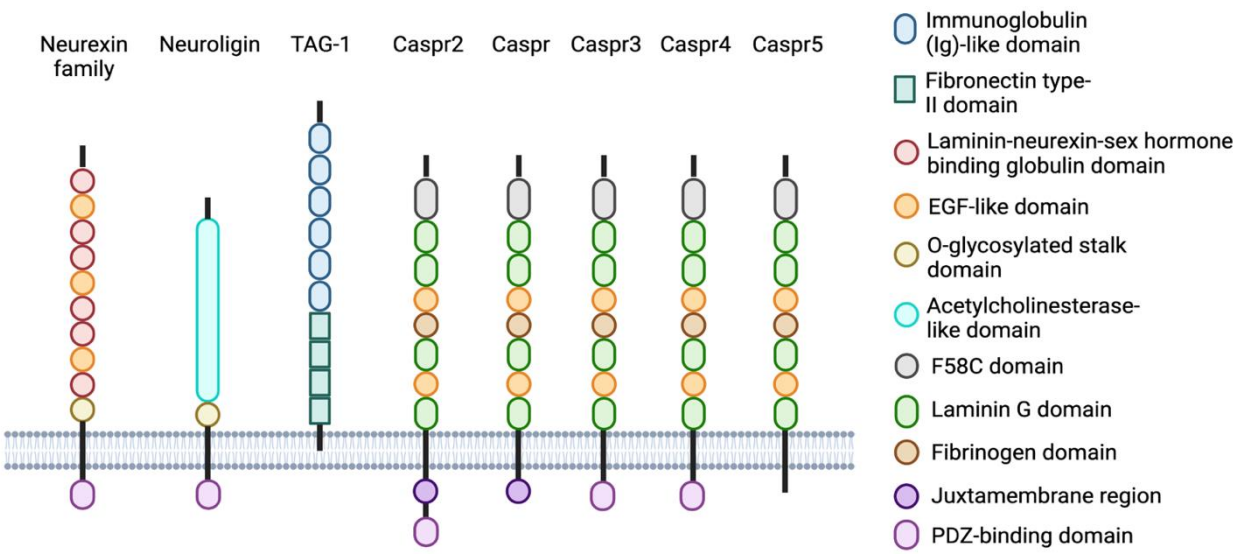

Figure 7: Cell adhesion molecules and their structure.

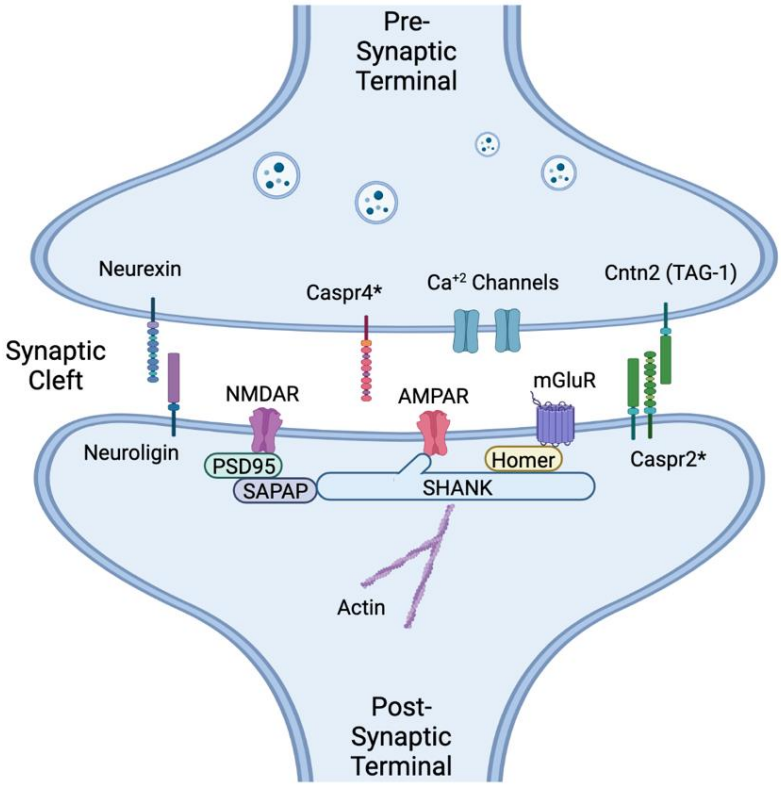

Figure 8: Schema of the synaptic compartment with proteins implicated in ASD. Adapted from (Monteiro and Feng 2017; Doldur-Balli et al. 2022; Jang et al. 2022).

SHANK proteins

The SHANK proteins are multidomain scaffolding proteins present in excitatory synapses and are encoded by the genes *SHANK1*, *SHANK2*, and *SHANK3*. They are major scaffolding proteins responsible for linking other intermediate scaffolding proteins in the post-synaptic density (PSD) (Fig. 8). The PSD is a protein-rich region just below the post-synaptic membrane which contains more than 1,000 proteins including NMDARs, mGluRs, and AMPARs, as well as cytoskeletal and adhesion proteins like actin and neuroligin (Monteiro and Feng 2017). Within the PSD, MAGUK scaffolding proteins enable a multitude of protein-protein interactions, and aid in the formation of a large protein complex which links SHANK, PSD95, Homer, and SAPAP proteins. Together, these proteins form a quaternary complex which joins mGluR and NMDAR complexes in the PSD.

The three SHANK proteins are differently expressed based on developmental stage, cell type, and brain region. Many mutations in *SHANK3* particularly have been observed in ASD patients, including microdeletions, nonsense mutations, breakpoints and missense mutations (Monteiro and Feng 2017). Recently mutations have also been found in *SHANK1* and *SHANK2* in ASD patients, and a meta-analysis study showed that disruptions in the SHANK family account for about ~1% of all ASD cases (Leblond et al. 2014). Additionally, the same study showed a correlation between the *SHANK* mutations and the level of cognitive impairment, with *SHANK3* mutations causing more severe defects than *SHANK1* or *2*. To study *Shank3* mutations, 13 different mutant mouse lines have been generated, 9 of which display ASD-like behaviors such as intense self-grooming and repetitive behaviors, along with social deficits and ultrasonic vocalization abnormalities (Monteiro and Feng 2017). Mice with mutations in *Shank1* and *2* (3 mutant lines) also show ASD-like phenotypes, with increased repetitive behavior and social deficits (Monteiro and Feng 2017). It is clear that mutation or deletion of the *Shank* genes can affect E/I balance and lead to some ASD phenotypes, but what is particularly noteworthy is how different isoform-specific mutations can lead to different phenotypes. In a study by Zhou and colleagues, two *Shank3* mutations were studied, both of which are located in exon 21, only 325 nucleotides apart, and both resulting in a stop codon. The two mouse lines display some shared defects and some distinct defects at the molecular through behavioral levels (Zhou et al. 2016). This study shows how different mutations in ASD-risk genes, such as *SHANK3*, can lead to mutation-specific defects that manifest differently in individual patients.

Contactin-Associated Proteins

Contactin-associated proteins (Caspr) are neurexin-like proteins (Fig.7) and are encoded by the *CNTNAP* genes. They consist of small intracellular domain, one transmembrane domain and a long extracellular domain which includes laminin G, EGF, fibrinogen and discoidin (F58C) domains. Of the 5 Caspr members, Caspr2 and Caspr4 can be localized in the synaptic compartment (Fig. 8).

Caspr2, while canonically residing in the juxtaparanodal region of the node of Ranvier, exists at the post-synaptic area of excitatory synapses, where it colocalizes with AMPAR subunit GluA1 (Varea et al. 2015), and is likely associated with the cell-adhesion molecule TAG-1 (Pinatel et al. 2015). Varea and colleagues demonstrated that mature glutamatergic synapses are affected in *Cntnap2* KO mice, potentially leading to defects in the E/I balance at later stages of maturation. Additionally, Antoine and colleagues recently showed that elevated E/I conductance ratio is present in several different ASD mouse models, including in *Cntnap2* KO mice (Antoine et al. 2019), giving further evidence that Caspr2 could play a role in synapse formation and/or stabilization. Regarding *CNTNAP2* mutations found in ASD patients, I will discuss this at length in Chapter 2.

Caspr4, encoded by the gene *CNTNAP4*, is highly homologous to Caspr2. Caspr4 exists within the pre-synaptic compartment, where it plays a role in the maturation of inhibitory synapses. Caspr4 associates with other pre-synaptic proteins such as Contactin5, Mint1, and CASK, all of which are important members of the inhibitory synapse. Here, Caspr4 helps to attenuate dopamine release through a pre-synaptic mechanism and is also necessary for the maturation of PV+ interneurons; studies in *Cntnap4* KO mice show that Caspr4 strongly contributes to the structural integrity of inhibitory synapses and acts in a dose-dependent manner. It's also been shown that reduced levels of Caspr4 affects membrane expression of $GABA_AR$, suggesting that Caspr4 is likely involved in their transport (Shangguan et al. 2018). *CNTNAP4* mutations have been identified in patients with ASD, as well as schizophrenia and epilepsy (Glessner et al. 2009; O'Roak and State 2008; Roohi et al. 2009). *Cntnap4* KO mice exhibit severe over-grooming behavior and an elevated startle response, indicating impaired processing of sensory information (Karayannis et al. 2014), supporting the potential contribution of *CNTNAP4* mutations to ASD.

CNTNAP5 has also been proposed as a risk gene for ASD, with a microdeletion identified in an ASD sibling pair and subsequent research discovering four additional rare missense mutations in the gene in an ASD patient screen (Pagnamenta et al. 2010). Genome-wide association study by another group more recently showed statistically significant SNPs in the *CNTNAP5* gene in ASD patients, further suggesting that this gene could play a role in the disorder (Narita et al. 2020). It has also been shown that mutations in the *CNTNAP3* gene, identified in Chinese Han ASD cohorts, can confer ASD risk; *Cntnap3* knockdown in mice was shown to cause decreased excitatory synapse and increased inhibitory synapse formation, with mice also exhibiting deficits in social behavior, cognitive tasks, and notable repetitive behaviors (Tong et al. 2019).

1. E. ii. The mTOR Pathway and Axon Development

The mTOR Pathway

While a handful of signaling pathways have been associated with increased ASD risk when altered, including met proto-oncogene–RTK signaling (MET RTK signaling) or HGFR signaling, as well as the ERK and PI3K signaling pathways (Levitt and Campbell 2009), I will focus on the mTOR pathway, as it is particularly relevant for my project. Abnormalities in the mammalian target of rapamycin (mTOR) signaling pathway have been observed in ASD models. The protein mTOR is a serine/threonine protein kinase in the PI3K-related kinase family that forms the catalytic subunit of two different protein complexes: mTOR complex 1 (mTORC1) and mTOR complex 2 (mTORC2) (Fig. 9). The mTOR pathway is involved in integrating a multitude of both intracellular and extracellular signals and translating them into cellular responses, including protein synthesis, cell growth, and proliferation in multiple cell types. Many syndromic disorders with ASD components are caused by mutations in genes which affect the mTOR signaling pathway to some degree, including tuberous sclerosis (affecting *TSC1/2*), Fragile X Syndrome (*FMR1*), Neurofibromatosis type 1 (*NF1*), PTEN mutation syndrome, and Rett's syndrome (Levitt and Campbell 2009). The frequent mutation of *TSC1*, *TSC2*, and *PTEN* in ASD patients has led researchers to suggest that mTORC1 hyperactivation is a probable cause of ASD symptoms, owing to these genes' primary role in the mTOR pathway (Winden, Ebrahimi-Fakhari, and Sahin 2018).

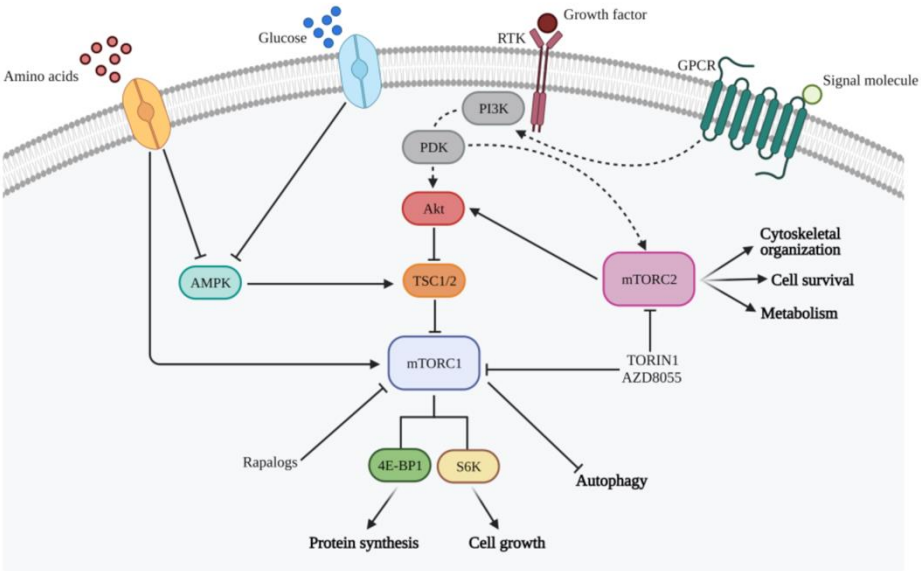

Figure 9: Schema of the main signaling pathways that regulate mTOR. mTORC1 is able to capture and transduce signals from different stimuli, such as the presence of growth factors, amino acids, and glucose through the mechanisms indicated. Once activated, mTORC1 promotes cell growth and proliferation, inducing various anabolic processes, including protein synthesis, and inhibiting catabolic processes, such as autophagy. mTORC2, on the other hand, performs an important regulatory function of the cytoskeleton, cell survival, and metabolism and phosphorylates the Akt kinase, determining its activation (Colardo, Segatto, and Di Bartolomeo 2021).

mTOR hyperactivation in the brain was observed in *Cntnap2* KO mice, suppression of which rescued social deficits in the KO mice (Xing et al. 2019). Furthermore, it was shown that *Cntnap2* KO mouse dorsal root ganglion (DRG) also have hyperactive mTOR signaling. When treated with mTOR inhibitors, pain-related hypersensitivity due to noxious stimuli and heat was reduced, as was DRG neuronal excitability (Xing et al. 2019, 2020). Using forebrain organoids from ASD patients expressing a homozygous protein-truncating mutation in *CNTNAP2*, de Jong and colleagues ascertained that patient-derived organoids had increased volume due to increased cell growth and proliferation (de Jong et al. 2021), which may result from mTOR activation. Deletion of the gene *Pten* in the central nervous system of mice led to abnormal social interaction and response to sensory stimuli, along with an enlarged brain (Kwon et al. 2006). This morphology was associated with an overactivation of the mTOR pathway as well (Kwon et al. 2006). Another study investigated the gene *TSC2*. They found that the TSC1/2 complex inhibits the p70 protein S6 kinase 1 and activates eukaryotic initiation factor 4E binding protein 1 (4E-BP1); these functions are mediated by mTOR, and TSC2 is directly phosphorylated by Akt. Therefore, when TSC2 is properly functioning, the mTOR signaling pathway is suppressed (Inoki et al. 2002). If *TSC1/2* is mutated, such as in ASD patients, this function can be affected and lead to dysregulation of the mTOR pathway. Furthermore, Price and colleagues studied the gene *FMR1*. mTOR inhibitor Rapamycin inhibited peripheral nociception in WT mice, but had no effect in *Fmr1* KO mice, suggesting that regulation of translation via FMRP and mTOR in an important part of nociception plasticity (Price et al. 2007), which is also interesting given the often perturbed sensory perception of ASD patients. Taken together, these studies and others suggest an important role of the mTOR pathway in ASD.

Axon Development

Among the wide variety of processes in which the mTOR pathway plays a role, axon development has been suggested as one which contributes to ASD. The implication of the mTOR pathway in axon morphology is supported by several studies. Pagani and colleagues recently showed that in *Tsc2* mutant mice, mTOR-dependent increased spine density is associated with ASD-like stereotypies and cortico-striatal hyperconnectivity; furthermore, these effects are completely rescued when mTOR is inhibited (Pagani et al. 2021). Choi and colleagues showed that when Tsc2 is inhibited, mTORC1 is activated in the axon, which allows it to initiate and maintain axon growth signals. They also showed evidence that Tsc2 plays a role in axon polarization by which a single neurite is “chosen” to become the axon (Choi et al. 2008). mTOR activation has also been shown to increase axonal growth capacity during regeneration in peripheral nerve injury, and up-regulation of the pathway via *Tsc2* deletion in DRGs can augment axon growth capacity both *in vitro* and *in vivo* (Abe et al. 2010). Similarly, when *PTEN* (an mTOR inhibitor) is deleted *in vivo*, robust axon regeneration is observed in adult retinal ganglion cells. Additionally, when knocking out *Tsc2*, another mTOR inhibitor, axon regeneration is also observed (Park et al. 2008). Several missense mutations have also been identified in ASD patients in the ASD risk gene *MECP2*. These variants

were shown to impair axon morphology and outgrowth in mouse cortical neurons *in vitro*, which could be linked to mTOR dysregulation (Wen et al. 2017). The ASD risk genes *Nuak1* and *Cntnap2* were also shown to have a dose-dependent effect on axon length in cortical neurons *in vitro* (Courchet et al. 2018; Canali et al. 2018) although a potential link with the mTOR pathway has not yet been evaluated.

1. E. iii. Myelin Dysregulation

In addition to the above elements, it has also been shown that the regulation of myelination can be perturbed in ASD patients and animal models. Myelination, in brief, is the process by which glial cells contact and ensheath neuronal axons; this will be explained in detail in Section 7. In the CNS, oligodendrocyte precursor cells (OPCs) mature during early development and become oligodendrocytes (OLs), which will wrap the axons in layers of myelin to insulate this region and boost the conduction speed of action potentials.

Khanbabei and colleagues recently showed increased myelination in the frontal brain of neonatal male and female BTBR mice, a common model of idiopathic ASD. This increase was no longer observed in adulthood, suggesting an accelerated phase of myelin development. They also observed a decrease in the platelet-derived growth factor alpha (PDGFα) signaling, indicating perturbed regulation of OPC maturation in the frontal brain (Khanbabaei et al. 2019). Another study conducted a network analysis of gene expression of cerebellar tissue of ASD patients and found up-regulation of OL markers, suggesting that aberrant expression of OL genes could contribute to anomalous cerebellar development in ASD (Zeidán-Chuliá et al. 2016). While these and other studies have given evidence for increased myelination and increased expression of myelin-related genes, other studies have shown data to the contrary. An investigation of OL-lineage cells and myelination was conducted in the VPA ASD mouse model. These mice showed hypomyelination in the basolateral amygdala and piriform cortex, as well as a decrease in the number of OL-lineage cells and mature OLs in the piriform cortex and the medial prefrontal cortex; however, the number of OPCs was unchanged (Graciarena et al. 2018). Overall, studies from both mouse models and human ASD patients seem to indicate dysregulation of the OL maturation process, leading to myelination and white matter abnormalities, though the specific types of abnormalities seem to be dependent on several factors, including age and type of mutation.

Interestingly, the gene encoding chromatin helicase DNA binding protein 7 and 8 (CHD7 and CHD8) has been implicated in ASD and myelin abnormalities. *CHD8* haploinsufficiency is known to result in ASD phenotypes in both humans and mice. *Chd8* deletion in mice induces behavioral defects including increased social interaction and anxiety-like behavior (Kawamura et al. 2020). *Chd8* was shown to regulate myelin-related gene expression and to be required for OL maturation and myelination. It was recently reported that *Chd7* protects non-proliferative OPCs from apoptosis and controls OPC differentiation, while CHD7 and CHD8 bind to a majority of ASD-risk genes in

OPCs, which suggests an involvement of OL-lineage cells in some ASD-related defects (Marie et al. 2018). In addition to the effects of CHD7 and CHD8, several growth factors have also been shown to regulate the maturation and proliferation of OPCs in the brain, including EGF and IGF-1, both of which are activators of the mTOR signaling pathway; overactivation has been shown to prevent glutamate-mediated apoptosis in immature OLs, which could potentially lead to abnormal myelination (Galvez-Contreras et al. 2020). While some results show an increase in myelination in ASD models and others show decreased myelination, it is clear that the myelination process is often perturbed in ASD patients and can be affected at different stages in different manners depending on the genes mutated.

2. The *CNTNAP2* Gene in Neurodevelopmental Disorders and ASD

CNTNAP2 is one of the largest genes in the human genome and is located on chromosome 7q35. It is composed of 24 exons and 4 transcripts are translated into functional proteins. The main transcript encodes a protein consisting of 1,331 amino acids, which is the protein referred as Contactin-associated protein 2 or Caspr2 (Fig. 10). A secondary isoform (Caspr2-Iso2) consisting of 108 amino acids, was identified more recently, but its functions are not yet known (N. Chen et al. 2015). The two other suspected isoforms consist of 119 and 390 amino acids, respectively, though these have yet to be proven experimentally (N. Chen et al. 2015).

Caspr2 is a cell adhesion glycoprotein comprised of: a large extracellular domain containing a Discoidin domain, 4 Laminin-G domains, an EGF and an EGF-like domain, and a fibrinogen-like domain; a single-pass transmembrane domain; and, a small intracellular portion composed of a PDZ-binding domain and a glycophorin C-neurexin IV-paranodin motif (GNP motif) that gives it the capacity to associate with the actin-spectrin cytoskeleton through proteins of the 4.1 family (Fig. 10). Caspr2 is very well conserved amongst mammals, with 94% amino acid identity between mouse and human. Caspr2-Iso2 corresponds to just the C-terminal intracellular region of the protein and the transmembrane domain, and is expressed at roughly a 10-fold lower amount in the whole brain (N. Chen et al. 2015).

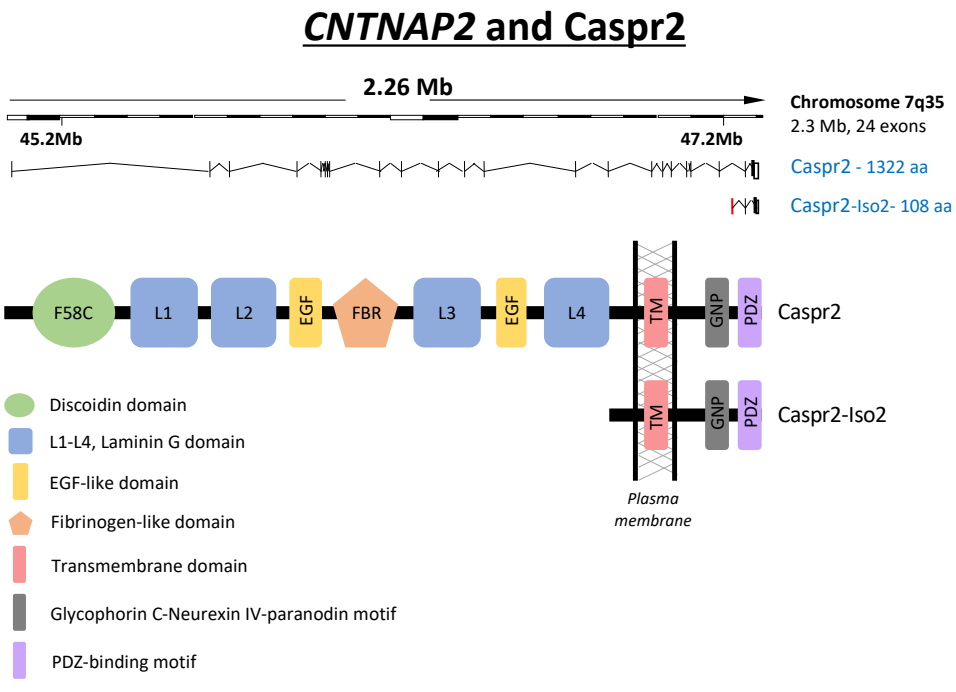

Figure 10: Scheme of *CNTNAP2* gene showing the two transcripts which encodeCaspr2 and Caspr2-Iso2, and the corresponding proteins below, with labeled domains

Caspr2 is heavily glycosylated during its maturation process, with 12 N-glycosylation sites along its extracellular domain (Rubio-Marrero et al. 2016). The number of glycosylation sites implies a complex maturation, protein folding, and trafficking process before it reaches its final location at the cell membrane. While Caspr2 has not yet been crystallized, Lu and colleagues were able to ascertain a reliable structure from electron tomography experiments and subsequent 3D modeling (Fig. 11). This work revealed that the extracellular domain of the protein has three distinct globular densities: a large lobe composed of the Discoidin domain and Laminin-G domains 1 and 2, a middle lobe composed of the fibrinogen-like domain and Laminin-G domain 3, and a small lobe corresponding to Laminin-G domain 4. The large, middle, and small lobes are maintained as well-defined entities within themselves, while the lobes can flex in relation to each other – with the small lobe displaying the greatest freedom of movement (Z. Lu et al. 2016). Their analysis suggests that Caspr2 also contains molecular hinges which correspond with the EGF-like repeats, which is what permits the lobes to flex with respect to each other. Caspr2 is now thought to have two main orientations: the vertical and the horizontal, which could alter where Caspr2 is localized within the cell and could change its capacity to bind different protein partners (Z. Lu et al. 2016; Saint-Martin et al. 2018).

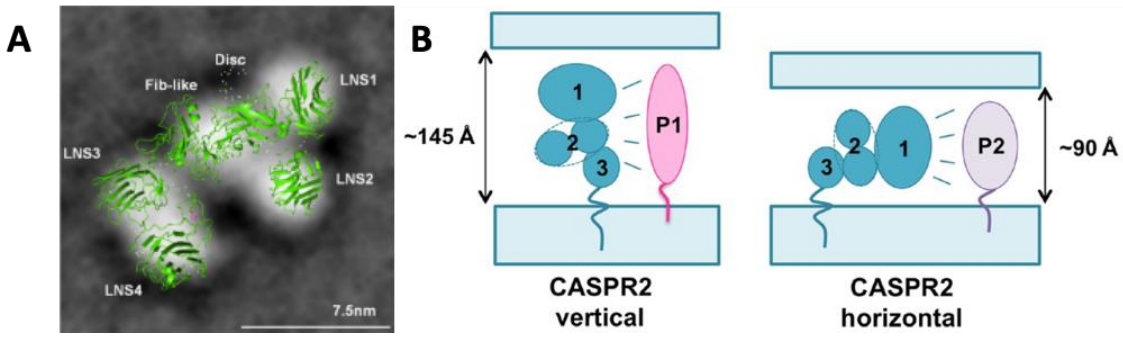

Figure 11: Conformation of Caspr2. A) Single particle EM of the extracellular domain of Caspr2 with overlay of one of the rigid body models obtained with Coral to show the structure of Caspr2. LNS1-4, Laminin-G domains 1-4; Disc, Discoidin domain; Fib-like, fibrinogen-like domain. B) Proposed conformation of Caspr2. Caspr2 is a ~145 Å- long, ~90 Å- wide, and ~50 Å- thick protein composed of three lobes (1, 2, and 3) flexible between each other allowing vertical or horizontal presentations. Such flexibility could reveal different domains of the protein and thus modulate its binding capability with multiple partners (P1 and P2). Furthermore, the localization of the protein at multiple neuronal subcellular regions could vary depending on its orientation. For example, only horizontal Caspr2 could fit in the narrow inhibitory synaptic cleft. Adapted from (Z. Lu et al. 2016; Saint-Martin et al. 2018).

2. A. Genetic Alterations in Neurodevelopmental Disorders

Many genetic alterations have been found in the *CNTNAP2* gene in NDDs including ASD, schizophrenia, intellectual disability, obsessive compulsive disorder (OCD), Pitt-Hopkins-like syndrome, ADHD, Gilles de la Tourette syndrome, and cortical dysplasia-focal epilepsy (CDFE) (Fig. 12) (Poot 2015). In 2003, *CNTNAP2* was found to be mutated in a family with Gilles de la Tourette

syndrome and obsessive-compulsive disorder. The mutation involved a chromosomal insertion on chromosome 7q35-36, which interrupted the gene (Verkerk et al. 2003). In 2006, researchers identified a group of patients in an Old Order Amish family who all had CDFE, a disorder which is characterized by seizures, language regression, hyperactivity, aggressive behavior, and intellectual disability. All patients in the study were found to have a single-base deletion at nucleotide 3709 in exon 22 of the gene; this frameshift mutation creates a stop codon prematurely and is predicted to generate a non-functional protein due to the lack of cytoplasmic and transmembrane domains (Strauss et al. 2006). All patients in the study were homozygous for this mutation. In 2009, a homozygous deletion of exons 2-9 in *CNTNAP2* were identified in siblings with Pitt-Hopkins-like syndrome, which results in a predicted loss of some functional domains of the protein (Zweier et al. 2009); another patient exhibited a compound-heterozygous mutation resulting in the deletion of exons 5-8, and subsequent loss of 2 Laminin-G domains in the protein (Zweier et al. 2009). Many of the mutations observed in patients with the aforementioned disorders are deleterious due to frame shift or loss of functional regions of the protein, and are caused by inherited recessive alleles from both parents. However, patients with other NDDs, such as ASD, often inherit mutations in *CNTNAP2* from only one parent, but present symptoms strong enough to be diagnosed.

Additionally, in a genome-wide study to investigate CNVs in patients with epilepsy and schizophrenia, Friedman and colleagues found unique CNVS all affecting the *CNTNAP2* gene; they also showed that there are dosage variations at this gene which can result in the previously mentioned disease phenotypes (Friedman et al. 2008). These results indicate that rare mutations and varying dosage of *CNTNAP2* could cause both neurological and psychiatric disorders.

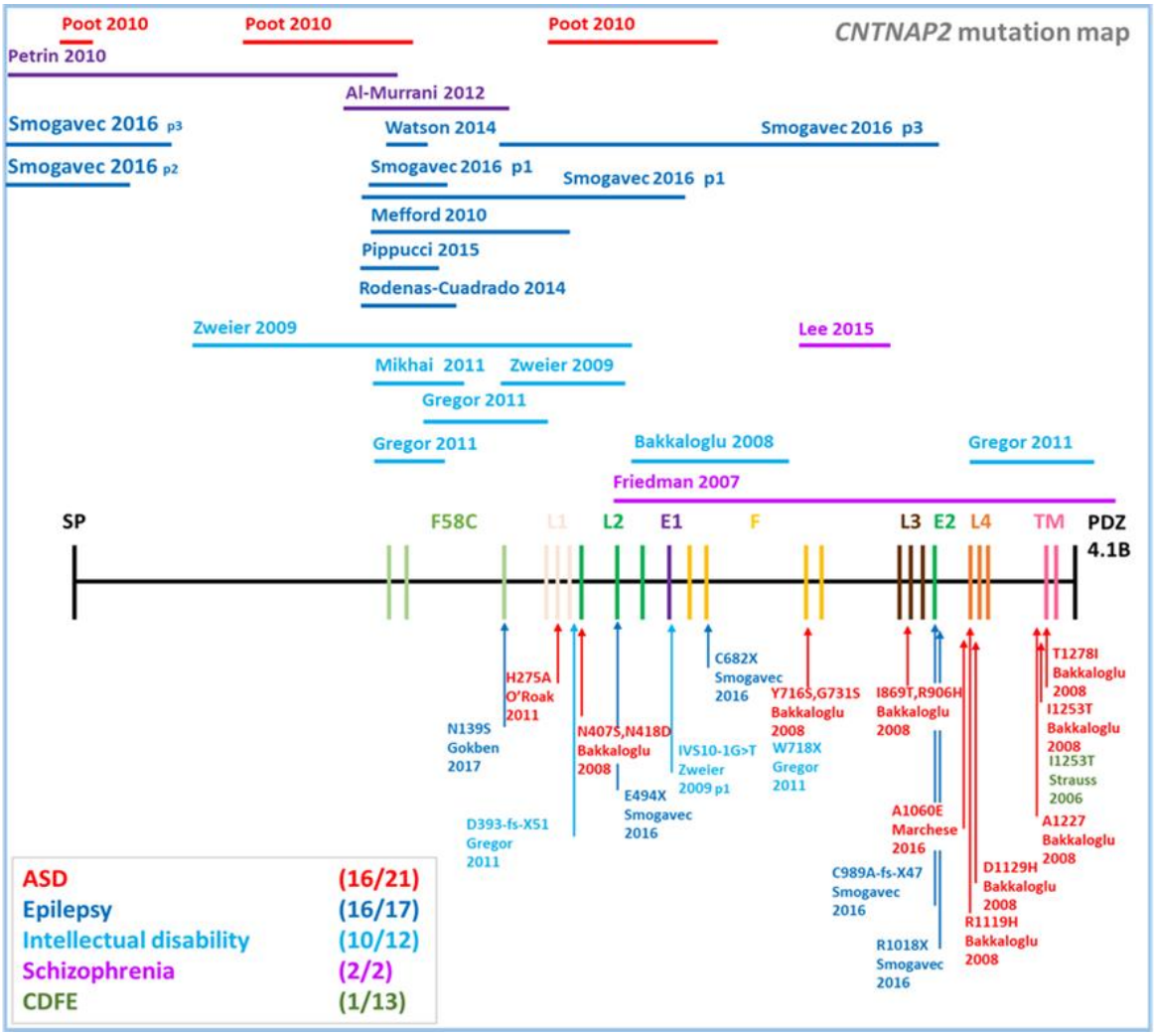

Figure 12: *CNTNAP2* mutation map. The *CNTNAP2* gene and its 24 exons coding for Caspr2. Lines above the gene represent large DNA deletions or duplications (Copy Number Variations, CNVs), while arrows indicate point mutations below the gene. References (author's name) are specified for each mutation. Patients presenting multiple *CNTNAP2* mutations are indicated with p1 (patient 1) to p4 (patient 4). The legend box presents the main pathologies associated with the mutations in different colors, and in brackets the number of distinct mutations and the number of patients for each disease. SP: single peptide; F58C: Discoidin domain; L: Laminin G domain; E: Epidermal growth factor-like domain; TM: Transmembrane domain; 4.1B: 4.1B-binding domain/GNP motif; PDZ: PDZ-binding domain (Saint-Martin et al. 2018).

2. B. *CNTNAP2* Mutations in ASD patients

CNTNAP2 was proposed to be an ASD-susceptibility gene in 2008 by Alarcón and colleagues, who used SNP analysis of the chromosomal region 7q34-36, encompassing the language quantitative trait locus which known to exist at 7q35 (Maricela Alarcón et al. 2008). Their analysis identified 4 genes for further study, one of which was *CNTNAP2*. Within the same month, Bakkaloglu and colleagues identified a *de novo* 7q inversion disrupting Autism susceptibility candidate 2 (*AUTS*) and *CNTNAP2* in a child displaying cognitive and social delay (Bakkaloglu et al. 2008). Further study of two of the previously identified SNPs were found to have no significant association with ASD, suggesting that while *CNTNAP2* dysregulation could play a role in some ASD

cases, it has a limited contribution to ASD susceptibility at the population level (Sampath et al. 2013).

More recently, a study by Shiota and colleagues assessed 67 children with ASD and 57 healthy children and genotyped them for the single-nucleotide polymorphism rs2710102 (G/A) of *CNTNAP2*; they found a significant association between genotype and ASD group (Shiota et al. 2021). While this study does not imply causation, it does suggest that variations in SNPs along the *CNTNAP2* gene – and specifically at rs27101012 – are associated with at least some ASD traits. Another SNP, rs7794745, was identified by Arking and colleagues, and was determined to be a common variant associated with increased risk for ASD in independent family-based sample groups; what's more, this mutation was found to exhibit a parent-of-origin bias (Arking et al. 2008). The group also references another study which identified *CNTNAP2* as a gene which maps onto a region of chromosomal instability; this could be one contributing factor to the fact that mutations in this gene are linked to so many neurodevelopmental disorders (Smith et al. 2006). Several other studies have linked *CNTNAP2* mutations to ASD (Gregor et al. 2011; Poot et al. 2010; Qiu et al. 2022).

A study by Bakkaloglu and colleagues investigated *CNTNAP2* mutations in ASD patients (Bakkaloglu et al. 2008). They sequenced *CNTNAP2* to investigate for mutations in a group of 635 patients and 942 controls. Within the 635 ASD patients, they found a total of 27 nonsynonymous variants, with 13 of these being rare variants; 8 of these were missense variants and were predicted to be deleterious via bioinformatic analysis (SIFT and/or PolyPhen) (Fig. 13). Interestingly, most rare heterozygous variants were inherited from unaffected parents, and are all localized to the extracellular region of the protein, except one (T1278I). One variant, I869T, was identified in 4 individual patients from 3 unrelated families but was not found in 4,010 control chromosomes. This variant was predicted to be deleterious by SIFT, and was shown to be conserved across several species (Bakkaloglu et al. 2008). While the group did strongly suggest that these rare *CNTNAP2* variants could contribute to ASD, it must be noted that they also identified variants in the control individuals. Within the 942 controls, 35 nonsynonymous variants were identified, with 11 being rare and 6 predicted to be deleterious (SIFT, PolyPhen).

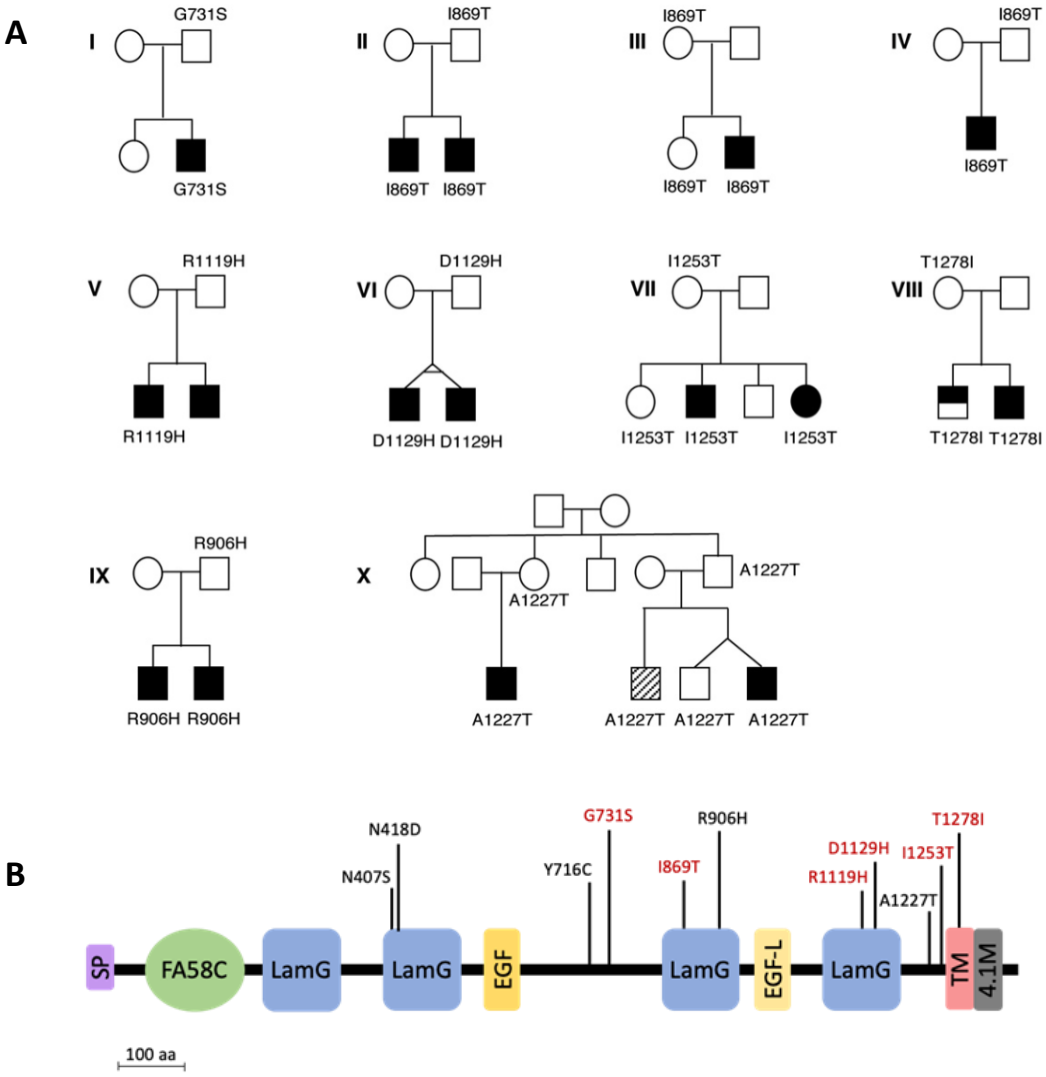

Figure 13: A) Pedigrees for all families with variants predicted to be deleterious at conserved sites (I to XIII) or which all affected relatives carry the identified variant (IX–X). The individuals carrying the suspect allele are noted and are heterozygous. The brothers inheriting the D1129H variant are monozygotic twins. Affected status was calculated with the AGRE diagnosis algorithm, which is based on ADI-R scores. Blackened symbols represent an ASD diagnosis, half-filled symbols indicate a not-quite-autism (NQA) diagnosis, and crosshatched individuals have a broad-spectrum diagnosis. B) Distribution of the variants identified by Bakkaloglu et. al. along the extracellular region of the Caspr2 protein. Adapted from (Bakkaloglu et al. 2008).

While some groups have found ample evidence of *CNTNAP2* mutations in ASD patients, others have questioned this link (Toma et al. 2018; Murdoch et al. 2015) and have pointed to the observation that many *CNTNAP2* mutations also are present in healthy individuals (Fig. 14). A study by Murdoch and colleagues evaluated existing sequence data of 2,704 ASD cases and 2,747 controls. In their combined cohorts, they found 26 rare variants in ASD cases and 28 rare variants in controls; therefore, they found no evidence for significant association of rare heterozygous mutations in any of the *CNTNAP* genes, including *CNTNAP2*, and ASD diagnosis (Murdoch et al. 2015). Additionally, Toma and colleagues used summary data from the Psychiatric Genomics Consortium GWAS, along with all reported structural variants in patients and controls, performed a cross-disorder analysis of previously identified SNPs, and conducted burden tests for rare

pathogenic variants using sequencing data from 4,483 ASD cases, 6,135 schizophrenia cases, and 13,042 controls. They found that the distribution of CNVs across *CNTNAP2* in psychiatric patients was no different from that of control cases, and that the rare variant burden of *CNTNAP2* in cases versus controls showed no difference as well (Toma et al. 2018). These studies show that while many rare *CNTNAP2* variants have been identified in ASD patients, many have also been identified in healthy individuals, therefore questioning the pathogenicity of these variants.

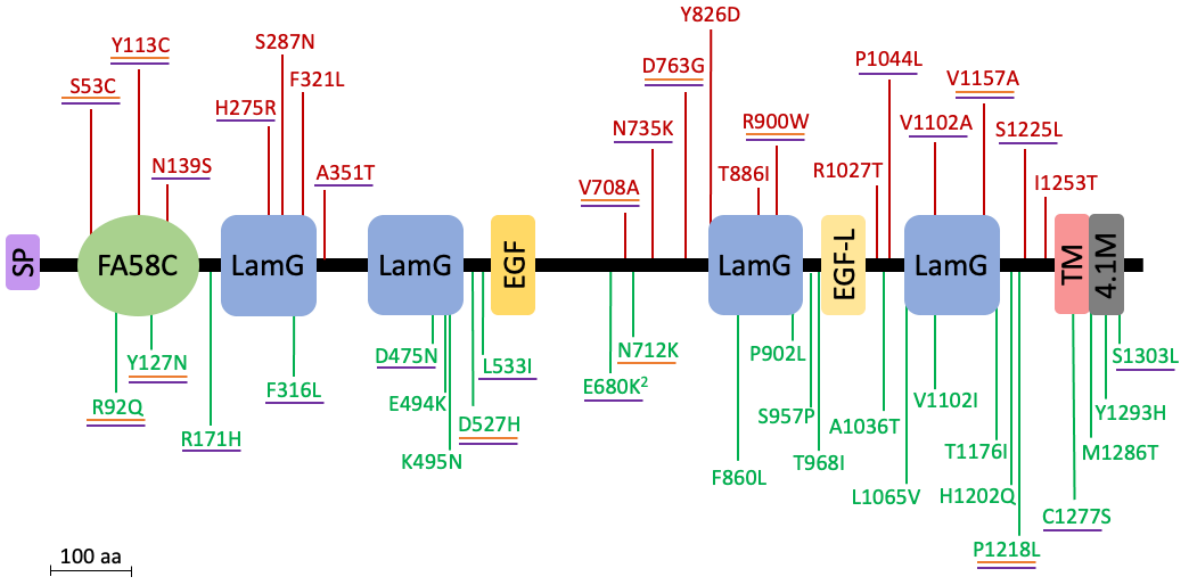

Figure 14: *CNTNAP2* heterozygous missense mutations in ASD patients and controls. All variants are localized in the extracellular domain of the protein. Variants shown in red were identified in patients (n=2704); variants in green were identified in controls (n=2747). Those predicted to be deleterious by SIFT are underlined in orange and those predicted to be deleterious by PolyPhen2 are underlined in purple. Adapted from (Murdoch et al. 2015).

Of note, in recent years, several tools have been developed to help predict the effects of mutations on protein function or pathogenicity level. One such software is MetaDome, which uses input from several genetic databases to create mutation intolerance map, generating amino acid resolution of genetic intolerance profiles for human protein domains (Wiel et al. 2019). This allows insight into which domains of a protein may be most affected by mutation. Using this tool for *CNTNAP2*, we can see that most of the extracellular domain of the Caspr2 is predicted to be intolerant to amino acid changes, suggesting that *CNTNAP2* variants identified so far could have damaging effects (Fig. 15). However, one has to be cautious with this prediction since Caspr2 presents a tightly compact structure (Fig. 11), which the modeling program does not take into account.

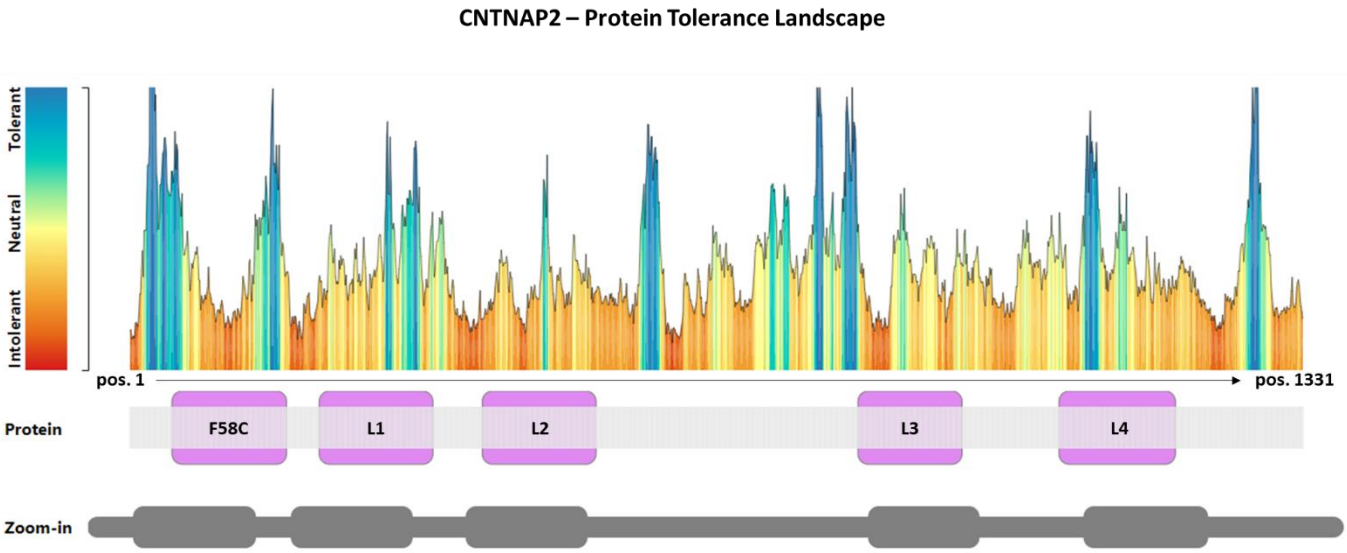

Figure 15: Protein tolerance landscape for CNTNAP2/Caspr2 protein. Blue indicates residues which are tolerant of mutation, while red indicates residues which are sensitive and are likely to have a greater effect when altered. Image adapted from MetaDome webserver (https://stuart.radboudumc.nl/metadome/dashboard).

2. D. *Cntnap2* Mouse Model and ASD

The *Cntnap2* KO mouse was generated in 2003 and has since been extensively studied, with multiple groups showing evidence of nervous system impairments and behavioral abnormalities, supporting genetic data. In initial studies, *Cntanp2* KO mice were shown to have epilepsy, neuronal migration abnormalities, and ASD-related defects (Peñagarikano et al. 2011; Sebastian Poliak et al. 2003). The *Cntnap2* KO mice are often compared with other mouse models for ASD-risk genes, including *Shank3b* KO*, Fmr1* KO*, Pten* KO*, Pcdh10* KO*, Tsc1* KO*,* and *16p11.2* KO (Brunner et al. 2015; Zerbi et al. 2018; Angelakos et al. 2019; Binder et al. 2020) in order to identify common pathways, behaviors, or brain structures that are altered.

When studying these ASD-risk genes in rodents, there are several behavioral tests which can be used to evaluate how certain genes could contribute to ASD-like behaviors. For anxiety-like behaviors, the open field test is often used to assess activity (distance traveled during a set time), resting time, and the amount of time spent in the center of the open field versus the edge. Increased activity and increased time spent around the edges of the field is associated with an anxious phenotype in mice. The rotarod test is also commonly used to assess learning capacity and locomotive performance. The mice are placed on a thick horizontal rod which is fixed on both ends and rotates/rolls/turns at steadily increasing speeds. The mice must hang on while walking and maintain balance for as long as possible, and duration is measured over consecutive days. Another test used to assess locomotion is the cyclotron test, in which mice are placed in a circular corridor for a fixed amount of time while the number of quarter-turns and rears they make are recorded by sensors. This test allows mice to be assessed for both locomotion and exploration behavior.

Peñagarikano and colleagues demonstrated that *Cntnap2* KO are hyperactive in the open field test and rotarod test, and another group showed that *Cntnap2* KO mice exhibit increased distance moved in a novel environment, indicating increased exploratory behavior and potential hyperactivity (Peñagarikano et al. 2011; R. Scott et al. 2019).

In addition to these tests, mice can be assessed for other ASD-like behaviors, such as stereotypical movements and repetitive behaviors. Mice can be observed via a home-cage scan which monitors their behavior over longer periods of time in a natural environment, and they can also be observed by eye for shorter periods of time with repetitive movements like scratching, twitching, or grooming recorded. Increased grooming and rubbing time as well as increased spontaneous/involuntary movements have been reported in *Cntnap2* KO by Scott and colleagues (R. Scott et al. 2019). Increased self-grooming time was also reported in *Cntnap2* KO mice by Kim and colleagues (Kim, Park, Kang, Gonzales, Oh, et al. 2019). Another study attempted to characterize different types of grooming behavior in detail, and showed that *Cntnap2* KO mice displayed more body grooming compared to their WT littermates (Klibaite et al. 2022).

Another key aspect of ASD is the lack of normal social interaction and communication deficits. Some ASD mouse models show perturbed social interaction, while others have more recently been shown to have altered communication, a trait which is now able to be studied more thoroughly due to advanced recording devices and high-throughput data analyses of ultrasonic vocalizations. Peñagarikano and colleagues observed that *Cntnap2* KO mice produced a lower number of ultrasonic calls at all developmental stages than WT mice (Peñagarikano et al. 2011). Mice can also be tested for social interaction via the juvenile play test or the three-chamber test. The juvenile play test involves recording the amount of time young mice spend interacting with each other versus other behaviors like digging or grooming. The three-chamber test consists of placing a mouse in an open field with three areas: an empty area, an area with a stranger mouse in a cup, and an area with an inanimate object in a cup. Normally, mice are very social animals and will prefer to spend time with the other mouse rather than in the other areas. However, in the study by Jang and colleagues, *Cntnap2* KO mice were shown to have no preference for the mouse over the inanimate object (Jang et al. 2022). Another study showed that *Cntnap2* KO mice displayed reduced preference for the conspecific mouse in the three-chamber test, as well as reduced interaction time in the juvenile play test (Kim, Park, Kang, Gonzales, Oh, et al. 2019).

In addition to these social and cognitive deficits, *Cntnap2* KO mice have also been reported to have motor and sensory defects. The mice show forelimb lag during their walking gait and defects in multi-day adaptation to motor tasks, according to a recent study (Klibaite et al. 2022). Hypersensitivity to both pain and heat were also reported in *Cntnap2* KO mice (Z. Zhang et al. 2021). Sensitivity can be measured in several ways, such as placing mice on a hot plate or conducting a thermal preference test and recording the time to hind paw withdrawal from the stimulus or poking the hind paws with fibers of increasing rigidity to record the mechanical stimulus

threshold (von Frey test). Using these tests, Dawes and colleagues observed that *Cntanp2* KO mice show increased sensitivity to mechanical stimuli and nociceptive stimuli (capsaicin injection) when compared to WT mice (Dawes et al. 2018).

In a recent study by our lab, *Cntnap2* HET mice were shown to have motor abnormalities, making more errors in the grid test (Cifuentes-Diaz et al. 2023); this test involves placing the mice in a box with a grid on the bottom made of evenly spaced thin metal bars. The mouse is left to wander the box for a fixed amount of time, and the number of slips/errors in foot placement is recorded. These results were especially interesting as *Cntnap2* HET mice are not often studied. This suggests that even a 50% reduction in Caspr2 protein level can lead to behavioral deficits.

3. *CNTNAP2* and Caspr2 Tissue Expression

Caspr2 was first characterized in 1999 by Poliak and colleagues, who demonstrated that it was located in the juxtaparanodal region of the node of Ranvier in central and peripheral mature myelinated fibers (S. Poliak et al. 1999); this will be detailed later in the Introduction. More recently, genetic data as inspired many studies to further investigate the expression patterns of Caspr2 and its potential functions during brain development, which could support the implication of the *CNTNAP2* gene in NDDs and ASD.

While overall Caspr2 tissue expression is thought to be comparable in mouse and human, much more data is available concerning Caspr2 expression in mouse and rat than in human, as samples are more abundant. When it was first described, *CNTNAP2* was shown to be expressed primarily in the nervous system – specifically human brain and spinal cord, with some light expression in the prostate and ovaries as well (Fig. 16A). During development, *CNTNAP2* expression was shown to overlap with cortico-striato-thalamic circuitry involved in higher cognitive processes, as well as in the frontal gray matter, subcortical structures, dorsal thalamus, caudate putamen, and amygdala in human fetuses (Fig. 16B) (Abrahams et al. 2007; Maricela Alarcón et al. 2008). In rat brain, Caspr2 was found to be expressed mainly in neurons, in pyramidal cells in the CA3 region of the hippocampus, in the subicular complex, the amygdala, and the cortex (S. Poliak et al. 1999). In mouse brain, *Cntnap2* expression was detected from around E14-15 (Fig. 16C) and is enriched in the cortex, ventricular zone, marginal zone, subplate and ganglionic eminence (Canali et al. 2018; Maricela Alarcón et al. 2008), continuing into adulthood and has been shown to have different expression patterns during different developmental time periods.

The expression pattern was more deeply evaluated in mice by Gordon and colleagues, who generated a Caspr2/tau-LacZ mouse line in which the first exon encoding ATG of Caspr2 was replaced with a tau-LacZ gene, which, when expressed, would allow and X-gal staining to mark all Caspr2 expressing brain regions through development to adulthood. They observed that Caspr2 is dynamically expressed from early developmental stages (Fig. 17). In adulthood, a particularly strong expression was detected in the cortex, hippocampus, substantia nigra, interpeduncle nucleus, pontine nucleus, and the medial mammillary nucleus. Furthermore, Gordon and colleagues showed that Caspr2 was also expressed in sensory areas. The areas showing Caspr2 expression were observed in all sensory pathways (auditory, visual, gustatory, somatosensory, and olfactory), and at all levels of perception, from sensory organs and brain stem nuclei to the thalamus and cortex. Of note, the Caspr2/tau-LacZ mouse line allowed detection of the expression of Caspr2-isoform 1 only, and little is known about Caspr2-isoform 2. One recent study by Montalban et al. indicates that the two isoforms could present differential expression patterns in mouse: Caspr2-isoform 1 was shown to be enriched in the dorsal striatum while Caspr2-isoform 2 is enriched in the nucleus accumbens, suggesting potential specific roles for the different isoforms (Montalban et al. 2022).

Importantly, Gegenhuber and colleagues recently showed that the transcription factor oestrogen receptor-α (ERα) could underlie several sex differences in the brain by studying the genomic targets of ERα (Gegenhuber et al. 2022). They identified brain-specific ERα binding events enriched for synaptic and neurodevelopmental disease Gene Ontology terms, including *CNTNAP2*/Caspr2, indicating *CNTNAP2* expression could be regulated by oestradiaol. This suggests that Caspr2 expression could vary by sex

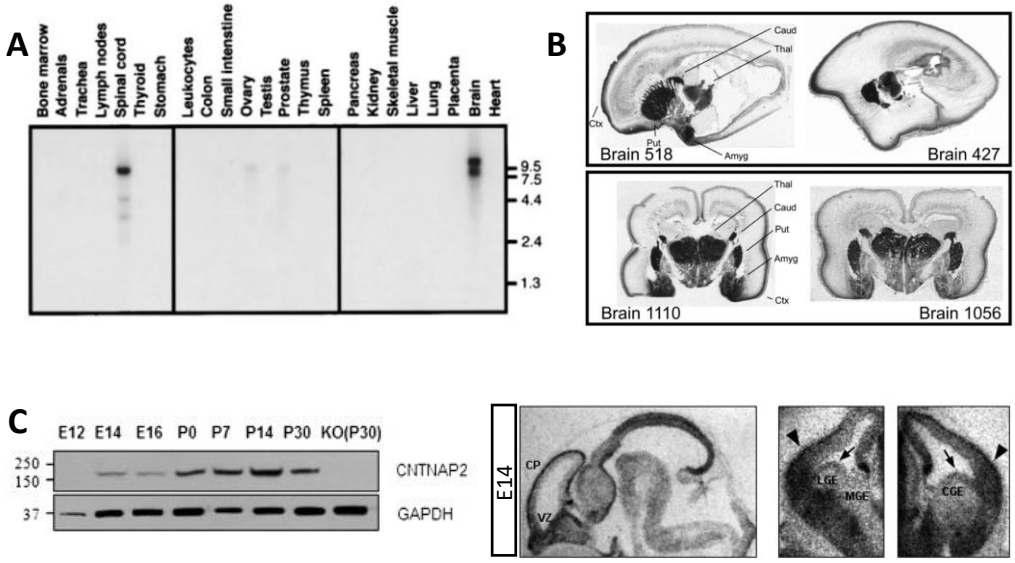

Figure 16: A) *CNTNAP2* tissue expression in human. Northern blots containing mRNA from various human tissues were hybridized with a Caspr2-specific probe. The autoradiogram is shown along with MW markers on the right. B) *CNTNAP2* expression in human brain. Top: autoradiograms of midline sagittal sections obtained from an 18-week and a 20-week fetal brain show striking enrichment of *CNTNAP2* in frontal gray matter, corresponding roughly to a region between the orbital gyrus and superior frontal cortical anlagen. Strong labeling is also observed in basal ganglia, thalamus, and amygdala. Bottom: Autoradiograms of coronal sections from two 19-week fetal brains demonstrate high levels of *CNTNAP2* in amygdala, caudate, cortical plate, dorsal thalamus, and putamen. Abbreviations: Amyg, amygdala; Caud, caudate; Ctx, cortex; Put, putamen; and Thal, thalamus. C) Left: Western blot of Caspr2 expression during development. Right: In situ hybridization of *Cntnap2* in WT embryos. CP, cortical plate; VZ, ventricular zone; LGE, lateral ganglionic eminence; MGE, medial ganglionic eminence; CGE, caudal ganglionic eminence. Arrows show expression of *Cntnap2* in the ganglionic eminences, arrowheads show expression of the gene in regions that contain migrating interneurons. n = 3 embryos/mice for each age. Adapted from (S. Poliak et al. 1999; Maricela Alarcón et al. 2008; Peñagarikano et al. 2011).

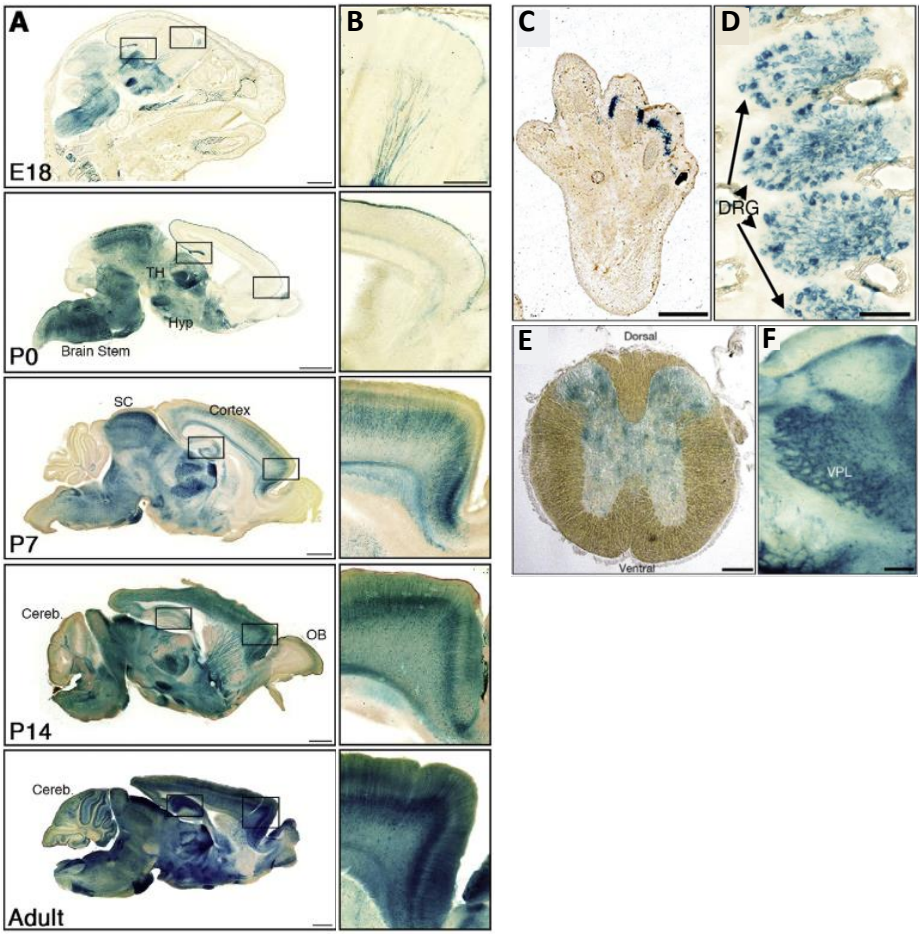

Figure 17: Caspr2 is dynamically expressed during development. A) Staining of mouse brains sagittal sections from E18 to adult. Caspr2 can be seen throughout many brain regions. TH-thalamus, Hyp-hypothalamus, SC-superior colliculus, Cereb-cerebellum, OB-olfactory bulb. B) High magnification of the cortex reveals expression starting at the surface and later moving into deeper layers of the cortex. C) Caspr2 is expressed in nerves innervating the footpad of E15 mice. D) DRG of E15 mice also express Caspr2. E) Expression is also seen in the dorsal (sensory) part of the spinal cord. F) Caspr2 is expressed in the ventral posterolateral thalamic nucleus (VPL), an area of the brain involved in somatosensory processing. Adapted from (Gordon et al. 2016).

.

4. Caspr2 functions in synapse formation and brain connectivity

Due to its capacity to interact with both cell adhesion molecules and cytoskeletal elements and its large expression in the brain from early developmental stages to adulthood, Caspr2 was found to play multiple roles during development in neuronal migration and interneuron maturation, as well as in the formation of synapses and brain connectivity *in vivo*, which I will detail forthwith.

4. A. Caspr2 and Synaptogenesis

As discussed briefly in section 1. E. i., Caspr2 has been shown to localize at the synaptic compartment. Anderson and colleagues strove to further study the role of Caspr2 in early development by using cortical neurons cultured from newborn mouse pups and knocking down (KD) Caspr2 expression *in vitro* (Anderson et al. 2012). They reported that reduced expression of Capsr2 suppresses neural network activity, an effect which is rescued when Caspr2 is fully expressed again. They then measured the size of evoked AMPA receptor and NMDA receptor-mediated excitatory postsynaptic currents (EPSCs) and found that KD of Caspr2 decreased the amplitudes of all synaptic responses in a cell-autonomous manner. In an effort to better understand these mechanisms, they investigated neuron morphology and found that Caspr2 KD impairs dendritic arbor and spine development (Anderson et al. 2012). The method by which this could occur was further explored by Varea and colleagues, who studied the subcellular localization of Caspr2 using mature cortical neurons cultured *in vitro* (DIV21) and found that Caspr2 is localized in axons, dendrites, spines, and soma (Varea et al. 2015). They also observed colocalization of Caspr2 and AMPA receptor subunit GluA1, indicating that Caspr2 is present in excitatory synapses. Furthermore, *Cntnap2* KO neurons showed reduced AMPA receptor levels and had large aggregates of GluA1 in the soma, indicating that Caspr2 could be involved in GluA1 trafficking (Varea et al. 2015). More recently, it was shown that Caspr2 stabilizes interneuron dendritic arbors via CASK, and that Caspr2-CASK and Caspr2-GluA1 complexes are formed *in vivo*, suggesting that Caspr2 and CASK work together to effectively traffic GluA1 to the membrane (Gao et al. 2019). However, despite this role in trafficking of key synaptic components, Caspr2 expression is not able to induce synaptic sites *in vitro*, while neuroligin and neurexin are, indicating that Caspr2 is not necessary for synapse formation.

While Varea et al. showed that Caspr2 could be present in excitatory synapses, other studies have shown that the protein is also present in inhibitory synapses. Caspr2 labelling was shown in about 58% of inhibitory (GAD65+) neurons as opposed to only 4% of excitatory (GD65-) neurons at DIV4; of the 81% of neurons in the culture that expressed Caspr2, 81% were inhibitory neurons (Pinatel et al. 2015). Caspr2 was also shown to colocalize with presynaptic vesicular glutamate transporter 1 (vGLUT1) at pre-synaptic sites, and presynaptic sites labeled for GAD65 were also strongly labeled with Caspr2 at the contact with the soma (Fig. 18) (Pinatel et al. 2015). Another

study showed that RNAi-mediated knockdown of Caspr2 led to a decrease in dendritic arborization and spine development in pyramidal neurons, leading to an overall reduction in the number of both excitatory and inhibitory synapses (Anderson et al. 2012). Furthermore, *Cntnap2* KO mice were shown to display a 20% decrease in the number of inhibitory interneurons, along with decreased GABA receptor-mediated inhibitory postsynaptic currents (IPSCs) (Anderson et al. 2012). *Cntnap2* deletion has also been shown to affect inhibition onto CA1 pyramidal cells, with reduced evoked IPSCs in the *Cntnap2* KO mice (Jurgensen and Castillo 2015). This study demonstrated that *Cntnap2* deletion can affect hippocampal inhibition while leaving excitation unchanged (Jurgensen and Castillo 2015).

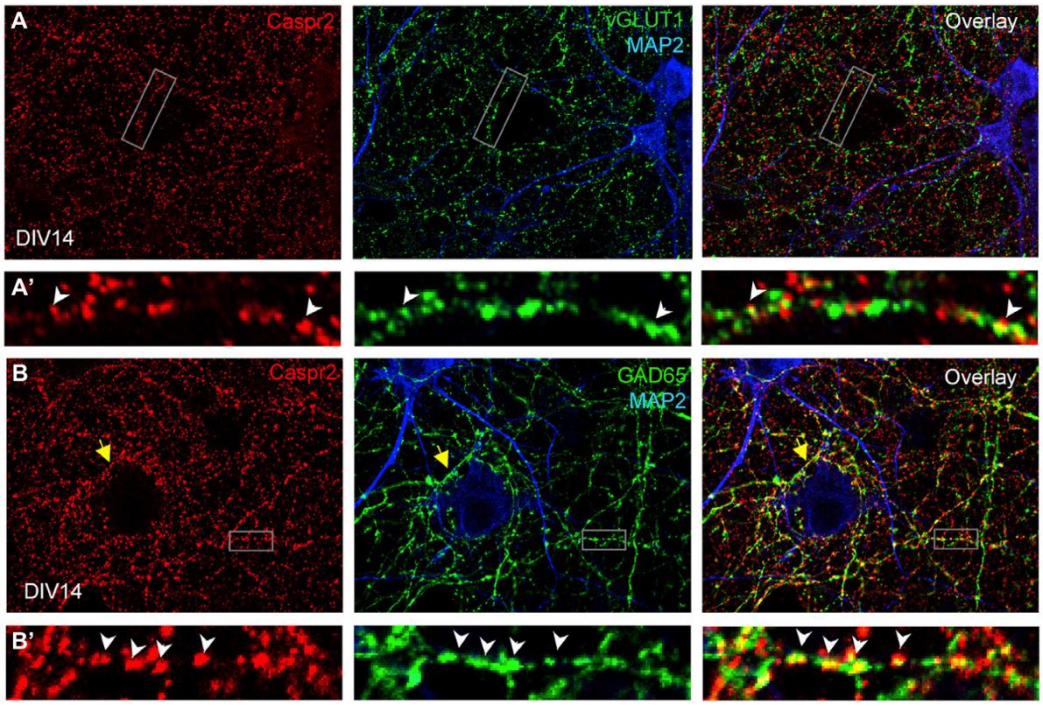

Figure 18: Distribution of Caspr2 at pre-synaptic sites of inhibitory axons. Confocal images of hippocampal neurons at DIV14 (A,B) that were surface labeled for Caspr2 using LE1 IgGs (red). Cells were fixed and permeabilized before double-staining for MAP2 (blue), vGLUT1 (A, green) or GAD65 (B, green). (A') Enlarged areas shows glutamatergic pre-synaptic sites stained for Caspr2. (B') Inhibitory pre-synaptic sites labeled for GAD65 (arrowheads) were intensely stained for Caspr2 at the contact with the soma or dendrites (B'). Adapted from (Pinatel et al. 2015).

4. B. Caspr2 and Connectivity *in vivo* + E/I Balance

Given that Caspr2 has been implicated in the synaptic compartment and possible contributions to synaptic organization and receptor trafficking, the potential role of Caspr2 in brain connectivity has been studied by several groups, though the jury is still out on this topic. Kim et al. showed that *Cntnap2* KO mice have reduced excitatory synaptic transmission in layer II/III neurons of the prefrontal cortex – specifically a reduced mEPSC amplitude, while the frequency remained

unchanged (Kim, Park, Kang, Gonzales, Kim, et al. 2019). Fernandes et al. also showed that upon treatment with Caspr2 antibodies in layer II/III pyramidal neurons, mEPSCs showed smaller amplitudes and unaltered frequency (Fernandes et al. 2019). Meanwhile, a study by Scott et al. showed that *Cntnap2* KO mice have abnormal action potential (AP) waveform when fiber volleys (FV) were measured from the contralateral hemisphere. FV are significantly reduced in *Cntnap2* KO mice, which indicates possible changes in AP waveform. Sure enough, they observed that the anti-peak amplitudes are significantly reduced in 8-week old *Cntnap2* KO mice (R. Scott et al. 2019). Furthermore, they observed increased amplitude of EPSCs likely due to increased neurotransmitter release from wider APs in the presynaptic excitatory neurons; their results point to perturbed excitatory connectivity and normal inhibitory connectivity in *Cntnap2* KO mice (R. Scott et al. 2019).

At the tissue scale, Liska and colleauges performed fMRI studies and retrograde viral tracing in *Cntnap2* KO mice to map large-scale functional connectivity and white matter deficits. They found that the loss of Caspr2 results in reductions of both local- and long-range connectivity in prefrontal regions which serve as functional connectivity centers in the brain, suggesting that Caspr2 could modulate functional network assembly (Fig. 19) (Liska et al. 2018). When Balasco and colleagues investigated the primary somatosensory cortex (S1) in *Cntnap2* KO mice, they found that the mutants showed focal hyperconnectivity within this area, with no change between it and other sensory areas, which could explain the sensory alterations observed in *Cntnap2* mutant mice (Balasco et al. 2022). In the medial prefrontal cortex (mPFC), Lazaro and colleagues demonstrated a reduction in both excitatory and inhibitory synaptic inputs onto excitatory neurons, along with decreased excitatory neurotransmission and a decrease in dendritic spine and synapse densities (Lazaro et al. 2019). Their results point to alterations in synchronous activity in the mPFC and, more globally, alterations in microcircuit connectivity and abnormal population activity in the absence of *Cntnap2*. Perturbed connectivity has also been reported in the auditory cortex in the absence of *Cntnap2*. In a recent study by Scott and colleagues, they showed that loss of *Cntnap2* leads to abnormal auditory-evoked potentials in the cortex, in addition to decreased spontaneous activity in the auditory cortex of *Cntnap2* KO rats. Furthermore, they report that auditory cortical neurons lacking *Cntnap2* have a lower stimulation threshold for depolarization accompanied by altered AP features and spiking kinetics (K. E. Scott et al. 2022). It could be that Caspr2 contributes differentially to connectivity in different regions of the brain, as it evidenced by these studies.

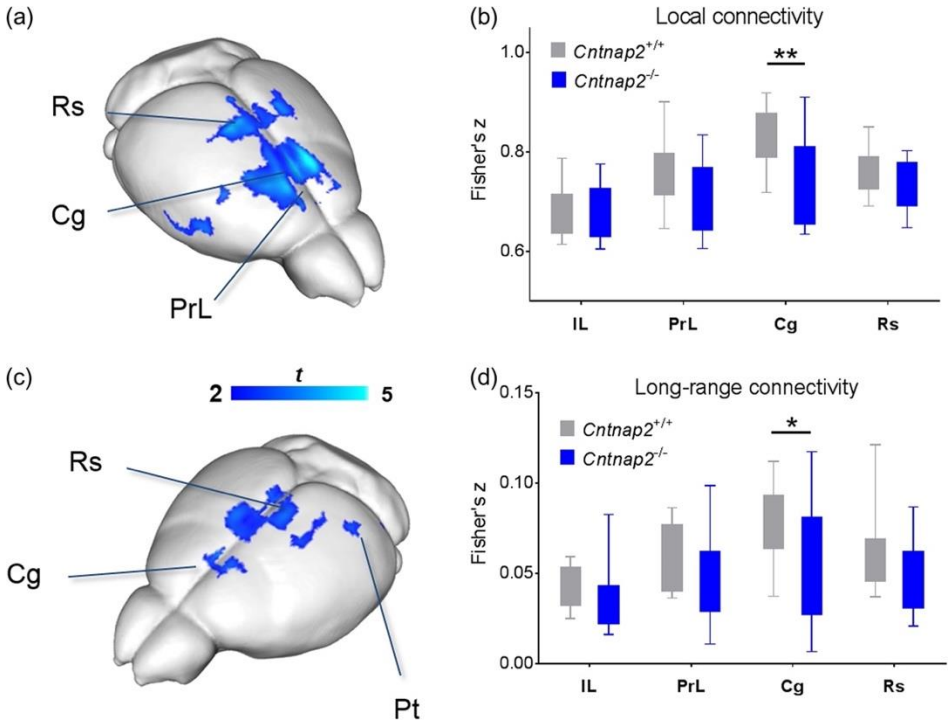

Figure 19: Reduced local and long-range connectivity in *Cntnap2*$^{-/-}$ mutants. (a) Foci of reduced local connectivity in *Cntnap2*$^{-/-}$ versus control *Cntnap2*$^{+/+}$ littermates (t-test; P < 0.05 FWE cluster-corrected, with cluster-defining threshold of t_{24} > 2.06, P < 0.05). (b) Mean local connectivity in regions of interest (t-test; Cg: t_{24} = 3.11, P = 0.005). (c) Foci of reduced long-range connectivity in *Cntnap2*$^{-/-}$ versus control *Cntnap2*$^{+/+}$ littermates (t-test; P < 0.05 FWE cluster-corrected, with cluster-defining threshold of t_{24} > 2.06, P < 0.05). (d) Mean long-range connectivity in regions of interest (t-test; Cg: t_{24} = 2.26, P = 0.03). IL, infralimbic cortex; PrL, prelimbic cortex, Cg, cingulate cortex; Rs, retrosplenial cortex, *P < 0.05, **P < 0.01. (Liska et al. 2018).

One interesting concept that has been explored in *Cntnap2* mice is the E/I ratio, which could be perturbed. Different ASD models have been proposed to show an increase in E/I ratio in the cortex, which could drive hyperexcitability in cortical circuits. Antoine and colleagues studied the feedforward circuit from layer IV to layer II/III pyramidal cells, which is mediated by PV+ interneurons, in *Cntnap2* KO mice. These mutants exhibited decreased inhibition and slightly decreased excitation, which yields an increased E/I ratio, though synaptic depolarization and spiking remained relatively unchanged (Antoine et al. 2019). They posit that this E/I ratio increase could be a sort of compensatory mechanism which stabilizes synaptic depolarization and excitability, rather than directly causing circuit hyperexcitibilty (Antoine et al. 2019). More recently, Lu and colleagues examined a *CNTNAP2* variant discovered in an ASD infant (R777G). When this variant was electroporated into primary mouse neurons, the mutant neurons showed decreased neurite extension and abnormal E/I balance (P. Lu et al. 2021). It seems that although the contributions of Caspr2 to connectivity in the brain may be region-specific, the E/I ratio is generally increased in the *Cntnap2* KO mouse models that have been studied.

Interestingly, recent evidence also suggests that some of the functions of Caspr2 in brain connectivity may be sex-dependent. A study by Townsend and colleagues showed that the visually

evoked activity in dorsal stream-associated visual areas was altered in male *Cntnap2* HET and *Cntanp2* KO mice, but unchanged in female mice (Townsend and Smith 2017). Another group demonstrated that female *Cntnap2* KO rats displayed increased pontine reticular nucleus firing rates compared to WT, while males showed no differences, implying that a loss of function mutation in the *Cntnap2* gene can have differential effects depending on sex (A. Zheng et al. 2023).

5. Caspr2 and Cortical Development

One of the most complex parts of the human brain is the cortex. The correct development of this brain region in a highly organized manner is part of what ensures a healthy overall brain development, and if any step of the process is perturbed, developmental delays or defects and deformations may ensue. The mammalian cortex is comprised of six different layers of cells, all originating from the innermost part of the neural tube during early development, called the ventricular zone (VZ). As more cells are produced, they begin to migrate to their final destinations. In the cortex, cells migrate in an inside-out manner, each time using the basal processes of previously generated neurons to "climb" up through the inner layers of the cortex to reach the outer layers. This process is called radial migration and is outlined below (Fig. 20). By following this process, the early-born neurons will form the deeper cortical layers, while late-born neurons will end up in the external layers of the cortex. This type of migration applies to roughly 70-80% of migrating neurons in the brain (Tierney and Nelson 2009). Once the migrating neurons which originate in the VZ have made their way up to the cortical plate (CP), these neurons will leave the basal processes of their predecessors and differentiate to form the neurons of their specific cortical layer (I-VI).

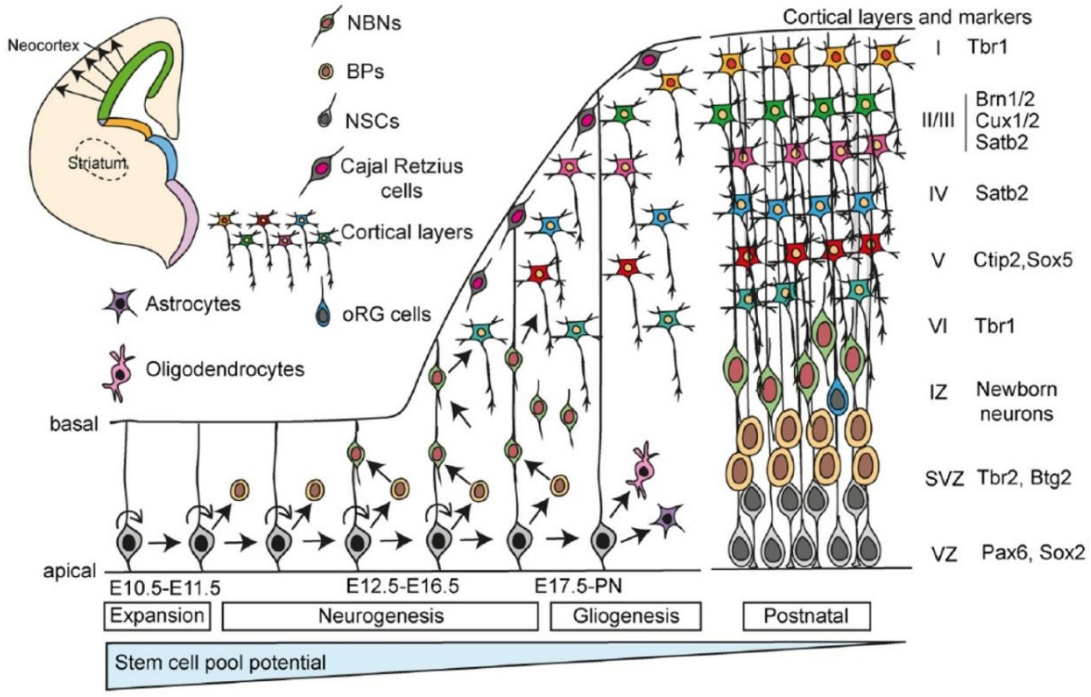

Figure 20: Systematic formation of cortical layers. During early stages of cerebral cortical development, neural stem cells (NSCs) undergo predominantly symmetric cell division to expand the NSC pool (expansion phase). The first neurons to be formed are generated by direct neurogenesis of the NSCs. During late embryogenesis, NSCs undergo more asymmetric divisions to generate 1 NSC and 1 basal progenitor (BP). The BPs generate mature neurons. Neurons are generated in inside-out fashion and are specified to their layers by transcription factors, shown at right. At later stages of development NSCs generate other cell types such as astrocytes and oligodendrocytes. BP, basal progenitors; IZ, intermediate zone; NBNs, newborn neurons; NSCS, neural stem cells; SVZ, subventricular zone; VZ, ventricular zone (Mukhtar and Taylor 2018).

A key aspect of cortical development is the generation and migration of interneurons. Interneurons are a type of neuron which act as a mediator between sensory and motor neurons and the central nervous system. These neurons comprise approximately 20-30% of neurons in the neocortex, and are mostly inhibitory, operating within the GABAergic system. Different types of interneurons express distinct neuropeptides; for example, basket cells, which make up about 50% of inhibitory interneurons, express parvalbumin (PV) and calbindin (CB) (Markram et al. 2004). Martinotti cells are a type of interneuron which expresses somatostatin (SST); these interneurons have ascending axons which arborize in Layer I of the cortex and spread horizontally, making synapses on pyramidal neurons. Many of these cells are found in cortical Layer V (Rudy et al. 2011). Interneurons are generated from progenitor cells in the embryonic subpallium from around E11.5; soon after becoming postmitotic, these young interneurons will undergo a long tangential migration around E14.5 and finally reach the pallium via several streams. Once here, interneurons will disperse throughout the cortex starting from P0 (Lim et al. 2018).

5. A. Caspr2 in Cortical Migration and Interneuron Maturation

Strauss and colleagues studied temporal lobe samples from Old Order Amish children with cortical dysplasia and focal epilepsy who carried homozygous mutation of *CNTNAP2* (Strauss et al. 2006). They found that in multiple cortical areas, neurons were abnormally arranged into tightly packed columns, while in the hippocampus and temporal neocortex, neuron density was increased. They also observed ectopic neurons located in the subcortical white matter. These results suggested that Caspr2 could be involved in corticogenesis and could mediate intercellular interactions during neuroblast migration and laminar organization. While these results are interesting, there were not many samples available for staining and analysis. Further evidence for the role of Caspr2 in neuronal migration came in 2011 from Peñagarikano and colleagues. They observed ectopic neurons in the CC of KO mutant mice at P14, after neuronal migration is completed, which was maintained into adulthood (Peñagarikano et al. 2011). These results are interesting given the ectopic neurons also observed in human samples by Strauss et al. Staining with cortical markers CUX1 (upper layer marker) and FOXP2 (deeper layer marker) revealed increased CUX1+ cells in deep cortical layers in the KO mice, while FOXP2+ cells showed no differences (Peñagarikano et al. 2011). Their data indicate that Caspr2 is necessary for the normal migration of cortical projection neurons in the brain. However, a more recent study by Scott and colleagues has shown conflicting results. In adult mice, they found no differences in the number of CUX1+ (upper layer) or Ctip2+ (deeper layer) cells in *Cntnap2* KO mouse brains (R. Scott et al. 2019).

In addition to the above observations by Peñagarikano and colleagues, they also observed a reduced number of GABAergic interneurons in *Cntnap2* KO mice via GAD1 immunostaining at P14; this was revealed to be due to a reduction specifically in PVALB+ interneurons (Peñagarikano et al. 2011). Vogt and colleagues observed concordant results in which PV+ interneurons were decreased in P30 somatosensory cortex of *Cntnap2* KO mice, with no change in SST+ cortical interneurons

(Vogt et al. 2018). Contrarily, Scott and colleagues observed no differences in PV+ or SST+ cell number in the neocortex of *Cntnap2* KO mice at P56 (R. Scott et al. 2019). Evidence for both sides was reported by Lauber and colleagues, who undertook a deeper study into different types of interneurons in *Cntnap2* KO mice at P25. They observed no decrease in PVLAB+ neurons in the striatum, somatosensory cortex, or medial prefrontal cortex when staining for VVA+ perineuronal nets; however, the number of PV+ neurons was decreased in the striatum. No changes were observed in PV+ cell numbers in cortical regions (Lauber, Filice, and Schwaller 2018). These studies suggest that Caspr2 could contribute to the maturation of specific types of interneurons, rather than to their migration, and questions whether observed reductions in PV+ interneuron number could be due to a down-regulation of PV expression in lieu of a physical decrease in the number of interneurons (Lauber, Filice, and Schwaller 2018).

6. Caspr2 and Interhemispheric Myelinated Tracts

In the brain, there are two main myelinated tracts which are made up of long-distance axons covered by a myelin sheath. These neurons may have their somas in the cortex or other brain regions, and project their axons through these tracts to communicate information to the contralateral side of the brain; therefore, they are often referred to as projection neurons. There are different types of cortical projection neurons (CPNs) which will be formed in the different layers of the cortex. Associative projection neurons send their axons to other locations within the same hemisphere of the brain, connecting local areas. Commissural and callosal projection neurons extend their axons to the contralateral hemisphere which will form the CC and the anterior commissure (AC) (Mukhtar and Taylor 2018). These tracts connect different brain regions and allow communication between both sides of the brain. Deep layer CPNs typically have long-distance projecting axons, while superficial layer CPNs participate in local circuitry within cortical columns (Leyva-Díaz and López-Bendito 2013).

6. A. The Corpus Callosum

In human the corpus callosum is comprised of over 200 million myelinated axons which are extended from the neuronal somas of the cortex and projected contralaterally to the opposite side of the brain. This large brain structure can be thought of as a highway relaying information from one side of the brain to the other, connecting right and left hemispheres. In 1989, Sandra Witelson conducted post-mortem studies on healthy individuals with varying handedness; this led to the definition of distinct regions with the CC. These include the rostrum, the genu, the body, the isthmus, and the splenium (Witelson 1989). Upon further investigation of the substructure of the CC, several studies showed that the myelinated fibers of the CC are organized by size and density in the different regions (Aboitiz et al. 1992; Hofer et al. 2015). These are outlined in Fig. 21.

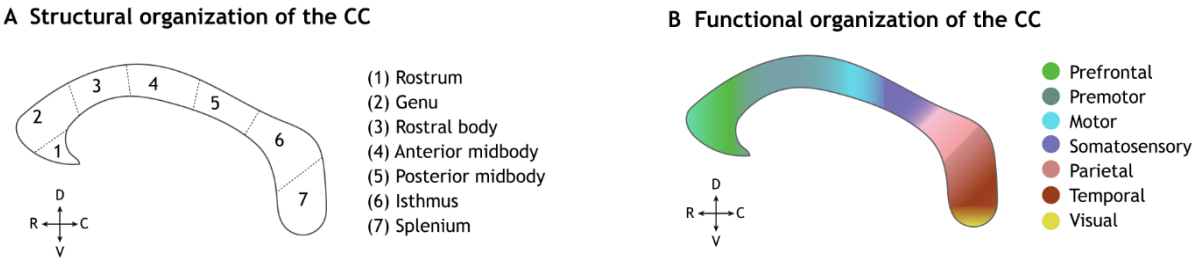

Figure 21: A) Structural organization of the human corpus callosum (hCC) represented from rostral to caudal. B) Functional organization of the hCC represented from rostral to caudal. (De León Reyes, Bragg-Gonzalo, and Nieto 2020).

In mouse, the CC is formed in the dorsomedial region of the cerebral cortex along the boundary between the septum and the cortex. The CC is comprised of CPNs from layers II/III (~ 80%) and layer V (~ 20%) and a small amount of CPNs from layer VI (Fame, MacDonald, and Macklis 2011). The first step of CC formation is the fusion of the telencephalic midline of the brain, which

will act as a substrate through which the callosal axons can grow. The CC consists of two populations of axons that come from different cortical areas: the neocortex and the cingulate cortex. The axons from the cingulate cortex arrive at the midline first, with neocortical axons following about 24 hours later (in mice). Because the cingulate cortical axons arrive at the midline first, they are deemed "pioneering axons" of the CC (Donahoo and Richards 2009). There are several other groups of cells which help to form the CC, including the midline zipper glia, the glial wedge, the indusium griseum glia, and the subcallosal sling (Fig. 22). In mice, the formation of the CC begins around gestational day 16 (E16). By P3 in mice, all Layer IV neurons have a callosal axon (De León Reyes, Bragg-Gonzalo, and Nieto 2020).

Once the pioneering axons have crossed the midline, they will begin to project into the contralateral hemisphere of the brain to find their targets. Long-range signaling molecules such as Slit/Robo, Wnt, and Netrin aid in the guidance of these axons through the CC and into the contralateral domain. It's been shown in experiments using carbocyanine dyes to inject mouse brains at different time points *in vivo* that the CC also develops in a directional manner, with the structure forming in a rostral to caudal direction; these same results were observed in human (Ren et al. 2006; Richards, Plachez, and Ren 2004). Axons from rostral regions are shown to cross the midline by E15.5, followed by axons from medial regions around E16, and axons from caudal regions at E16.5, with axons from all regions having crossed the midline by around day E17 (Richards, Plachez, and Ren 2004).

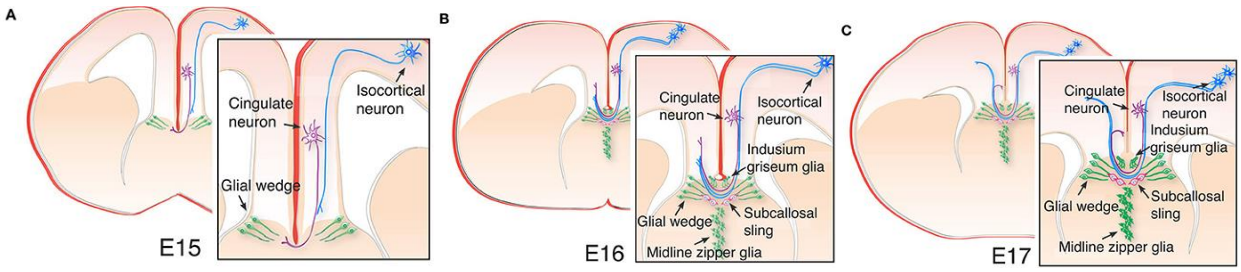

Figure 22: Cellular architecture of the telencephalic midline and callosal development in mouse. A) The ventral-most boundary of the corpus callosum is established by glial wedge cells, as cingulate pioneering axons first cross the midline at E15, while the more laterally located isocortical axons grow toward the midline following cingulate axons. B) At E16, a small number of isocortical axons have crossed the midline, and the indusium griseum glia and midline zipper glia are now detectable with Gfap immunohistochemistry. The indusium griseum glia provide the dorsal boundary of the corpus callosum. In addition, cells of the subcallosal sling begin to migrate toward the midline, just beneath the corpus callosum. C) By E17, isocortical axons have started crossing the midline, and cingulate pioneering axons are projecting to homotopic targets in the contralateral hemisphere. Midline crossing of callosal axons continues during early postnatal stages in mice (Suárez, Gobius, and Richards 2014).

After many of these cortical neurons have projected their axons through the CC, there is a period of exuberance and refinement in which underutilized callosal axons will be eliminated; this process does not involve cell death, but rather the elimination of transient axons (LaMantia and Rakic 1990; De León Reyes, Bragg-Gonzalo, and Nieto 2020). This refinement process will take place from around P3 to P21 in mice, when adult local connectivity is reached and axons are myelinated; this is based upon many factors, including activity-dependent mechanisms during critical periods. Human CC development parallels that of the mouse, with CC formation beginning around gestational week 11, first axons crossing the midline by week 13, and continuing until week 22 (Fig. 23) (Raybaud 2010). The rostral portion of the CC is visible from 15 gestational weeks, while the more caudal portion isn't observable until gestational weeks 18-19 (Ren et al. 2006).

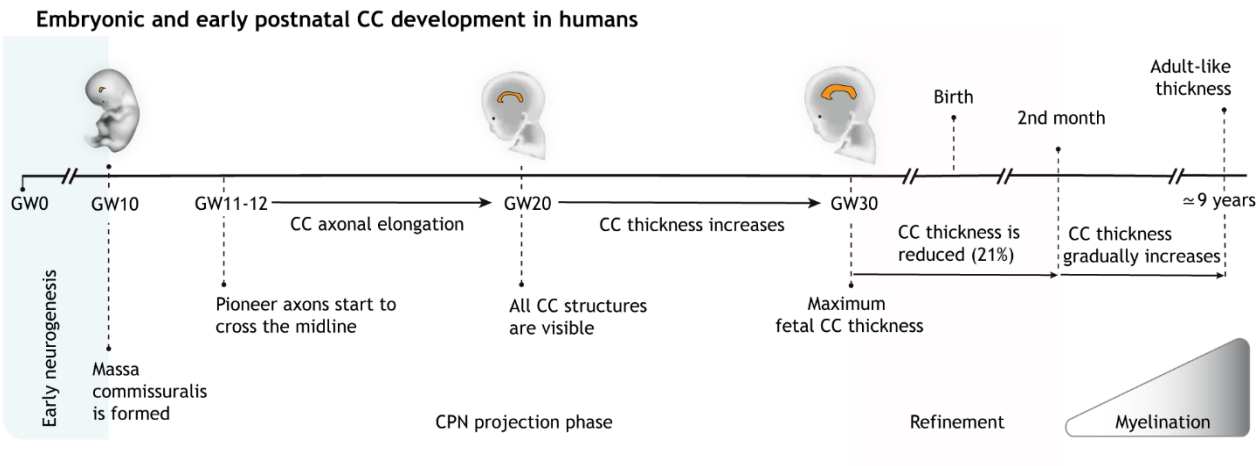

Figure 23: Embryonic and early postnatal development of the human CC. First, callosal projecting neurons (CPNs) project their axons through the midline. All CC structures are visible by gestation week (GW) 20. CC axonal elongation continues until GW30. Then, 21% of the total CC cross-sectional area is reduced. During the second postnatal month, myelination begins, and CC thickness gradually increases. Adult-like thickness is achieved by around 9 years (De León Reyes, Bragg-Gonzalo, and Nieto 2020).

6. B. The Anterior Commissure

The AC is the oldest interhemispheric connection among all vertebrates and conveys connections from diverse brain regions. These include the olfactory and amygdaloid regions, as well as the temporal lobes and the piriform cortex. The AC is comprised of three main branches: the anterior branch (ACa), comprised of fibers from the anterior olfactory nucleus to the contralateral olfactory bulb; the posterior branch (ACp), comprised of fibers from the piriform cortex, lateral entorhinal cortex, and ectorhinal and temporal association areas; and the stria terminalis branch, comprised of fibers from the cortical amygdala and nucleus of the lateral olfactory tract that join the dorsocaudal aspect of the AC after circling around the stria terminalis (Fig. 24A) (Fenlon et al. 2021).

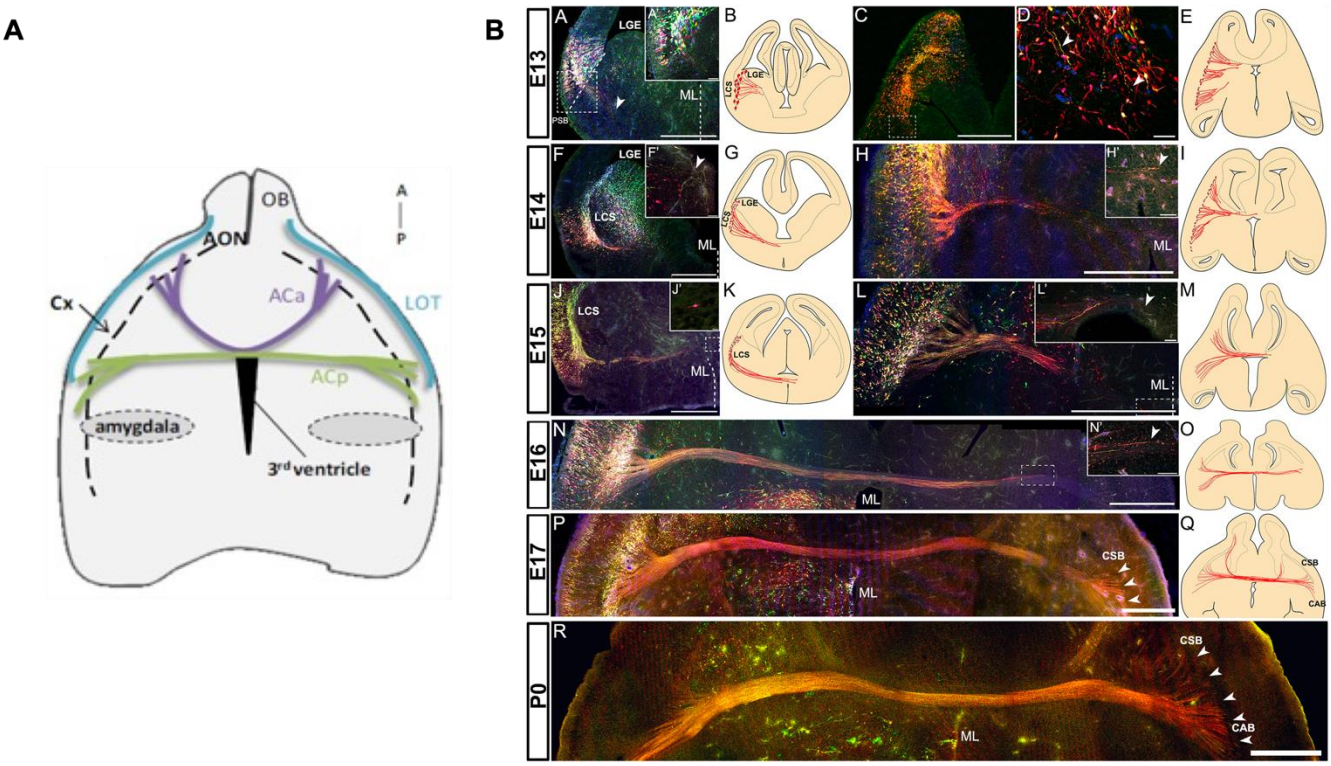

Figure 24: A) Schematic representation of the structure of the AC showing the ACa and the ACp. B) Timeline of anterior commissure development as demonstrated by labeling piriform cortex precursor cells with the piggyBac transposon system. Coronal sections and diagrams illustrating axon growth at E13, E14, E15, E16, E17 and P0. *CAB* cortico-amygdaloid border, *CSB* cortico-striatal border, *LCS* lateral cortical stream, *ML* midline. Scale bars = 500 µm in A, C, F, H, J, I, N, P and R; 50 µm in A', D, F', H', L', N'; 5 µm in J' (Martin-Lopez, Meller, and Greer 2018).

Development of the AC begins along the rostral midline domain, just after the closure of the anterior neuropore (Fig. 24B). The lamina terminalis grows dorsally and glial cells accumulate here, where they will help to channel pioneering axons of the AC. In mice, the ACp begins to form around E13, followed by the stria terminalis and ACa (E14-E15). The first axons will reach the midline around E14 (Klingler et al. 2015; Martin-Lopez, Meller, and Greer 2018). Once the pioneering axons arrive here, there is a slight pause in development; by E16, these axons progress once more to invade the contralateral hemisphere, growing consistently until E17, by which time they've successfully invaded their targets, such as the olfactory cortex). Following this growth period, there is another pause in which axon bundles begin to defasciculate and wait until P1 to begin innervating the cortex (Fenlon et al. 2021). After these axons have reached their destinations, oligodendrocytes can begin the myelination process around P10, undergoing a rapid phase starting at P14, and reaching full adult myelination levels around P30.

6. C. Caspr2 in Axon and Myelinated Tract Development

Development of both the CC and the AC relies on the processes of axon elongation and subsequent myelination to properly form these white matter tracts. The lab provided evidence that Caspr2 contributes to the development of both the CC and the AC. It showed that Caspr2 plays an important role in axon development, regulating axon growth in a dose-dependent manner: primary E14.5 cortical neurons from *Cntnap2* HET mice present an intermediate phenotype between neurons from WT and KO mice, which is rescued by expression of Caspr2 in these neurons (Fig. 25) (Canali et al. 2018).

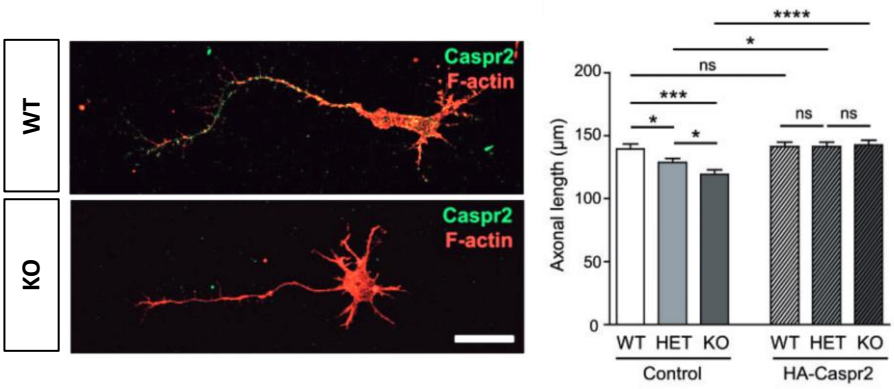

Figure 25: Caspr2 modulates axonal outgrowth of primary E14.5 cortical neuron in a dose-dependent manner. At left, representative images of Caspr2 cell surface immunostaining on WT and KO cortical neurons at DIV3 (green). Co-staining of actin with phalloidin (red). At right, rescue of axon growth by expression of HA-Caspr2 in cortical neurons. Quantification of axon lengths at DIV3 in WT, HET and KO neurons electroporated with the control vector or the HA-Caspr2-expressing vector. Data are means +/- SEM. n=8–10 embryos/genotype, n=40–43 neurons/embryo. Statistical analyses: Kruskal–Wallis one-way ANOVA test, $P < 0.0001$; Dunn's Multiple Comparison post-test, *$P < 0.05$, **$P < 0.01$, ***$P < 0.001$; ns, not significant (Canali et al. 2018).

Furthermore, the lab showed that in *Cntnap2* HET and KO mouse brains compared with WT, the reduced amount of Caspr2 has different effects at different developmental stages on the morphology of the CC. In adult mice (P90), lower Caspr2 levels lead to reduced CC midline thickness in coronal sections of KO mice (Fig. 26), and reduced CC area in sagittal sections of KO mice as well, while HET mice show no differences from WT (Cifuentes-Diaz et al. 2023). A similar effect was observed in CC area of mice at P30, though at P7 and P2 there were no differences between any genotypes. However, at E17.5 CC thickness was found to be significantly increased in HET embryos and tends to be increased in KO embryos (Fig. 26). These differences are particularly interesting given the fMRI results in human ASD patients, which show increased CC thickness in young children/toddlers compared to healthy individuals, with reduced CC thickness in ASD adults compared to healthy adults (R. Chen, Jiao, and Herskovits 2011; Wolff et al. 2015).

Caspr2 was similarly shown to control the morphology of the AC through development. When measuring the area of the AC in sagittal sections, the lab found that KO mice have a significantly reduced AC area compared to WT and HET at P90, which was also observed at P30. No differences were present at P7, but an increased AC area compared to both WT and HET was found at E17.5 (Fig. 27) (Cifuentes-Diaz et al. 2023).

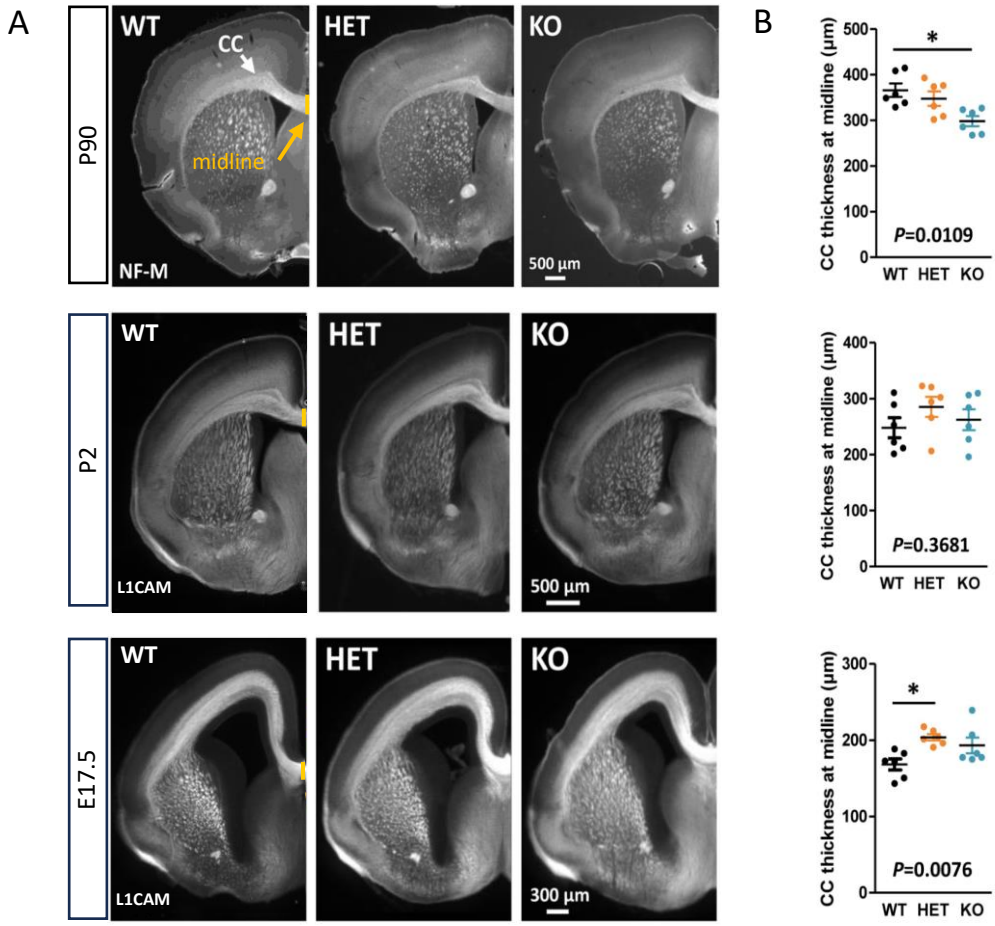

Figure 26: CC morphological differences in *Cntanp2* HET and KO mice. A) Representative images of coronal sections of brains at P90, P2, and E17.5. B) Quantification of CC thickness at midline of coronal sections at P90, with KO being significantly thinner than WT. No differences were observed at P2. At E17.5, HET brains show increased CC thickness compared to WT. Unpaired t-test to compare HET or KO mice to WT mice, and one-way ANOVA test to compare the three genotypes: ∗P< 0.05, ∗∗P< 0.01, ∗∗∗P< 0.001 (Cifuentes-Diaz et al. 2023).

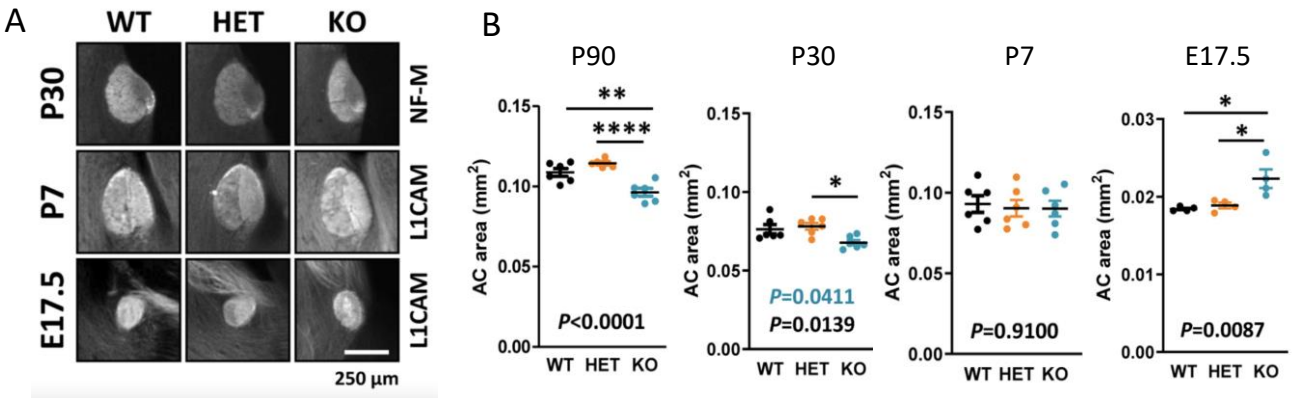

Figure 27: AC morphological differences in *Cntnap2* HET and KO mice. A) Representative images of sagittal sections of WT, HET, and KO mice at E17.5, P7, and P30. B) Quantification of AC area through development. Unpaired t-test (P90, P7, E17.5) or Mann–Whitney test (P30) to compare HET or KO mice to WT mice, and one-way ANOVA test (P90, P7, E17.5) or Kruskal–Wallis test (P30) to compare the three genotypes; ∗P < 0.05, ∗∗P < 0.01, ∗∗∗∗P < 0.0001 (Cifuentes-Diaz et al. 2023).

7. Myelination and the Node of Ranvier

7. A. General Introduction to Myelination and the Node of Ranvier

From our previous work and the work of other groups, Caspr2 has been found to play a role in myelination and node of Ranvier formation. Myelination is the process by which the axons of neurons are ensheathed with a substance known as myelin, a lipid-rich material which serves three main purposes: it insulates the axons thus increasing conduction speed; it gives trophic support to axons; and it conserves energy. A myelinated axon consists of a long axon with many large areas covered by myelin, each separated by a small uncovered area, called the node of Ranvier (NOR), where voltage-gated sodium channels (Na_v) responsible of action potential (AP) propagation are localized (Fig. 28). The space between nodes is called the internode.

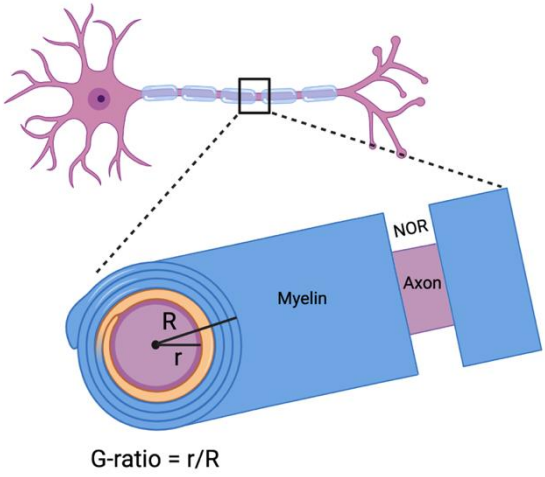

Figure 28: Myelinated axon showing the myelin sheaths with nodes of Ranvier spaced between them. The scheme illustrates a zoomed-in version of the myelinated axon indicating the inner myelin tongue in yellow, and the subsequent myelin wrappings in blue, with the axon in purple. The G-ratio measurement is also indicated.

Myelin is composed mainly of proteins and lipids in a ratio of roughly 1:186 (proteins : lipids) (O'Brien and Sampson 1965), the major proteins being Myelin Basic Protein (MBP), Myelin-Associated Glycoprotein (MAG), Myelin oligodendrocyte glycoprotein (MOG), Proteolipid Protein (PLP), and 2'3'-cyclic-nucleotide 3'-phosphodiesterase (CNP) in the CNS (Fig. 29). Myelin isolates the axon between two NOR and helps to increase the speed of conduction by allowing signals to be transmitted via saltatory conduction, hopping from one NOR to the next rather than travelling down the entire length of the axon. This type of conduction is advantageous because it allows signals to reach the correct speed for information transfer based on the size of each axon. The G-ratio is a unit which is commonly used to assess myelin thickness, as it is the ratio of the inner myelin diameter to the outer myelin diameter (Fig. 28). Modifications of the myelin sheath, such as altered thickness or differences in NOR size, can influence the speed of action potential conduction.

Likewise, the diameter and length of the axon can influence its myelination pattern, as well as its location in the nervous system.

The mechanisms of myelination in the CNS and in PNS are different (Fig. 30). Myelinating glial cells are OLs in the CNS, while they are Schwann cells in the PNS. Schwann cell myelination differs from OL myelination in that there is not one cell which extends multiple processes to wrap several different axons, but a single cell which is responsible for one segment of the myelin sheath of one single axon.

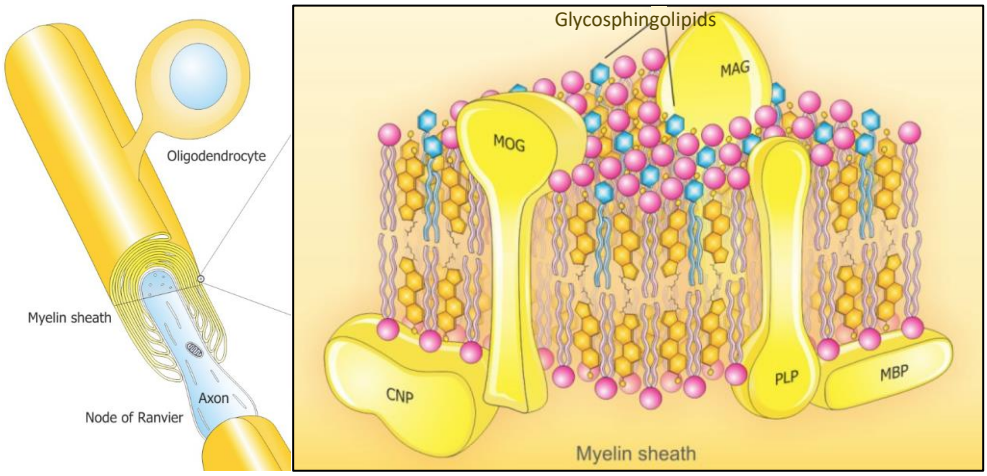

Figure 29: A composite diagram summarizing features of CNS myelin, including architecture and 3D-molecular composition and conformation-based assembly of the myelin sheath. CNP - 2'3'-cyclic-nucleotide 3'-phospodiesterase; MAG - myelin-associated glycoprotein; MBP - myelin basic protein; MOG - myelin oligodendrocyte glycoprotein; PLP - proteolipid protein. Adapted from (Podbielska et al. 2013).

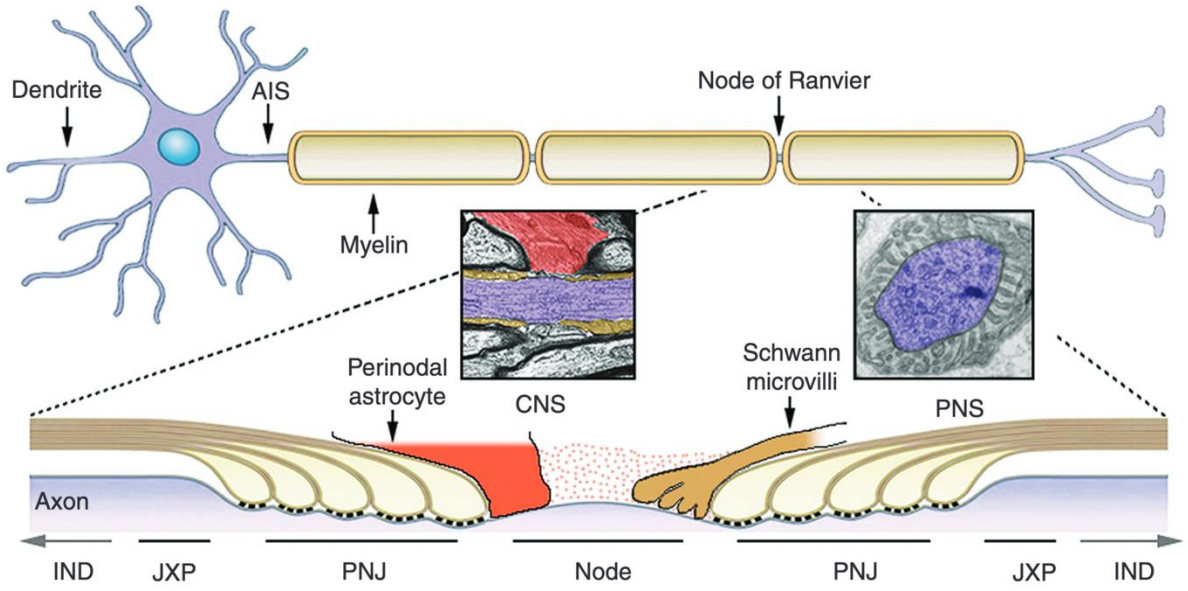

Figure 30: Myelinated fibers in the CNS (left side) and PNS (right side) (Matthew N. Rasband and Peles 2015).

7. B. Structure of the Node of Ranvier

The NOR is a highly specialized domain which is divided into three main subdomains, each of which is molecularly, structurally, and functionally unique. These are the node, the paranode (PN), and the juxtaparanode (JXP) (Fig 30, 31). While these three domains are very similar in the CNS and the PNS, there are some slight differences to the overall node structure (Fig. 31). In the PNS, the entire myelin compartment is covered by a basal lamina and the outermost layer of the Schwann cell extends microvilli which cover the nodes; there is also a perinodal space (space between the axon and the basal lamina) that contains a filamentous matrix. In the CNS, there is no basal lamina, and the nodes are covered by perinodal astrocytes, which aid in providing nutritional and energetic support to the node and the axon (Sebastian Poliak and Peles 2003).The three subdomains of the NOR, the node, the PN and the JXP, are characterized by specific molecular complexes which mediate axo-glial contacts.

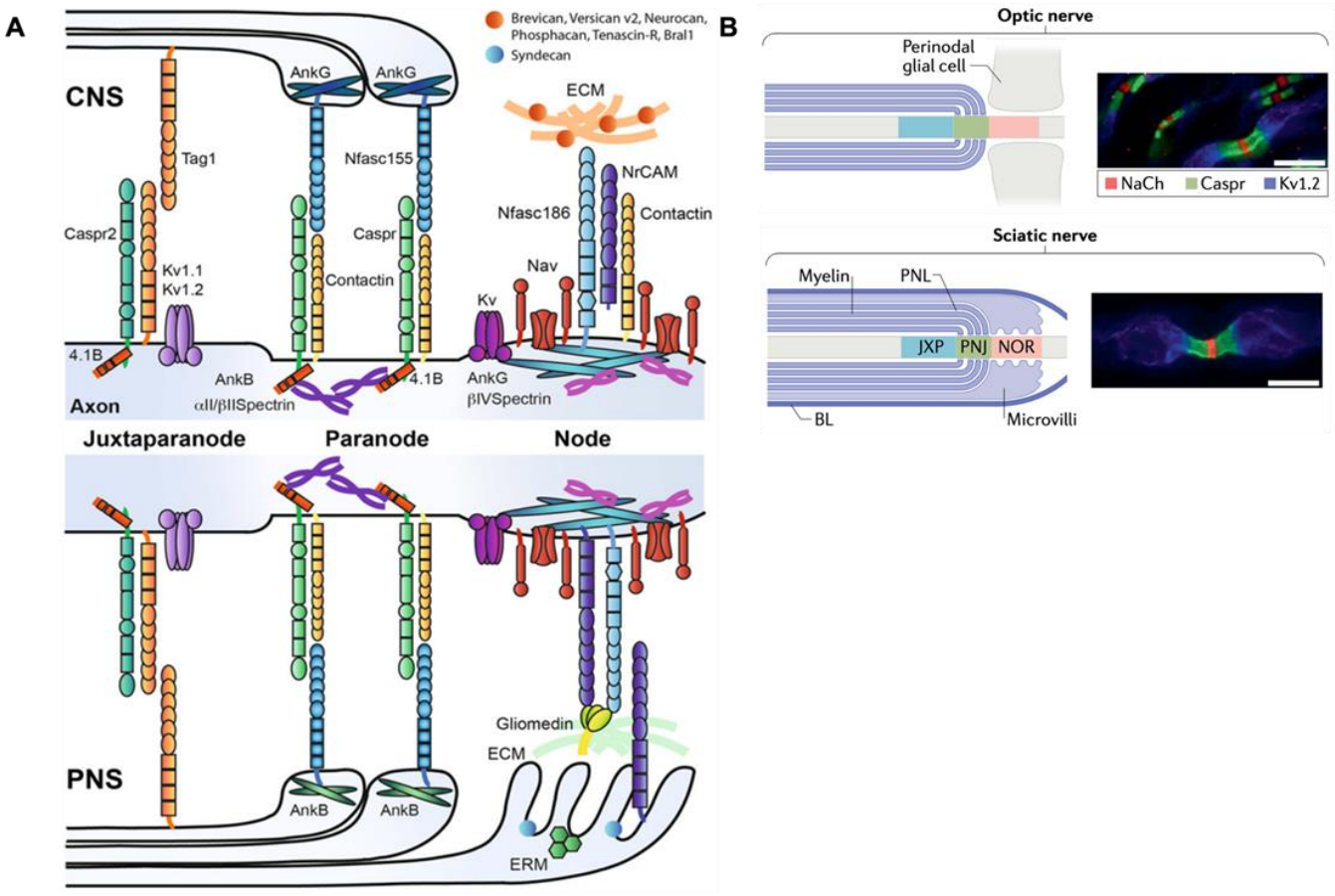

Figure 31: The node of Ranvier (NOR) and its subdomains in the CNS and PNS. A) The NOR is comprised of distinct regions including the node, the paranode, the juxtaparanode, and the internode. Resident proteins of each subdomain are indicated along with their cytoskeletal connecting elements. Slight differences exist between the CNS (top) and PNS (bottom), namely in the nodal domain. B) NOR diagrams indicated with immunostaining for NaCh (node), Caspr (paranode), and Kv1.2 (JXP). Top, Optic nerve (CNS). Bottom, Sciatic nerve (PNS). Scale bars 10 µm. Adapted from (Freeman et al. 2016; Matthew N. Rasband and Peles 2021).

7. B. i. The Node

The node is the center of the NOR complex. This area is characterized by a high density of sodium channels (Na^+, Na_V), which are essential for AP conduction and mediate ion flux across the membrane. When the axonal membrane depolarizes, the resulting influx of Na^+ ions initiates the AP once again and in this manner, it propagates along the axons. It is specifically the β-subunit of Na^+ channels which modulate channel gating and assist in the proper trafficking of Na^+ channels to the cell surface at the node, and to act partially as cell adhesion molecules (CAMs) (Isom 2002). In addition to these channels, the node also contains cytoskeletal proteins and cell-adhesion molecules, which are illustrated in Fig. 30. The CNS nodes contain several ECM proteins which interact with the cell adhesion molecules, including Brevican, Versican, Neurocan, and Phosphacan. The PNS nodes also contain ECM proteins, as well as cell adhesion molecules located on the membrane of the Schwann cell microvilli extending into the node. These include Gliomedin, Syndecan, and ERM proteins (ezrin, radixin and moesin) (Freeman et al. 2016; Ramesh 2004).

Various nodal parameters have been shown to affect AP transmission and node function when altered. For example, in a study by Arancibia-Cárcamo and colleagues in 2017, they showed that node length can vary over a 4.4-fold range in rat optic nerve, and an 8.7-fold range in cerebral cortical axons; not only this, but they found that node length varies much more between axons than along the same axon. They used these results to create a model that allowed them to predict the effects of changes in node length on conduction speed and electrophysiological properties. When the node length was increased but number of ion channels was held constant, the predicted conduction speed decreased as node length increased; however, when the ion channel density at the node was held constant, increased node length led to increased conduction speed until a peak/threshold node length, after which point the conduction speed decreased (Fig. 32) (Arancibia-Cárcamo et al. 2017). This work shows how drastic the effects of node and internode length changes can be on conduction speed along axons and suggests that node length may be adjusted physiologically to fine tune axon conduction speed depending on an organism's needs.

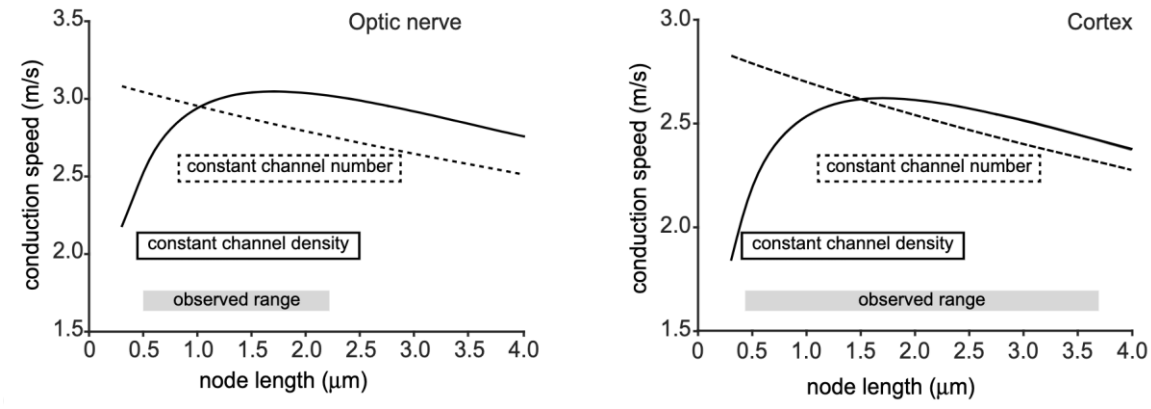

Figure 32: Predicted effect on conduction speed of different node lengths. Calculated conduction speed as a function of node length for axons in the optic nerve (left) and the cortical grey matter (right). Simulations were carried out assuming either that the density of ion channels at the node is constant as the node length is changed (solid lines), or that the number of ion channels is kept constant (dashed lines) at the value assumed for the mean node length. Adapted from (Arancibia-Cárcamo et al. 2017).

7. B. ii. The Paranode

The PN flank the node on either side and are the largest vertebrate intercellular junction (Matthew N. Rasband and Peles 2021). They are areas of the node in which the edges of the myelin sheath attach to the axonal membrane through septate-like junctions; these paranodal loops are cytoplasm-filled loops or tongues of myelin which wrap around the axon. Each paranodal loop represents one turn or layer of the wrapped myelin sheath. The PN have been thought of as "fences" separating the node from the juxtaparanodal and internodal regions of the axon (Sebastian Poliak and Peles 2003; Boyle et al. 2001; Bhat et al. 2001; Dupree, Girault, and Popko 1999). They restrict the lateral movement of juxtaparanodal proteins from moving out from under the myelin sheath, and additionally separating the juxtaparanodal K^+ channels physically from the Na^+ channels at the node.

The PN are demarcated by CAM complexes including Caspr, Contactin, and NF155. Caspr and Contactin exist along the axonal membrane, while NF155 interacts with Contactin in trans from its niche in the paranodal loops of the glial cell (OL or Schwann cell). Caspr and Contactin are essential for the formation of axo-glial junctions in the PN, and disruption in the expression of these proteins can lead to impaired adhesion of the paranodal loops and widening of the nodes (Boyle et al. 2001) and impaired nerve conduction velocity (Bhat et al. 2001). Caspr binds the scaffolding protein 4.1B on its intracellular domain, which allows it to link with Ankyrin B (AnkB) and subsequently the actin/spectrin cytoskeleton (Denisenko-Nehrbass et al. 2003; Menegoz et al. 1997). It is thought that Caspr acts as a sort of transmembrane scaffold that stabilizes the Caspr/Contactin complex and its interacting partners (NF155) to the axonal cytoskeleton (Sebastian Poliak and Peles 2003). The localization of Caspr, Contactin, and 4.1B are interdependent, and disruption of any one of these proteins affects PN organization.

7. B. iii. The Juxtaparanode

The JXP is the nodal subdomain which flanks the paranodes on either side of the NOR. As with the node and paranode, the JXP is characterized by its protein complexes, which include Kv1 channels, Contactin2 (TAG-1), and Caspr2, which mirrors the interaction of Contactin and Caspr in the paranode. TAG-1 and Caspr2 form a tight complex and are both required for proper clustering of the Kv1 channels in the JXP (Traka et al. 2003; Sebastian Poliak et al. 2003; Horresh et al. 2008). The clustering of TAG-1 and Caspr2 are interdependent, and both are required for Kv1 channel clustering at the JXP. Savvaki and colleagues showed that in axons of the CC in *Tag1* KO mice, only

5-6% of JXPs showed normal Kv1 clustering, emphasizing the importance of this protein in correct JXP formation (Savvaki et al. 2008). The Kv1 channels are important for maintaining the fidelity of conduction by ensuring the resting potential of the internode during and after the action potential, which is mediated by the Na^+ channels of the node (Arancibia-Carcamo and Attwell 2014). It's also been proposed that Kv1 channels could serve a protective purpose in axons with damaged or decreased myelination, or that their interaction with Caspr2 and TAG-1 could be used maintain stability if the axoglial junctions are compromised (Sebastian Poliak and Peles 2003).

Disintegrin and metalloproteinase domain-containing protein 22, or ADAM22, is another protein which has been identified in the JXP via its co-immunoprecipitation with both Kv1 channels and membrane-associated guanylate kinases (MAGUKS) PSD93 and PSD95, which link ADAM22 to the cytoskeletal components (Ogawa et al. 2010). It's thought that Caspr2 and Kv1 interact via their carboxyl-terminal region, likely through proteins which bind their PDZ-binding domains (Sebastian Poliak and Peles 2003). Caspr2 and TAG-1 also interact with the scaffolding protein 4.1B, which serves to associate these cell adhesion complexes with the cytoskeleton. In *4.1b* KO mice, Caspr is disorganized in the PN and clustering of Caspr2 and TAG-1 in the JXP was absent, with the juxtaparanodal proteins being diffusely spread along the axon (Cifuentes-Diaz et al. 2011). This demonstrates that 4.1B is required for the localization of the JXP complexes.

7. C. Assembly of the Node of Ranvier

The process by which the NOR assembles and sequesters its protein components to their subdomains is clearly highly synchronized, though it happens slightly differently in the CNS versus the PNS (Fig. 33). PNS node assembly begins by the clustering of Na^+ channels at the future node site, which is then followed by the establishment of the paranodal junction and then by the K^+ channel clustering at the JXP and subsequent protein partner recruitment. CNS node assembly begins with paranode formation, which is then followed by Na^+ channel clustering (M. N. Rasband et al. 1999; Matthew N. Rasband and Peles 2015). While this stepwise clustering of Na^+ channels and paranodal junctions varies between CNS and PNS, the overall mechanism remains the same. At the onset of node formation, Na^+ channels will accumulate immediately next to axo-glial connection sites where either OL or Schwann cell processes are extending to meet the axon. As these myelinating processes grow and elongate into sheaths, they push these Na^+ channel clusters along the axonal membrane until two adjacent clusters will fuse to form the NOR (Matthew N. Rasband and Peles 2015).

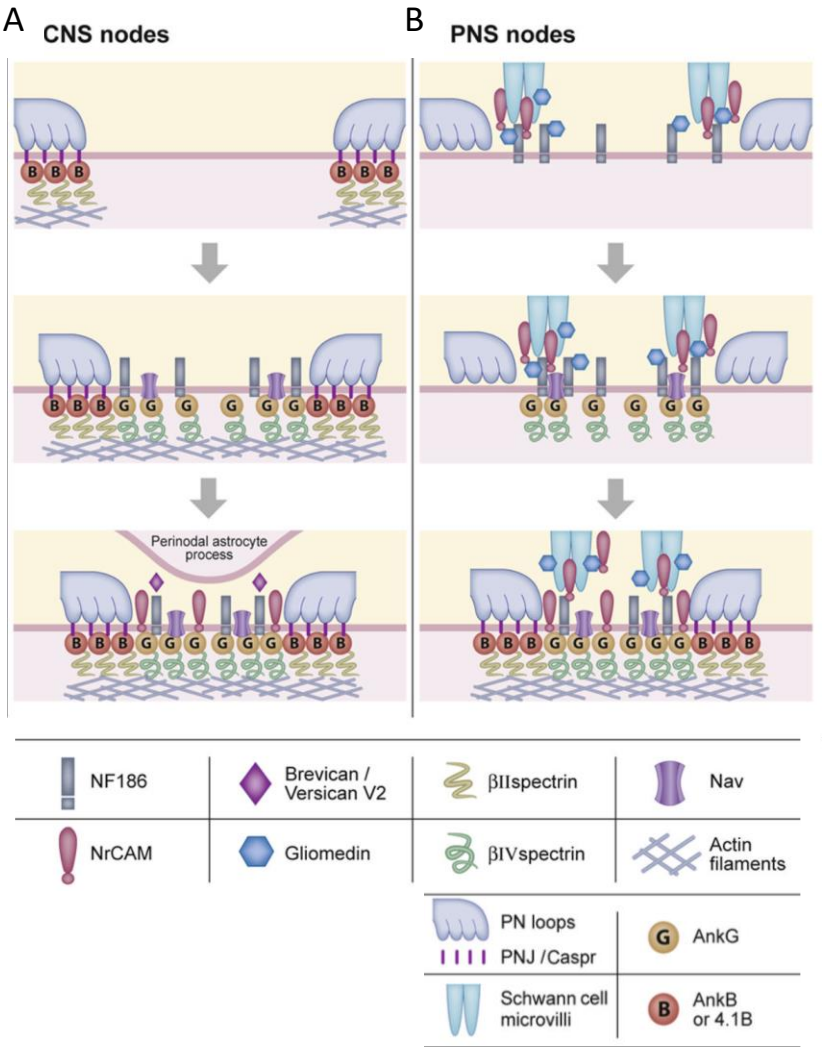

Figure 33: Current models for the formation of nodes and AIS. A-B) CNS and PNS nodes. The assembly of both the AIS and CNS nodes starts by the formation of a diffusion barrier marked by ankB and 4.1B. For nodes, this occurs at the base of the formed paranodal junction. In the adjacent AIS or nodal axolemma, accumulation of ankG results in the clustering of Nav and of NF186. ECM is the last to appear, and together with NF186, is probably required for the stabilization of AIS and nodal complexes. An asctrocyte process may contact CNS nodes late in development, although the exact timing is still to be determined. C) PNS nodes. The assembly of PNS nodes is induced by glial gliomedin and NrCAM that cluster NF186 on the axolemma, resulting in the accumulation of ankG and Nav. Linkage of the forming complex to the submembranous actin cytoskeleton likely occurs earlier in CNS nodes formation and later in AIS and PNS nodes (Eshed-Eisenbach and Peles 2013).

7. D. Caspr2 and Node of Ranvier Formation

In 2001, Poliak and colleagues used mice with defective myelin synthesis and perturbed paranodes to study the NOR. They showed that the localization of Caspr2 and Kv1 channels were perturbed in the mutant mice, settling closer to the nodes and not the JXP. Thus, when the paranodes were perturbed, the localization of JXP proteins was perturbed as well, leading to the conclusion that paranodal proteins may restrict the movement of JXP protein complexes like

Caspr2/Kv1 and act as a sort of barrier for this nodal domain (S. Poliak et al. 2001). Furthermore, they showed that the Caspr2/Kv1 complex forms during development at the PN/JXP border and later migrates to the JXP region; when the paranodal domain is not well defined, the Caspr2/Kv1 complex remains at the PN and does not migrate to its proper location. They conclude that paranodal protein Caspr and JXP protein Caspr2 appear sequentially during development and help to differentiate the nodal domains, as Caspr2 is present in the paranode and JXP in sciatic nerve of mice at P8, but only in the JXP of adult mice (S. Poliak et al. 2001). This was confirmed by Traka and colleagues who observed that at P8 in rat, Caspr2, TAG-1, and Kv1 colocalization was observed in a few fibers, but not all, also indicating that these complexes are formed prior to their relocation to the JXP (Traka et al. 2003). Another study used CGT mutant mice to investigate the localization of Caspr2's known interacting partner at the JXP, TAG-1, and found that in the mutant mice, TAG-1 was also no longer restricted to the JXP but found diffusely expressed in the paranodes as well (Traka et al. 2002). These results show that not only Caspr2 but also its JXP complexes help to orchestrate the proper formation of the NOR subdomains.

Hivert and colleagues used myelinating co-cultures of DRGs and Schwann cells to observe NOR formation *in vitro*. They found that Kv1/Caspr2 complexes were localized at the paranodes at DIV21-28, while they were mainly enriched at the distal paranodes and JXP at DIV35-42; this indicates that both Caspr2/Kv1 and Caspr/4.1B complexes are first assembled at the paranode before the former migrates to the JXP. Not only this, but at DIV21, Kv1 channels and Caspr2 were found to be enriched in the nodal gap between two heminodes; the heminodes are a precursor to the NOR found in early development (Fig. 34) (Hivert et al. 2016). Similar results were also observed in the developing sciatic nerve of young mice at P5 as well, where Caspr2 is located in the nodal gap but then migrates to the JXP by P14, where it remains into adulthood. These results are imperative in demonstrating Caspr2's role in NOR formation during early development and better understanding how the protein contributes to this process.

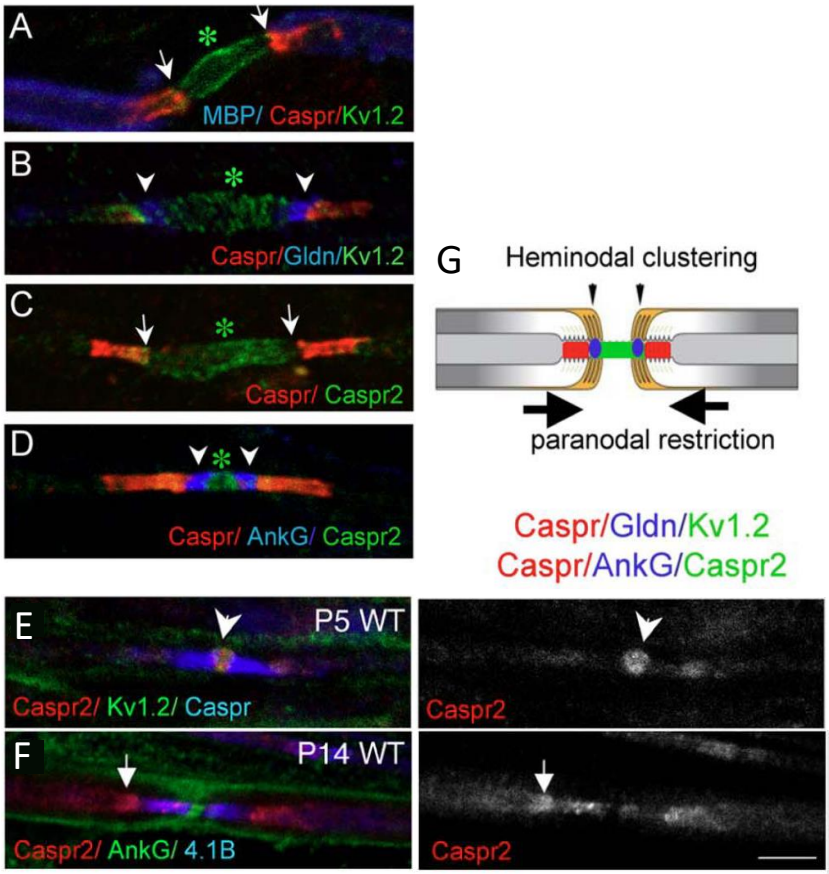

Figure 34: Transient trapping of Kv1.2 and Caspr2 between heminodes in myelinating DRG cultures. Rat DRG cultures at DIV21 after myelin induction. (A–D): Kv1.2 (A, B, green) and Caspr2 (C, D, green) were concentrated between the heminodes of two myelinated segments. The paranodes were stained for Caspr (red) and heminodes for Gliomedin (Gldn) or AnkyrinG (AnkG) (blue). Kv1.2 and Caspr2 were concentrated between the two heminodes and also enriched at paranodes. (E-F) Distribution of Kv1.2 and Caspr2 in the developing sciatic nerves of WT mice. Teased sciatic nerves of P5 and P14 sciatic nerves shown. In P5 WT mice, Kv1.2 (green) and Caspr2 (red) colocalized at the juxtaparanodes (arrows in E and F) and paranodes labeled for Caspr (blue). Strikingly, Caspr2 and Kv1.2 were enriched at some nodal gaps (arrow in E). In P14 wild-type mice, 4.1B (blue) was strongly enriched at paranodes whereas Caspr2 (red) located to juxtaparanodes indicated with arrows. G) Schema showing heminodal clustering and localizations of proteins during this process. Adapted from (Hivert et al. 2016).

Recently, Cifuentes-Diaz and colleagues showed that not only is Caspr2 present in the node during early development, but reduced protein levels of Caspr2 can affect the size of the node structure. In *Cntnap2* HET and KO mice, they showed that node length was significantly reduced in a dose-dependent manner; however, the node diameter was unaffected (Fig. 35) (Cifuentes-Diaz et al. 2023). These results are interesting and show that although the NOR organization can remain unaltered when Caspr2 is mutated or levels are reduced, the size of the different domains are affected.

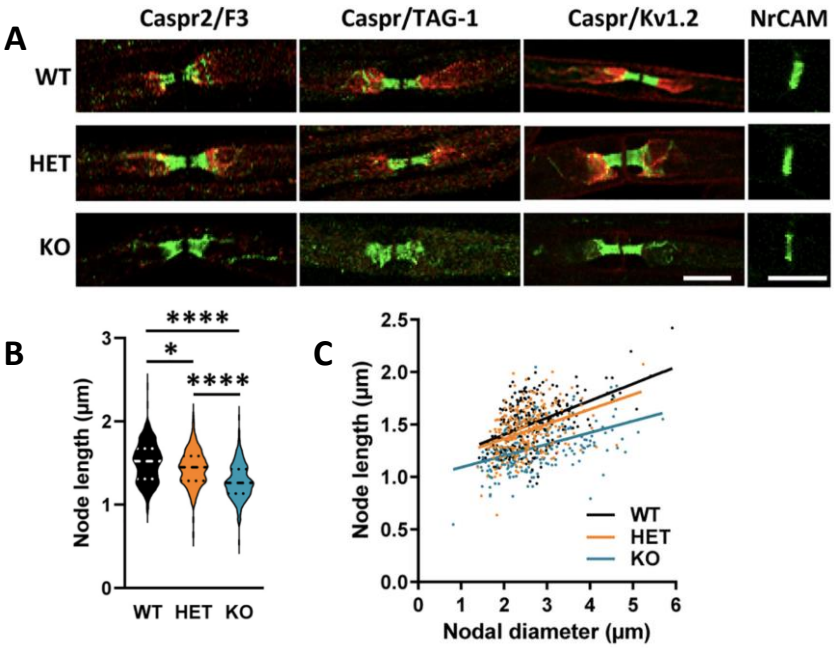

Figure 35: Node size altered in *Cntnap2* HET and KO mice. A) Representative confocal images of immunostainings of sciatic nerves fibers from WT, HET, and KO adult mice, for nodal (NrCAM), paranodal (Caspr, F3), and juxtaparanodal (Caspr2, TAG-1, Kv1.2) proteins. B) Length of the nodes measured on NrCAM immunostainings. C) Scatter plot graph displaying length of individual node as a function of the respective nodal diameters, and the linear regression of the node length measurements for each genotype. n= 243 nodes/genotype, 3 mice/genotype, 81 nodes/mouse. Adapted from (Cifuentes-Diaz et al. 2023).

7. E. CNS Myelination and the Role of Caspr2

7. E. i. Oligodendrocyte Development

In the CNS, the myelinating cells are OLs. The OLs originate from OPCs during development during a phase called oligodendrogenesis. This process occurs in spatially and temporally distinct waves directed by gradients of signaling molecules which emanate from different areas to facilitate tissue patterning (Newville, Jantzie, and Cunningham 2017). The first wave of OPC production starts at E12.5, and is generated by Nkx2.1-expressing progenitors; as these OPCs begin to migrate and populate the telencephalon, the second wave of OPC (Gsh2+ progenitors) production begins at E15.5; finally, the third wave occurs at birth (P0) from Emx1-expressing progenitors (Fig. 36) (Kessaris et al. 2006; Newville, Jantzie, and Cunningham 2017). By P10, the Nkx2.1+ OPCs from the first wave have completely disappeared, while the OPCs from the second and third waves remain in an approximate ratio of 1:4 (Gsh2:Emx1).

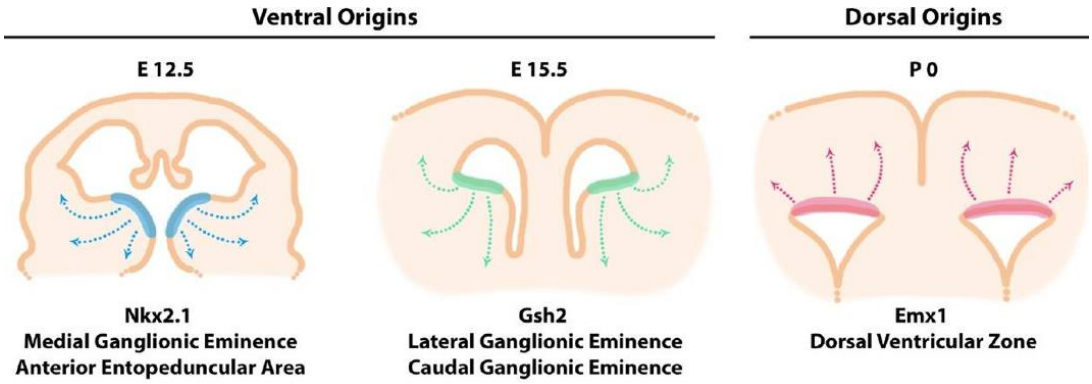

Figure 36: Oligodendrocytes arise from three distinct waves of production during development. These can be distinguished by their spatial location and their migration pattern, as well as the transcription factors they express (Newville, Jantzie, and Cunningham 2017).

OLs undergo a lineage that includes four separate maturational stages which are defined by proliferative capacity, temporal expression of cell surface markers, and morphological complexity. These stages are 1) OPCs, 2) pre-OLS, 3) immature pre-myelinating OLs, and 4) mature myelinating OLs (Butts, Houde, and Mehmet 2008). The first stage (OPCs) express platelet-derived growth factor receptor alpha (PDGFRα), which is regulated by Olig1 and Olig2, which are influenced by SHH morphogen (Butts, Houde, and Mehmet 2008). Olig2 is unique in that it is expressed throughout all OL maturation stages. The second stage of OL maturation begins when OLs have migrated to their target area, where they lose their migratory ability and express O4 and O1, as well as developing more complex morphology. These cells can then differentiate into immature pre-myelinating OLs, the third stage of OL maturation. OLs in this stage will still express O4 and O1 and will begin to express myelin protein like MAG. The fourth and final stage of mature OLs will express myelin regulatory factor (MYRF), which in turn initiates the expression of the major myelin proteins (Kitada and Rowitch 2006; Newville, Jantzie, and Cunningham 2017). The four main stages of OL maturation are outlined in Fig. 37; however, it is important to note that in recent years, some scientists have suggested that there may be more separate mature states of OLs defined by their transcriptional profile (Marques et al. 2016).

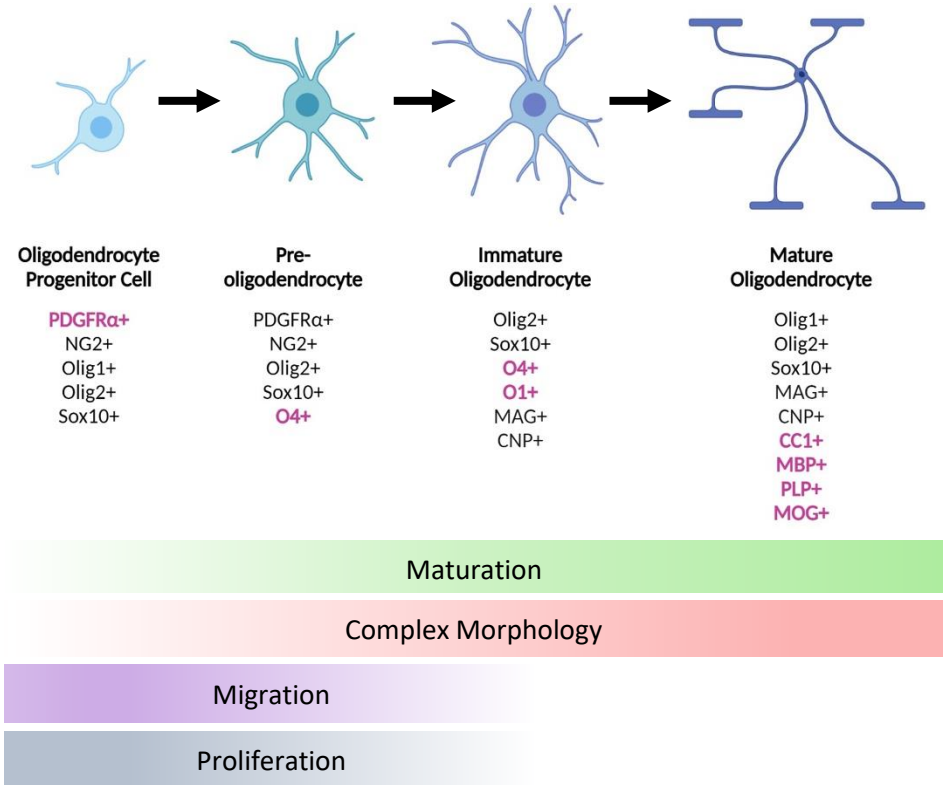

Figure 37: Stages of oligodendrocyte maturation over time. Transcription factors (TFs) expressed are indicated underneath images, which depict the increasingly complex morphology of the cells as they mature. TFs in pink are considered defining markers of the indicated stage. Adapted from (Barateiro and Fernandes 2014; Newville, Jantzie, and Cunningham 2017).

7. E. ii. CNS Myelination Process

The physical process of how myelin actually ensheathes the axons of the CNS was first suggested to occur in a "jelly roll" manner, with the myelinating cells migrating around the axon or sending an inner tongue around the axon multiple times to generate wrapped layers (Geren and Schmitt 1954). This model involved an inner myelin sheath extending in both a concentric and lateral movement down the length of the axon, generating a spirally wrapped axon with a concurrently compacting myelin sheath (Bercury and Macklin 2015). With live imaging advancements in more recent years, several studies were able to confirm this model of axon wrapping, being coined the "liquid croissant" model by Sobottka and colleagues, proposing that the myelin "pours" out of the oligodendrocytes in a triangular-shaped process which attaches to the axon and allows the myelin layer to spread laterally as it wraps around the axon and more myelin is continuously "poured" in (Sobottka et al. 2011). Other modern techniques, such as high pressure freezing and subsequent electron microscopy coupled with 3D reconstructions, were utilized by other researchers. These studies also confirmed what Geren and Schmitt observed previously, in which axon wrapping consists of an inner myelin tongue expanding and extending down the axon and compacting bit by bit with each new layer that forms (Snaidero et al. 2014). Transport of nutrients through these expanding myelin layers is achieved through cytoplasmic channels which

can connect layers of the sheath; this will disappear as the myelin matures and compacts. This process is illustrated in Fig. 38.

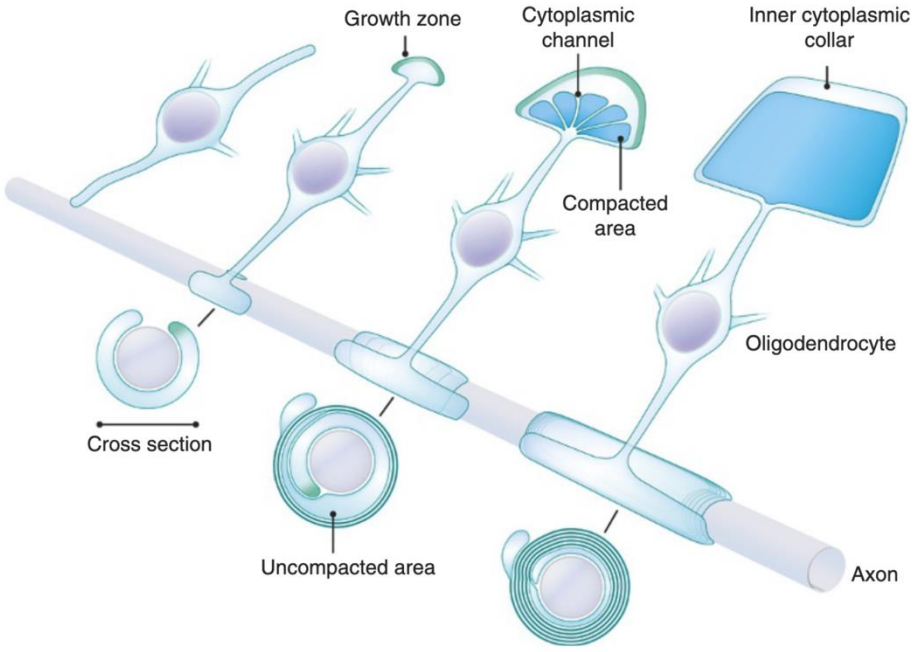

Figure 38: Model of a developing myelin sheath in wrapped (center along axon), unwrapped (top/right), and cross-section (bottom/left) views. Early development at left and mature state at far right. The unwrapped representation shows the development of the sheath and the localization of the cytoplasmic channels, which connect the cell body and the growth zone at the inner tongue. The growth zone is colored in dark teal, and the compacted myelin is in darker blue. The wrapped representation shows the position of the layers when wrapped around the axon. The cross- sections show the state of compaction during myelin growth. The area just adjacent to the axon is the uncompacted inner tongue of the axon; as the myelin develops, this will compact to become mature myelin (Chang, Redmond, and Chan 2016).

Not all axons of the CNS will be myelinated by OLs. Certain axons will begin to be myelinated, while others will not, in a selection process that is not so straightforward. While the cross-sectional size (caliber) of an axon plays a large role in whether it is myelinated (usually $\geq 1\mu m^2$), there are some axons as small as 200-300nm which can be myelinated in some regions of the CNS, but not others (Simons and Lyons 2013). Almeida and colleagues showed that large caliber axons are among the first to be myelinated, and demonstrated the plasticity of OLs by showing that the number and size of axons each OL myelinates can vary with physiological conditions (Almeida et al. 2011). Furthermore, Lee and colleagues proved the essential role of axon caliber in myelination by conducting *in vitro* experiments to observe the myelination capacities of OLs when presented with polystyrene nanofibers of different sizes. They observed that in these neuron-free conditions, the minimum threshold diameter for fibers to be myelinated was 0.4μm; axons smaller than this would not be ensheathed by OLs, and axons with diameters above 0.5μm were largely preferred (Lee et al. 2012) (Fig. 39). While previous studies had shown that artificial fibers could be

myelinated, Lee and colleagues demonstrated that fiber size/caliber also plays an important role. Not only does axon caliber determine whether an axon will be myelinated, but it can also determine how thick the myelin sheath will be. This was demonstrated by Waxman and colleagues in 1984, who showed that myelin thickness is dependent on axon diameter, with thicker axons having thicker myelin sheaths (Waxman and Sims 1984). Interestingly, another study established that when knocking out either mid-sized or heavy neurofilaments (NF-M and NF-H), CNS axons were smaller in diameter but maintained normal myelin thicknesses, thus suggesting that myelination relies mainly on axon size and can adapt, while cell surface molecules are not essential for this adaptation (Elder, Friedrich, and Lazzarini 2001).

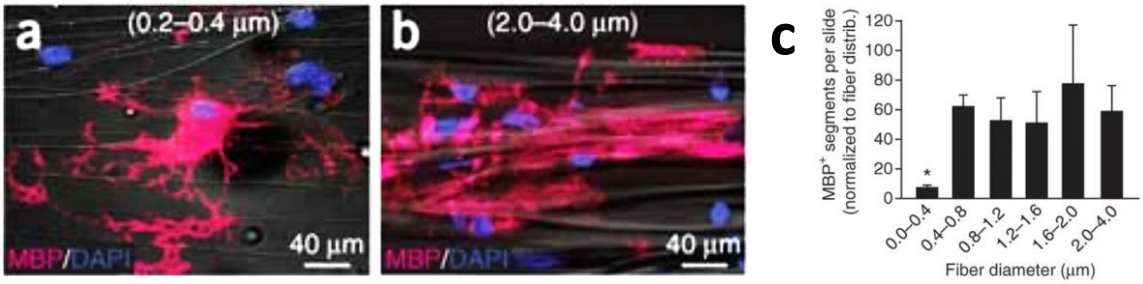

Figure 39: OL wrapping of polystyrene nanofibers. A-B) Immunostaining of cultures for MBP and DAPI in the presence of small (0.2-0.4µm) and large (2.0-4.0µm) diameter fibers. C) Quantification of MBP+ segments normalized to the distribution of fiber diameters (n=3, mean±SEM, $p<0.001$, Tukey post-hoc comparison after one-way ANOVA). Adapted from (Lee et al. 2012).

While axon caliber plays an essential role in CNS myelination, signaling molecules and axo-glial crosstalk have also been suggested to aid in the process. Some groups have shown an effect of the protein Neuregulin 1 (Nrg1). Overexpression of Nrg1 type I and III have been shown to increase myelin thickness in the CNS, as well as increased myelination of smaller axons (<400µm) that normally wouldn't be myelinated (Brinkmann et al. 2008; Taveggia et al. 2005). Not much is currently known about other specific signals in the CNS which could initiate the myelination process, though there is evidence that molecules such as integrins, Laminin, Wnt, and GPR17 (Câmara et al. 2009; Y. Chen et al. 2009; Fancy et al. 2009; Kang and Yao 2022) could play a role in myelination onset.

Additionally, electrical activity has been shown to influence the myelination process, with the overall idea being that the more active an axon is (the more it is used), the more myelinated or more quickly myelinated it will be. In 1993, Barres and colleagues demonstrated that proliferation of OPCs in the developing rat optic nerve depends on electrical activity in neighboring axons; in the absence of electrical activity, increasing concentration of PDGF will have the same effect. These results insinuate that electrical activity controls the release of growth factors responsible for OPC proliferation (Barres and Raff 1993). OPCs are now known to have AMPA, NMDA, GABA, and kainite

receptors, which can create viable neuron-glia synapses in the brain (Bergles et al. 2000; Káradóttir et al. 2005). Moreover, stimulation of GABAergic receptors has been shown to induce OPC proliferation and differentiation early in the myelination process (Zonouzi et al. 2015). Li and colleagues stimulated corticospinal axons of adult rats and found that this promoted the proliferation and differentiation of OPCs, further demonstrating the importance of neural activity in OPC development even in the adult CNS (Li et al. 2010). Furthermore, vesicular release of glutamate from axons and subsequent Fyn signaling has been shown to regulate the local synthesis of MBP in oligodendrocytes, which suggests that electrical activity of axons can also play a role in their myelination by OLs (Wake, Lee, and Fields 2011).

Myelination in the CNS is timely regulated. In the mouse, the process begins around postnatal day 10, or P10. Slightly before this, at P7, a few MBP+ cells are labeled in the white matter tracts of the brain, such as the optic chiasm and olfactory tracts. The number of MBP+ cells increases sharply until P11 (Foran and Peterson 1992). Myelination begins to ramp up around P10 and continues robustly until around P30, at which point the vast majority of the CNS is myelinated. During adulthood, though initial myelination is completed, adaptive myelination can continue to occur. The timeline of myelination in the mouse CNS is outlined in Fig. 40.

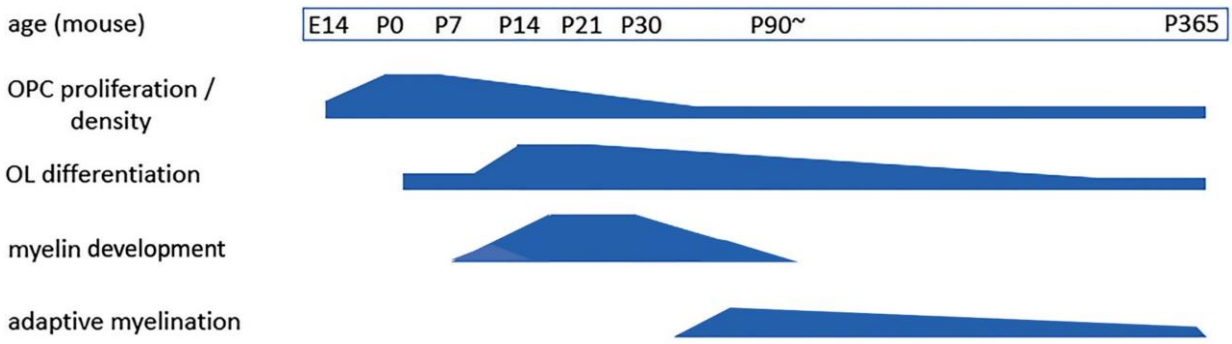

Figure 40: Diagram showing the timeline of OPC proliferation and density, OL differentiation, myelination, and adaptive myelination in the mouse. Age of the mouse is indicated across the top. Not drawn to scale. (Nishiyama et al. 2021).

7. E. iii. Role of Caspr2 in CNS Myelination

Evidence that Caspr2 could play a role in myelination came in 2019 when Scott et al. showed delayed myelination of the gray matter (neocortex) in *Cntnap2* KO mice. In these mice, they observed comparable fiber density in the corpus callosum (CC), but did find reduced density in the upper layers of the neocortex (R. Scott et al. 2019). Along with this reduced fiber density, they observed reduced MBP intensity and a significant reduction in the number of Sox10+ cells in the neocortex of *Cntnap2* KO mice at 3 weeks of age compared WT (Fig. 41); as Sox10 labels all OLs, from OPCs to mature OLs, this result indicates that there are fewer myelinating cells in the *Cntnap2* KO mice. These results were further proven when the researchers performed electrophysiological

recordings in the brains of KO mice, which revealed no changes in the speed of AP propagation in the CC, but did reveal significantly slower speeds of AP propagation in the neocortex (R. Scott et al. 2019). These functional results are consistent with the reduction of myelinated fibers in the neocortex of *Cntnap2* KO mice. In 8-week-old mice, no differences were seen between the *Cntnap2* mutants and WT mice, suggesting that myelin defects are transitory and recover with age, or are delayed in their progress.

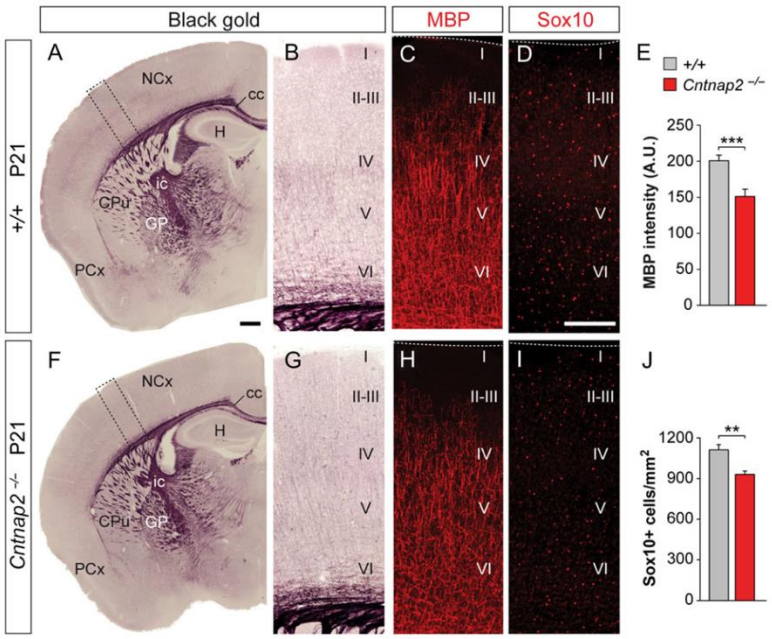

Figure 41: Delayed myelination of cortical gray matter in *Cntnap2* mutant mice. (A–D, F–I) Histological staining of myelin by Black gold (A, B, F, G) and immunohistochemistry for MBP (C, H) and Sox10 (D, I) in the neocortex of 3-week-old control (A–D) and Cntnap2 mutant (F–I) mice. (E) Quantification of MBP intensity in the somatosensory cortex; n = 4 control and 4 Cntnap2 mutant mice, t-test, ***P < 0.001. (J) Quantification of the density of Sox10+ cells in the somatosensory cortex; n = 4 control and 4 *Cntnap2* mutant mice, t-test, **P < 0.01. Adapted from (R. Scott et al. 2019).

Further evidence for Caspr2's role in myelination came earlier this year in work from our lab, which analyzed myelinated fiber development in the CC and AC of *Cntnap2* HET and *Cntnap2* KO mice at P30. The team investigated the axonal parameters and myelination at the ultrastructural level using electron microscopy to measure axon diameter as well as G-ratio reflecting the myelination status. Differential patterns of myelination were observed in the CC and the AC, and between *Cntnap2* HET and *Cntnap2* KO mice. In the CC, the lab found that KO mice have reduced axon diameter compared to WT and KO mice, while G-ratio is unaffected (Fig. 42) (Cifuentes-Diaz et al. 2023). By contrast, axon diameters we not affected in HET mice, but the G-ratio was decreased, indicating hypermyelination. Interestingly, the number of myelinated fibers was also increased in HET mice. Also, at P7, before the onset of myelination, axon diameter was increased in HET mice compared to WT, while diameter of KO axons was reduced compared to WT and HET (see Figure 6, paper in annex).

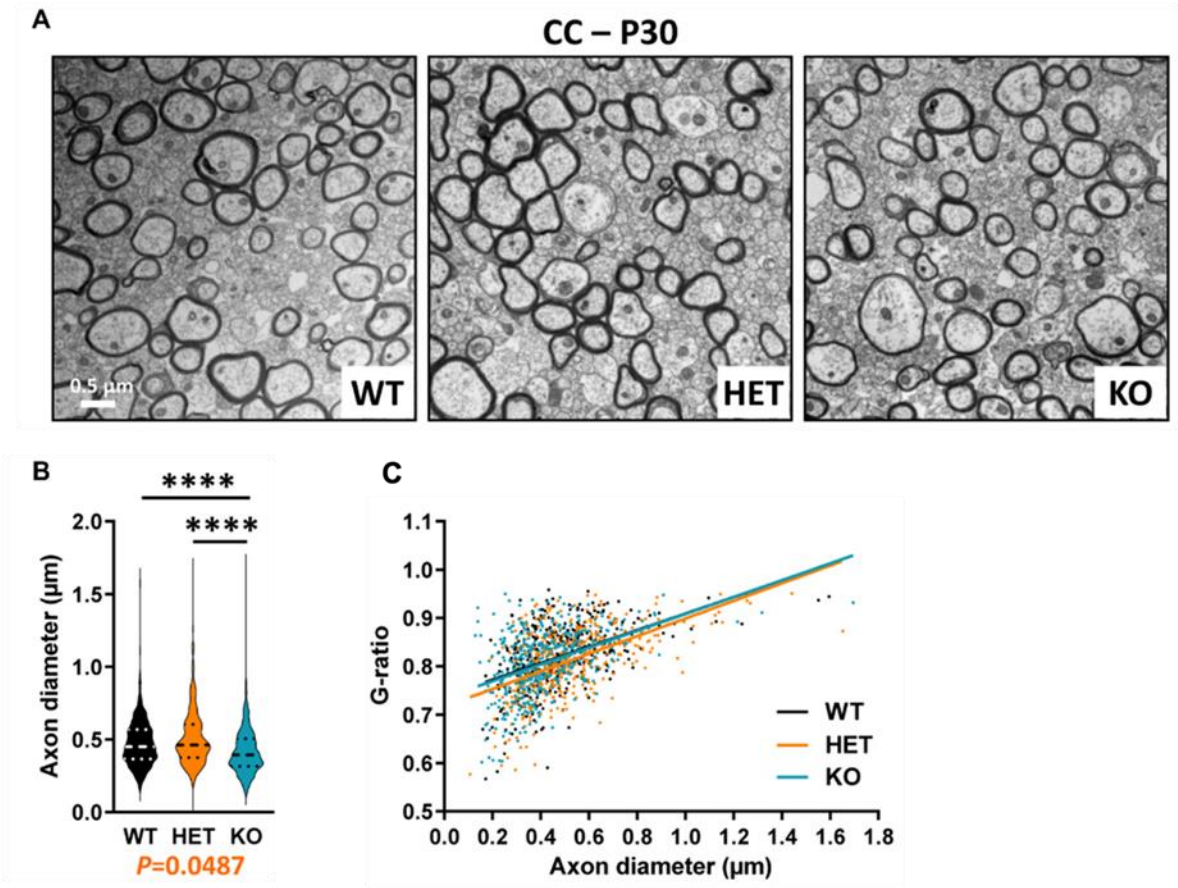

Figure 42: CC Ultrastructural abnormalities of corpus callosum (CC) myelinated fibers in P30 mice. A) Electron micrographs of transversal sections of the CC at brain midline, from wild-type (WT), HET, and KO P30 mice. B) Axonal diameters of CC myelinated fibers. C) Scatter plot graph displaying G-ratios of individual myelinated axons as a function of the respective axon diameters, and linear regression of the G-ratio measurements for each genotype (Cifuentes-Diaz et al. 2023).

For the AC, opposite effects were observed for the ACa and the ACp. *Cntnap2* HET and KO mice have increased axon diameter compared to WT in the ACa, while only the KO show increased axon diameter in the ACp. Additionally, HET mice were shown to have a decreased G-ratio and thus hypermyelination compared to WT in the ACa, while both HET and KO mice showed hypermyelination in the ACp (Fig.43). At P7, the ACa was more affected in Cntnap2 HET and KO mice, with KO mice showing a significantly reduced axon diameter in the ACa when compared to WT and HET mice (Fig. 43). There was no difference in axon diameter between genotypes observed at P7 in the ACp.

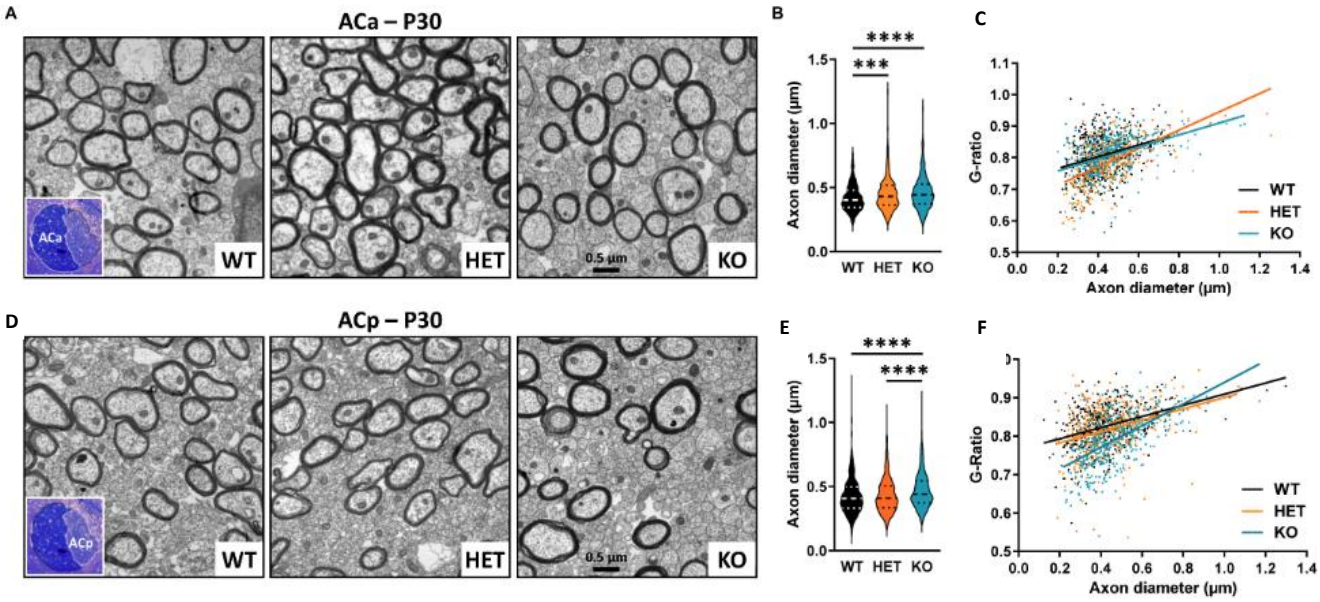

Figure 43: Ultrastructural abnormalities of anterior branch (ACa) and posterior branch (ACp) myelinated fibers in P30 mice. Electron micrographs of transversal sections of the ACa (A) and ACp (D) at brain midline, from wild-type (WT), HET, and KO P30 mice; insets, semi-thin transversal sections of the AC stained with toluidine blue, showing the ACa and the ACp. Axonal diameters of ACa (B) and ACp (E) myelinated fibers. Scatter plot graphs displaying G-ratios of individual myelinated axons as a function of the respective axon diameters, and the linear regression of the G-ratio measurements for each genotype, for the ACa (C) and the ACp (F).

In addition to these effects of Caspr2 in myelinated fiber development, overall myelin protein levels were altered in *Cntnap2* HET and KO mice in a region-specific manner. KO mice showed reduced levels of myelin proteins MBP and MAG in the neocortex, but not in the CC, compared to WT mice, while HET mice showed no differences (Fig. 44) (Cifuentes-Diaz et al. 2023). These results are particularly interesting as they show that Caspr2 can modulate myelination in specific regions, while seemingly having no effect in other areas. Furthermore, the same study showed that in *Cntanp2* HET mice, Caspr2 levels are downregulated just before the onset of myelination; while expected to be at 50% of WT Caspr2 levels in whole brain extracts, they are in fact at just 35% of WT Caspr2 level until P15, after myelination has already begun (Fig. 45). This time point corresponds with a switch in CC and AC morphologies observed around P7-P10, indicating that Caspr2 levels could be modulating myelination around the onset of this process. Interestingly, the group also found that *Cntnap2* mutant mice displayed increased firing of Layer III cortical neurons at P10-P12, further strengthening the idea that Caspr2 could be helping to mediate the cross-talk between the axon and OLs at this stage (Fig. 46) (see Figure 7 in annex).

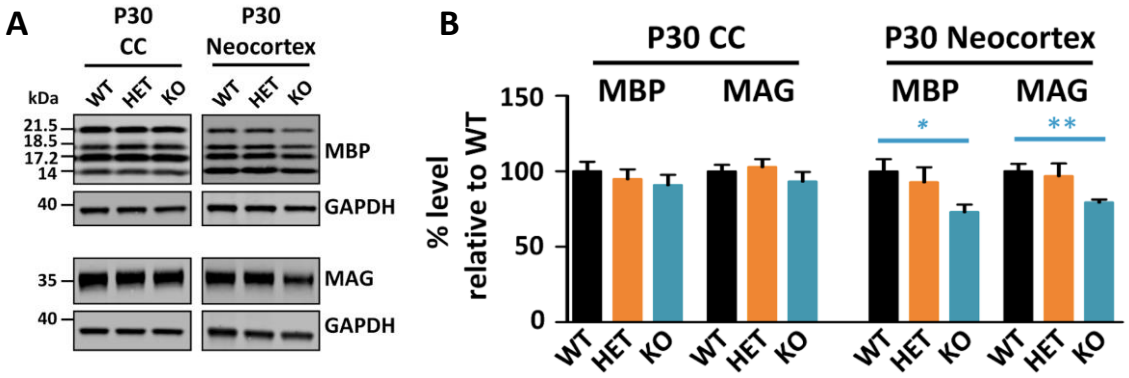

Figure 44: Myelin protein levels in brain extracts. A) Representative immunoblots showing levels of MBP and MAG normalized to GAPDH levels and relative to mean WT (in %) in extracts from the neocortex and the CC of mice at P30. B) Quantifications of western blots relativized to WT protein level (Cifuentes-Diaz et al. 2023).

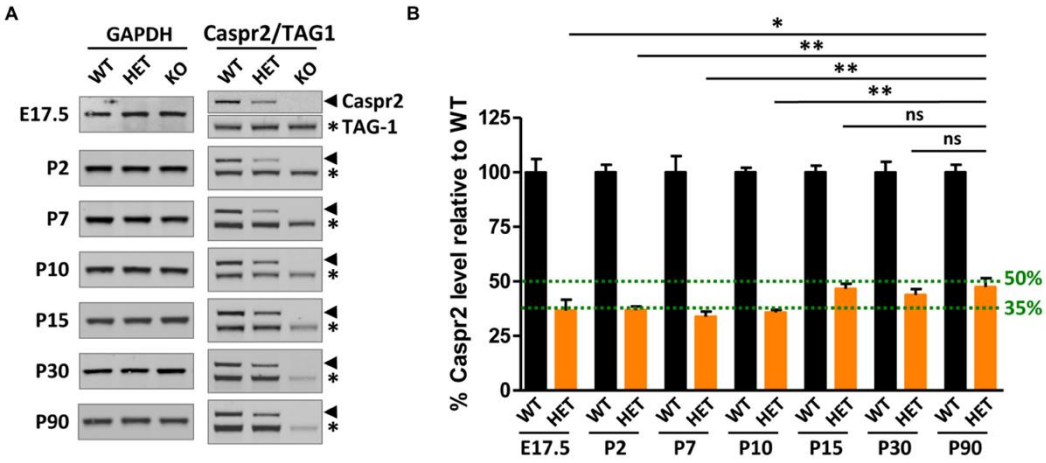

Figure 45: Caspr2 levels in mouse brains during development. A) Representative immunoblots showing Caspr2, TAG-1 and GAPDH levels in brain lysates of WT, HET, and KO mice at different developmental stages and at adulthood. B) Levels of Caspr2 normalized to GAPDH levels and relative to mean WT (in %) (Cifuentes-Diaz et al. 2023).

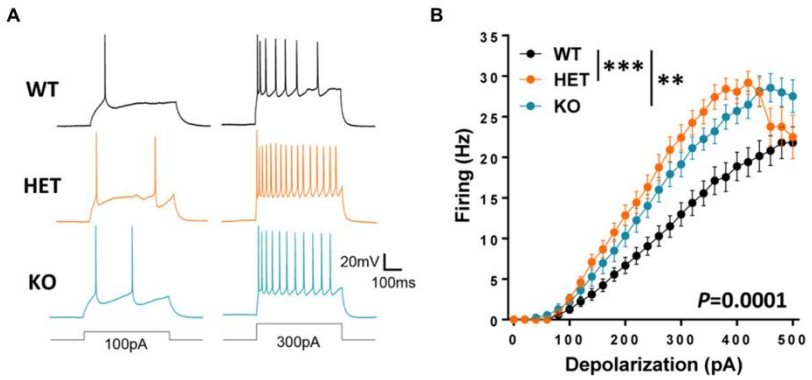

Figure 46: Intrinsic excitability in cortical pyramidal cells from P10–P12 pups. A) Sample spike trains evoked by a 100-pA (left) or a 300-pA somatic current injection (right) in a WT (top), HET (middle) and KO (bottom) neuron. B) Mean f-i curve for WT (n = 27 cells from three mice), HET (n = 24 cells from three mice), and KO (n = 27 cells from three mice) (Cifuentes-Diaz et al. 2023).

7. F. PNS Myelination and the Role of Caspr2

7. F. i. Schwann Cell Development

As mentioned previously, myelination in the PNS is a bit different from that in the CNS as it is conducted by Schwann cells (SCs). SCs derive from neural crest (NC) cells early in development, along with fibroblasts, melanocytes, and what will become the connective tissue of the PNS. SC development begins around E12-13 in mice; nerves at this stage consist of tightly packed axons with flattened glial cell processes (Jessen, Mirsky, and Lloyd 2015) (Fig. 47). These glial cell bodies derived from NC cells are situated among the peripheral axons within the nerve or at the nerve surface and are called the SC precursors. By E15-16, SC precursors will then give rise to immature SCs, along with endoneurial fibroblasts, and parasympathetic neurons. These immature SCs will envelop groups of axons forming columns of axons/SCs covered by a basal lamina and surrounded by extracellular. From this point, immature SCs can undergo two distinct differentiation programs depending on their final phenotype – myelinating or non-myelinating. Once myelinating SCs reach the axon, they reduce their mitotic activity and adopt a pro-myelinating phenotype, expressing P0 and MAG.

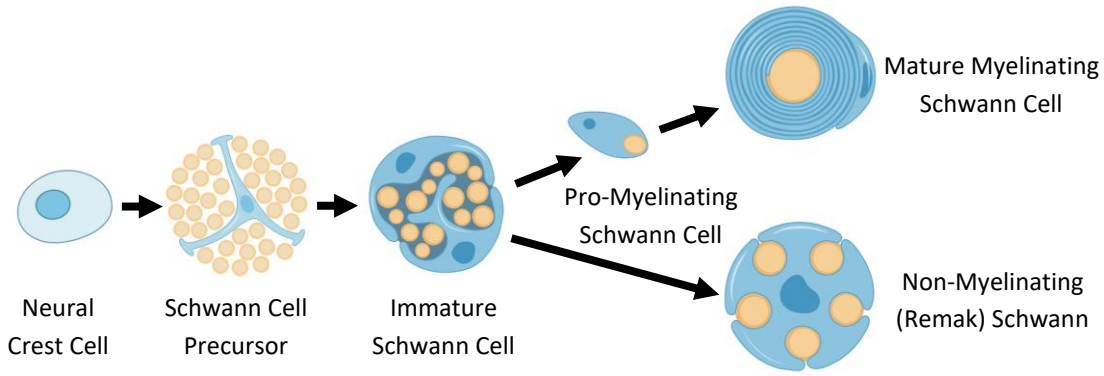

Figure 47: Schwann cell development. Neural crest cells will give rise to Schwann cell precursors, which will then develop into immature Schwann cells (SCs). After radial sorting, SCs will either mature into pro-myelinating and subsequently myelinating SCs, or into non-myelinating SCs, which will form the Remak bundles. Adapted from (Castelnovo et al. 2017; Jessen, Mirsky, and Lloyd 2015).

Myelination of fibers in the PNS depends on axon diameter, with larger axons being individually myelinated and smaller axons being surrounded by non-myelinated SCs in groups. These groups of small-diameter axons are called Remak bundles and consist of a Schwann cell pushing its cytoplasm in between the small fibers to isolate them from each other (Fig. 47). PNS myelination also depends upon electrical activity, with increased firing rates inducing more myelination than in non-stimulated fibers. This is illustrated by Liang and colleagues, who show that co-cultures of DRG and Schwann cells displayed increased myelination after 7 days of electrical stimulation than non-stimulated cells (Fig. 48) (Liang et al. 2019).

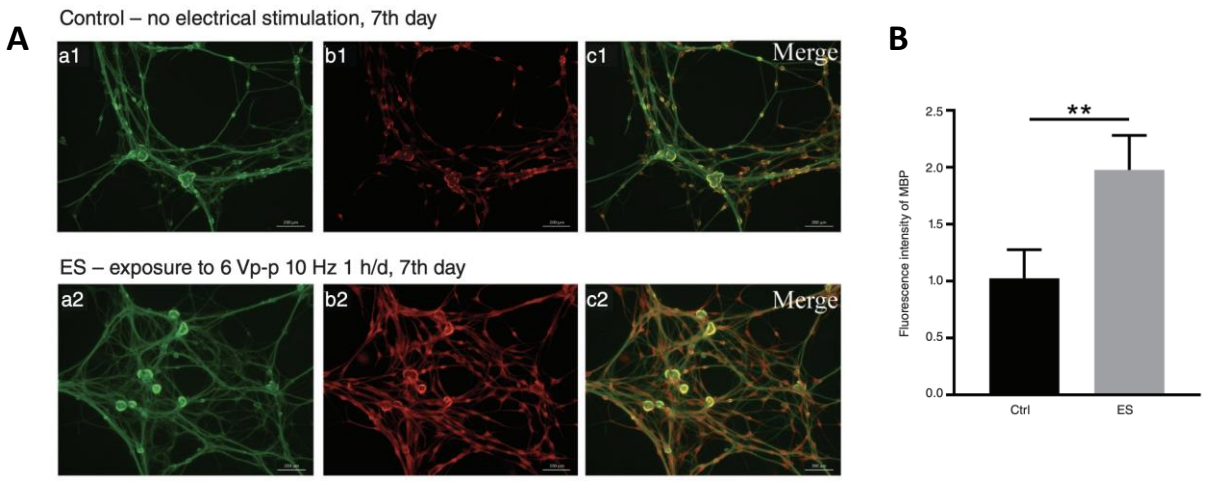

Figure 48: Immunofluorescent for MBP of co-cultured DRG/SC cells after 7-day electrical stimulation. (A) Ctrl group, no electrical stimulation. a1: The neurite network by NF200 staining (green); b1: myelinated segments (red) by MBP staining; c1: MBP protein is expressed on axons after co-culture 7 days; ES group, exposure to 6 Vp-p,10 Hz. a2: NF200 (green); b2: MBP (red); c2: MBP positive section are abundant throughout the co-cultures after electrical stimulation compared with Ctrl group. (B) The semi-quantitative results of fluorescence intensity of MBP in Ctrl and ES groups. Values represent mean ± SEM of 3/group, **p < 0.01, statistically significant compared with the Ctrl group. Ctrl: Control; DRG: Dorsal root ganglion; ES: Electrical stimulation; MBP: Myelin basic protein; SC: Schwann cell (Liang et al. 2019).

7. F. ii. PNS Myelination Process

The myelin sheath of the PNS is wrapped around axons in much the same manner as in the CNS. The SCs are both radially and longitudinally polarized, which allows them to organize into distinct membrane domains, also similar to OLs (Pereira, Lebrun-Julien, and Suter 2012). The myelin sheath is more loosely wrapped at first, and then it compacts with the upregulation of mature myelin proteins such as P0 (Kidd, Ohno, and Trapp 2013). The SC nucleus remains adjacent to the axon, while the inner tongue of the myelin wraps around the axon, with the initial wraps being narrower and gradually expanding as the myelin sheath grows. The organization of myelinated fibers in the PNS is illustrated in Fig. 49.

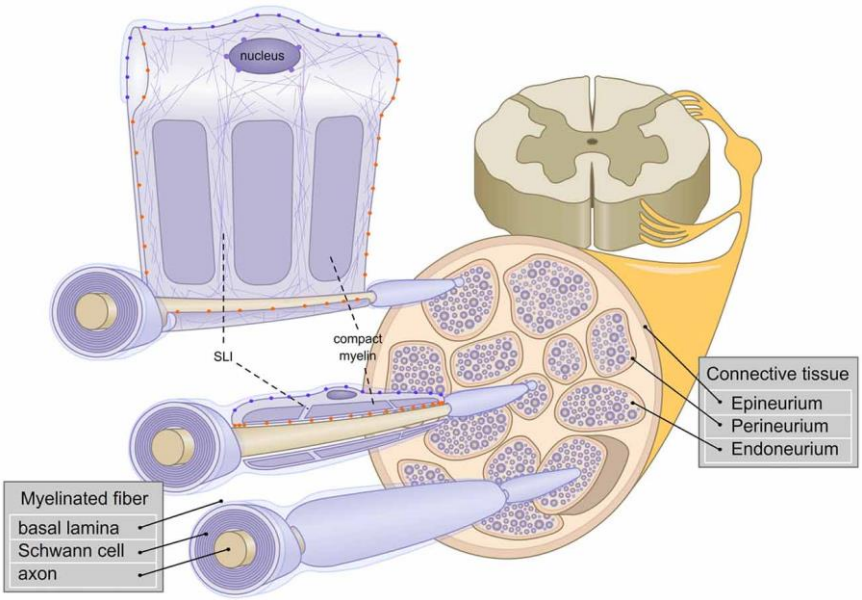

Figure 49: Schematic representation of the architecture of Schwann cells wrapping myelinated fibers in the PNS. The three layers of connective tissues are depicted, and three myelinated fibers are enlarged. The first fiber (bottom) represents a rolled Schwann cell (SC). The second fiber (middle) shows a longitudinal section of a Schwann cell. The third fiber (top) is a view of Schwann cell unrolled. Axonal (orange) and basal lamina (blue) cell adhesion molecules (CAMs) and Linker of Nucleoskeleton and Cytoskeleton complex (LINC; purple) are represented. Actin filaments are depicted with thin purple lines. SLI: Schmidt-Lanterman incisures (Belin, Zuloaga, and Poitelon 2017).

7. F. iii. Role of Caspr2 in PNS Myelination

Caspr2 has been shown to modulate also axonal parameters and myelination in the axons in the PNS. When studying sciatic nerve fibers at the ultrastructural level, it was observed that *Cntnap2* HET and KO mice show increased axon diameters compared to WT, and not only this, but HET mice have an increased G-ratio and therefore show hypomyelination compared to WT mice (Fig. 50) (Cifuentes-Diaz et al. 2023). This is important because it demonstrates that effects on myelination may be different in the CNS versus the PNS, and that *Cntnap2* HET mice can also show distinct phenotypes from both WT and KO in the PNS.

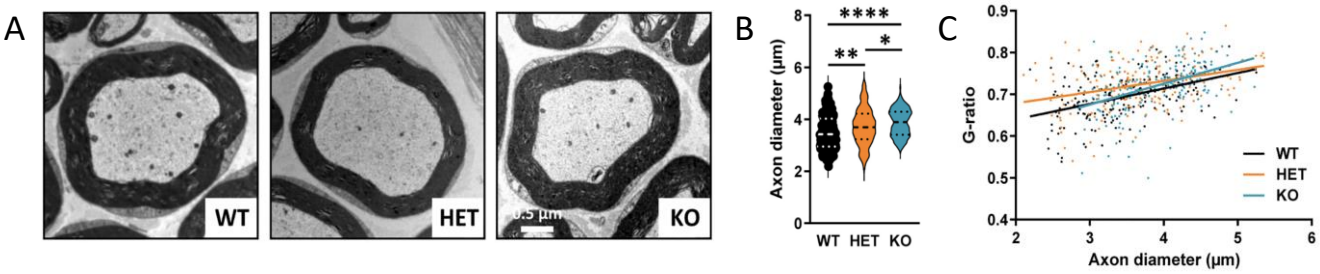

Figure 50: Myelinated fiber abnormalities in *Cntnap2* HET and KO mouse sciatic nerve (PNS). A) Representative images of sciatic nerve transversal sections. B) Axonal diameters of myelinated fibers. C) Scatter plot graph displaying G-ratios of individual myelinated axons as a function of the respective axon diameters, and the linear regression of the G-ratio measurements for each genotype (Cifuentes-Diaz et al. 2023).

8. Caspr2, Nociception, and Sensitivity

8. A. Sensory Fibers of the PNS

Myelinated fibers are responsible for conducting many different types of signals in the body, from thoughts and ideas to motor and sensory information from the PNS. Large-caliber axons from the periphery convey motor information, while small-caliber fibers can convey sensations such as touch, pressure, pain, temperature, and other mechanical sensations. The different types of fibers in the PNS nerves were defined by Erlanger and Gasser in the 1920s and are classified into three main categories: A fibers, B fibers, and C fibers. A and B fibers are larger in diameter and are individually myelinated to allow for rapid conduction of electrical signals. C fibers correspond to small caliber axons which are wrapped in groups by a single non-myelinated Schwann cell into the Remak bundles. The types of fibers are outlined in Fig. 51.

A fibers can be subdivided into different categories: Aα fibers, which are responsible for somatic motor information and proprioception; Aβ fibers, which are responsible for touch and pressure sensations; Aγ fibers, which conduct motor information to muscle spindles; and Aδ fibers, which conduct information about sharp pain, cold sensation, and touch. B fibers are preganglionic sympathetic nerve fibers which are less myelinated than A fibers and are classified as afferent fibers. Finally, C fibers have the slowest conduction speed. They include both postganglionic fibers in the autonomic nervous system and nerve fibers in the dorsal roots, and carry sensory information such as slow or chronic pain, heat sensation, mechanical sensation, and are also responsible for some reflexes. Injury or disruption of these C fibers can lead to neuropathic pain in human patients. While these classifications have remained the standard, there is increasing evidence that there are more specific subtypes of fibers which could be classified based on molecular markers and RNA sequencing experiments (Usoskin et al. 2015).

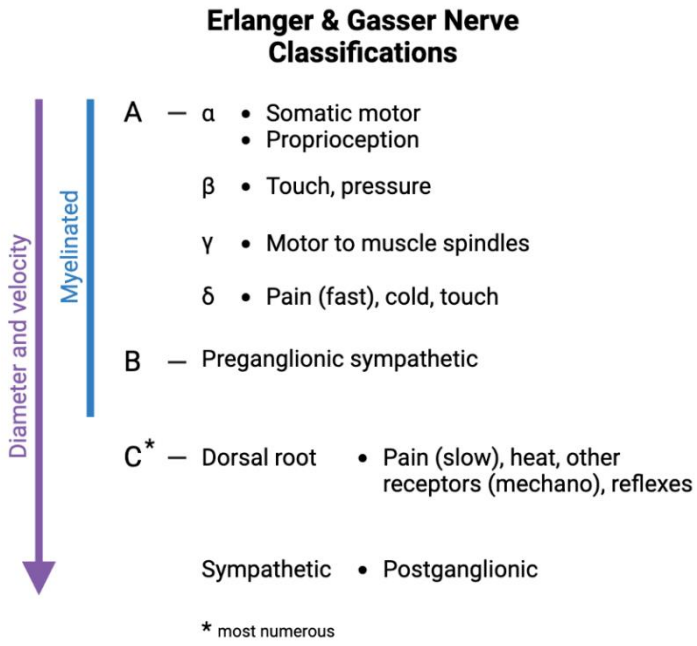

Figure 51: Sensory fiber classifications. Adapted from (Goel 2013).

8. B. Dorsal Root Ganglia and CNS Integration

The DRG is a cluster of neurons located in the dorsal root of a spinal nerve, containing up to 15,000 neurons at each limb-innervating segment (Ahimsadasan et al. 2022). The axons of these neurons are afferents, meaning that they extend into the PNS and relay sensory information into the CNS. These DRG neurons are pseudo-unipolar, meaning that a single long axon projects from the cell body and bifurcates at the T-junction; one segment extends into the periphery, and the other extends into the CNS. In this way, the two processes can function as a single axon, sometimes bypassing the cell body completely to relay information from the PNS into the CNS. These neuronal clusters are heterogeneous, consisting of A, B, and C fibers. Each fiber type will be directed through a different spinal cord segment or layer in the dorsal horn, which will then project the sensory information into the target brain region via second-order neurons (Fig. 52). The neurons of the DRG also play an active role in sensory transduction and modulation, with their T-junctions able to impede the full propagation of APs from the periphery, therefore acting as a sort of filter (Utzschneider, Kocsis, and Devor 1992). Furthermore, it's been shown that DRG neurons have unique membrane properties and are kept separate from each other by a layer of satellite glia cells, which support these neurons. Because the different neurons with different membrane properties are close together, they can experience sub-threshold excitation when other cell bodies near them are activated; this is known as cross-depolarization or cross-excitation, and can affect up to 90% of neighboring neurons when just one DRG neuron is stimulated (Z. Lu et al. 2016). The primary afferent neurons will conduct signals from the PNS and can generate synapses with both excitatory and inhibitory neurons in the dorsal horn of the spinal cord, though the patterns in which certain types of fibers synapse onto certain types of secondary neurons is still being determined (Harding, Fung, and Bonin 2020). Cell-autonomous classifications based on molecular markers are being

investigated as a more accurate way to identify dorsal horn neurons, similar to those trying to identify more accurate PNS fiber types. Descending modulation of the dorsal horn neurons can also come from regions within the brainstem; these regions can modify the excitability or neurons in the spinal cord (Hao et al. 2023; Huang et al. 2019; Porreca, Ossipov, and Gebhart 2002). This regulatory mechanism could be especially relevant in the context of chronic pain.

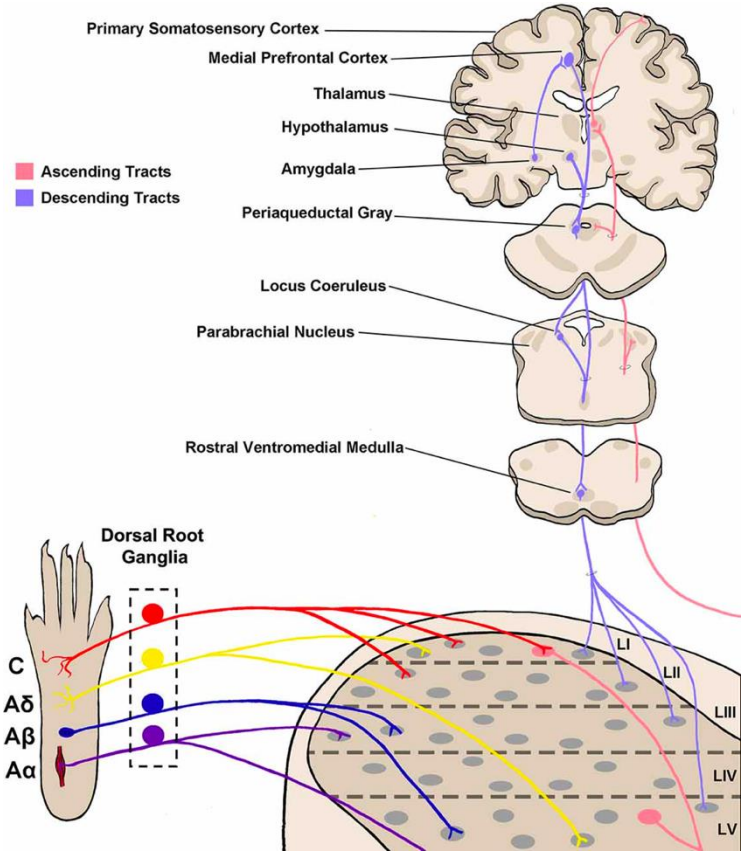

Figure 52: Somatosensory circuitry from the periphery to the brain. Somatosensory information is first transmitted into the spinal dorsal horn by primary afferent neuron fibers, which extend from peripheral tissue into the spinal cord and synapse onto neurons within the dorsal horn. There are four main types of primary afferent fiber, separated by transduction velocity, and each type (Aα, Aβ, Aδ, C) shows some selectivity in somatosensory modality transmitted and synapses into different laminae as shown here. Projection neurons within lamina I and V send axons up to the brain via ascending tracts including the spinothalamic tract and dorsal column–medial lemniscal tract. Some projections terminate within other brainstem regions including the parabrachial nucleus and periaqueductal gray. Descending tracts originate from several brain regions including the medial prefrontal cortex, hypothalamus, and amygdala, and project first to the periaqueductal gray. From here, descending projections then synapse within the rostral ventromedial medulla (RVM), and join with locus coeruleus (LC) descending projections. RVM/LC projection targets including the superficial dorsal horn and lamina V (Harding, Fung, and Bonin 2020).

8. C. Caspr2, Temperature / Pain Sensitivity and the mTOR Pathway

Temperature can be detected by both Aδ fibers (cold) and C fibers (hot); this section will focus mainly on the latter. C fibers can express either peptidergic nociceptors, which are responsible for thermal sensation and pain stemming from noxious heat or capsaicin, or nonpeptidergic nociceptors, which sense noxious mechanical pain or an itch response (Crawford and Caterina 2020; J. Zhang et al. 2013). The terminals of the peptidergic C fibers are located within the epidermis of hairy and glabourous skin, where they can sense any injury or disruption in the epidermal barrier. There is a well-defined line between mild warmth and noxious heat which reaches temperatures able to cause tissue damage, and it's this noxious type of heat which is transmitted by the C fibers. For most of these nociceptive fibers, the threshold sits around 43°C, with a smaller group being activated by higher heat – around 50°C (Z. Lu et al. 2016).

The mTOR pathway has been implicated in many different physiological systems, including heat sensitivity. It has been shown that mTOR can regulate local mRNA translation in the skin and afferent fibers. Jiménez-Diaz and colleagues injected rapamycin (mTOR inhibitor) into the hind paw of mice and found that this significantly increased the threshold temperatures for paw withdrawal in the hot plate test, suggesting that local translation regulated by mTOR could play a role in A fibers and potentially in C fibers as well (Jiménez-Díaz et al. 2008). A more recent study sought to investigate the effects of mTORC1 activation in sensory neurons on target innervation and sensory behavior by deleting Tsc2 in mice and found that mice lacking Tsc2 exhibited reduced sensitivity to heat, while sensitivity to cold and to mechanical stimuli remained unaffected (Carlin et al. 2018). These results are interesting considering heat and cold sensitivity are known to be communicated via different sensory fibers (C fibers and Aδ fibers, respectively), and perhaps indicates a role of Tsc2 in C fibers specifically.

Interestingly, a recent study aimed to unravel some of the sensory defects often observed in ASD patients, as altered sensitivity to various physical stimuli is a characteristic of the disease. Xing and colleagues used *Cntnap2* KO mice and found that they had increased mTOR activity in the brain, which, when suppressed, rescued social deficits (Xing et al. 2019); using this same model, they next strove to characterize mTOR signaling in the PNS of these mice. They observed that *Cntnap2* KO mice also show hyperactive mTOR signaling in the DRG, and that treatment with an mTOR inhibitor rapamycin reduced hypersensitivity to heat and noxious mechanical stimuli, as well as reduced DRG hyperexcitability (Fig. 53) (Z. Lu et al. 2016).

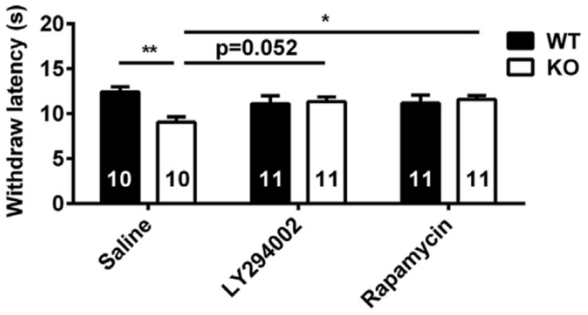

Figure 53: Treatment with the Akt inhibitor LY294002 and mTOR inhibitor rapamycin rescued the hypersensitivity of *Cntnap2* KO mice to heat as assayed with a hot plate set at 54.5 °C. The number of mice was indicated in the respective graphs. *p < 0.05, **p < 0.01, ***p < 0.001. Data are expressed as the mean ± sem (standard error of the mean). A repeated-measure ANOVA followed by Bonferroni post hoc tests or unpaired two-tail Student's t-test was used (Xing et al. 2020).

The potential implication of Caspr2 in regulating sensitivity also came from the identification of Caspr2 autoantibodies in patients with autoimmune encephalitis, limbic encephalitis (LE), neuromyotonia, Morvan syndrome, and neuropathic pain (Joubert et al. 2016, 2017; Muñiz-Castrillo et al. 2020). In 2015, several groups strove to discern where the Caspr2 autoantibodies bound to the Caspr2 protein by using neurons treated with patient sera. Olsen and colleagues found that patient antibodies bound to the extracellular domain of Caspr2, regardless of glycosylation pattern (Olsen et al. 2015). Another study in the same year by Pinatel et al. conducted a similar study by treating Caspr-2 trasnfected N2A cells, rat sciatic nerves, and rat hippocampal neurons in culture with serum from seven different patients with LE. They observed that the majority of patient samples bound to Caspr2 in these different conditions, and discerned that the different N-terminal modules of the protein can actually be selectively targeted by different patient autoantibodies (Pinatel et al. 2015).

In a study of patients with Caspr2 and leucine-rich glioma-inactivated (LGI1) autoantibodies, a study was conducted to investigate neuropathic pain. Of 147 patients studied, 52% of those with Caspr2 antibodies and only 19% of those with LGI1 antibodies experienced pain. When patient antibodies were tested in DRG cultures of WT and *Cntnap2* KO mice, no Caspr2 antibody binding was observed in the KO mice, indicating that patient antibodies are indeed specific for Caspr2 (Fig. 54). In the Caspr2 antibody patients, pain was more localized to the distal regions of the body, including hands, legs, and feet (Ramanathan et al. 2021). These symptoms of neuropathic pain reported in the limbs in the presence of Caspr2 autoantibodies is very interesting given recent findings from Gendre et al., who reported a patient with neuropathic pain and paresthesia in the lower limbs. Paresthesia refers to a burning or prickling sensation which is usually experienced in the hands, arms, legs, or feet. They confirmed that the patient showed serum anti-Caspr2 positivity, which was used to treat rat sciatic nerve samples. Reactivity along the C-fibers and also at the JXP of the rat sciatic nerve was observed when treated with patient serum, indicating not only that

Caspr2 is located along the sensory C-fibers of peripheral nerves but also that Caspr2 autoantibody binding can be linked with different types of pain sensation (Fig. 55) (Gendre et al. 2021).

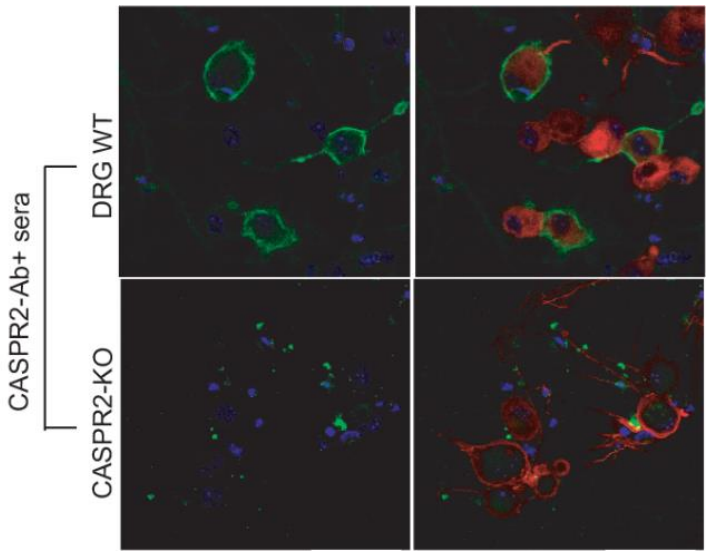

Figure 54: Serum IgG from 10 of 16 CASPR2 antibody patients bound to wild-type (WT) mouse DRG cultures at endpoint dilutions > 1:400 compared to 1 of 12 healthy controls. Binding of human IgG colocalized with nucleated (blue, DAPI) rodent WT DRG neurons (red, β3-tubulin), but not to DRG neurons derived from CASPR2 knockout mice (CASPR2-KO). Scale bar = 50µm. Adapted from (Ramanathan et al. 2021).

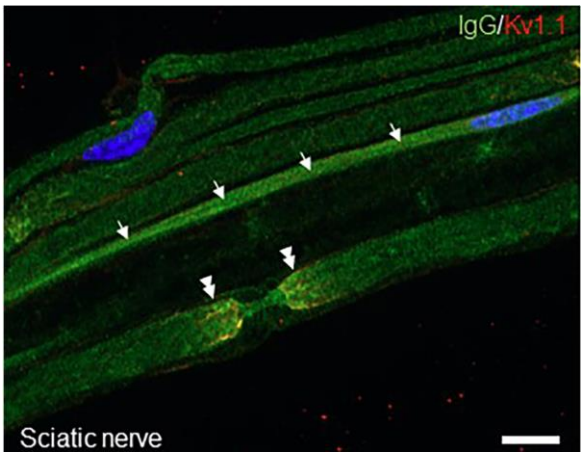

Figure 55: The patient's IgG are reactive against CASPR2 and stain C-fibers and the juxtaparanodes of myelinated fibers. Serum anti CASPR2 positivity was screened by indirect immunofluorescence against the constant fraction of heavy chain γ. These are teased mouse sciatic nerve fibers immunostained with the patient's IgGs (green) and a mouse antibody to Kv1.1 (Kv1.1; red) to labels juxtaparanodes (double arrowheads). Nuclei are stained in blue with 40,6-diamidino-2-phenylindole (DAPI). Scale bar: 10 µm. Immunofixation can be seen on C-fibers (arrows) and the juxtaparanodes of myelinated fibers (double arrowheads) (Gendre et al. 2021).

The PhD Project

In Section 2 of the introduction, I discussed *CNTNAP2* heterozygous missense variants found patients with ASD. Since their identification, two studies have been conducted using *in vitro* methods to investigate the pathogenicity of some of them. Falivelli and colleagues studied the variants identified by Bakkaloglu and colleagues (Falivelli et al. 2012). They first evaluated the glycosylation patterns of variants using Endoglycosidase-H and PNGase F treatment and discovered that Endo-H fully digests the Caspr2 mutant protein bearing the variant D1129H (Caspr2-D1129H), indicating that trafficking of this variant is severely impaired; most of it is not addressed to the cell surface and remains in the endoplasmic reticulum (ER). These results were confirmed by immunofluorescence in transfected HEK293 cells and in rat hippocampal neurons (Fig. 56A). They also showed that Caspr2-D1129H presents delayed clearance from the ER after cycloheximide treatment (Fig. 56B) and is preferentially degraded by the proteasome, activating the unfolded protein response (UPR) via the ATF6 signaling pathway.

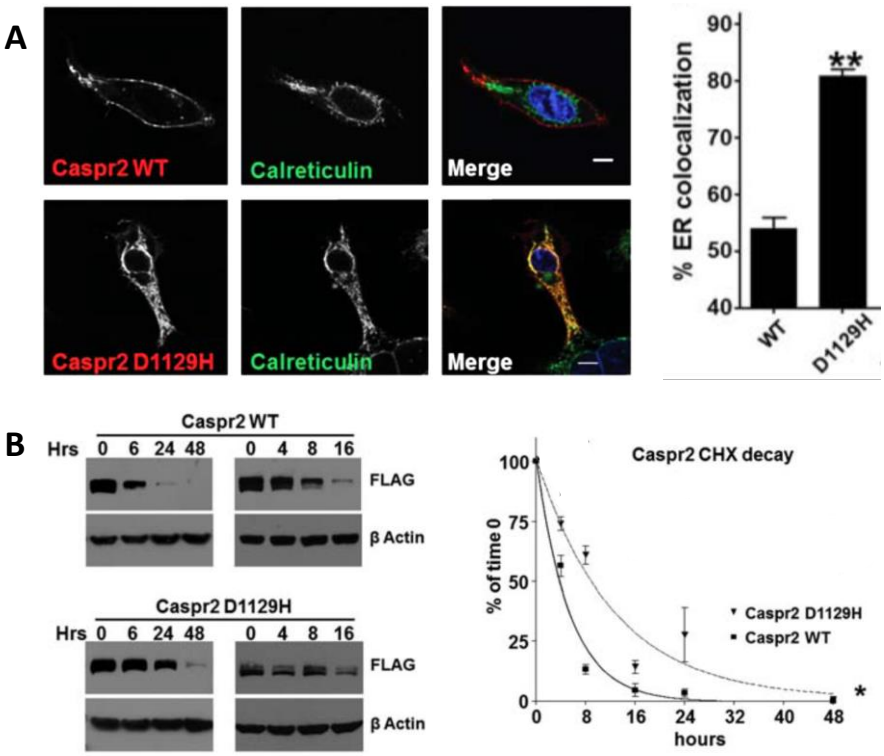

Figure 56: *CNTNAP2* variant D1129H can affect Caspr2 protein in vitro. A) In transfected HEK cells, the D1129H variant was shown to be heavily retained in the ER. B) The D1129H variant shows delayed clearance from the cell compared to wild-type Caspr2 after Cycloheximide (CHX) treatment. Adapted from (Falivelli et al. 2012).

Several *CNTNAP2* variants identified by Bakkaloglu and colleagues were further studied *in vitro* by our lab, who sought to better characterize the downstream effects of these mutations in cultured cortical neurons. As mentioned previously, the lab showed that Caspr2 regulates axon growth in a dose-dependent manner, with an intermediate phenotype for cortical neurons from

Cntnap2 HET mice between neurons from WT and KO mice (Canali et al. 2018). The team tested several variants in *Cntnap2* HET neurons, as this background is more relevant for *CNTNAP2* heterozygosity in ASD patients, and found they could be divided into two main groups. The first group includes variants leading to protein retention in the ER, including the variant D1129H, supporting results from Falivelli et al. The lab demonstrated that these variants oligomerize with the WT Caspr2 and have a dominant-negative effect on its localization in transfected cells, leading to its retention in the ER; these variants consequently display a dominant-negative effect on cortical axon growth (Fig. 57A, variant D1129H). The second group of variants were those which were well localized at the cell membrane, but lost their ability to interact in *trans* with TAG-1, such as variant G731S, and do not seem to affect axon outgrowth (Fig. 57B).

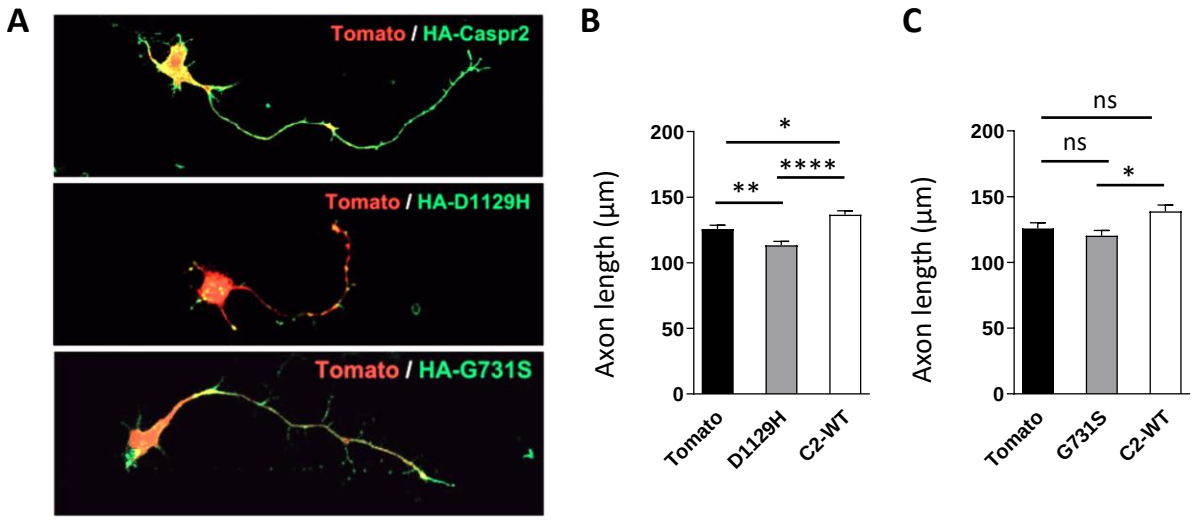

Figure 57: A) Representative images of cell surface immunostaining of HET electroporated neurons co-expressing Tomato (red) and HA-Caspr2 or the variants HA-D1129H or HA-G731S (green). B) The variant D1129H has a dominant-negative effect on cortical neuron axon growth, with decreased length compared to WT. Expression of WT Caspr2 induces increased axon length compared to WT. C) Variant G731S is defective in axon growth, with no change in axon length compared to WT neurons. N= 4–6 embryos/genotype, 36 neurons/embryo. Statistical analyses: Dunn's Multiple Comparison post-test, *P < 0.05, **P < 0.01, ***P < 0.001; ns, not significant. Adapted from (Canali et al. 2018) + unpublished lab data.

These findings underscore a potential pathogenicity of heterozygous *CNTNAP2* variants, and led the lab to propose a hypothetic model showing how *CNTNAP2* heterozygous missense variants could impact Caspr2 functions when dose dependent (Fig. 58).

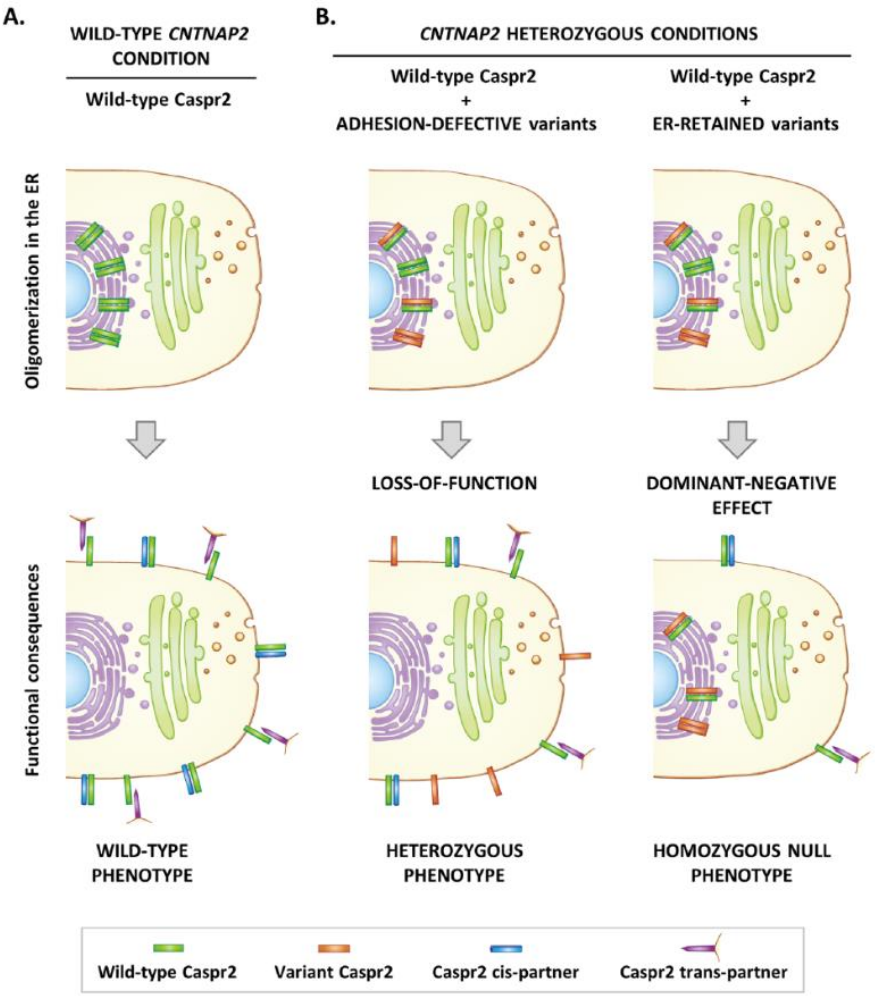

Figure 58: Hypothetic model showing how *CNTNAP2* heterozygous missense variants could impact Caspr2 functions when dose dependent. A) In wild-type condition, Caspr2 self-associates during its intracellular processing but is expressed in a monomeric form at the plasma membrane where it interacts with its cis and trans extracellular partners. B) *CNTNAP2* heterozygous conditions. After oligomerization during intracellular processing, adhesion-defective variant proteins are correctly addressed to the plasma membrane but do not interact with their extracellular partners (loss-of-function), a situation leading to phenotypes mimicking *CNTNAP2* heterozygosity. On the other hand, misfolded variant proteins retain wild-type Caspr2 in the endoplasmic reticulum (ER), leading to a decrease in functional protein at the plasma membrane (dominant-negative effect) and phenotypes mimicking homozygous *CNTNAP2* null mutation (Canali and Goutebroze 2018).

Given this background, the lab collaborated with Dr. Christel Depienne and Dr. Caroline Nava at the Hôpital la Pitié-Salpêtrière in Paris, France, who performed a screen for *CNTNAP2* mutations in French ASD patients. They identified a novel variant, I236S, which was present in a young male ASD patient, and was inherited from the patient's mother, who did not present ASD symptoms; the father carried no mutation and was healthy as well (Fig. 59). Variant I236S was classified as "Deleterious" (score 0), "Possibly damaging" (score 0.993), and "Disease causing" (*P* value: 1) by the SIFT, PolyPhen-2, and Mutation Taster software, respectively. A recently developed deep-learning model, ESM1b, also predicted I236S to be pathogenic; this model gives each variant an effect score, the log-likelihood ratio (LLR) between the variant and wild type residue. Variant

I236S (LLR of -13.25) is beneath the LLR threshold of -7.5 considered to be pathogenic (Brandes et al. 2023). Preliminary studies in the lab further showed that the mutant Caspr2 protein bearing the variant I236S is heavily retained in the ER *in vitro*, comparable to some other previously studied variants. The goal of my PhD project was thus to better understand the effects of ER-retained heterozygous missense *CNTNAP2* variants *in vivo*, using variant I236S as an example, and asses how such variants could contribute to ASD.

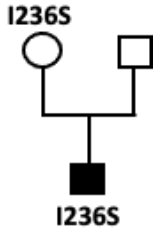

Figure 59: Pedigree of ASD patient bearing the I236S mutation.

To address this, the lab generated a novel knock-in (KI) mouse line expressing this variant endogenously, called "KI-I236S", which I used to shed light on **how the variant could contribute to ASD pathogenicity *in vivo***, and to better understand **whether and how it could impact Caspr2 function** by analyzing alterations in animal behavior which could indicate an ASD phenotype, along with studying nervous system morphology and biochemical changes induced by the I236S mutation. As Caspr2 is known to play a major role in axon development, including in NOR organization and in myelination, I investigated these processes in both the PNS and the CNS of KI-I236S HET male and female mice. I also studied their behavior to better understand if the *CNTNAP2* variant I236S could, via altered Caspr2 function, affect cognitive, sensory, or motor performance of the mice, or induce classical ASD behaviors like restrictive or repetitive movements.

The results of my PhD led to the writing of the following article, "Sex-dependent impact of an ASD-related *CNTNAP2* missense variant on mouse behavior and axon and myelinated fiber development," presented in Results I. We demonstrate that *CNTNAP2* heterozygous missense variant I236S affects Caspr2 function *in vivo*, including myelination and axon diameter of the PNS, CNS white matter tract morphology, NOR formation, sensory behavior, muscular strength, and social preference. Interestingly, we also reveal that many of these effects are sex-dependent in KI-I236S HET mice. Additionally, I present complementary results in Results II, in which we further studied myelination in the CNS. This work is still in progress and will be further considered, along with my other results, in the Discussion. At the beginning of my PhD, I also contributed to the characterization of *Cntnap2* HET and KO mice, work which was published earlier this year (February 2023). The article is presented in the Annex.

Results I

Sex-dependent impact of an ASD-related *CNTNAP2* missense variant on mouse behavior and axon and myelinated fiber development

Manett T.[1,2,3], Cifuentes-Diaz, C.[1,2,3], Nosten-Bertrand M.[1,2,3], Devaux J.[4], Savariradjane M.[1,2,3], François A.[1,2,3], Grannec G. [1,2,3], Nava C.[5], Mignot C.[6], Garcia M.[1,2,3], Goutebroze L.[1,2,3] *

[1]Inserm, UMR-S 1270, F-75005, Paris, France

[2]Sorbonne University, Faculté des sciences et ingénierie, F-75005, Paris, France

[3]Institut du Fer à Moulin, F-75005, Paris, France

[4]Institut de Génomique Fonctionnelle, Université de Montpellier, CNRS, INSERM, Montpellier, France

[5]Institut du Cerveau et de la Moelle épinière (ICM), Sorbonne Université, UMR S 1127, Inserm U1127, CNRS UMR 7225, F-75013, Paris, France

[6]Department of Genetics, La Pitié-Salpêtrière Hospital, APHP, Sorbonne University, Paris, France.

Correspondance: Laurence Goutebroze, Ph.D, laurence.goutebroze@inserm.fr

INTRODUCTION

Autism Spectrum Disorder (ASD) represents a group of early neurodevelopmental disorders which are characterized by the presence of repetitive/restricted behaviours and deficits in social interaction and communication (DSM-V) and can be associated with additional symptoms such as motor deficits and/or impaired sensitivity. ASD affects approximately 1 in 36 children in the U.S., with a male-to-female ratio of roughly 4:1 (Maenner et al., 2023). It presents complex etiology, with contributions from both the environment and genetics, the latter of which is estimated to contribute to 40-80% of ASD susceptibility (Rylaarsdam & Guemez-Gamboa, 2019). *CNTNAP2*, encoding the protein Caspr2, is considered to be one of the major ASD risk genes. *CNTNAP2* genetic alterations identified in ASD patients include complex genomic rearrangements, deletions, and a particularly large number of heterozygous missense variants (Arking et al., 2008; Bakkaloglu et al., 2008; Murdoch et al., 2015; Sampath et al., 2013). *Cntnap2*$^{-/-}$ mice display ASD-like behaviors (Balasco et al., 2022; Choe et al., 2022; Dawes et al., 2018; Deemyad et al., 2022; Mishra, 2022; Peñagarikano et al., 2011; Scott et al., 2019; Xing et al., 2019), supporting genetic data. However, most of the missense variants identified in ASD patients are inherited from an unaffected parent (Bakkaloglu et al., 2008). Furthermore, heterozygous missense *CNTNAP2* variants have been found in control individuals (Murdoch et al., 2015), thus questioning the clinical significance of the variants identified in ASD patients and their contribution to the development of the pathology.

Caspr2 is a neurexin-like cell-adhesion transmembrane glycoprotein originally identified in the juxtaparanodal regions (juxtaparanodes) of the nodes of Ranvier in mature myelinated neurons of the central (CNS) and peripheral (PNS) nervous system, where it contributes to the formation of axoglial contacts, forming a complex *in cis* and *in trans* with the immunoglobulin cell-adhesion molecule CNTN2/Contactin2/TAG-1 (S. Poliak et al., 1999, 2001). Caspr2 is also required for the clustering of *Shaker*-type voltage-gated potassium channels (Kv1.1 and Kv1.2) in these regions (Sebastian Poliak et al., 2003). Mislocalization of Kv1 channels in *Cntnap2*$^{-/-}$ mice is associated with modifications of axonal action potential wave form and increases in postsynaptic excitatory responses, suggesting that Caspr2 is important for proper conductivity of CNS myelinated fibers (Cifuentes-Diaz et al., 2023; Scott et al., 2019). More recently, Caspr2 has been proposed to also play multiple functions during brain development, including in axon growth and myelination. We showed that Caspr2 controls cortical neuron axon growth *in vitro* in a dose-dependent manner (Canali et al., 2018). Moreover, Scott et al. (2019) reported a delay in myelination of the cortex in juvenile *Cntnap2*$^{-/-}$ mice (Scott et al., 2019). Comparing wild-type (WT), *Cntnap2*$^{-/-}$ and *Cntnap2*$^{+/-}$

mice, we further demonstrated that Caspr2 controls the morphology of two major brain interhemispheric myelinated tracts, the corpus callosum (CC) and the anterior commissure (AC), throughout development, as well as axon diameter at early developmental stages, cortical neuron intrinsic excitability at the onset of myelination, and axon diameter and myelin thickness at later developmental stages (Cifuentes-Diaz et al., 2023). Changes in axon diameter, myelin thickness and node of Ranvier morphology were also detected in the sciatic nerves of the mutant mice (Cifuentes-Diaz et al., 2023). Importantly, most of the parameters analyzed were affected in *Cntnap2*$^{+/-}$ mice, either specifically, more severely, or oppositely as compared to *Cntnap2*$^{-/-}$ mice, indicating that both *Cntnap2* heterozygosity and *Cntnap2* null homozygosity impact axon and central and peripheral myelinated fiber development, but in a differential manner, and suggesting that *CNTNAP2* alterations could lead to a multiplicity of phenotypes in humans.

All the *CNTNAP2* heterozygous missense variants identified so far in ASD patients are localized in the exons encoding the extracellular domain of Caspr2 (Bakkaloglu et al., 2008; Murdoch et al., 2015; Saint-Martin et al., 2018). This domain is composed of different structural subdomains and is likely to present an overall compact architecture, suggesting complex structure-function relationships, which may be affected by the variants (Lu et al., 2016). *In vitro* studies accordingly showed that some of the variants lead to protein misfolding and retention in the endoplasmic reticulum (ER), with activation of the unfolded protein response (UPR) and delayed clearance (Falivelli et al., 2012). We further demonstrated that mutant proteins bearing such variants (R1119H, D1129H) display a dominant-negative effect on axon growth *in vitro* in a *Cntnap2*$^{+/-}$ background through their oligomerization with wild-type Caspr2, indicating that ER-retained mutant proteins may be pathogenic (Canali et al., 2018; Canali & Goutebroze, 2018). However, whether ER-retained misfolded variants could have functional consequences *in vivo* remains to be determined.

In this study, we address this question by studying a novel knock-in mouse model bearing a *CNTNAP2* heterozygous missense variant, c.707T>G, identified young ASD male patient. We show that the corresponding Caspr2 mutant protein is strongly retained in the ER, facilitating comparison with other Caspr2 ER-retained variants. Studying both male and female heterozygous (HET) mutant mice, we evaluate the impact of the variant on their behavior using a battery of tests which may indicate peripheral deficits and/or ASD-related symptoms. We also characterized brain interhemispheric myelinated tract and sciatic nerve abnormalities in mutant mice. Overall, our

observations show differential behavioural deficits and morphological alterations between males and females.

MATERIAL AND METHODS

Knock-in mouse generation and animal procedures

KI-I236S mutant mice were generated using a sgRNA CRISPR/Cas9 technology in a C57BL/6J background at the Centro Nacional de Biotecnología (CSIC) in Madrid (Spain), thanks to the European INFRAFRONTIERS program (**Suppl. Fig. 1A, B**). The mutation c707T>G in *Cntnap2* exon 5 leads to the introduction of a digestion site for the restriction enzyme TaaI (HpyCH4III) site (**Suppl. Fig.1A**). The genotypes were analyzed by PCR of tail-tip genomic DNA with primers Forward 5' TTCTCCTCTCAGGGGCTGAC and Reverse 5´TGAATGATTTGCCTGCCTGT 3´ amplifying a 468-bp product (both WT and mutant allele), and subsequent digestion with TaaI leading to 2 products for the WT allele (426 bp, 42 bp), and three products for the mutant allele (299 bp, 127bp, 42 bp) (**Suppl. Fig.1C, D**).

Mice were group housed with *ad libitum* access to food and water and a 12 h–12 h light–dark cycle (light phase onset at 8 a.m.). All the experiments complied with all relevant ethical regulations. They were approved by the French Ministry of Higher Education, Research, and Innovation (Institute agreement D750522; project agreements APAFIS#5496-20160519l5l48075 v8 and APAFIS#31520-2021051709364077 v3).

Behavioral tests

The behavioral phenotype of the mice was examined with three groups of males and females during the following tests: Group 1, 2-month-old animals, circular corridor; Group 2, 2.5-month-old animals submitted successively to grid, pole, wire-hanging, grip, and hot plate tests; Group 3, >3.5-month-old animals, marble burying and social interaction tests. All tests were performed in sound-attenuated rooms between 9 am and 5 pm, and always at the same time for a given test. For all experiments the experimenter was blinded to the genotype of the mice tested and analyzed.

Spontaneous locomotor and rearing activities: Locomotor and rearing activities were measured using a circular corridor with four infrared beams placed at every 90° near the floor of the corridor and one infrared beam placed high above the floor (Imetronic, Pessac, France), in a low luminosity environment, avoiding stress. Locomotor activity was counted when mice interrupted two infrared beans near the floor and thus had traveled ¼ of the circular corridor. Rearing activity was counted each time the mice interrupt the infrared beam placed high above the floor. Activities were evaluated during three consecutive days, by 5 minutes intervals for 60 minutes.

Grid test: Coordination between forelimbs and hind limbs and accurate limb placement were examined by assessing the ability to walk on metal grid bars with 1.5 cm gaps on the bottom of a 30

x 20 x 20 cm box. The number of steps was automatically registered by the apparatus. All sessions were video tracked to analyze the performance of each animal by counting the number of errors in foot placement/total number of steps, during 2-minute sessions, once a day, for two consecutive days. On the two days prior to data collection, each mouse was allowed to walk on the grid for 2 minutes to habituate.

Pole test: The vertical pole-test was used to evaluate motor coordination and balance. The apparatus consists of a vertical metal bar (2 cm in diameter, 40 cm in height) covered with "Tensoplast" fabric adhesive bandages, placed in a home cage with litter on the bottom. Mice were placed with the head facing upwards, and their ability to turn and descend along the bar to its home cage was assessed. Mice were recorded during 5 consecutive trials and the average of the 5 trials was used for analysis. On the two days prior to data collection, each mouse performed a habituation session.

Wire-hanging test: The wire-hanging test was performed to measure motor coordination and neuromuscular strength. Mice were gently placed on a wire-cage lid, which was then slowly waved and turned upside down above the soft bedding (50 cm). The time (in seconds) the animal spent hanging on the grid before falling in the cage was recorded. Each mouse underwent three trials each day for two consecutive days. The best performance for day 2 was used for quantification.

Grip strength analysis: Forelimb grip strength was measured using a Grip Strength Meter (Bioseb). Mice were held by the tail and allowed to grasp a small grill with their forepaws. Once the mouse grasped the grill with both paws, the mouse was pulled away from the grill until the mouse released the grill. The digital meter displays the level of tension (in grams) exerted on the bar by the mouse. The average of 3 trials was used for analysis.

Hot plate: A standard hot plate (Bioseb), adjusted to 52°C, was used to assess motor reactions in response to noxious stimuli. Mice were confined on the plate by a Plexiglas cylinder (diameter 19 cm, height 26 cm). The latency to a hind paw response (licking or shaking) or jumping, whatever happened first, was taken as the nociceptive threshold.

Marble burying test: The purpose of this test was to detect stereotypical behaviors and also assess anxiety. The mice were evaluated individually in a clean cage (25 x 20 x 14cm) filled with a 3cm-thick layer of sawdust on which were placed 12 glass balls in 3 lines of 4 equidistant balls. The number of buried balls (>75% covered) was recorded every minute for the first 10 minutes of the test, then every 5 minutes for 20 minutes, and one last time after 30 minutes of testing.

Social preference test: This test was performed in an "Open-field" unit (40 x 40 x 30 cm, white Plexiglass on the sides and the floor) illuminated with 600 lux, and was divided in three phases. During the habituation phase, the mouse was placed in the empty open-field and left free to explore for 10 minutes. Then, two perforated round boxes (10 cm diameter) were inserted into the space, and the mouse was left to explore for 10 minutes. Finally, a novel object was added to one box and an unfamiliar congener of the same age and sex was added to the other, which the mouse was free to explore the two boxes for 10 consecutive minutes. The behavior of the mouse was automatically recorded by the video-tracking system (Viewpoint, Lyon) and the recordings were used to quantify the number of entrances and the time spent in an area of 5 cm diameter around the boxes. Videos could also be used to assess other behaviors such as stereotyped behaviors, which can vary depending on the environment in which the animal is placed.

COS-7 culture, transfections, immunofluorescence staining and image acquisition

The pCDNA-HA-Caspr2 construct encode human Caspr2 (Accession number NM_014141, KIAA0868) with the HA epitope inserted downstream of the signal peptide between the residues Trp26 and Thr27, in the pCDNA3 vector (Canali et al., 2018). Mutated pCDNA-HA-Caspr2-I236S expressing the Caspr2 variant protein was generated by site-directed mutagenesis using the oligonucleotides 5'-CAGCAAGGAGATTACA*G*TACCTTGGAACTGAAA-3' (sense) and 5'-TTTCAGTTCCAAGGTA*C*TGTAATCTCCTTGCTG-3' (antisense), and the whole sequence of the mutated cDNA was verified by sequencing.

For protein expression and localization analysis, COS-7 grown in DMEM containing 10% fetal calf serum were transiently transfected using Polyethylenimine (PEI), using 3 µg of plasmid/10 µg PEI/15 x 10^4 cells/30 mm-diameter dish and 1 µg of plasmid/3 µg PEI/5 x 10^4 cells/20 mm-diameter coverslip, respectively. After transfection, cells were grown for 24 h before processing.

For immunofluorescence staining, cells were fixed with paraformaldehyde (PFA, 40 mg/ml) in buffered saline (PBS) for 30 min at room temperature (RT) and permeabilized in PBS-Triton X-100 2 µl/ml for 5 min at RT. Coverslips were incubated in a saturation solution (50 mg/ml bovine serum albumin in PBS), and then sequentially with primary antibodies (anti-HA, rat clone 3F10 #11 867 423 001, Roche; anti-KDEL, mouse #SPA-827, Stressgen; diluted in the saturation solution) at RT for 2 hours and Alexa Fluor-conjugated-secondary antibodies (Thermo Fisher Scientific; diluted in the saturation solution) at RT for 1 hour. Coverslips were finally washed with PBS and mounted with Fluoromount-G medium (Thermo Fisher Scientific). To visualize the subcellular

localization of WT or variant HA-Caspr2, images were acquired using a Leica SP5 confocal laser-scanning microscope (Leica microsystems, Z stack 1µm) with constant parameters.

Biochemical experiments

To analyze expression of WT and variant HA-Caspr2 in transfected COS-7 and protein levels in brains and sciatic nerves, cells and tissues were lysed in RIPA buffer (50 mM Tris, pH 8.0, 150 mM NaCl, 10 µl/ml NP-40, 5 µg/ml sodium deoxycholate, 1 µg/ml SDS) containing Complete protease inhibitors (Roche), and immunoblotting was performed as previously described (Canali et al., 2018; Cifuentes-Diaz et al., 2023). Briefly, equal amounts of proteins (40 µg) were loaded on NuPAGE 8 % Bis-Tris gels (COS-7 cell lysates) or NuPAGE 8-12% Bis-Tris gels (brain and sciatic nerve lysates) (Thermo Fisher scientific) and transferred to 0.45 µm Nitrocellulose membranes. Membranes were blocked with 50g/l non-fat dry milk in Tris-Buffered Saline solution/0.1 ml/l Tween 20 for 1 hour at RT, incubated with primary antibodies in the same solution for 2 hours at RT or O/N at 4°C, 1 hour at RT with appropriate IRDye-conjugated secondary antibodies, and imaged using Odyssey Imaging System (LI-COR Biosciences). The expression levels of the proteins were quantified using Image Studio Lite Quantification Software version 5.2 (LI-COR Biosciences) and normalized on actin (sciatic nerves) or GAPDH (brains) expression. The commercial antibodies were from the following sources: anti-HA, rat clone 3F10 #11 867 423 001, Roche; anti-K_v1.2 α subunit, mouse clone K67/25 #75-075, NeuroMab, 1:400; anti-F3, goat #AF904, R&D Systems, 1:400; anti-NrCAM, rabbit #ab24344, Abcam, 1:300; anti-TAG-1, goat #AF4439, R&D Systems, 1:500; anti-Caspr2 (191) and anti-Nfasc155/186 previously described (Denisenko-Nehrbass et al., 2003; Martin et al., 2017).

RT-qPCR experiments

For mRNA expression analysis, total mRNA was extracted from brains using the TRIzol™ Reagent (Invitrogen) following the manufacturer's recommendations. Reverse transcription was performed with the SuperScript II reverse transcriptase (Invitrogen, #18064-022) and random primers, and qPCR in a Stratagene™ Mx3005P qPCR instrument (Agilent Technologies) using the Brilliant II SYBR ® Green QPCR Master Mix (Agilent Technologies, #600828). The MxPro QPCR Software (Agilent Technologies) was used to perform expression analyses. The expression level of *Cntnap2* mRNA was normalized to *Psap* mRNA level. Primers for *Cntnap2* were designed on two different exons: primer sense 5'CAGCGCTCTCGCTCTGGATT (accession number NM_001004357, nucleotides 261-280), primer anti-sense 5'CCCCAGCACCTCCTCGTTTATT (nucleotides 425-446), amplified DNA fragment 186 bp. Primers for *Psap* were the following: primer sense 5'CTGGTGTCAGAACATGGAGACTG

(accession number NM_001146120, nucleotides 1708-1730), primer anti-sense 5'TGACTTCTGCAGCTGGGAAA (nucleotides 1781-1800), amplified DNA fragment 93 bp.

Tissue processing, immunostainings, and image analyses

Brains: Adult P90 mice were deeply anesthetized by intraperitoneal injection of ketamine (100 mg/kg) and xylazine (10 mg/kg) and transcardially perfused with 4% paraformaldehyde (PFA) in 0.12 M phosphate buffer pH 7.4. Brains were post-fixed overnight (O/N) at 4°C in 4% PFA. After washing with PBS, 45 µm-thick serial coronal sections and 500 µm-thick horizontal sections were performed using a VT1000S vibratome (Leica, France). Thirty-five µm-thick serial sagittal sections were obtained similarly on brains embedded in 35g/l agarose and 80g/l sucrose in PBS. All floating sections were conserved at 4°C in PBS with 1g/l sodium azide until use. For morphological analysis of the CC and AC, coronal and sagittal sections were incubated in a permeabilization /saturation solution (PS: PBS, 2 g/l porcine skin gelatin, 2.5 ml/l Triton X-100) for 1 hour at RT and then O/N at 4°C with the anti-NF-M antibody (Sigma, mouse clone NN18, #N5264, 1:300) diluted in PS. Sections were then washed 3 times for 10 minutes in PBS/2.5 ml/l Triton X-100 (WS) and incubated for 2 hours at RT with adequate Alexa Fluor 488-conjugated-secondary antibodies (Thermo Fisher Scientific) diluted in PS. After secondary antibody incubation, sections were washed 3 times for 10 minutes in WS and nuclei were stained for 10 minutes with Hoechst before mounting with Fluoromount-G medium (Thermo Fisher Scientific). Images of immunostained coronal and sagittal sections or phase-contrast images of horizontal sections were acquired using a macroscope MVX10 (Olympus). Thickness and area measurements were performed using the ImageJ software.

Sciatic nerves: Nerves of mice 4-month-old, 3 of each genotype, were dissected and fixed in 2% PFA for 30 min at RT, teased apart to yield single fiber preparations, air-dried and kept at –20°C until use. Immunofluorescent staining was performed as described previously (Martin et al., 2017). Briefly, slides were treated with 0.1M glycine for 30 min at RT or with methanol 50%/acetone 50% for 20 min at -20°C, pre-incubated for 1 hour at room temperature in the permeabilization/saturation solution PS, before incubation with primary antibodies diluted in PS overnight at 4°C (anti-K_v1.2 α subunit, mouse clone K67/25 #75-075, NeuroMab, 1:400; anti-F3, goat #AF904, R&D Systems, 1:400; anti-NrCAM, rabbit #ab24344, Abcam, 1:300; anti-TAG-1, goat #AF4439, R&D Systems, 1:500; anti-Caspr (L51, 1:500) and anti-Caspr2 (191, 1:400) previously described (Denisenko-Nehrbass et al., 2003; Menegoz et al., 1997). After washing with PBS, coverslips were incubated for 2 hours at room temperature with Alexa Fluor-conjugated-secondary antibodies (Thermo Fisher Scientific) secondary antibodies diluted in PS2, washed again with PBS,

and mounted with Fluoromount-G medium. Images were acquired using a Zeiss Celldiscoverer 7 imaging system for quantification analyzes, and a STELLARIS 5 confocal laser-scanning microscope (Leica microsystems) to acquire representative images. Measurements of node length, node axonal diameter and paranodal length were performed manually on NrCAM and Caspr stainings using the ImageJ software.

Electron microscopy and morphometry

For ultrastructural analyses of peripheral myelinated fibers, the sciatic nerves of 4.5 month-old mice were fixed *in situ* for ~1 min with 3% glutaraldehyde in Milloning's phosphate buffer 0.1M pH 7.4, dissected out, placed in fixative O/N at 4°C, rinsed in PB, post-fixed in 2% osmium tetroxide in PB, dehydrated in an ascending series of ethanol, and embedded in epoxy resin. The global morphology of the nerves and the number of myelinated fibers were evaluated on 0.5 µm-thick semi-thin transversal sections stained with toluidine blue and imaged with a DM6000 Leica microscope. Measurements of the number of myelinated fibers were performed manually using the Fiji software.

For ultrastructural studies, transversal and longitudinal sections ultra-thin sections (40 nm) of the nerves were stained with Reynold's lead citrate and uranyl acetate and examined with a Philipps CM-100 TEM electron microscope. Images were acquired using an Orius (Gatan) digital camera. Axon diameters, fiber diameters and G-ratios were measured on the transversal sections using the semiautomatic software MyelTracer (Kaiser et al., 2021). A least ten nodes of Ranvier per mice were examined in longitudinal sections of sciatic nerves.

Electrophysiological analysis

Mice (~6-month-old, 6/genotype) were euthanized, and the sciatic nerves were quickly dissected out and transferred into artificial CSF containing 126 mM NaCl, 3 mM KCl, 2 mM $CaCl_2$, 2 mM $MgSO_4$, 1.25 NaH_2PO_4, 26 mM $NaHCO_3$ and 10 mM dextrose, pH 7.4-7.5. The sciatic nerves (2 cm segments) were placed in a three-compartment recording chamber and perfused at 1-2 ml/min in medium equilibrated with 95%O_2-5%CO_2. The distal end was stimulated supramaximally (40 µs duration) through two electrodes isolated with petroleum jelly, and recordings were performed at the proximal ends. Signals were amplified and digitized at 500 kHz. The duration of the compound action potentials (CAPs) was calculated at the half maximal amplitude ($V_{1/2}$). The delay of the CAPs was measured at $V_{1/2}$ and at the maximal amplitude (V_{max}). The conduction velocity was derived from the delay. For recruitment analysis, the CAP amplitude was measured and plotted as a

function of the stimulation intensity. For the refractory period analysis, two successive stimuli were applied at different intervals, and the amplitude of the second CAP was measured and plotted as a function of the delay between the two stimuli.

Statistical analysis

Statistical analyses were performed with the GraphPad Prism 9 Software (GraphPad Software, San Diego, CA, USA). Results are provided as mean ± SEM or median ± quartile (Violin plot, medium smoothing). The normality of the samples was tested using the Shapiro-Wilk test. To compare the 2 genotypes or 2 conditions, statistical analyses were carried out using the unpaired t test when the variables followed a normal distribution and the Mann Whitney test when the variables did not follow a normal distribution, eventually followed by a Kolmogorov-Smirnov test to compared cumulative distribution. For the weight of the mice in function of the age, the marble burying test and the electrophysiological experiments, the 2 genotypes were compared using Two-way RM ANOVA tests, followed by Dunnett's multiple comparisons tests or Šídák's multiple comparisons tests. Linear regression analyzes were performed after checking the correlations between the variables (Pearson coefficient). The significance was established at a *P*-value < 0.05.

RESULTS

The *CNTNAP2* variant c.707T>G induces protein retention in the ER

The *CNTNAP2* variant c.707T>G was identified in a French ASD patient. It was transmitted by the mother, who is not obviously affected by the pathology (**Fig. 1A**), but reported at a very low frequency in the Genome Aggregation Database (GnomAD; frequency, ~ 10^{-6}). Caspr2 is a protein of 1331 residues, which presents a large extracellular domain composed of eight defined structural subdomains: a discoidin (F58C) domain, four laminin G (L1-L4) domains, two epidermal growth factor-like (EGF) domains, and a fibrinogen-like (FBR) domain (**Fig. 1B**). The variant leads to a replacement of the isoleucine at position 236 within the distal L1 subdomain by a serine (I236S mutation). SIFT, Polyphen-2, and Mutation Taster software, and the deep-learning model ESM1b, predicted that this variant could be “Deleterious” (score 0), “Possibly damaging” (score 0.993), “Disease causing” (*P* value: 1), and “Pathogenic” (LLR score -13.25), respectively. According to electron microscopy studies of the extracellular domain of the protein, Caspr2 probably displays a very compact F-shaped monomeric architecture organized into three major lobes composed of the L4 domain, L3 and FBR domains, and L1, L2 and F58C domains, respectively, while the EGF-like domains may serve as molecular hinges permitting the lobes to flex with respect to each other (Lu et al., 2016). The DynaMut software (Rodrigues et al., 2018) predicted that the Serine 236 positioned on the external part of L1 domain could be destabilizing (ΔΔG value: -2.682; **Fig. 1C**) and could increase protein flexibility (ΔΔSvib: 0.910 kcal.mol-1.K-1; **Fig .1D**).

The impact of the variant on folding and trafficking of the corresponding mutant protein, Caspr2-I236S, was evaluated in transfected heterologous COS-7 cells expressing HA-tagged proteins. Our previous work showed that in these conditions, Caspr2 appears as two bands in immunoblotting: an upper band which corresponds to a mature, fully glycosylated form which is trafficked appropriately and is expressed at the plasma membrane; and a lower band which corresponds to an immature, partially glycosylated, intracellular form (Canali et al., 2018; Falivelli et al., 2012) (**Fig. 1E**). Quantification of the percentage of the immature glycosylated form for HA-Caspr2-I236S on immunoblots showed that the mutant protein was mainly expressed as the immature form when compared to HA-Caspr2 (**Fig. 1E**), and in manner similar to that of the mutant protein bearing the variant D1129H (**Fig. 1B,E**; HA-Caspr2-D1129H), which was extensively studied previously and shown to induce protein misfolding and ER retention, with UPR activation. The subcellular localization of HA-Caspr2-I236S was further monitored by immunohistochemistry. The mutant protein showed a strong co-localization with an ER marker while HA-Caspr2 was mainly

detectable at the plasma membrane (**Fig. 1F**). These experiments demonstrated that the I236S variant is heavily retained in the ER and presents maturation defects.

Knock-in mice are viable and do not display major developmental defects

The knock-in mutant mice bearing the c.707T>G/I236S variant (KI-I236S mice) were generated using a sgRNA CRISPR/Cas9 technology in a C57BL/6J background at the Centro Nacional de Biotecnología (CSIC) in Madrid (Spain) (**Suppl. Fig. 1A,B**). Crossing heterozygous (HET) mice with C57BL/6J WT mice generated litters in which HET pups were obtained at a Mendelian ratio with comparable proportion of males and females (**Fig. 2A**), demonstrating that the variant does not have a major impact on mouse development. Also, both HET males and females appeared normal and survived as long as WT mice (>2 years), although HET males were slightly heavier than WT males during the first post-natal weeks (**Fig. 2B**), but not at later stages (**Fig. 2C**). Gross morphology of the brain appeared unaffected in both males and females (**Fig. 2D**). However, immunoblotting on brain lysates showed a significantly reduced level (~30% reduction) of total Caspr2 protein in HET animals (**Fig. 2E**) while RT-qPCR analysis showed no significant difference in *Cntnap2* mRNA levels (**Fig. 2F**), suggesting post-translational degradation of the mutant protein, either alone or together with WT Caspr2 through oligomerization.

KI-I236S HET mice show sex-dependent abnormalities in heat sensitivity and muscular strength but not in motor ability and coordination

We first characterized the behavioral phenotype of adult mutant mice using a battery of tests which may indicate peripheral deficits. Considering that boys are more often affected by ASD than girls, the performances of male and female mice were evaluated independently. The animals were tested successively for spontaneous locomotor activity and exploration during three consecutive days in a circular corridor, motor ability and coordination in grid, pole and hanging wire tests, muscular strength using the grip test, and heat sensitivity on a hot plate. Tests for motor ability and coordination did not reveal significant differences between WT and HET mice, males or females, as they showed comparable number of steps and of falls per 100 steps in the grid test (**Fig. 3B**) and similar time to descend along the vertical bar in the pole test (**Fig. 3C**) and to fall from the grid in the hanging wire test (**Fig. 3D**). In the pole test, WT and HET mice (males and females) displayed differences in descent strategy, HET mice showing a propensity to descend the pole in a turning manner rather than a straight manner (**Fig. 3C**), but what exactly this could indicate is not clear as there is conflicting evidence in the literature on this topic. Male and female HET mice did not

demonstrate impairments in the circular corridor during the two first days of the test (**Fig. 3A**), showing comparable horizontal locomotor activity (number of 1/4 turns per 60 minutes) and rearing activity (number of rears per 60 minutes) to WT mice, and decreased activities from day 1 to day 2, indicating habituation. However, on day 3 of testing HET female mice showed significantly decreased horizontal locomotor and rearing activities as compared to WT mice, while the rearing activity of HET males tended to be increased (*P*=0.0845), indicating likely differences in exploration capacities and/or interest between male and female HET mice. Also, differences were detected between males and females in the grip and hot plate tests: HET males displayed decreased muscular strength compared to WT males (**Fig. 3E**) and decreased heat sensitivity, that could reflect sensory defects (**Fig. 3F**; latency to a hind paw response or jumping), while no differences were observed between WT and HET females.

KI-I236S HET mice show sex-dependent abnormalities in social preference but no stereotypical behaviors

We next characterized the phenotype of adult mutant mice in two tests which may reveal ASD-related behaviors: stereotypical and anxious behaviors using the marble burying test, and social interaction deficits using a social preference test. In the marble burying test, mice were evaluated individually for the time spent to bury 12 glass balls placed on sawdust over a 30 minute-session. No difference was detectable between WT and HET mice, males or females (**Fig. 4A**), and no specific stereotypical behavior was observed either. The social preference test was conducted in an open field where mice were free to explore two boxes, one containing a novel object and one containing an unfamiliar congener of the same age and sex. As expected, WT mice showed a preference for the box with the congener (**Fig. 4B**; number of entrances and time spent in the area of the two boxes). HET males also demonstrated a preference for the box with the congener. By contrast, no significant difference for interaction with the box containing the congener and the empty box was observed for HET females, indicating that female HET mice display some social interaction deficits. Note that in this test, WT and HET mice, males and females showed comparable activity (**Fig. 4B**; right panels). Also, the behavior of the mice was automatically recorded by the video-tracking system and the observation of the videos did not reveal either stereotyped or anxiety behaviors, which can vary depending on the environment in which the animal is placed.

KI-I236S HET mice show sex-dependent morphological alterations of brain interhemispheric myelinated tracts

As we previously observed morphological alterations of the corpus callosum (CC) and of the anterior commissure (AC) in *Cntnap2*$^{-/-}$ and *Cntnap2*$^{+/-}$ mouse brains (Cifuentes-Diaz et al., 2023), we next examined brain morphology on coronal sections (**Fig. 5A,D;** Bregma + 0.55), sagittal sections (**Fig. 5B,E**) and horizontal sections (**Fig. 5C,F**). The CC is the most prominent white matter structure in the brain, formed by ~80% of axons coming from neocortical neurons in layers II/III and ~20% of axons coming from cortical neurons in layer V (**Fig. 5A,D**). The AC is formed by two main branches, contacting each other at the midline of the brain (**Fig. 5E**). The anterior branch (ACa) is composed mainly of axons from the anterior piriform cortex and the anterior olfactory nucleus, whereas the posterior branch (ACp) is composed mostly of axons from the posterior piriform cortex and the amygdala**.** Immunostaining of coronal and sagittal slices with antibodies directed against the neurofilament subunit NF-M, which is expressed in myelinated commissural axons, and phase-contrast images of horizontal sections did not reveal gross abnormalities in mutant mice either in the global morphology of the brain or in the global structure of the CC or AC. The thicknesses of the motor cortex (MC) and sensorimotor cortex (SSC) measured on coronal sections were not affected (data not shown). When measuring the thickness of the CC at the midline on coronal sections (**Fig. 5A**), and CC area, minimum and maximum calipers on sagittal sections (**Fig. 5B**), no significant difference was observed between HET and WT males (**Fig. 5G**), but a significant decrease of CC maximum caliper and a decreased tendency of CC area were detected in HET females as compared to WT females (**Fig. 5I**). Conversely, measurements of AC area on sagittal sections and ACa thickness on horizontal sections did not reveal differences between HET and WT females (**Fig. 5J**), but a significant decrease of AC area in HET males as compared to WT males (**Fig. 5H**). The fact that the ACa thickness was not significantly decreased in males suggested that decreased AC area was preferentially due to a decrease in ACp thickness.

KI-I236S HET mice show sex-dependent myelinated fiber anomalies in the peripheral nervous system

Since we previously showed that Caspr2 also controls axon diameter, myelin thickness, and node of Ranvier morphology in peripheral nerves (Cifuentes-Diaz et al., 2023), we further assessed whether the organization of peripheral myelinated fibers could be perturbed in HET adult mice, focusing on sciatic nerves. As for the brains, immunoblotting on nerve lysates showed a ~30% reduction of total

Caspr2 protein in HET animals as compared to WT animals (**Fig. 6A**). Semi-thin transversal sections of the nerves stained with toluidine blue did not reveal any major difference in the global morphology of the nerves between adult WT and HET (**Suppl. Fig. 2**), nor in the total number of myelinated fibers (**Fig. 6B**), although it tends to be slightly decreased in HET males. At the ultrastructural level, the structure of the myelin appeared normal in HET mice (**Fig. 6C**). We measured myelinated fiber and axon diameters, to subsequently calculate the G-ratio, which is the ratio *between the inner and outer diameters of a fiber* whose variations can reveal myelin thickness defects. When plotting the G-ratios as a function of axon diameter, we did not detect any difference between HET and WT female mice (**Fig. 6E**), but a significant difference between HET and WT male mice with an increased G-ratio in HET male, indicating hypomyelination (**Fig. 6D**).

We further examined the organization of myelinated fibers in males, looking at the nodes of Ranvier. Fluorescent immunolabelling on teased myelinated fibers revealed that their global organization was preserved in HET mice (**Fig. 7A,B**). Caspr2 was detectable in more than 96% of the juxtaparanodes (> 96%) (**Fig. 7A,B,E**), together its partner TAG-1 (**Fig. 7A,B**), although the enrichment of latter might be reduced since immunoblotting revealed a decreased level (~12%) of the protein in nerve lysates (**Fig. 7C,D**). *Shaker*-type voltage-gated potassium channels (Kv1.2) were observed in the vast majority of the juxtaparanodes stained for Caspr2 (**Fig. 7A,B,E**), and their global level in nerve lysates was not significantly different from that in WT mice (**Fig. 7D**). The localization of proteins enriched in the two other regions of the nodes of Ranvier, the paranode and the node, as well as their level in nerve lysates, also appeared unchanged (**Fig. 7A,B,** F3, Caspr, NrCAM; **Fig. 7C,D,** Nfasc155, Nfasc186). However, a detailed examination revealed a significant increase in the axonal diameter of the nodes (labelled for NrCAM) together with a significant increase in their length (**Fig. 7F-H**), and a decrease of the length of the paranodes (labelled for F3) (**Fig. 7I**) in HET mice. We thus examined the ultrastructure of the nodes of Ranvier by electron microscopy on ultra-thin longitudinal sections of the nerves. No major abnormalities were observed in the juxtaparanodes in mutant mice (**Fig. 8A,B**). The cytoplasmic glial loops contacting the axons at paranodes appeared globally normal (**Fig. 8C**). The transverse bands, the ultrastructural hallmark of paranodal junctions, were visible in mutant as well as in WT mice (**Fig. 8C,** arrowheads). Schwann cells microvilli filled the nodal gap and contacted the axon, and their organization was indistinguishable in mutant and WT mice (**Fig. 8C**). However, in agreement with morphometric analyses on immunostained myelinated fibers, the nodes often appeared larger and longer, and paranodes shorter, both in large and thin myelinated fibers of HET mice (**Fig. 8A,B**).

KI-I236S HET mice show sex-dependent Remak bundle anomalies in the peripheral nervous system

During development of peripheral nerves, myelination takes place in Schwann cells wrapped around large-diameter axons whereas immature Schwann cells give rise to non-myelinating cells, which ensheath groups of small-diameter C-fiber axons (<1µm) to form the Remak bundles. C-fibers carry sensory input such as nociception from touch or heat from the periphery to the central nervous system. Non-myelinating Schwann cells keep the axons from touching each other by squeezing their cytoplasm between the axons. Upon examination of sciatic nerve transversal sections, we noticed that the cytoplasm of non-myelinating Schwann cells might be more dense in HET males than in the WT males (**Fig. 9A**). We thus asked whether this could be associated with modifications in the global organization of the Remak bundles. We did not observe differences in the number of C-fibers per Remak bundle between WT and HET mice, males or females (**Fig. 9B**). However, the diameters of the axons were significantly increased in HET males as compared to WT mice, while no difference was observed in females (**Fig. 9C**).

Considering the morphological abnormalities of the myelinated fibers and Remak bundles observed in mutant males, we finally asked whether they may influence peripheral nerve functions. To this end, we examined the electrophysiological properties of the sciatic nerves. Recording did not reveal any alteration in compound action potentials (CAPs) recruitment for increasing intensities of stimulation amplitude at 35°C in myelinated fibers of HET mice (**Suppl. Fig. 3A**). The mean conduction velocity at the peak (CV_{max}) or at the mid-amplitude ($CV_{½}$) of the CAPs, as well as the mean amplitude and duration of the CAPs, were not affected (**Table 1; Suppl. Fig. 3C,D**). The refractory period was also identical in WT and HET mice (**Suppl. Fig. 3B**). No impairment in CAP propagation fidelity was detected upon high frequency stimulation (**Suppl. Fig. 3E**). Additionally, the recruitment of the CAPs in C-fibers at 35°C was essentially unchanged in HET mice (**Suppl. Fig. 3F**).

DISCUSSION

It has previously been shown that *Cntanp2* null homozygosity and *Cntnap2* heterozygosity can affect several parameters of neurodevelopment. The *Cntnap2*$^{-/-}$ mouse has often been used as an ASD mouse model, displaying behavioral and morphological abnormalities which at best suggest a possible contribution of *CNTNAP2* mutations to ASD pathology, but at least establish a key role of the protein Caspr2 in neurodevelopment. In the present study, we illustrate that an ER-retained *CNTNAP2* heterozygous missense variant can indeed alter the function of the protein Caspr2, indicating that these types of variants found in ASD patients could potentially contribute to disease pathogenicity. Interestingly, we also provide strong evidence that *CNTNAP2* variants could have sex-dependent effects.

We herein show that the ASD patient variant protein Caspr2-I236S is heavily ER-retained and could be misfolded due to its predicted increased instability in the large N-terminal lobe of the protein. Caspr2 is a large protein with an extracellular region which consists of three main lobes, likely adopting a very compact structure (Lu et al., 2016). The predicted structural changes incurred by the I236S mutation could impact the trafficking of only the mutant protein, or of WT Caspr2 also through oligomerization with the mutant protein in the ER (Canali et al., 2018). Thus, the abnormalities observed in KI-I236S HET mice could be due to reduced Caspr2 levels at the cell surface due to ER-retention and subsequent degradation, or/and to altered Caspr2 function at the cell surface caused by the I236S mutation. Our current data showing a ~30% decrease of Caspr2 level in brains and sciatic nerves of KI-I236S HET mice compared to WT mice strongly suggest that both phenomena co-exist in these mice, although the exact proportion of WT Caspr2 versus Caspr2-I236S cannot be assessed in tissue lysates. Considering the results from the study of the heavily ER-retained Caspr2 variant Caspr2-D1129H by Falivelli et al., misfolding of Caspr2-I236S likely leads to activation of the UPR, including pathways such as ATF6 (Falivelli et al., 2012).

Myelination is a developmental process which relies on cross-talk between the axon and the myelinating glial cells. It is influenced by axonal parameters such as axon diameter and firing rate (Kato & Wake, 2019; Lee et al., 2012). Caspr2 has been implicated in these processes both in the CNS and in the PNS (Scott et al., 2019), (Cifuentes-Diaz et al., 2023). Caspr2 is also known to modulate node of Ranvier formation and organization (Hivert et al., 2016; Horresh et al., 2010; Sebastian Poliak et al., 2003; Traka et al., 2003). We recently showed that both myelination processes and node of Ranvier organization are differentially impacted by *Cntnap2* heterozygosity and *Cntnap2* null homozygosity (Cifuentes-Diaz et al., 2023). Here we observe that the variant

Caspr2-I236S has similar effects on myelin thickness of peripheral fibers of adult male mice as previously observed in *Cntnap2*$^{+/-}$ mice (Cifuentes-Diaz et al., 2023), with an increased G-ratio indicating hypomyelination. By contrast, the variant Caspr2-I236S has opposite effects on node morphology to those observed in *Cntnap2*$^{-/-}$ and *Cntnap2*$^{+/-}$ mice (Cifuentes-Diaz et al., 2023); node diameter and length are increased in KI-I236S HET males whereas decreased node length was observed in *Cntnap2*$^{-/-}$ and *Cntnap2*$^{+/-}$ mice. In addition, the enrichment of TAG-1 at the juxtaparanodes is maintained in KI-I236S HET males as in *Cntnap2*$^{+/-}$ mice, but the global level of the protein in sciatic nerve lysates is decreased whereas it is not affected in as *Cntnap2*$^{+/-}$ mice. Overall, these observations demonstrate that the variant has varying effects on both PNS myelination and node of Ranvier formation in male mice which, apart from being sex-dependent, do not recapitulate either *Cntnap2* heterozygosity or *Cntnap2* null homozygosity. Of note, previous morphological studies in *Cntnap2*$^{-/-}$ and *Cntnap2*$^{+/-}$ mice were performed on pool of male and female mice in so far as the independent analysis of males and females did not reveal obvious differences.

In addition to PNS abnormalities, the I236S variant shows effects on the morphology of myelinated white tracts of the brain, indicating that the variant likely impacts CNS myelination as well. However, CC and AC morphological modifications in KI-I236S HET mice here again do not recapitulate either *Cntnap2* heterozygosity or *Cntnap2* null homozygosity (Cifuentes-Diaz et al., 2023). Both decreased AC area and decreased CC thickness and area were previously observed in *Cntnap2*$^{-/-}$ mice (Cifuentes-Diaz et al., 2023). In this study, we find a decreased AC area in in KI-I236S HET male mice, but without major morphological alterations of the CC. Furthermore, KI-I236S HET female mice do not show AC morphological alterations, but a decrease in CC area. These data strongly suggest that even for a given sex the variant impacts different types of myelinated fibers differentially, likely because of differences in the molecular mechanisms in which Caspr2 could be implicated from one axon to another. Further investigations will be necessary to evaluate the impact of the variant on fiber morphology and myelination at the ultrastructural level.

Sex-dependent morphological alterations KI-I236S HET mice are accompanied by sex-dependent behaviors; KI-I236S HET male mice, but not female mice, show decreased muscular strength and in heat hyposensitivity, which once again contrasts with the heat hypersensitivity previously observed in *Cntnap2*$^{-/-}$ males (Dawes et al., 2018; Xing et al., 2020; Zhang et al., 2021). Decreased muscular strength questions whether the variant could affect neuromuscular junction integrity as previously observed in 6 months-old *Cntnap2*$^{-/-}$ mice (Saifetiarova et al. 2017). Although

electrophysiological studies on sciatic nerves did not reveal obvious conduction abnormalities, heat hyposensitivity in males may be related to the specific morphological alterations observed in C-fibers, which are responsible for relaying nociceptive sensory information from the periphery. A role for Caspr2 in C-fibers is supported by the reactivity along the C-fibers of rat sciatic nerve observed when treated with patient serum containing Caspr2 auto-antibodies, indicating that Caspr2 is located along sensory C-fibers (Gendre et al., 2021). Also and interestingly, increased C-fiber axon diameter was previously observed when the mTORC1 signaling pathway was activated in mouse peripheral sensory neurons by conditional deletion of its negative regulator Tuberous Sclerosis Complex 2 (Tsc2) (Carlin et al., 2018); Tsc2-deleted mice also exhibited reduced noxious heat sensitivity. Hyperactive mTOR signaling was reported in dorsal root ganglia neurons (DRG) of *Cntnap2*$^{-/-}$ mice and treatment with an mTOR inhibitor rapamycin reduced hypersensitivity to heat as well as reduced DRG hyperexcitability (Xing et al., 2020). Given these observations, we could speculate that the increased C-fiber axon diameter and reduced heat sensitivity in KI-I236S HET male mice could be potentially due to a dysregulation of the mTOR pathway.

Previously, *Cntnap2*$^{-/-}$ male mice were shown to present social defects (Jang et al., 2022), and this contributed to conclude that *CNTNAP2* may indeed be an ASD susceptibility gene given the known gender bias in ASD patients (Maenner et al., 2023). Here, behavioral tests revealed that KI-I236S HET female mice, but not male mice, present perturbed social preference, indicating that the I236S variant could favor ASD-like cognitive behaviors in females rather than in males. This assumption is supported by the fact that KI-I236S HET females also showed decreased horizontal locomotor and rearing activities on day 3 of testing in the circular corridor, suggesting decrease in exploration capacities. However, these observations are puzzling since the variant was identified in a boy affected by ASD and in his mother who was described as non-affected by the pathology. One explanation for the mother's lack of diagnosis could be that any social abnormalities are very mildly affected and isolated. We indeed found that KI-I236S HET females do not present obvious stereotypical behaviors, indicating that the I236S variant could likely be not sufficient to induce the full clinical presentation of ASD in women. Regarding male gender, Caspr2 dysfunction might not be sufficient for the development of ASD cognitive symptoms, additional genetic, epigenetic and/or environmental events being required.

One can question the mechanisms that may underlie both morphological and behavioral differences between KI-I236S HET male and female mice. Recently, Gegenhuber and colleagues showed that the transcription factor oestrogen receptor-α (ERα) could underlie several sex

differences in the brain by studying the genomic targets of ERα (Gegenhuber et al., 2022). They interestingly identified brain-specific ERα binding events enriched for synaptic and neurodevelopmental disease Gene Ontology terms, including *CNTNAP2*/Caspr2, indicating that *CNTNAP2* expression could be regulated by oestradiaol. Our results show that the overall level of Caspr2 proteins in brains and sciatic nerves of KI-I236S HET mice are not significantly different between males and females. However, we cannot totally exclude the existence a slight but sufficient difference in Caspr2 level between the two sexes that could account for a differential impact of the I236S variant at the cellular level, as we observed a decreased tendency for *Cntnap2* mRNA level in the brains of KI-I236S HET females (Fig. 2F). This issue merits further study.

In conclusion, we have characterized an ER-retained *CNTNAP2* variant identified in an ASD patient *in vivo* for the first time, providing evidence that this group of variants can affect the functions of Caspr2, leading to PNS and CNS morphological and behavioral alterations in a sex-dependent manner. Further investigations will be required to determine whether the variant alters brain function, notably synapse function, and local and long-range brain connectivity in which Caspr2 has been implicated (Liska et al., 2018; Zerbi et al., 2018). Our observations nevertheless strongly suggest that at least some ER-retained *CNTNAP2* variants could provide a genetic background conferring susceptibility for the development of ASD-like symptoms. However, our study also raises the intriguing question of whether in a non-pathological context ER-retained *CNTNAP2* missense variant could contribute to inter-individual variability. Currently more than 400 heterozygous *CNTNAP2* missense variants have been identified in individuals of the global population (https://gnomad.broadinstitute.org). Studying eight variants distributed in different subdomains of the extracellular of Caspr2, we previously showed that they lead to various degrees of ER retention of the mutant proteins (Canali et al, 2018), suggesting that the *CNTNAP2* variants could induce a continuum of phenotypes *in vivo*.

REFERENCES

Arking, D. E., Cutler, D. J., Brune, C. W., Teslovich, T. M., West, K., Ikeda, M., Rea, A., Guy, M., Lin, S., Cook, E. H., & Chakravarti, A. (2008). A common genetic variant in the neurexin superfamily member CNTNAP2 increases familial risk of autism. *American Journal of Human Genetics*, *82*(1), 160–164.

Bakkaloglu, B., O'Roak, B. J., Louvi, A., Gupta, A. R., Abelson, J. F., Morgan, T. M., Chawarska, K., Klin, A., Ercan-Sencicek, A. G., Stillman, A. A., Tanriover, G., Abrahams, B. S., Duvall, J. A., Robbins, E. M., Geschwind, D. H., Biederer, T., Gunel, M., Lifton, R. P., & State, M. W. (2008). Molecular cytogenetic analysis and resequencing of contactin associated protein-like 2 in autism spectrum disorders. *American Journal of Human Genetics*, *82*(1), 165–173.

Balasco, L., Pagani, M., Pangrazzi, L., Chelini, G., Viscido, F., Chama, A. G. C., Galbusera, A., Provenzano, G., Gozzi, A., & Bozzi, Y. (2022). Somatosensory cortex hyperconnectivity and impaired whisker-dependent responses in Cntnap2-/- mice. *Neurobiology of Disease*, *169*, 105742.

Canali, G., Garcia, M., Hivert, B., Pinatel, D., Goullancourt, A., Oguievetskaia, K., Saint-Martin, M., Girault, J.-A., Faivre-Sarrailh, C., & Goutebroze, L. (2018). Genetic variants in autism-related CNTNAP2 impair axonal growth of cortical neurons. *Human Molecular Genetics*, *27*(11), 1941–1954.

Canali, G., & Goutebroze, L. (2018). CNTNAP2 Heterozygous Missense Variants: Risk Factors for Autism Spectrum Disorder and/or Other Pathologies? [Review of *CNTNAP2 Heterozygous Missense Variants: Risk Factors for Autism Spectrum Disorder and/or Other Pathologies?*]. *Journal of Experimental Neuroscience*, *12*, 1179069518809666.

Carlin, D., Golden, J. P., Mogha, A., Samineni, V. K., Monk, K. R., Gereau, R. W., 4th, & Cavalli, V. (2018). Deletion of Tsc2 in Nociceptors Reduces Target Innervation, Ion Channel Expression, and Sensitivity to Heat. *ENeuro*, *5*(2). https://doi.org/10.1523/ENEURO.0436-17.2018

Choe, K. Y., Bethlehem, R. A. I., Safrin, M., Dong, H., Salman, E., Li, Y., Grinevich, V., Golshani, P., DeNardo, L. A., Peñagarikano, O., Harris, N. G., & Geschwind, D. H. (2022). Oxytocin normalizes altered circuit connectivity for social rescue of the Cntnap2 knockout mouse. *Neuron*, *110*(5), 795-808.e6.

Cifuentes-Diaz, C., Canali, G., Garcia, M., Druart, M., Manett, T., Savariradjane, M., Guillaume, C., Le Magueresse, C., & Goutebroze, L. (2023). Differential impacts of Cntnap2 heterozygosity and Cntnap2 null homozygosity on axon and myelinated fiber development in mouse. *Frontiers in Neuroscience*, *17*. https://doi.org/10.3389/fnins.2023.1100121

Dawes, J. M., Weir, G. A., Middleton, S. J., Patel, R., Chisholm, K. I., Pettingill, P., Peck, L. J., Sheridan, J., Shakir, A., Jacobson, L., Gutierrez-Mecinas, M., Galino, J., Walcher, J., Kühnemund, J., Kuehn, H., Sanna, M. D., Lang, B., Clark, A. J., Themistocleous, A. C., … Bennett, D. L. (2018). Immune or Genetic-Mediated Disruption of CASPR2 Causes Pain Hypersensitivity Due to Enhanced Primary Afferent Excitability. *Neuron*, *97*(4), 806-822.e10.

Deemyad, T., Puig, S., Papale, A. E., Qi, H., LaRocca, G. M., Aravind, D., LaNoce, E., & Urban, N. N. (2022). Lateralized Decrease of Parvalbumin+ Cells in the Somatosensory Cortex of ASD Models Is Correlated with Unilateral Tactile Hypersensitivity. *Cerebral Cortex* , *32*(3), 554–568.

Denisenko-Nehrbass, N., Oguievetskaia, K., Goutebroze, L., Galvez, T., Yamakawa, H., Ohara, O., Carnaud, M., & Girault, J.-A. (2003). Protein 4.1B associates with both Caspr/paranodin and Caspr2 at paranodes and juxtaparanodes of myelinated fibres. *The European Journal of Neuroscience*, *17*(2), 411–416.

Falivelli, G., De Jaco, A., Favaloro, F. L., Kim, H., Wilson, J., Dubi, N., Ellisman, M. H., Abrahams, B. S., Taylor, P., & Comoletti, D. (2012). Inherited genetic variants in autism-related CNTNAP2 show perturbed trafficking and ATF6 activation. *Human Molecular Genetics*, *21*(21), 4761–4773.

Gegenhuber, B., Wu, M. V., Bronstein, R., & Tollkuhn, J. (2022). Gene regulation by gonadal hormone receptors underlies brain sex differences. *Nature*, *606*(7912), 153–159.

Gendre, T., Lefaucheur, J.-P., Devaux, J., & Créange, A. (2021). A patient with distal lower extremity neuropathic pain and anti-contactin-associated protein-2 antibodies. *Muscle & Nerve*, *64*(3), E15–E17.

Hivert, B., Pinatel, D., Labasque, M., Tricaud, N., Goutebroze, L., & Faivre-Sarrailh, C. (2016). Assembly of juxtaparanodes in myelinating DRG culture: Differential clustering of the Kv1/Caspr2 complex and scaffolding protein 4.1B. *Glia*, *64*(5), 840–852.

Horresh, I., Bar, V., Kissil, J. L., & Peles, E. (2010). Organization of myelinated axons by Caspr and Caspr2 requires the cytoskeletal adapter protein 4.1B. *The Journal of Neuroscience: The Official Journal of the Society for Neuroscience*, *30*(7), 2480–2489.

Jang, W. E., Park, J. H., Park, G., Bang, G., Na, C. H., Kim, J. Y., Kim, K.-Y., Kim, K. P., Shin, C. Y., An, J.-Y., Lee, Y.-S., & Kim, M.-S. (2022). Cntnap2-dependent molecular networks in autism spectrum disorder revealed through an integrative multi-omics analysis. *Molecular Psychiatry*. https://doi.org/10.1038/s41380-022-01822-1

Kaiser, T., Allen, H. M., Kwon, O., Barak, B., Wang, J., He, Z., Jiang, M., & Feng, G. (2021). MyelTracer: A Semi-Automated Software for Myelin g-Ratio Quantification. *ENeuro*, *8*(4). https://doi.org/10.1523/ENEURO.0558-20.2021

Kato, D., & Wake, H. (2019). Activity-Dependent Myelination. *Advances in Experimental Medicine and Biology*, *1190*, 43–51.

Lee, S., Leach, M. K., Redmond, S. A., Chong, S. Y. C., Mellon, S. H., Tuck, S. J., Feng, Z.-Q., Corey, J. M., & Chan, J. R. (2012). A culture system to study oligodendrocyte myelination processes using engineered nanofibers. *Nature Methods*, *9*(9), 917–922.

Liska, A., Bertero, A., Gomolka, R., Sabbioni, M., Galbusera, A., Barsotti, N., Panzeri, S., Scattoni, M. L., Pasqualetti, M., & Gozzi, A. (2018). Homozygous Loss of Autism-Risk Gene CNTNAP2 Results in Reduced Local and Long-Range Prefrontal Functional Connectivity. *Cerebral Cortex* , *28*(4), 1141–1153.

Lu, Z., Reddy, M. V. V. V. S., Liu, J., Kalichava, A., Liu, J., Zhang, L., Chen, F., Wang, Y., Holthauzen, L. M. F., White, M. A., Seshadrinathan, S., Zhong, X., Ren, G., & Rudenko, G. (2016). Molecular Architecture of Contactin-associated Protein-like 2 (CNTNAP2) and Its Interaction with Contactin 2 (CNTN2)*. *The Journal of Biological Chemistry*, *291*(46), 24133–24147.

Maenner, M. J., Warren, Z., Williams, A. R., Amoakohene, E., Bakian, A. V., Bilder, D. A., Durkin, M. S., Fitzgerald, R. T., Furnier, S. M., Hughes, M. M., Ladd-Acosta, C. M., McArthur, D., Pas, E. T., Salinas, A., Vehorn, A., Williams, S., Esler, A., Grzybowski, A., Hall-Lande, J., … Shaw, K. A. (2023). Prevalence and Characteristics of Autism Spectrum Disorder Among Children Aged 8 Years - Autism and Developmental Disabilities Monitoring Network, 11 Sites, United States, 2020. *Morbidity and Mortality Weekly Report. Surveillance Summaries* , *72*(2), 1–14.

Martin, P.-M., Cifuentes-Diaz, C., Devaux, J., Garcia, M., Bureau, J., Thomasseau, S., Klingler, E., Girault, J.-A., & Goutebroze, L. (2017). Schwannomin-interacting Protein 1 Isoform IQCJ-SCHIP1 Is a Multipartner Ankyrin- and Spectrin-binding Protein Involved in the Organization of Nodes of Ranvier. *The Journal of Biological Chemistry*, *292*(6), 2441–2456.

Menegoz, M., Gaspar, P., Le Bert, M., Galvez, T., Burgaya, F., Palfrey, C., Ezan, P., Arnos, F., & Girault, J. A. (1997). Paranodin, a glycoprotein of neuronal paranodal membranes. *Neuron*, *19*(2), 319–331.

Mishra, S. K. (2022). The Role of CNTNAP2 in Itch Sensation. *The Journal of Investigative Dermatology*, *142*(1), 251–253.

Murdoch, J. D., Gupta, A. R., Sanders, S. J., Walker, M. F., Keaney, J., Fernandez, T. V., Murtha, M. T., Anyanwu, S., Ober, G. T., Raubeson, M. J., DiLullo, N. M., Villa, N., Waqar, Z., Sullivan, C.,

Gonzalez, L., Willsey, A. J., Choe, S.-Y., Neale, B. M., Daly, M. J., & State, M. W. (2015). No evidence for association of autism with rare heterozygous point mutations in Contactin-Associated Protein-Like 2 (CNTNAP2), or in Other Contactin-Associated Proteins or Contactins. *PLoS Genetics*, *11*(1), e1004852.

Peñagarikano, O., Abrahams, B. S., Herman, E. I., Winden, K. D., Gdalyahu, A., Dong, H., Sonnenblick, L. I., Gruver, R., Almajano, J., Bragin, A., Golshani, P., Trachtenberg, J. T., Peles, E., & Geschwind, D. H. (2011). Absence of CNTNAP2 leads to epilepsy, neuronal migration abnormalities, and core autism-related deficits. *Cell*, *147*(1), 235–246.

Poliak, S., Gollan, L., Martinez, R., Custer, A., Einheber, S., Salzer, J. L., Trimmer, J. S., Shrager, P., & Peles, E. (1999). Caspr2, a new member of the neurexin superfamily, is localized at the juxtaparanodes of myelinated axons and associates with K+ channels. *Neuron*, *24*(4), 1037–1047.

Poliak, S., Gollan, L., Salomon, D., Berglund, E. O., Ohara, R., Ranscht, B., & Peles, E. (2001). Localization of Caspr2 in myelinated nerves depends on axon-glia interactions and the generation of barriers along the axon. *The Journal of Neuroscience: The Official Journal of the Society for Neuroscience*, *21*(19), 7568–7575.

Poliak, Sebastian, Salomon, D., Elhanany, H., Sabanay, H., Kiernan, B., Pevny, L., Stewart, C. L., Xu, X., Chiu, S.-Y., Shrager, P., Furley, A. J. W., & Peles, E. (2003). Juxtaparanodal clustering of Shaker-like K+ channels in myelinated axons depends on Caspr2 and TAG-1. *The Journal of Cell Biology*, *162*(6), 1149–1160.

Rodrigues, C. H., Pires, D. E., & Ascher, D. B. (2018). DynaMut: predicting the impact of mutations on protein conformation, flexibility and stability. *Nucleic Acids Research*, *46*(W1), W350–W355.

Rylaarsdam, L., & Guemez-Gamboa, A. (2019). Genetic Causes and Modifiers of Autism Spectrum Disorder. *Frontiers in Cellular Neuroscience*, *13*, 385.

Saint-Martin, M., Joubert, B., Pellier-Monnin, V., Pascual, O., Noraz, N., & Honnorat, J. (2018). Contactin-associated protein-like 2, a protein of the neurexin family involved in several human diseases. *The European Journal of Neuroscience*, *48*(3), 1906–1923.

Sampath, S., Bhat, S., Gupta, S., O'Connor, A., West, A. B., Arking, D. E., & Chakravarti, A. (2013). Defining the contribution of CNTNAP2 to autism susceptibility. *PloS One*, *8*(10), e77906.

Scott, R., Sánchez-Aguilera, A., van Elst, K., Lim, L., Dehorter, N., Bae, S. E., Bartolini, G., Peles, E., Kas, M. J. H., Bruining, H., & Marín, O. (2019). Loss of Cntnap2 Causes Axonal Excitability

Deficits, Developmental Delay in Cortical Myelination, and Abnormal Stereotyped Motor Behavior. *Cerebral Cortex* , *29*(2), 586–597.

Traka, M., Goutebroze, L., Denisenko, N., Bessa, M., Nifli, A., Havaki, S., Iwakura, Y., Fukamauchi, F., Watanabe, K., Soliven, B., Girault, J.-A., & Karagogeos, D. (2003). Association of TAG-1 with Caspr2 is essential for the molecular organization of juxtaparanodal regions of myelinated fibers. *The Journal of Cell Biology*, *162*(6), 1161–1172.

Xing, X., Wu, K., Dong, Y., Zhou, Y., Zhang, J., Jiang, F., Hu, W.-P., & Li, J.-D. (2020). Hyperactive Akt-mTOR pathway as a therapeutic target for pain hypersensitivity in Cntnap2-deficient mice. *Neuropharmacology*, *165*, 107816.

Xing, X., Zhang, J., Wu, K., Cao, B., Li, X., Jiang, F., Hu, Z., Xia, K., & Li, J.-D. (2019). Suppression of Akt-mTOR pathway rescued the social behavior in Cntnap2-deficient mice. *Scientific Reports*, *9*(1), 3041.

Zerbi, V., Ielacqua, G. D., Markicevic, M., Haberl, M. G., Ellisman, M. H., A-Bhaskaran, A., Frick, A., Rudin, M., & Wenderoth, N. (2018). Dysfunctional Autism Risk Genes Cause Circuit-Specific Connectivity Deficits With Distinct Developmental Trajectories. *Cerebral Cortex* , *28*(7), 2495–2506.

Zhang, Z., Yao, Z., Wu, K., Zhang, T., Xing, C., & Xing, X.-L. (2021). Resveratrol rescued the pain related hypersensitivity for Cntnap2-deficient mice. *European Journal of Pharmacology*, *891*, 173704.

TABLE 1: Electrophysiological characteristics of sciatic nerves from WT and HET males at 35°C.

	WT	HET
	A-fibers	
Amplitude (mV)	13.8 ± 4.2	13.0 ± 4.1
CV $V_{1/2}$ ($m.s^{-1}$)	76.0 ± 6.5	73.1 ± 5.2
CV V_{max} ($m.s^{-1}$)	47.1 ± 4.4	45.9 ± 4.7
Duration $V_{1/2}$ (ms)	0.33 ± 0.04	0.32 ± 0.04

n represents the number of nerves tested, the number of animals is indicated in parentheses. Data are means ± SD. Statistical analyses: two-tailed *t*-tests for two samples of equal variance, non-significant.

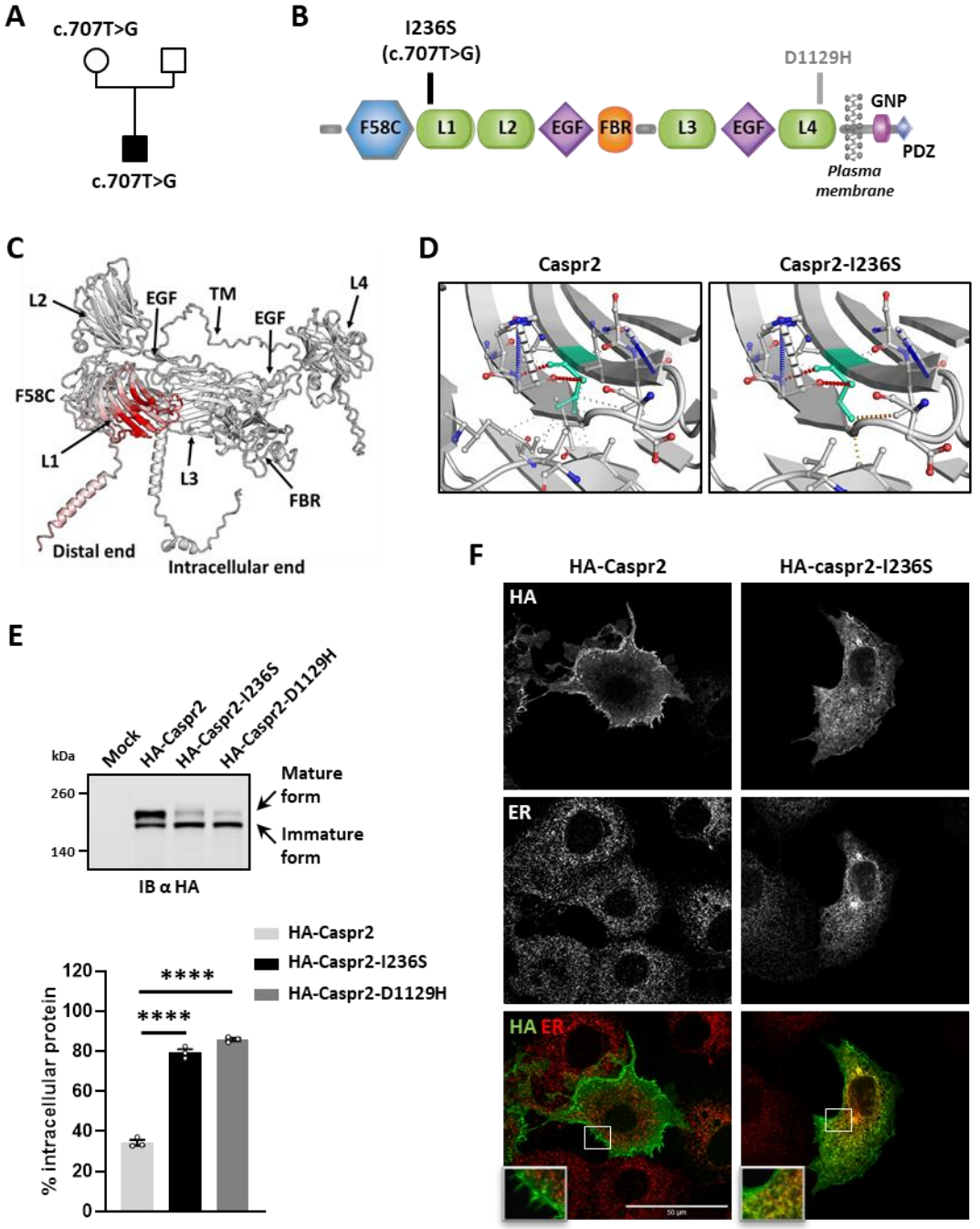

FIGURE 1 | Identification and characterization of the I236S variant. (A) Pedigree of the family where the variant c.707T>G/I236S was identified. **(B)** Domain organization of Caspr2 and position of the variants I236S and D1129H. F58C, discoidin domain; L1-L4, laminin G domains; FBR, fibrinogen-like domain; EGF, EGF-like domains; GNP, "Glycophorin C-Neurexin IV-Paranodin" motif; PDZ-B, PDZ-binding motif. **(C)** Caspr2-I236S overall structure, with amino acids colored according to the vibrational entropy change upon mutation with red representing a gain in flexibility (DynaMut software). **(D)** Caspr2 and Caspr2-I236S structure predictions around position 236 (DynaMut software). Position 236 is in light blue. Hydrogen bonds and halogen bonds are indicated in red end blue, respectively. For wild-type Caspr2,

weak interactions at position 236 are indicated in light gray dotted lines. For Caspr2-IS236S, notable change is a gain in weak hydrogen bonds shown in orange and Ionic interactions in yellow, and loss of several other weak interactions. **(E)** Intracellular retention of the variants I236S and D1129H in transfected COS-7 cells. Upper panel, representative immunoblotting (IB) of 3 independent experiments performed on lysates from transfected COS-7 cells expressing HA-Caspr2 or the HA-Caspr2 variants, with HA antibodies (αHA). The mature and immature forms of the proteins are indicated by arrows. Molecular mass markers are shown in kDa on the left of the panels. Bottom panel, quantification of the % of immature form for each protein normalized to its total expression (mature and immature forms). **(F)** Representative images of the subcellular localization of HA-Caspr2 and HA-Caspr2-I236S in transfected COS-7 cells immunolabeled with antibodies directed against HA (Caspr2/Caspr2-I236S, Green) and the ER marker KDEL (red). Single confocal sections. Inserts, high magnification of white squares. Statistical analyses: (E, bottom panel) Means ± SEM; Unpaired t test to compare each variant to HA-Caspr2, ****P<0.0001.

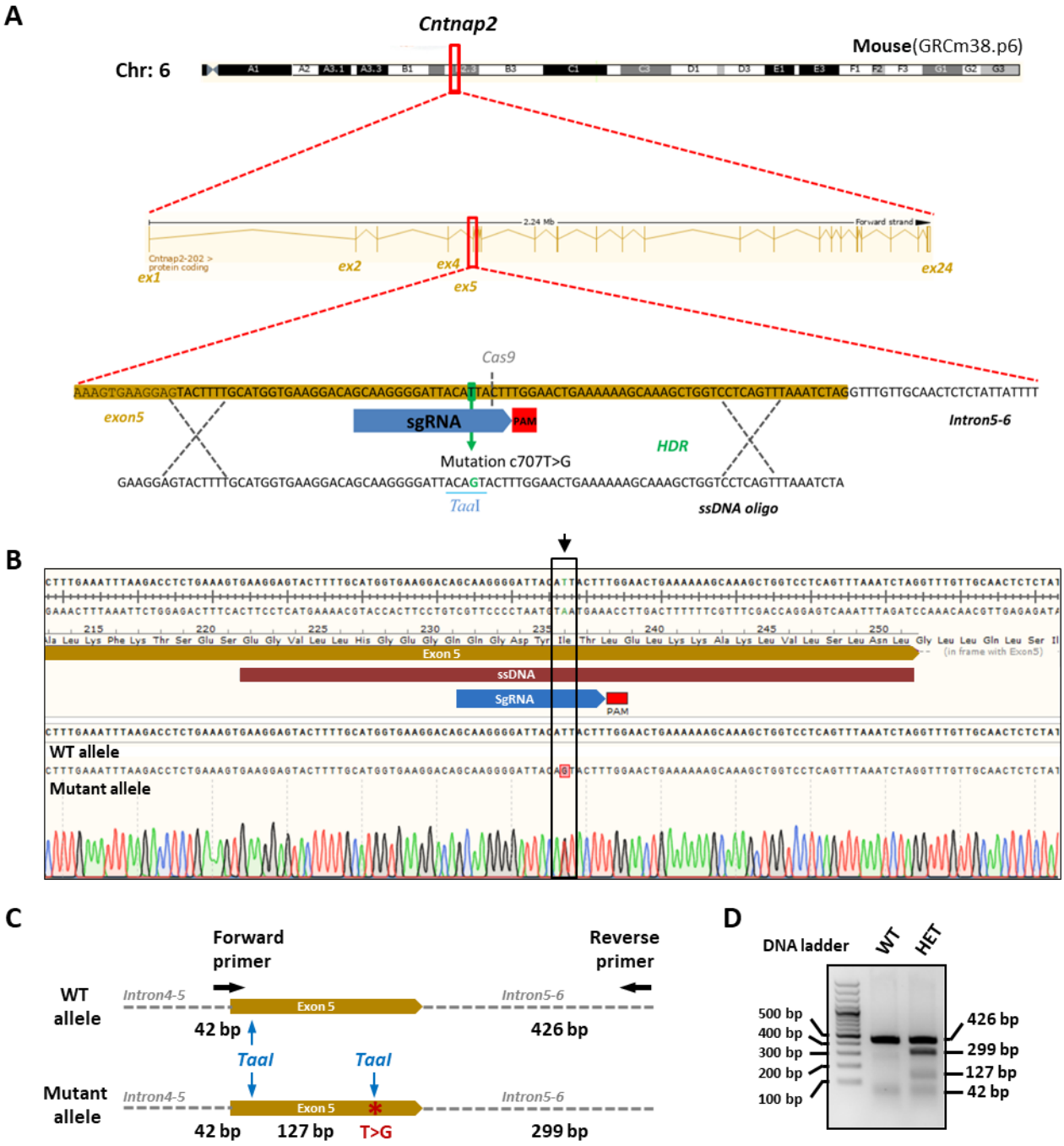

Supplementary Figure S1 | Generation of KI-I236S mice and genotyping. (A) Schema of the sgRNA CRISPR/Cas9 strategy used to generate the mutant mice, showing *Cntnap2* genomic locus and the sgRNA sequence. The mutation c707T>G in *Cntnap2* exon 5 leads to the introduction of a digestion site for the restriction enzyme TaaI (HpyCH4III) site. **(B)** Validation of the mutation by sequencing. **(C)** Schema of the genotyping strategy by PCR of tail-tip genomic DNA with primers Forward and Reverse amplifying a 468-bp product, and subsequent digestion with TaaI leading to 2 products for the WT allele (426 bp, 42 bp), and three products for the mutant allele (299 bp, 127bp, 42 bp). **(D)** PCR analysis on genomic DNAs of WT and HET mice (2% agarose gel, 100 bp ladder).

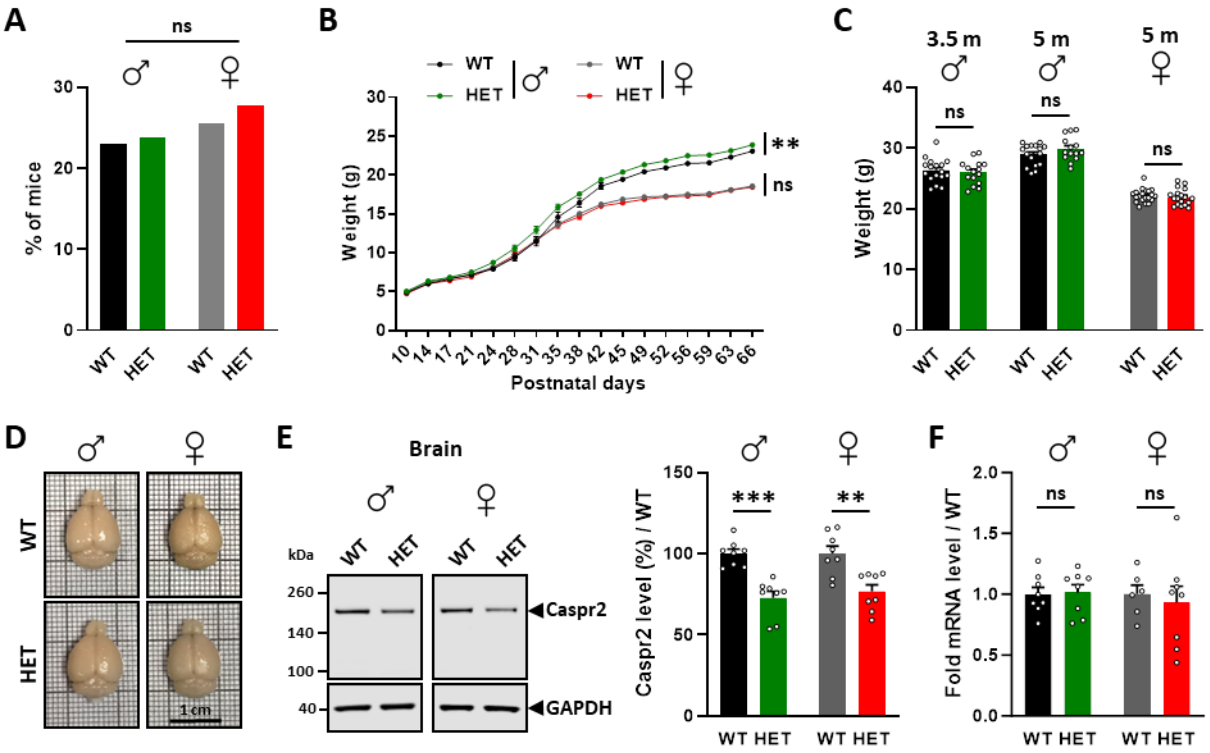

FIGURE 2 | General characterization of KI-I236S mouse model. (A) Percentage of males and females of different genotypes (WT/HET) in litters from WT x HET crossings. **(B)** Weights of males and females, WT or HET, from postnatal (P) day 10 to ~two months (P66). **(C)** Weights of males, WT or HET, at ~3.5 months (m) and ~5 months, and of females, WT or HET, at ~5 months. **(D)** Representative photos from the brains of adult males and females, WT or HET. **(E)** Left panel, representative immunoblots showing Caspr2 and GAPDH levels in the brains of adult males and females, WT or HET. Molecular mass markers are shown in kDa on the left of the panels. Right panel, Caspr2 levels normalized to GAPDH levels and relative to mean WT (in %). **(F)** Levels of *Cntnap2* mRNAs normalized to the *Psap* gene and relative to mean WT in the brains of adult males and females, WT or HET. (**A**) 576 mice from 89 litters, mean > 6 mice/litter; (**B**) Females n=28 WT-28 HET, males n=17 WT-27 HET; (**C**) 3.5 month-old males n =17 WT–15 HET; 5 month-old males n=16 WT-14HET, 5 month-old females n=20 WT–18 HET, (**E**) Left panel, 8 mice/genotype/sex; (**F**) 8 males/genotype; 6-8 females/genotype. Statistical tests: (A) Fisher's exact test; (B) Means ± SEM, Two-way RM ANOVA to compare the 2 genotypes for each sex; (C) Means ± SEM, Unpaired t test or Mann Whitney test to compare the 2 genotypes for each sex and each age; (E) Means ± SEM, Unpaired t test or Mann Whitney test to compare the 2 genotypes for each sex; (F) Means ± SEM, Unpaired t test to compare the 2 genotypes for each sex; ***P<0.001, **P<0.01, ns non-significant.

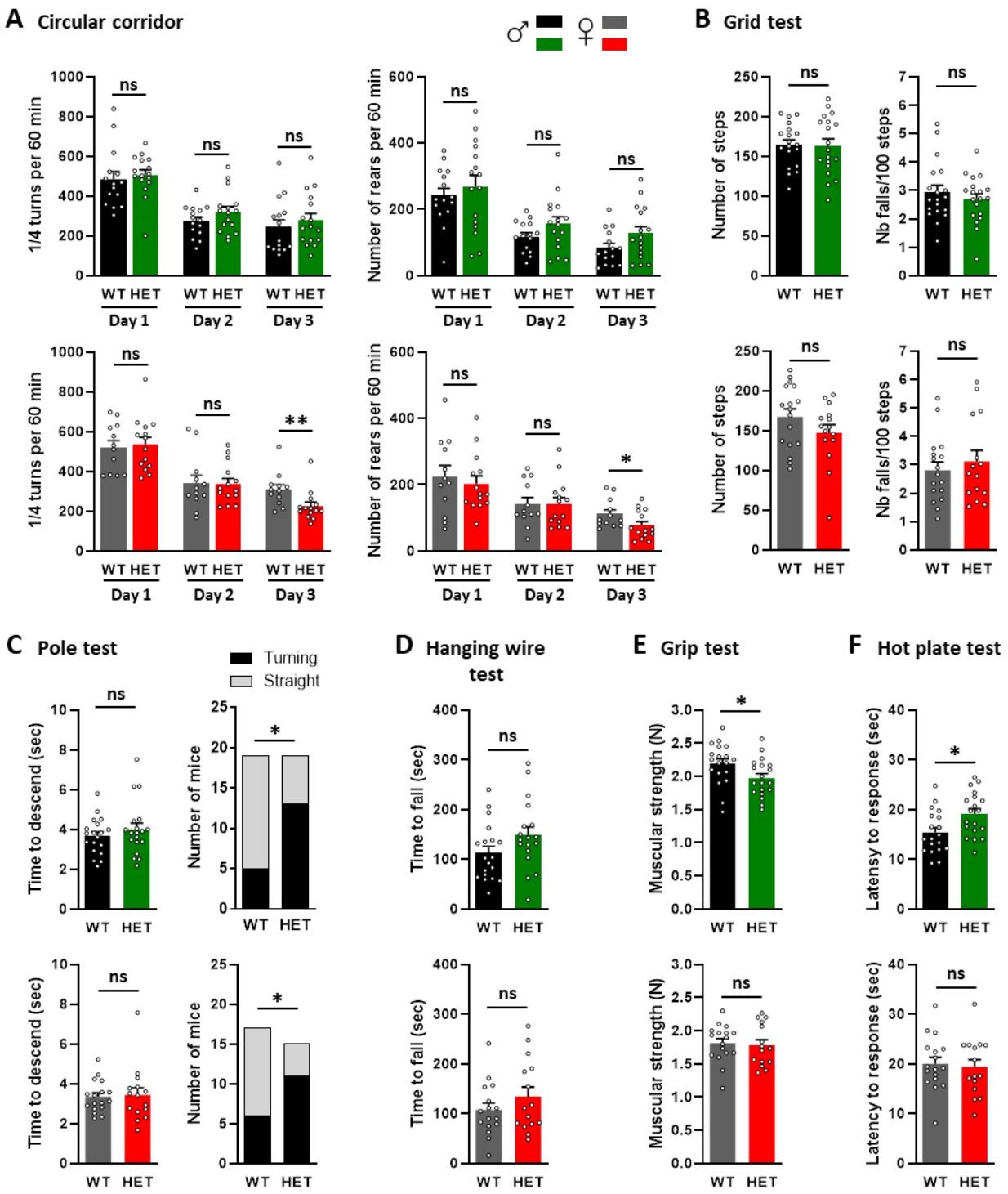

FIGURE 3 | Spontaneous locomotor activity, motor coordination, muscular strength and heat sensitivity of mutant mice. (A) Cumulative horizontal locomotor activity (left panels, number of

¼ turns) and rearing activity (right panels, number or rears) for 60 minutes during three consecutive days in the dark in a circular corridor. **(B)** Grid test: number of steps (left panels) and falls per 100 steps (right panels) during 2 min. **(C)** Pole test: time to descend in seconds (sec, left panels) and strategy adopted to descend (number of mice, right panels). **(D)** Hanging wire test: latency to fall from the grid in seconds (sec). **(E)** Grip test: muscular strength in Newton (N). **(F)** Hot plate test: latency in seconds (sec) to a hind paw response or jumping. (**A**) Females n=12 WT-14 HET, males n=15 WT–16 HET; (**B, C, E, F**) Females n= 17 WT-15 HET, males n=19 WT–19 HET; (**D**) Females n= 16 WT-15 HET, males n=19 WT–18 HET. Statistical analyses: (A, B, C left panel, D-F) Means ± SEM; Unpaired t test or Mann Whitney test to compare the 2 genotypes; (C, right panel) Fisher's exact test; (A) Two-way RM ANOVA for genotype effect, day effect, and genotype/day interaction, to compare the 2 genotypes over the 3 consecutive days, followed by Dunnett's multiple comparisons post-tests to compare Days 3 to Day 1 for each genotype. Males or females, locomotor or rearing activity: day, $P<0.0001$; interaction, non-significant. Day 3 *versus* Day 1: males, locomotion or rearing, WT $P<0.0001$, HET $P<0.001$; females, locomotion, WT $P<0.001$, HET $P<0.0001$; females, rearing, WT $P<0.01$, HET $P<0.001$. $^{**}P<0.01$, $^{*}P<0.05$, ns non-significant.

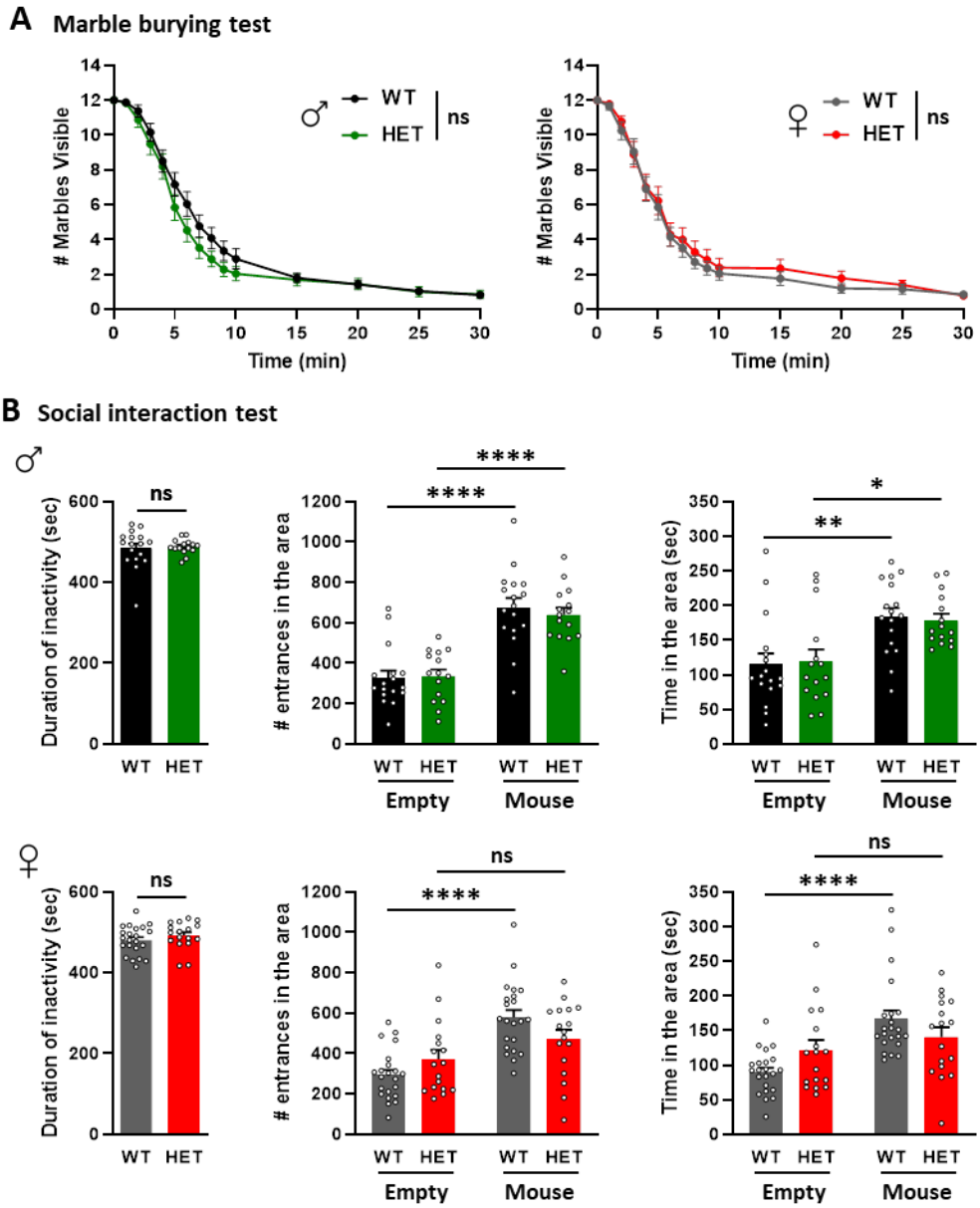

FIGURE 4 | Stereotypical, anxiety and social interaction behaviors of mutant mice. (A) Marble burying test: Number of buried marbles over time. **(B)** Social preference test. Duration of inactivity (left panels), number of entrances (central panels) and time spent (right panels) in the area of the empty box and of the box containing an unfamiliar congener, respectively, for 10 consecutive minutes. (**A**) Females n=20 WT-18 HET, males n=26 WT–25 HET; (**B**) Females n=22 WT-18 HET, males n=17 WT–15 HET. Statistical analyses: (A) Means ± SEM, Two-way RM ANOVA test to compare the 2 genotypes over time; (B, left panels) Means ± SEM, Unpaired t test to compare the 2 genotypes; (B, central and right panels) Means ± SEM, Two-way RM ANOVA test for genotype effect, box preference, and genotype/box preference interaction, followed by Šídák's multiple comparisons tests for to compare box preference for each genotype. Males, number of entrances and time spent in the area: genotype, non-significant; box preference, $P<0.0001$; interaction, non-significant. Females, number of entrances in the area: genotype, non-significant; box preference, $P<0.0001$; interaction, $P<0.05$. Females, time spent in the area: genotype, non-significant; box preference, $P<0.0001$; interaction, $P=0.0645$. ****$P<0.0001$, **$P<0.01$, *$P<0.05$, ns non-significant.

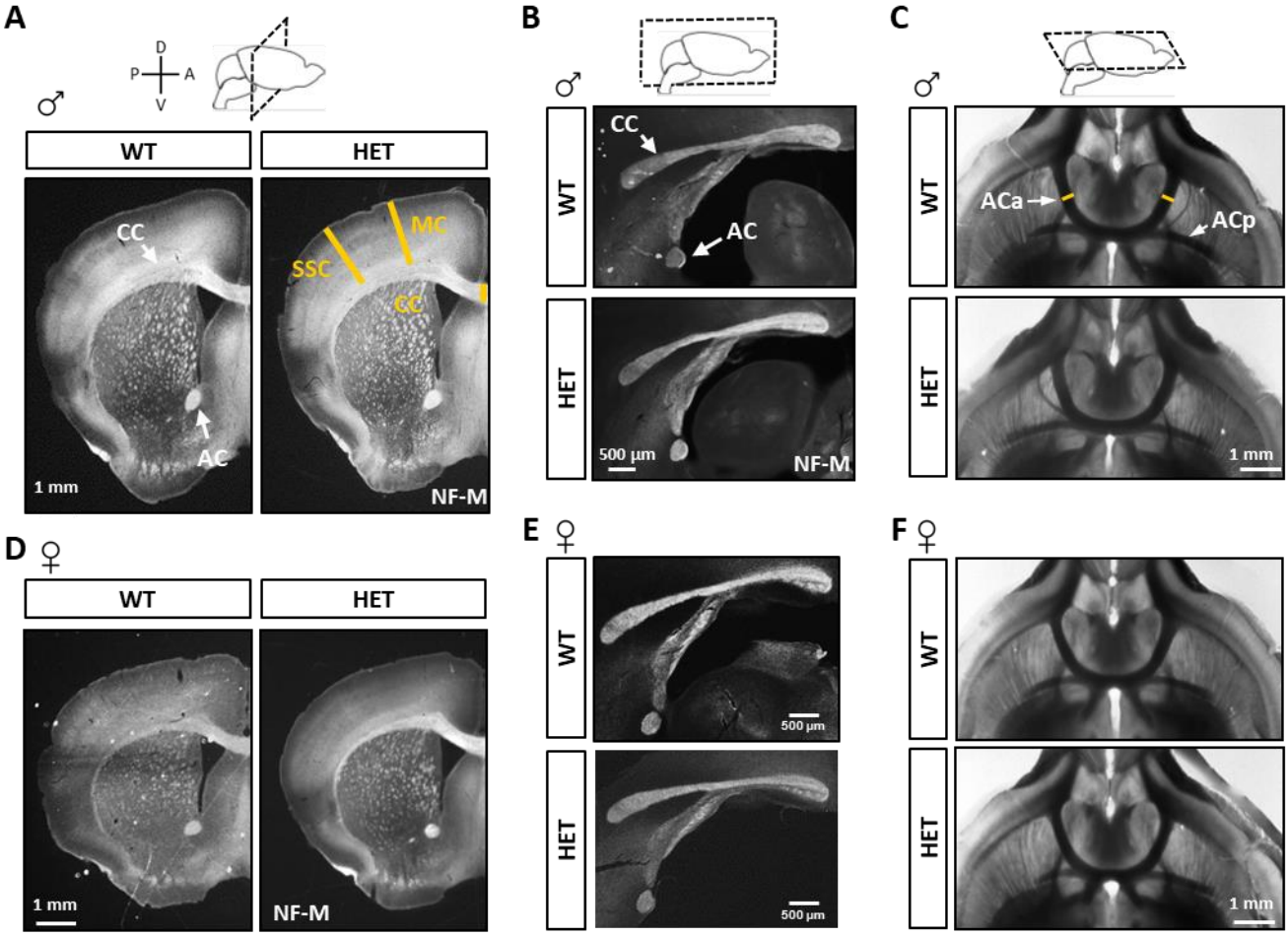
A
♂
D
P
A
V
WT
HET
CC
AC
1 mm
SSC
MC
NF-M
B
♂
WT
HET
CC
AC
500 µm
NF-M
C
♂
WT
HET
ACa
ACp
1 mm
D
♀
WT
HET
1 mm
NF-M
E
♀
WT
HET
500 µm
500 µm
F
♀
WT
HET
1 mm

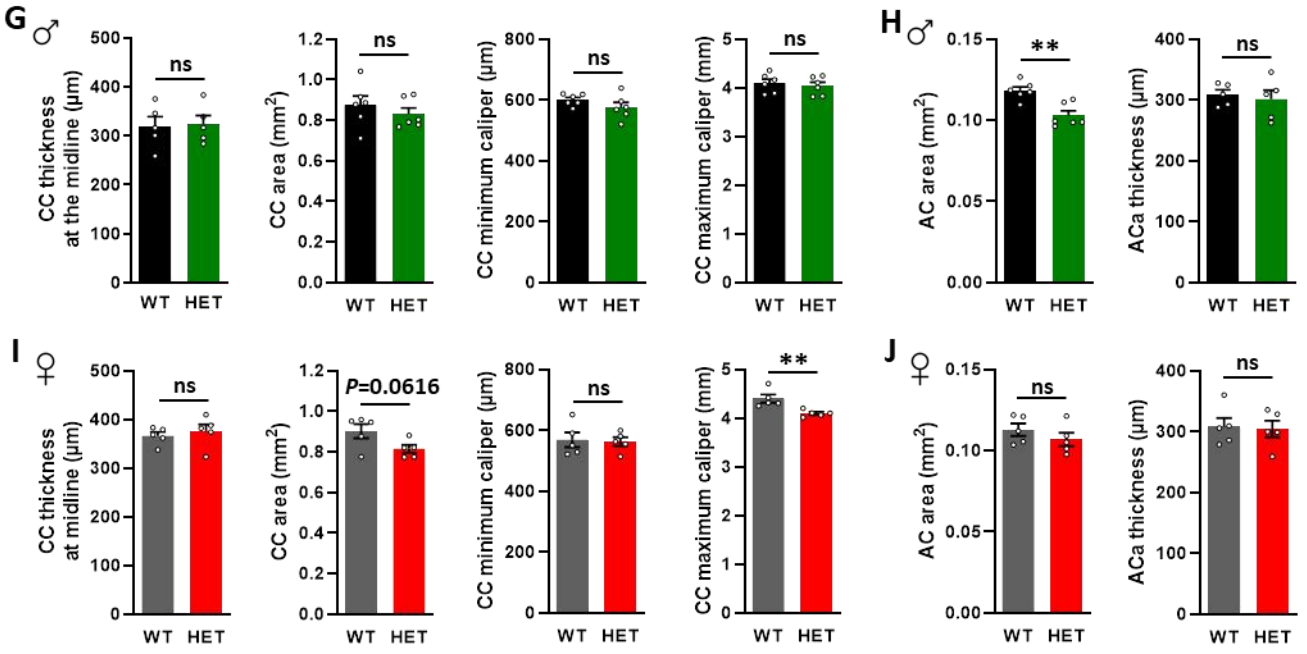
G
♂
CC thickness at the midline (µm)
ns
CC area (mm²)
ns
CC minimum caliper (µm)
ns
CC maximum caliper (mm)
ns
WT HET
H
♂
AC area (mm²)
**
ACa thickness (µm)
ns
WT HET
I
♀
CC thickness at midline (µm)
ns
CC area (mm²)
P=0.0616
CC minimum caliper (µm)
ns
CC maximum caliper (mm)
**
WT HET
J
♀
AC area (mm²)
ns
ACa thickness (µm)
ns
WT HET

FIGURE 5 | Brain morphology in 3 month-old mice. (A, D) Representative images of brain coronal sections at Bregma +0.55 of WT and HET males (A) and females (D) showing the CC and the AC immunostained with anti-NF-M antibodies; yellow lines, levels where MC, SSC and CC thickness measurements were performed. **(B, E)** Representative images of mid-sagittal brain sections of WT and HET males (B) and females (E), showing the CC and the AC immunostained with anti-NF-M antibodies. **(C, F)** Representative phase-contrast images of horizontal brain sections of WT and HET males (C) and females (E), showing the two branches of the AC, the anterior branch (ACa) and the posterior branch (ACp); yellow lines, levels where the thickness of the ACa was measured. **(G, I)** CC thickness at the midline measured on brain coronal sections (A, D), and CC area, minimum caliper and maximum caliper measured on mid-sagittal brain sections (B, E) in males (G) and females (I). **(H, J)** AC area measured on mid-sagittal brain sections (B, E) and ACa thickness measured on horizontal brain sections (C, F) in males (H) and females (J). (**G-J**) 5 animals/genotype; (**G, I**) CC thickness at the midline, average of measurements on three consecutive sections/animal; CC area, minimum caliper and maximum caliper, average of measurements on three consecutive sections/animal; (**H, J**) AC area**,** average of measurements on three consecutive sections/animal; ACa thickness, average of measurements on both hemispheres on one section/animal. Statistical tests: (G-J) Means ± SEM, Unpaired t test or Mann Whitney test to compare the two genotypes; $^{**}P<0.01$, ns non-significant.

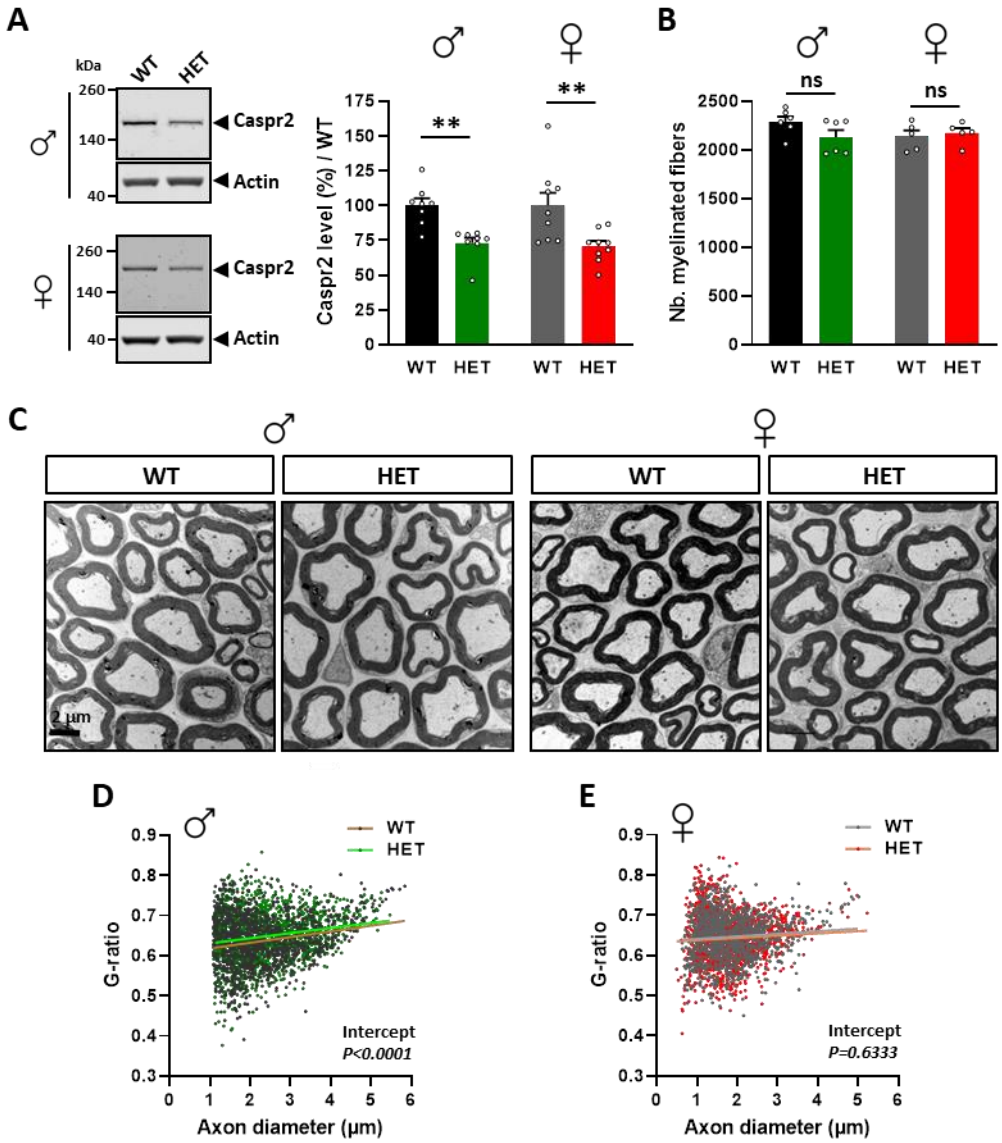

FIGURE 6 | Myelinated fiber abnormalities in sciatic nerves from ~4.5 month-old mice. (A) Left panel, representative immunoblots showing Caspr2 and actin levels in the sciatic nerves of adult males and females, WT or HET. Molecular mass markers are shown in kDa on the left of the panels. Right panel, Caspr2 levels normalized to actin levels and relative to mean WT (in %). **(B)** Number of myelinated fibers in sciatic nerves of males and females. **(C)** Representative electron micrographs showing myelinated fibers from sciatic nerves of males and females. **(D, E)** Scatter plot graph displaying G-ratios of individual myelinated axons as a function of the respective axon diameters, and the linear regression of the G-ratio measurements for each genotype, from sciatic nerves of males (D) and females (E). (**A**) Left panel, 8 mice/genotype/sex; (**B**) 5-6 mice/genotype/sex; (**D, E**) 450 myelinated fibers/genotype, 3 mice/genotype. Statistical tests: (A, B) Means ± SEM, Unpaired t test or Mann Whitney test to compare the 2 genotypes to compare the 2 genotypes; (D) Linear regression (WT, r=0.2065; HET, r=0.1857) for pairwise comparisons, HET *vs* WT, slope *P*=0.5719, elevation *P*<0.0001; (E) Linear regression (WT, r=0.08411; HET, r=0.0636) for pairwise comparisons, HET *vs* WT, slope *P*=0.8112, elevation *P*=0.1022; **P*<0.05, ***P*<0.01, ns non-significant.

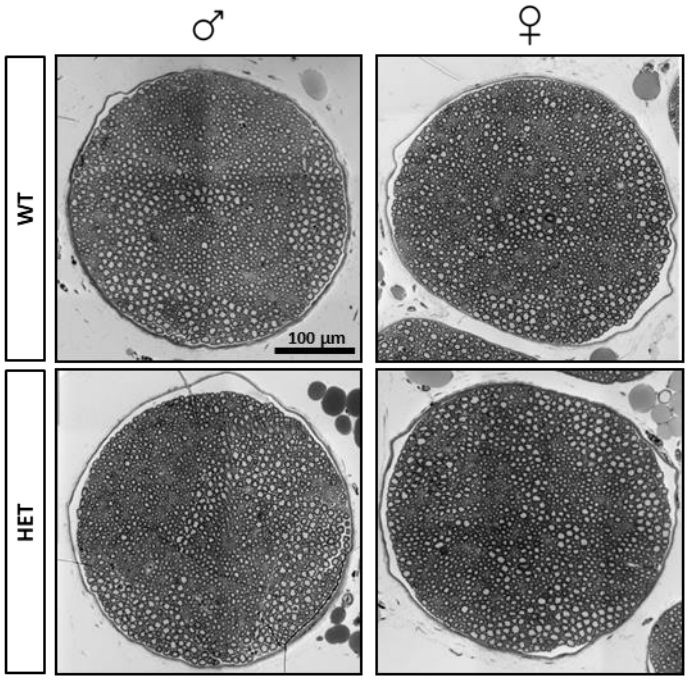

Supplementary Figure S2 | Representative transversal semi-thin sections of sciatic nerves from 4.5 month-old males and females.

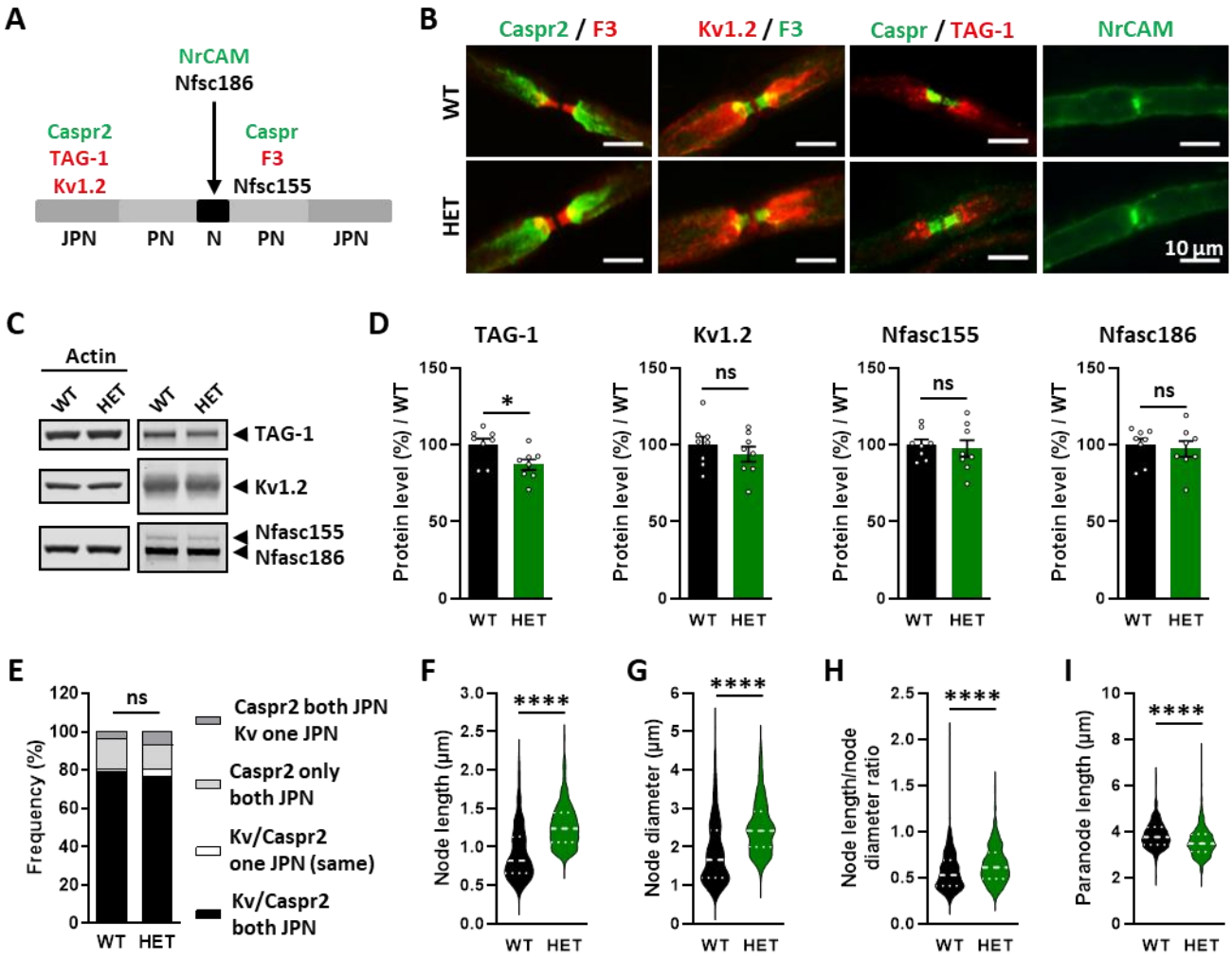

FIGURE 7 | Morphological alterations of the nodes of Ranvier in sciatic nerves from adult males. (A) Schematic representation of a node of Ranvier showing the node (N) surrounded on both sides by the paranodes (PN) and the juxtaparanodes (JPN). The major molecules enriched in the three sub-domains are indicated. **(B)** Representative confocal images of immunostainings of sciatic nerves fibers from WT and HET adult males, for nodal (NrCAM), paranodal (Caspr, F3), and juxtaparanodal (Caspr2, TAG-1, Kv1.2) proteins. **(C)** Representative immunoblots showing TAG-1, Kv1.2 channel, Nfsc155, Nfsc186 and actin levels in sciatic nerves of WT and HET males. **(D)** Levels of TAG-1, Kv1.2 channel, Nfsc155 and Nfsc186 normalized to actin levels and relative to mean WT (in %). **(E)**. Frequency of distribution of Caspr2 and Kv1.2 channels at juxtaparanodes in percentage. **(F-H)**. Length of the nodes (F), diameter of the nodes (G) and node length/node diameter ratio (H) measured on NrCAM immunostainings. **(I)** Length of the paranodes measured on Caspr immunostainings. (**D**) 8 mice/genotype; (**E**) 3 mice/genotype, > 100 nodes/mouse, n=343 WT-341 HET; (**F-I**) 3 mice/genotype, 100 nodes/mouse. Statistical tests: (D) Means ± SEM, Mann Whitney test to compare the 2 genotypes; (E) Two-way ANOVA; (F-I) Median ± quartile, Mann Whitney test to compare the 2 genotypes; **P*<0.05, *****P*<0.0001, ns non-significant.

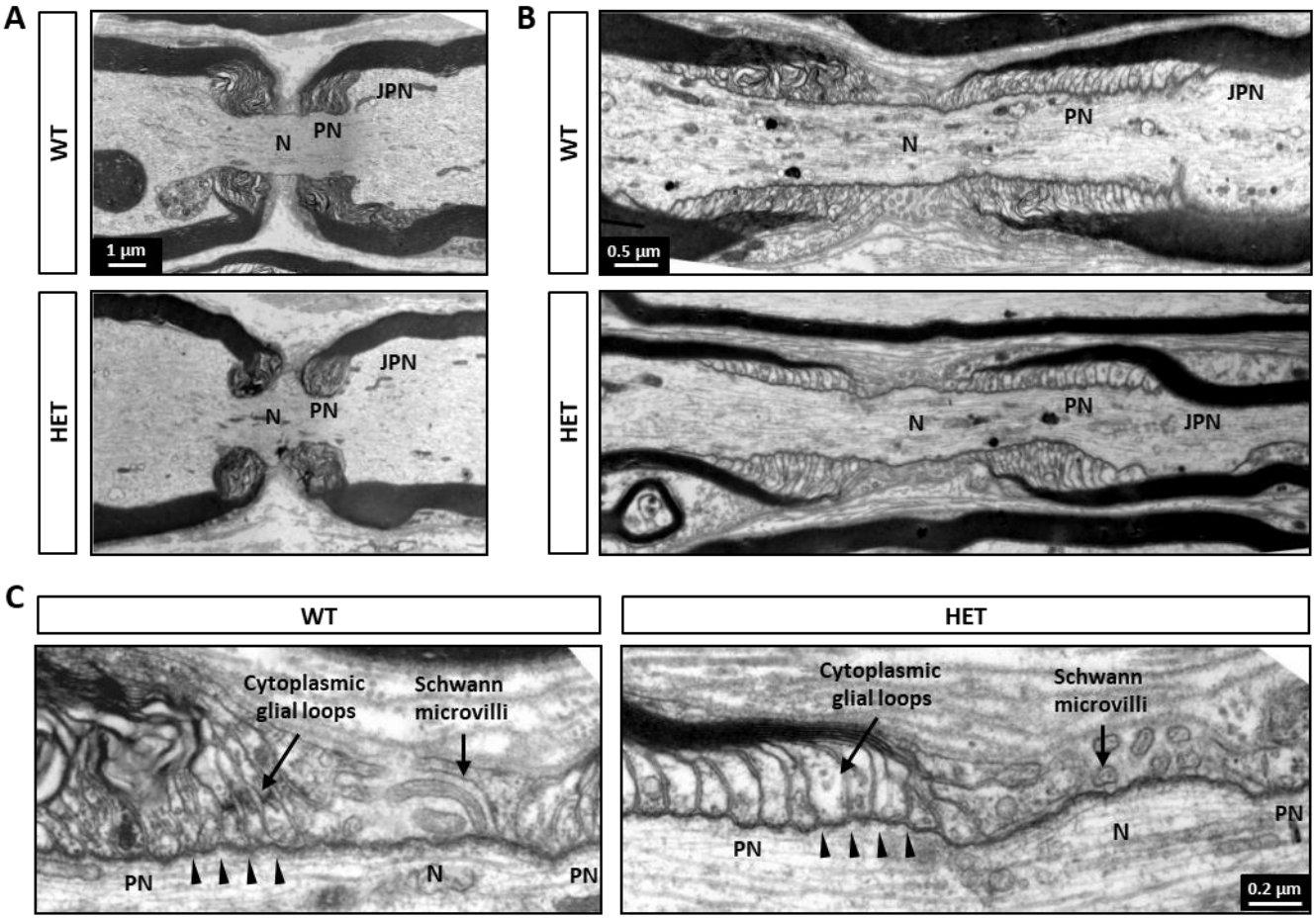

FIGURE 8 | Ultrastructural abnormalities of the nodes of Ranvier in sciatic nerves from ~4.5 month-old males. (A, B) Representative electron micrographs of sciatic nerve longitudinal sections of large **(A)** and thin **(B)** myelinated fibers, at the level of nodes of Ranvier, showing the node (N) surrounded on both sides by the paranodes (PN) and the juxtaparanodes (JPN). **(C)** High magnifications of the nodes presented in B. Schwann cell microvilli and the cytoplasmic glial loops contacting the axons at paranodes are globally normal in mutant mice, and the transverse bands (arrowheads) are visible in mutant mice as well as in WT mice.

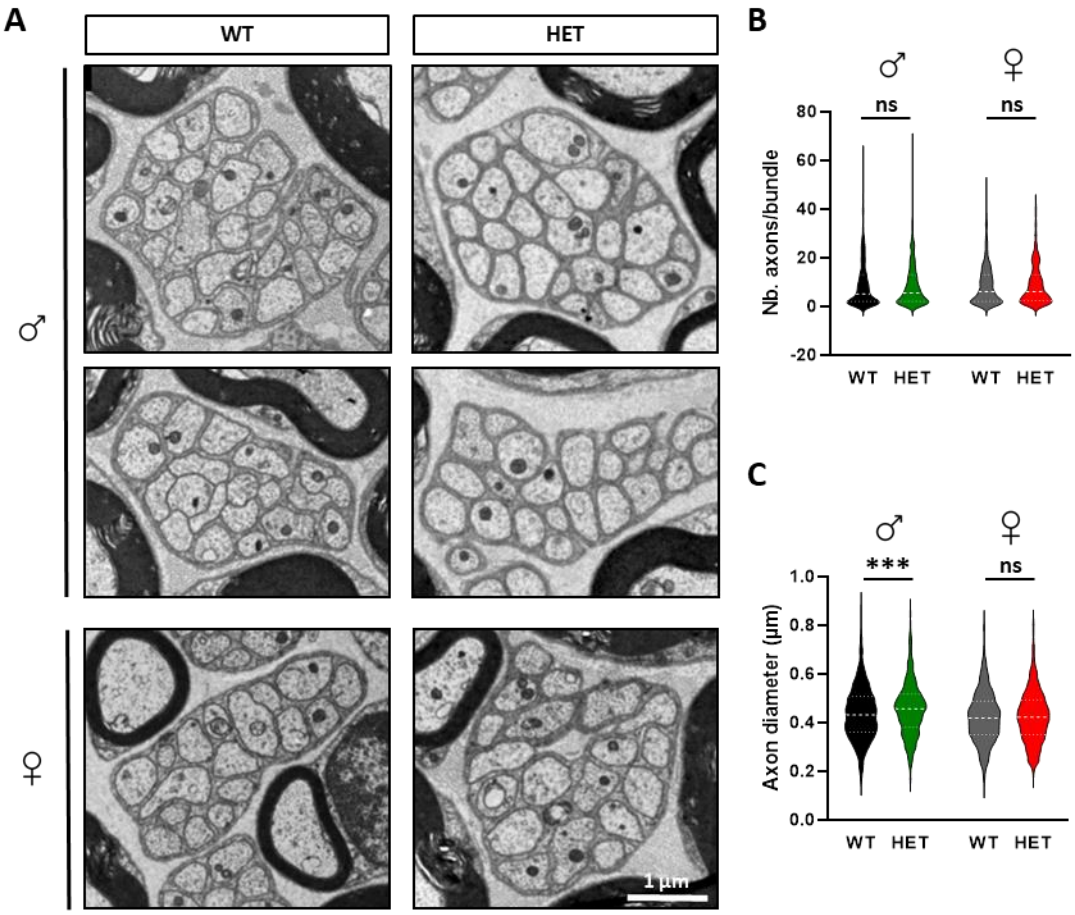

FIGURE 9 | Remak bundle abnormalities in sciatic nerves from ~4.5 month-old mice. (A) Representative high magnification electron micrographs showing Remak bundles in sciatic nerves of males (C) and females (D). **(B)** Number of axons per Remak bundle in sciatic nerves of males and females. **(C)** Diameter of the axons of Remak bundles in sciatic nerves of males and females. (**B**) 100 Remak bundles/mouse, 3 mice/genotype; (**C**) 343 axons/mouse; 3 mice/genotype. Statistical tests: (B, C) Median ± quartile, Mann Whitney test to compare the 2 genotypes: Kolmogorov-Smirnov test to compared cumulative distribution, males $P<0.000$, females non-significant; ***$P<0.001$, ns non-significant.

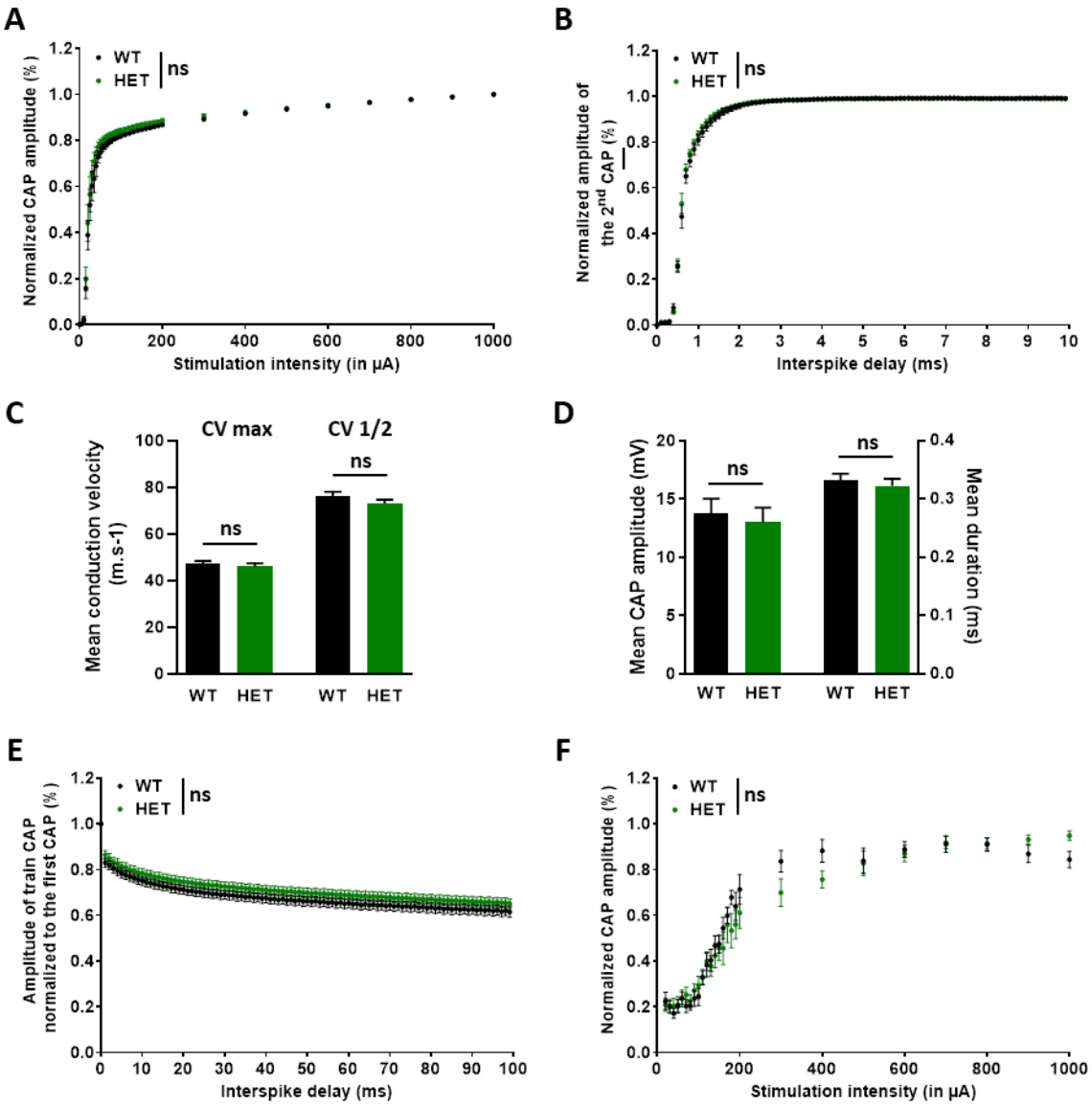

Supplementary Figure S3 | Electrophysiological characteristics of sciatic nerves from adult males at 35°C. (A-E) Characteristics of myelinated fibers at 35°C. **(A)** CAPs recruitment curves with increasing stimulation intensities. **(B)** Refractory period curves obtained by performing two stimulations at increasing intervals. The amplitude of the 2nd CAP is represented as a function of the interpulse delay. **(C)** Mean conduction velocity calculated at peak of the CAPs (CV_{max}) or at mid-amplitude ($CV_{½}$). **(D)** Mean amplitude and duration of the CAPs. **(E)** High frequency response of myelinated fibers. Nerves were stimulated at a frequency of 1kHz for 100ms, and the amplitude of each CAP was measured and normalized to that of the first CAP. **(F)** Characteristics of non-myelinated fibers at 35°C. Recruitment curve of C-fiber populations for increasing intensities of stimulation amplitude. (**A-F**) 6 mice/genotype, 2 nerves/mice. Statistical tests: (A, B, E, F) Means ± SEM, Two-way ANOVA; (C, D) Means ± SEM, Unpaired t test; ns non-significant.

Results II

CNS myelination abnormalities in KI-I236S mice

Manett T., Cifuentes-Diaz, C., Savariradjane M., Garcia M., Goutebroze L.

INTRODUCTION

Previous studies indicated that Caspr2 could play multiple functions in axon development and myelination in the CNS. Scott et al. (2019) reported a delay in myelination of the cortex in juvenile *Cntnap2*$^{-/-}$ mice (R. Scott et al. 2019). Comparing wild-type (WT), *Cntnap2*$^{-/-}$ and *Cntnap2*$^{+/-}$ mice, the team further demonstrated that Caspr2 controls the morphology of the CC and AC throughout development, as well as axon diameter at early developmental stages, cortical neuron intrinsic excitability at the onset of myelination, and axon diameter and myelin thickness at later developmental stages (Cifuentes-Diaz et al. 2023). Morphological alterations of the CC and AC observed in KI-I236S HET adult mice suggested that the variant could affect CNS myelination, we thus started to evaluate this hypothesis.

MATERIAL AND METHODS

Biochemical experiments

Protein analyses were performed as described in Result part I. The commercial antibodies were from the following sources: anti-MBP, Serotec, rat clone 82-87, #MCA409S, 1:250; anti-MAG, Zymed, rabbit, #34-6200, 1:1000; anti-GAPDH, Millipore, chicken, #AB2302, 1:5000. The anti-Caspr2 antibody has been described previously (Denisenko-Nerhbass, 2003).

Electron microscopy and morphometry

P10, P15, P21, and P90 animals were deeply anesthetized by intraperitoneal injection of ketamine (100 mg/kg) and xylazine (10 mg/kg) and transcardially perfused with 4% paraformaldehyde (Acros Organics) and 2.5% glutaraldehyde (P10) (Microm Microtech, G003) in phosphate buffer 0.1M pH 7.4. Brains were post-fixed in the same fixative solution O/N at 4°C. For P15, P21, and P90, we used 3% glytaraldehyde (P15, P21, P90) (Microm Microtech, G003) in Milloning's phosphate buffer 0.1M pH 7.4 at 14.5 mL/min (total volume 100mL) and immediately processed brains. For all ages, 1mm-thick sagittal sections were produced and post-fixed for 1hr at 4°C in fresh fixative solution, washed once with phosphate buffer 0.1M pH 7.4 (P10) or Milloning's phosphate buffer 0.1M (P15, P21, P90), and 3 times for 10 mins each with Palade buffer. Samples were then incubated in 2% osmium tetroxide in Palade buffer for 40 mins at RT, rinsed in Palade buffer for 3 mins and three times for 3 mins in distilled water, dehydrated in a series of ethanol baths, and flat embedded in epoxy resin (EPON 812, Polysciences). After polymerization, blocks containing the CC were cut in 50nM-thick sections using an ultramicrotome (Ultracute E, Leica). Sections were then examined with a Philips CM100 electron microscope and digital images acquired with a CCD camera (Gatan Orius). Axon diameters and G-ratios were measured on the transversal sections using the semiautomatic software MyelTracer. Periaxonal space was calculated by subtracting the axonal area from the inner myelin area (data from MyelTracer).

RESULTS

We first took a biochemical approach to study in parallel the levels of Caspr2 and myelin proteins in whole brain lysates at several key developmental stages of axon development and myelination: E17.5 and P7, before myelination; P10, at myelination onset, P15, P21 and P30, myelination ongoing; and P90, myelination completed. As we did not previously observe major difference in Caspr2 levels between male and female mice (Results I, Fig.2E), Caspr2 immunoblots were performed on male and female lysates pooled. Interestingly, we found that Caspr2 levels were not affected in KI-I236S HET mice at E17.5 and P7 relative to WT protein, but started to decrease progressively from P10, with this decrease becoming more pronounced over time (**Fig. 1A,B**). We conducted qPCR experiments to investigate *Cntnap2* mRNA levels at the same developmental stages and found that *Cntnap2* level in KI-I236S HET mice was not significantly different from that of WT mice at E17.5, P7 and P15, although slightly increased **(Fig. 1C).** By contrast, *Cntnap2* mRNA level was significantly increased at P10, indicating that cells might try to compensate decreased Caspr2 levels at the onset of myelination by increasing *Cntnap2* gene transcription. This is interesting given that the lab also previously observed changes in Caspr2 level in *Cntanp2*$^{+/-}$ mice at this stage (Cifuentes-Diaz et al. 2023).

As we previously observed differential impacts of the variant I236S on the morphology of the CC and AC in males and females, myelin protein levels in whole brain lysates were evaluated in mice of both sexes separately. We started to evaluate the levels of the myelin basic protein (MBP) and myelin-associated glycoprotein (MAG). Preliminary results seem to indicate that global levels of these myelin proteins are not affected in male or female KI-I236S HET mice from P15 to P90 **(Fig. 2A,B**). By contrast, protein levels tend to increase in both male and female KI-I236S HET mice at P7, a stage at which these proteins are very poorly detectable in WT mice, but to decrease at P10 in KI-I236S HET females only. These observations are intriguing since they indicate that the variant could affect very early myelination stages in a sex-dependent manner.

To further explore possible myelin abnormalities in the CNS, we began ultrastructural analysis of the axons and myelinated fibers of the CC in males at several developmental stages: P10, P15, P21 and P90, using electron microscopy (EM) (**Fig. 3A**). At P10, no myelinated fibers were detectable either in WT or mutant mice, despite increased levels of myelin protein at P7 in KI-I236S HET mice. Having the impression that the ultrastructure of myelinated fibers could be different between WT and mutant mice at P21, we performed a morphometric analysis. At this stage, myelination is well advanced, but some space persists between the axon and the compact myelin

sheath, forming the periaxonal area. We thus analyzed axon diameters, periaxonal area, myelin thickness, and G-ratio. No differences were observed in myelin thickness; however, G-ratio differences seemed to depend upon axon diameter, with the lines of best fit for HET and WT mice displaying different slopes. HET mice show a decreased G-ratio at smaller axon diameters, and an increased G-ratio at larger axon diameters (**Fig. 3D**). We did not observe significant difference in axon diameter (**Fig. 3B**) nor in myelin thickness (**Fig. 3D**) between WT and mutant mice. By contrast, the periaxonal area appeared significantly decreased in KI-I236S HET mice compared to WT (**Fig. 3C**). This effect was observable at all axon diameters, as visualized by the scatter plot in Fig. 3C (right panel), and thus was non-dependent upon axon diameter. A decreased area of either the periaxonal space implies more compacted myelin, thus evoking a more mature state of myelination. This suggests that KI-I236S HET male mice exhibit either an earlier onset of the myelination process, or/and an increased speed of the myelination processes, allowing myelinated fibers to be more mature by age P21 than the WT one. We therefore began to assess images at P15, which are currently under analysis. Additionally, we acquired images at P90 to better understand if the phenotype persists later into adulthood.

CONCLUSION AND PERSPECTIVES

Our results thus far in the CNS seem to indicate myelination defects in the KI-I236S HET mice, particularly during the onset and early stages of this process. We plan to further investigate this hypothesis by completing analysis of the axon diameter, myelin thickness, and periaxonal space in EM images from mice at P15 and P90 to better understand the nature of these defects. The ultrastructure of CC myelinated fibers shall also be examined in female mice. Our biochemical results also point to some interesting effects of variant I236S in early myelination, from P7 to P15. It would be interesting to study the origins of these defects by performing RT/qPCR experiments to question whether differences in myelin protein levels are due to altered mRNA expression of proteins such as MBP and MAG, or if they are due to post-translational problems in trafficking or localization of these proteins; experiments are currently being performed and analyzed at P10, P15, and P21. It should be noted that our biochemical experiments were performed on whole brain lysates, not specific brain regions. Preliminary data from our lab indicate that myelin abnormalities in the KI-I236S HET mice may be region-specific; we observed that in KI-I236S HET male mice, levels of MAG and MOG are slightly, though not significantly, increased in the CC and striatum, while levels in the somatosensory cortex are unaltered (data not shown). Caspr2 has previously been

shown to influence myelination in the brain, specifically in the somatosensory cortex, with reduced MBP levels shown in *Cntnap2*$^{-/-}$ mice (R. Scott et al. 2019). Specific brain regions have not yet been investigated in female mice, so whether these effects are sex-dependent or not is currently unknown.

Myelin regulatory factor (MYRF) is an oligodendrocyte transcription factor which is essential for myelination during development in the CNS (Emery et al. 2009). MYRF has also been shown to be required for the maintenance of myelin and mature oligodendrocyte identity in the adult CNS (Koenning et al. 2012), where it is cleaved to activate the transcription of myelin genes directly (Bujalka et al. 2013). It would be interesting to see if MYRF expression is altered in the CNS of KI-I236S HET mice to question if this transcription factor could play a role in the abnormal myelin levels observed in the brain. Experiments are currently being conducted to investigate this.

The preliminary defects observed in the myelin of the CNS indicate that Caspr2 is influencing this process at early stages. These early stages of myelination can be recapitulated *in vivo* by treating mice with demyelinating agents such as cuprizone for an extended period of time (Torre-Fuentes et al. 2020), then taking brain samples at several points during recovery to see if the re-myelination process post-damage shares similar effects to those seen in naïve myelination during early development. A pilot study is currently being conducted in female KI-I236S mice to investigate this further. Finally, similar to our study in the PNS, it would be interesting to investigate the nodes of Ranvier and electrophysiological properties of CC myelinated fibers in KI-I236S HET mice to more fully understand exactly how the variant I236S may perturb myelinated fiber organization and function in the CNS.

REFERENCES

Bujalka, Helena, Matthias Koenning, Stacey Jackson, Victoria M. Perreau, Bernard Pope, Curtis M. Hay, Stanlislaw Mitew, et al. 2013. "MYRF Is a Membrane-Associated Transcription Factor That Autoproteolytically Cleaves to Directly Activate Myelin Genes." *PLoS Biology* 11 (8): e1001625.

Cifuentes-Diaz, Carmen, Giorgia Canali, Marta Garcia, Mélanie Druart, Taylor Manett, Mythili Savariradjane, Camille Guillaume, Corentin Le Magueresse, and Laurence Goutebroze. 2023. "Differential Impacts of Cntnap2 Heterozygosity and Cntnap2 Null Homozygosity on Axon and Myelinated Fiber Development in Mouse." *Frontiers in Neuroscience* 17. https://doi.org/10.3389/fnins.2023.1100121.

Emery, Ben, Dritan Agalliu, John D. Cahoy, Trent A. Watkins, Jason C. Dugas, Sara B. Mulinyawe, Adilijan Ibrahim, Keith L. Ligon, David H. Rowitch, and Ben A. Barres. 2009. "Myelin Gene Regulatory Factor Is a Critical Transcriptional Regulator Required for CNS Myelination." *Cell* 138 (1): 172–85.

Koenning, Matthias, Stacey Jackson, Curtis M. Hay, Clare Faux, Trevor J. Kilpatrick, Melanie Willingham, and Ben Emery. 2012. "Myelin Gene Regulatory Factor Is Required for Maintenance of Myelin and Mature Oligodendrocyte Identity in the Adult CNS." *The Journal of Neuroscience: The Official Journal of the Society for Neuroscience* 32 (36): 12528–42.

Scott, Ricardo, Alberto Sánchez-Aguilera, Kim van Elst, Lynette Lim, Nathalie Dehorter, Sung Eun Bae, Giorgia Bartolini, et al. 2019. "Loss of Cntnap2 Causes Axonal Excitability Deficits, Developmental Delay in Cortical Myelination, and Abnormal Stereotyped Motor Behavior." *Cerebral Cortex* 29 (2): 586–97.

Torre-Fuentes, L., L. Moreno-Jiménez, V. Pytel, J. A. Matías-Guiu, U. Gómez-Pinedo, and J. Matías-Guiu. 2020. "Experimental Models of Demyelination and Remyelination." *Neurología (English Edition)* 35 (1): 32.

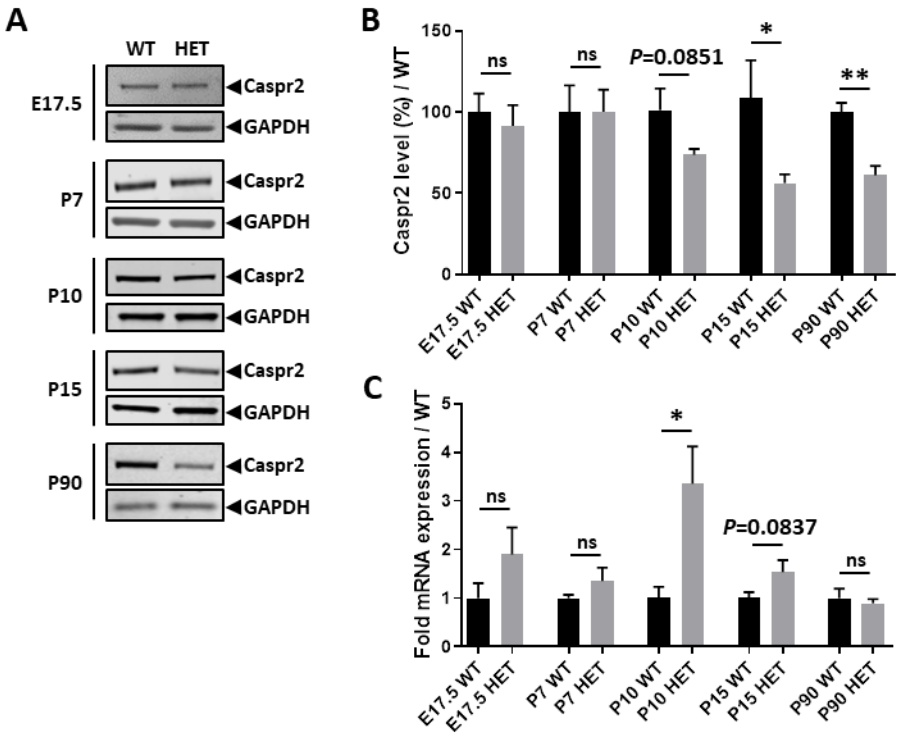

Figure 1 | Caspr2 protein levels of whole brain lysates of KI-I236S HET mice through development. (A) Representative immunoblots showing Caspr2 and GAPDH levels in the brains of adult at the ages indicated. **(B)** Levels of Caspr2 (pool of males and females) normalized to GAPDH levels and relative to mean WT (in %). **(F)** Levels of *Cntnap2* mRNAs (pool of males and females) normalized to the *Psap* gene and relative to mean WT. (**B**) E17.5-P7-P10 n=5 mice/genotype, P15 n=4 mice/genotype, P90 n=6 mice/genotype; (**C**) E17.5 n=4 mice/genotype, P7-P10-P15 n=5 mice/genotype, P90 n=6 mice/genotype. Statistical tests: (B, C) Means ± SEM, Unpaired t test or Mann Whitney test to compare the 2 genotypes at each age; **P*<0.05, ***P*<0.01, ns non-significant.

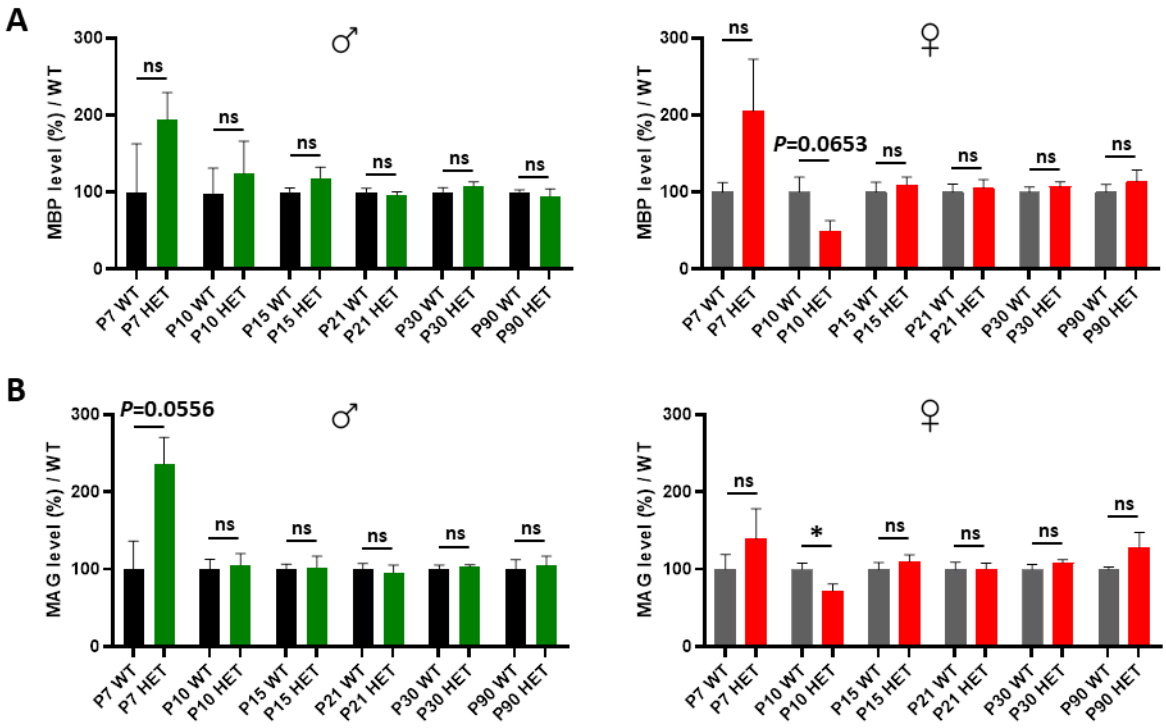

Figure 2 | Myelin protein levels of whole brain lysates of KI-I236S HET males and females through development. Levels of the Myelin basic protein (MBP) **(A)** and Myelin-associated glycoprotein (MAG) **(B)** normalized to GAPDH levels and relative to mean WT (in %) at the ages indicated. Statistical analyses: Means ± SEM; n=5 mice/genotype; Unpaired t test or Mann Whitney to compare the 2 genotypes at each age; **P*<0.05, ns non-significant.

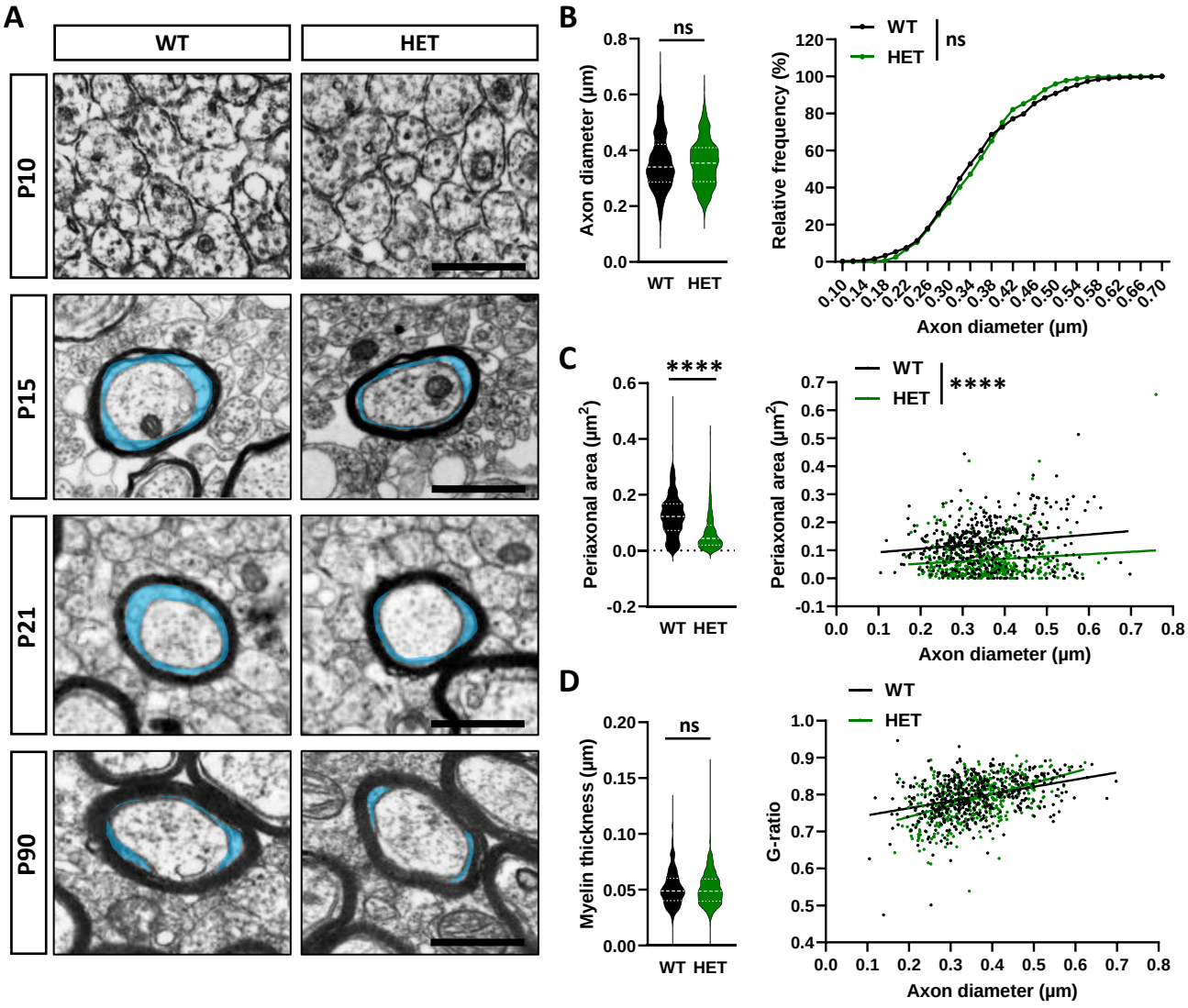

Figure 3 | Ultrastructural analysis of the CC of KI-I236S HET male mice. (A) Representative images from the CC of mice at the ages indicated. Periaxonal space in later stages is highlighted in blue. Scale bar 0.5µm. **(B-D)** Measurements of axon diameters (B), periaxonal area (C) and myelin thickness (D) in P21 mice. **(B)** Left panel, axon diameters; right panel, frequency distribution of axon diameters. **(C)** Left panel, periaxonal areas; right panel, scatter plot graph displaying periaxonal area of individual myelinated axons as a function of the respective axon diameter, and the linear regression of the periaxonal areas for each genotype as a function of axonal diameters. **(D)** Left panel, myelin thickness; right panel, scatter plot graph displaying G-Ratio of individual myelinated axons as a function of the respective axon diameter, and the linear regression of G-Ratio for each genotype as a function of axonal diameters. (**B-D**) n=150 axons/mouse, 3 mice/genotype. Statistical tests: (B-D, left panels), Median ± quartile, Mann Whitney test to compare the 2 genotypes; (B, right panel) Kolmogorov-Smirov test; (C, right panel) Linear regression (WT R^2=0.02766, HET R^2=0.01099), slope *P*=0.4178, intercept *P*<0001; (D, right panel) Linear regression (WT R^2=0.1259, HET R^2=0.2161), slope *P*=0.0025; ****P<0.0001, ns non-significant.

General Discussion

General Discussion

During my PhD, I questioned whether an ER-retained heterozygous missense *CNTNAP2* variant could impact Caspr2 function *in vivo* and contribute to ASD pathogenicity. To do so, we generated a knockin mouse model bearing the I236S variant, and proceeded to its characterization. The data I've gathered by studying these mice support that *CNTNAP2* heterozygous missense variants such as I236S could alter Caspr2 function *in vivo* and lead to sex-dependent CNS and PNS morphological alterations and behavior deficits.

1. How could the I236S *CNTNAP2* variant affect Caspr2 structure and function?

Many *CNTNAP2* heterozygous missense variants have been identified in ASD patients. Interestingly, these mutations are mostly located along the long extracellular domain of the Caspr2 protein and could thus affect its maturation and function in different ways. The variant I studied, I236S, leads to ER-retention and a reduced proportion of the mature form of the protein in the cell.

Our results show that variant I236S is strongly ER-retained, with its maturation impaired. As Caspr2 is a heavily glycosylated protein with 12 N-glycosylation sites, we could speculate that these maturation defects are due to abnormal glycosylation patterns. The Caspr2 protein has a highly compact structure, and therefore alterations within or far from glycosylation sites may impact the folding of the protein. Novel programs which allow the generation of high quality predicated folded protein structures, such as Alphafold, help visualize how intra-protein reactions such as Hydrogen bonds could be affected by amino acid substitutions. We used Dynamut, a recently developed web server which uses protein models to predict structural and stability changes when specific residues are mutated (Rodrigues, Pires, and Ascher 2018). The data generated indicate that when the isoleucine at position 236 of Caspr2 is changed to a serine, the H-bonds formed with neighboring residues are altered, causing an increased flexibility of this region of the protein (large N-terminal lobe). Given this information, we can suspect that the I236S mutation causes either misfolding of Caspr2 or a properly folded but less stable conformation which leads to most of the mutant protein to be sequestered in the ER. This heavy ER-retention leads to cellular stress and, importantly, less Caspr2 protein available at the cell membrane.

Notably, our results show that there is a reduced overall level of Caspr2 in both sciatic nerve tissue and brain of I236S mutant mice, which begins around age P10 in both males and females. A previous study investigating *CNTNAP2* variant D1129H *in vitro* showed that this misfolded Caspr2 variant displays delayed clearance from the cell, and activate the UPR via the ATF6 pathway (Falivelli et al. 2012). This might be also the case for the variant I236S, which would be them be submitted to degradation. However, prior to age P10 in the KI-I236S HET mice, there are no changes Caspr2 level. Perhaps, at these early stages of development, Caspr2 is co-trafficked with other proteins which allows even misfolded or immature forms of the protein to reach the cell

surface. Reduced levels of Caspr2 at the cell membrane, where it aids in axo-glial communication and cell adhesion, could alter these properties, and subsequently contribute to the myelination defects observed in the KI-I236S mice.

2. Effects of I236S variant in myelination and other roles of Caspr2?

Our team previously reported myelination abnormalities in *Cntnap2* HET and KO male mice in the CNS and PNS. Our current results demonstrate that variant I236S can also affect myelination, and that it can do so in a sex-dependent manner, in both the myelinated tracts of the CNS and the myelinated fibers of the PNS.

In the CNS, Caspr2 is expressed in neurons from an early age, around E14.5 in mice. Previous results from the lab showed that Caspr2 plays a role in myelinated fiver development from early development until adulthood, a proposed model which is illustrated in Fig. 60. Alterations in *Cntnap2* expression and Caspr2 protein levels impact this developmental program. Only *Cntnap2* HET mice show increased CC thickness at E17.5, while only *Cntnap2* KO mice show decreased CC thickness at P90; additionally, *Cntnap2* KO mice have a larger AC area at E17.5, but a reduced area at P90 (Cifuentes-Diaz et al. 2023). In the present study, we investigated myelinated tract morphology in adult mice only. As Caspr2 protein level also varies in the KI-I236S HET mice throughout development, it would be interesting to further study CC and AC morphology at earlier developmental time points to see if the variant could influence myelinated tract morphology differentially throughout development, as in the *Cntanp2* HET and KO mice.

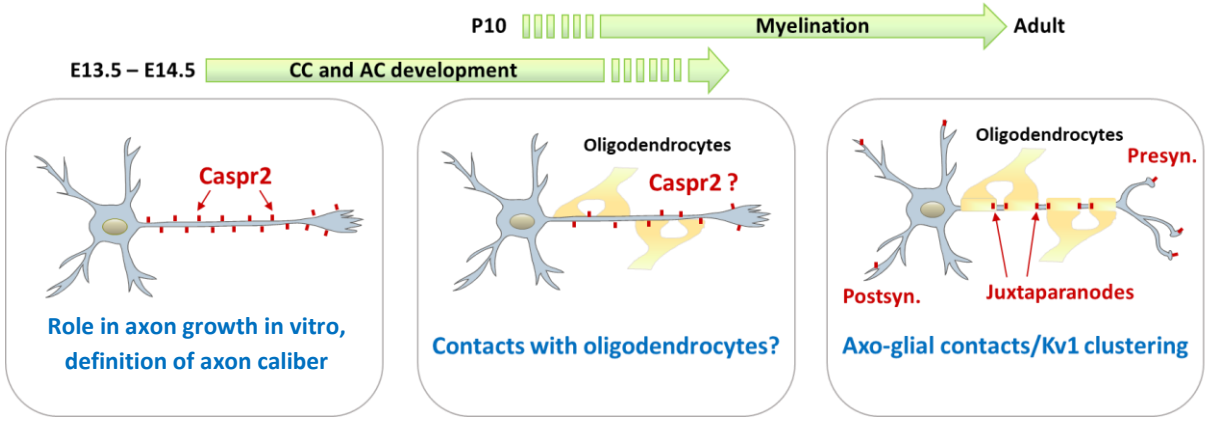

Figure 60: Proposed model of Caspr2's role in myelinated fibers throughout development.

CC and AC morphological alterations KI-I236S HET mice suggest myelination abnormalities. Our current ultrastructural analyses indicate that the speed or onset of myelin sheath wrapping could be affected in the CC of mutant males. Following the model proposed in Fig. 60, during the embryonic period, Caspr2 is localized along the entirety of the axon where it can play roles in several mechanisms, such as determining axon diameter/caliber. It has also been shown to play a

role in axon outgrowth at these early stages. Caspr2 was further shown to contribute to axon diameter and the electrical activity; firing rate of Layer II/III cortical neurons is altered in *Cntnap2* HET and KO mice (Cifuentes-Diaz et al. 2023). Both electrical activity and axon diameter early during development help to determine which and how axons are myelinated at the onset of myelination. Thus, it would also be interesting to study other parameters in which Caspr2 plays a role during CNS development, such as in white matter tract formation, axon diameter, electrophysiology, and myelination at earlier developmental stages in KI-I236S HET mice. We are currently starting this by assessing EM images of CC axons at P10 and P15 males.

While the functions of Caspr2 in the axon are becoming better understood, we recently found evidence that Caspr2 may be expressed in oligodendrocytes as well (preliminary data from the lab, Fig. 61). This further questions the respective contributions of axonal Caspr2 versus Caspr2 expressed in oligodendrocytes in myelination defects observed in KI-I236S HET mice. To address this question, we could perform myelinating co-cultures with cortical neurons and oligodendrocytes. By comparing several culture combinations (WT neurons + WT oligos; WT neurons + HET oligos; HET neurons + WT oligos; HET neurons + HET oligos), we could better understand exactly how alterations in Caspr2 are affecting the process of myelination from start to finish at the cellular level. Furthermore, it would be interesting to perform purely oligodendrocyte cultures to investigate OPC differentiation and OL maturation, which could be perturbed in mutant mice.

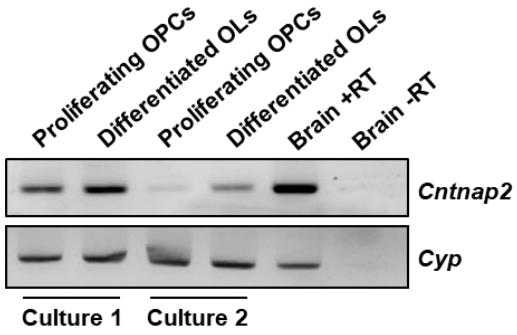

Figure 61: *Cntnap2* is expressed in OPCs at different stages of differentiation. Expression of *Cntnap2* in primary oligodendroglial cell cultures (rat), under proliferation conditions after 3 days (proliferating OPCs) and under differentiation conditions at 6 days (differentiated OLs). RT-PCR with brain cDNAs used as a control, with (+RT) and without (-RT) reverse transcription. *Cyp*, control gene. 50ng of cDNA was used per PCR reaction. Preliminary lab data. OPC cultures and mRNA isolation by M.A. Masson, B. Nait-Oumesmar Lab, ICM.

Currently, to further investigate how could myelination be perturbed *in vivo*, we plan to study both protein levels and mRNA transcription levels of key myelin proteins MBP, MAG, MOG, and PLP, as well as myelin regulatory factor protein MYRF. MYRF is required for CNS myelination during development as well as myelin maintenance in adults. It is a membrane-associated transcription factor which undergoes a proteolytic cleavage; this cleavage separates the C-terminal

region from a nuclear-targeted N-terminal region. The cleaved N-terminal part binds directly to the enhancer regions of OL-specific and myelin genes (Bujalka et al. 2013). If there are reduced levels of MYRF in the cell, this could lead to a decreased expression of myelin and OL genes, contributing to reduced myelin protein levels or potential hypomyelination. MYRF dysregulation could also contribute to differences in myelination speed or maturation. Moreover, it was recently shown that cells deficient for MYRF showed signs of ER stress and impaired proliferation, implying that MYRF has some role in the control of ER homeostasis and may regulate additional genes (Milan et al. 2020).

In addition to myelin thickness decrease in the PNS of KI-I236S HET males, we showed increased length and diameter of the nodes of Ranvier. During early developmental stages, Caspr2 is initially present within the node before being restricted to the JXP with TAG-1 and Kv1 channels, as demonstrated by co-culture experiments (Hivert et al. 2016); thus, it could potentially influence the length and diameter of the nodal subdomains, before being restricted to the JXP region, with variant I236S affecting its function, as per our results. Perhaps altered Caspr2 structure or trafficking problems could lead to the protein being trapped within the nodal compartment for longer than normal, contributing to altered node size later in life. Another phenotype we observed in the KI-I236S HET mice was a decreased paranodal length. This phenomenon does not seem to be the result of detachment of paranodal loops within this region (as per our observations of sciatic nerve longitudinal sections via EM), but could be due to a decrease in the number of paranodal loops per node. One could imagine that is a thinner myelin sheath consisting of fewer layers or wraps of myelin, which would in turn mean that fewer paranodal loops would be attached to the axon in this region.

Besides Caspr2's role in myelination, it is also known to play roles in axon development, synapse development, and brain connectivity. It would be very interesting to study these processes further in the KI-I236S mice to better understand which of Caspr2's roles could be affected by the I236S variant *in vivo*. Casrp2 is known to co-localize with AMPA receptor subunit GluA1; perhaps the misfolded I236S variant could affect the trafficking of this subunit and thus influence excitatory synapse formation. Caspr2 has also been shown to play a role in the migration of cortical projection neurons. Preliminary data from our lab indicate that there are no major migratory defects in the cortex of KI-I236S HET mice, though it would be worthwhile to study this further. Perhaps Caspr2 plays a role in the migration of other neuron types, whose function could be altered by the I236S mutation. Performing immunohistochemistry on coronal brain slices of KI-I236S mice by staining for interneurons (SST, PVALB), for example, would be intriguing, as patient autoantibodies for Caspr2 were shown to target interneurons. Studying different neuronal cell types *in vitro* to detail the cellular mechanisms affected, as well as using fMRI or other techniques in the KI-I236S mice *in vivo* to study connectivity perturbation would be extremely interesting and would further help to uncover how *CNTNAP2* variants such as I236S could affect Caspr2 functionality at different levels.

3. How could *CNTNAP2* variant I236S affect behavioral phenotypes?

The KI-I236S mice studied herein presented several interesting behavioral phenotypes which provide evidence that heterozygous missense *CNTNAP2* variants identified in ASD patients could contribute to some abnormal behaviors. The behavioral defects described in *Cntnap2* KO mice have been discussed in the introduction; however, our study is the first time that a patient *CNTNAP2* variant has been studied *in vivo*. We thoroughly characterized the KI-I236S heterozygous mice so as to recapitulate the clinical conditions as accurately as possible.

3. A. Muscular strength and sensory deficits

We showed that KI-I236S HET male mice displayed decreased muscle strength than WT mice particularly in the grip strength test, which measures the muscular force exerted by the mice when pulled against a resisting force in Newtons. How could a mutation in Caspr2 affect the muscular strength of these mice? Some insight comes from Saifetiarova and colleagues in 2017 (Saifetiarova et al. 2017). They report that ablation of Caspr and/or Caspr2 leads to differences in node organization which can in turn affect the neuromuscular junction (NMJ). *Cntnap2* mutant mice were shown to have a significant percentage of NMJs fully denervated by P180, along with smaller post-synaptic endplate areas and pre-synaptic and post-synaptic changes (Fig. 62). The researchers conclude that Caspr2 is not only essential for axonal domain organization, but also for NMJ integrity; they also state that while the loss of the JXP has no effect on nerve conduction, this does not exclude the development of muscle pathologies involving structural or functional impairment over time (Saifetiarova et al. 2017). We did not observe any differences in conduction in the sciatic nerve of KI-I236S mice, but a significant increase in node size, accompanied by a decrease in paranode size. Thus, we could speculate that NMJs could also be affected in KI-I236S HET male mice. The observations of Saifetiarova and colleagues, however, question the mechanisms through which Casp2 could play a role in NMJ integrity. The authors stated that they were not able to detect Caspr2 at the NMJ using standard immunostaining techniques. Be that as it may, previous work from our lab investigated Caspr2's partner 4.1B, which links Casrp2 and TAG-1 to the cytoskeleton at JXP, and showed that the NMJ is perturbed in *4.1b* KO mice (Cifuentes-Diaz et al. 2011). Perhaps if Caspr2 function is altered in the NMJ region, this could alter its interaction with 4.1B, and thus contribute to changes in the NMJ. We plan to investigate this in the lab in KI-I236S HET mice, to better understand the root of the differences in muscular strength observed herein.

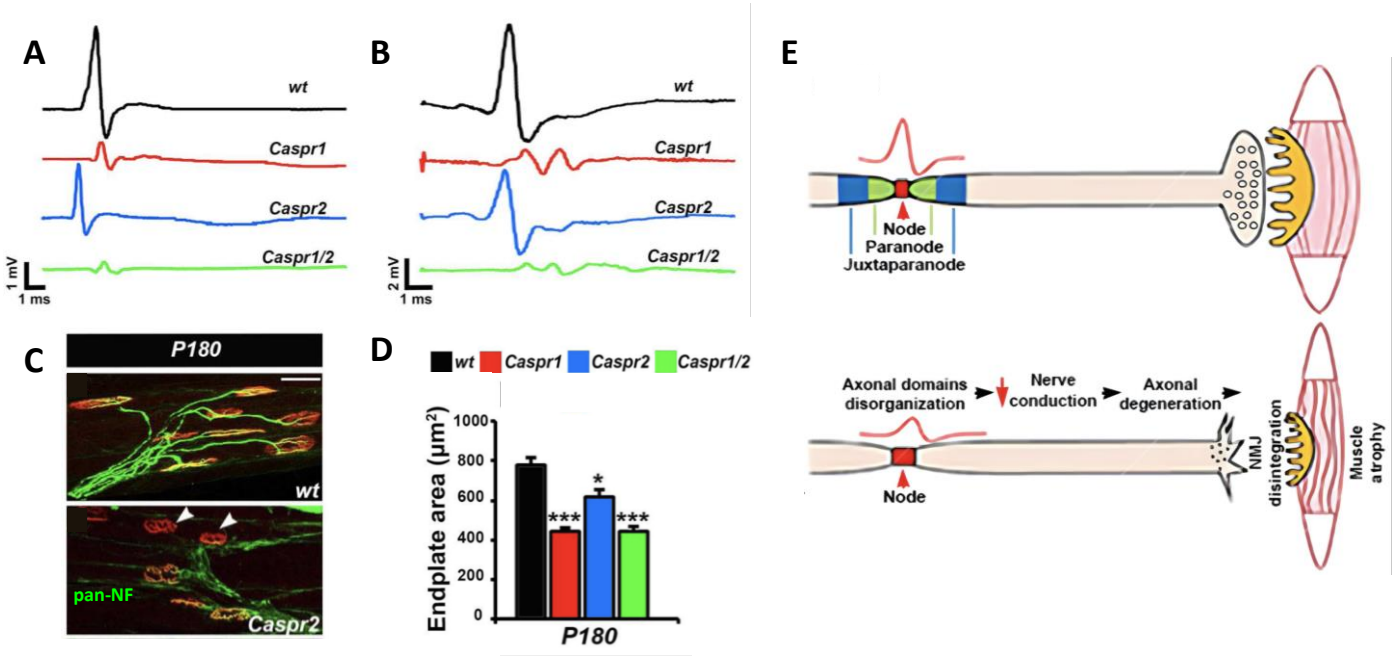

Figure 62: Nerve conduction and neuromuscular junction properties altered in *Cntnap2* KO mice. A) Representative electrophysiological profiles of CAPs from sciatic nerves and tails (B) of P180 WT, Caspr1, Caspr2 and Caspr1/2 mice. C) WT, Caspr1, Caspr2 and Caspr1/2 mice at age P180 immunostained with antibodies against pan-NF (green) together with α-BTX (red). Arrowheads indicate denervated NMJs. D) Quantification of α-BTX-positive endplate area from P180 WT, Caspr1, Caspr2 and Caspr1/2 mice (n=3, comparison of endplate areas between genotypes within the same age group is performed by 1-way ANOVA with Bonferroni's post hoc test; *P<0.05, ***P<0.001). E) Scheme illustrating how altered NOR parameters could influence nerve conduction in the PNS, leading to axonal degeneration and subsequent alteration of the NMJ, including disintegration and even muscle atrophy. Adapted from (Saifetiarova et al. 2017).

Besides the differences in muscular strength, KI-I236S HET male mice also display a decreased sensitivity to heat. These results are interesting given that *Cntanp2* KO mice and other mouse models investigating ASD risk genes show an increased sensitivity to heat. As Caspr2 is known to exist along the axons of sensory C-fibers of the PNS (Gendre et al. 2021), as well as within the glabrous skin of the paw (Gordon et al. 2016), it is not surprising that mutation of this protein could affect this level of the sensory system. It would be interesting to investigate the mechanisms of this sensory defect more deeply by studying the DRG of the KI-I236S mice to see if there are abnormalities at this level which could explain how Caspr2 mutation affects the signaling of sensory information from the periphery. Caspr2 is expressed in the dorsal radial glia (DRG) cells; recent work by Dawes and colleagues shows that Caspr2 antibodies bind to DRG cells *in vitro* (Dawes et al. 2018). They also demonstrate that Caspr2 can regulate sensory neuronal excitability along with membrane Kv1 channel expression in DRG cells, and that the loss of Caspr2 leads to dorsal horn hyperexcitability (Dawes et al. 2018). In addition, DRG of *Cntnap2* KO mice have been shown to have increased Akt-mTOR signaling, which was accompanied by a hypersensitivity to heat (Xing et al. 2020); since the KI-I236S mice display dysregulated heat sensitivity, perhaps the mTOR activation in the DRG of the KI mice are altered.

Another interesting result that furthers the idea that certain Caspr2 mutations such as I236S could affect the sensory perception in the PNS is the increased axon diameter of C-fibers in the Remak bundles of the sciatic nerve. A similar phenomenon was observed by Carlin and colleagues in *Tsc2* KO mice, which also exhibited reduced heat sensitivity (Carlin et al. 2018). Tsc2 is Tuberous sclerosis complex 2, a negative regulator of mTORC1. When *Tsc2* is deleted, the mTOR pathway is uninhibited, thus remaining activated (Carlin et al. 2018). The deletion of *Tsc2* also increases cell body and axon diameters of C-fiber neurons – peptidergic nociceptors that are CGRP- and NF200-positive (Fig. 63). Additionally, they found that peripheral and central target innervation is disrupted by Tsc2 loss, and that Tsc2 is required for full expression of ion channels in nociceptor neurons (Carlin et al. 2018). This further supports the assumption that the increased C-fiber axon diameter and reduced heat sensitivity in KI-I236S HET male mice may be potentially due to a dysregulation of the mTOR pathway by Tsc2 or other mTOR-regulating genes.

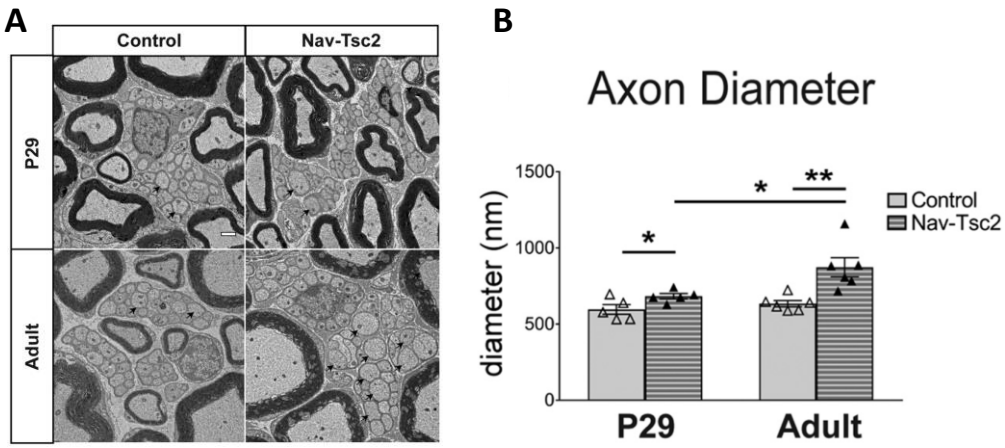

Figure 63: C-fiber axon diameter is increased in Nav-Tsc2 mice. A) Transmission electron micrographs of representative transverse sections of sciatic nerve of P29 (n=5) and adult (n=6) mice. Arrows point to axons greater than one micron in diameter. Scale bar: 1μm. B) Average diameter of axons bundled by Remak Schwann cells. Individual animals plotted with mean +/- SEM; *p<0.05, **p<0.01. Adapted from (Carlin et al. 2018).

3. B. ASD stereotype behaviors and social deficits

While the motor and sensory defects were prominent in the male KI-I236S HET mice, the female mice showed no differences from WT in these types of tests; on the other hand, they did display some social impairments which the males did not, specifically in the social preference test. While the female KI-I236S HET mice did not prefer to interact with the object versus the other mouse, they clearly showed no preference for the mouse. This reflects what has been observed in *Cntnap2* KO male mice (Jang et al. 2022), though the KI-I236S HET male mice are more similar to WT mice in this case. These results suggest that mutations in *CNTNAP2* could impact male and female patients in different ways and that the behavioral symptoms associated with ASD could manifest differently depending on sex. In addition to our results for social preference, the female

KI-I236S HET mice also show a decreased activity and decreased exploration behavior on day 3 of testing in the Cyclotron (circular corridor) test.

While the behavioral phenotypes observed are interesting, they do not fully represent a clinical phenotype of ASD, which typically requires impaired communication or social skills along with higher order repetitive stereotypic behaviors for diagnosis in humans. We tested KI-I236S mice for stereotypic behaviors via the marble burying test and observed no differences between HET and WT mice, in males or females, nor did we observe any repetitive behaviors such as self-grooming or twitching. To further explore the social deficits observed, it would be nice to conduct tests such as the Y-maze test; in fact, we conducted a pilot experiment of this test and observed no differences for the moment. Other social tests such as ultrasonic vocalization, social memory test, or the dominance test could be interesting to better understand social defects in KI-I236S mice. We performed additional preliminary experiments to study working memory, odor recognition, and lateralization, none of which seem to show defects in the KI-I236S mice, though these could be explored further.

The mild cognitive defects observed in KI-I236S HET mice do not fully recapitulate a classic ASD phenotype, and thus lead to the conclusion that *CNTNAP2* variant I236S alone likely does not lead to ASD; other elements are probably needed to contribute to an ASD phenotype in humans, such as environmental factors or other genetic variations. The combination of several factors could eventually surpass a tolerance threshold and result in a clinical presentation of ASD symptoms. While variant I236S alone may not produce an ASD phenotype, it most likely contributes to ASD susceptibility. The level of susceptibility carried by variant I236S may be sex dependent as well, potentially conferring increased susceptibility in males than in females. The ASD patient who bears the I236S variant studied in this project is male, supporting this idea. The boy inherited the I236S variant from his mother, who is not diagnosed with ASD. However, we do not know if she presents any type of social deficits, nor do we know about environmental factors which could have contributed to her child's ASD diagnosis. While both the patient and his mother carried variant I236S and thus ASD susceptibility, perhaps the patient was more susceptible due to the known increased risk of ASD in males or to other environmental factors.

Male sex is typically seen as a strong risk factor for ASD, what with a greatly increased ratio of males to females being diagnosed – a ratio which has remained very stable over time. The leading theory has been that a "female protective effect" exists, positing that males and females have a different threshold to disease development. The model postulates that females require either an increased number or a larger breadth of risk factors to manifest ASD than males (Dougherty et al. 2022). Many are beginning to question this model, however, searching for alternative models to explain sex differences in ASD.

4. Sex-dependent effects of the I236S variant?

Previous studies investigating *CNTNAP2* and its functions *in vivo* have used preferentially *Cntnap2* HET and/or KO male mice. Our study provides not only insights into the differences between WT male and female mice, but also shed light on the ways in which the same mutation can manifest differently in males and females. Interestingly, a recent study by Gegenhuber and colleagues aimed to investigate how gene regulation by sex hormones could influence sex differences in the brain. It's been shown that oestradiol can help to establish sex differences in vertebrates (MacLusky and Naftolin 1981; McEwen 1981; McCarthy 2008), which it does through activation of the transcription factor oestrogen receptor α (ERα). They first sought to identify all the genomic targets of ERα in the brain and found 1,930 ERα-bound loci in the brain (Gegenhuber et al. 2022). These brain-specific ERα binding events were specifically enriched for synaptic and neurodevelopmental disease Gene Ontology terms, including neurotransmitter receptors, ion channels, and extracellular matrix genes. Concentrating their study on the posterior bed nucleus of the stria terminalis (BNSTp), it was observed that this region contained higher numbers of inhibitory neurons in males, which allows stronger disinhibition of downstream sites (Gegenhuber et al. 2022). Interestingly, the researchers also analyzed CUT&RUN data from their sequencing to further analyze ERα expression in the adult mouse brain. Their results identify cell adhesion molecules as having enriched ERα-associated genes; they also identify several neurodevelopmental disorders (NDDs) associated with genes closest to ERα peaks, including ASD (Gegenhuber et al. 2022).

When examining the genes associated with the NDDs, they identified *CNTNAP2* as one such gene that could be regulated by oestradiol and ERα (Fig. 64) (Gegenhuber et al. 2022). This could mean that *CNTNAP2* expression may be influenced by certain hormone levels or steroids and that differential activation of *CNTNAP2/Cntnap2* in males and females could contribute to behavioral and morphological differences, including potentially altered expression patterns in the brain. Our results show that the overall level of Caspr2 proteins in brains and sciatic nerves of KI-I236S HET mice are not significantly different between the sexes. However, we cannot completely exclude the existence a slight but sufficient difference in Caspr2 level or *Cntnap2* expression between the two sexes that could account for a differential impact of the I236S variant at the cellular level, as we observed a decreased tendency for *Cntnap2* mRNA level in the brains of KI-I236S HET females. It could be interesting to complete more qPCR experiments with an increased sample size of males and females, using PSAP as a reference gene, to further study this trend towards reduced expression of *Cntnap2* in females. We could further investigate how *Cntnap2* is differentially affected in males and females by studying other proteins whose levels vary in males and females that may interact with Caspr2. Interestingly, *Cntnap2* is also expressed in the ovaries and the prostate. It could be interesting to study the role of Caspr2 and patient variants such as I236S in these tissues as well.

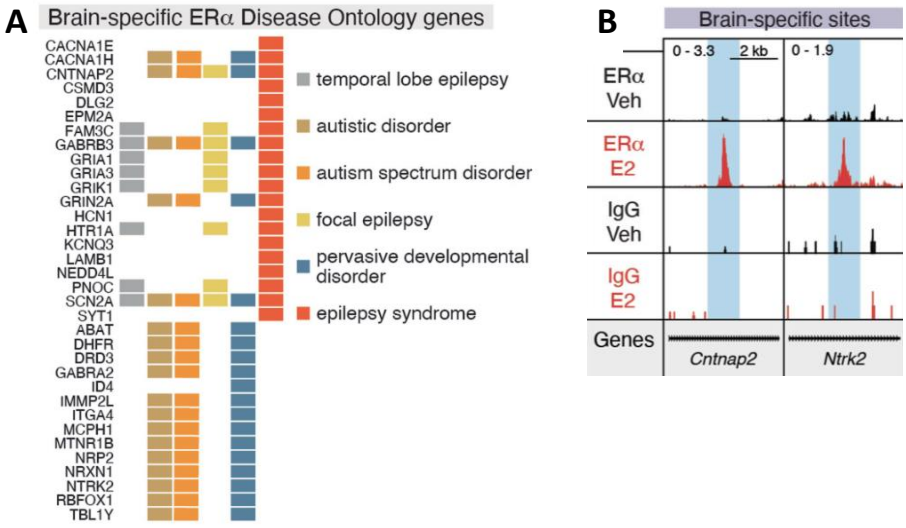

Figure 64: Additional analysis of adult brain ERα CUT&RUN dataset. A) Brain-specific ERα peak-associated genes within each enriched Disease Ontology (DO) term (clusterProfiler, padj < 0.1), colored by term. B) Example brain-specific (*Cntnap2*, *Ntrk2*) ERα peaks. Adapted from (Gegenhuber et al. 2022).

A recent study by Dawson and colleagues investigated sex differences in *Cntnap2* KO mice along with WT mice of both sexes and found several differences, notably in microglial expression and activation along with differences in spine density and social behavior (Dawson et al. 2023). They analyzed the ACC, as it is an important brain region controlling social behavior and observed that spine densities on apical dendrites of L2/L3 and L5 pyramidal excitatory neurons occurred only in male *Cntnap2* KO mice, while no differences were observed between female WT and KO mice. Furthermore, male KO mice exhibited increased microglial activation compared to WT, while female mice showed no difference between genotypes. Interestingly, microglia have been shown to be influenced by 17 β-oestradiol levels in zebrafish, along with displaying testosterone-induced differences in certain characteristics throughout development, indicating that sex-controlled differences of microglia could contribute to some ASD sex differences in *Cntnap2* mutant mice.

5. Contribution of other *CNTNAP2* variants to ASD?

Several *CNTNAP2* heterozygous missense variants have been previously studied *in vitro*. These variants have been shown to impact Caspr2 in two ways; some were misfolded and retained in the ER, while others were trafficked to the membrane but affected Caspr2 function once there. However, ER-retained variants displayed a varying degree of ER retention/maturation state, from being barely distinguishable from WT to being severely retained and containing little to no mature form of the protein (Fig. 65) (unpublished lab data).

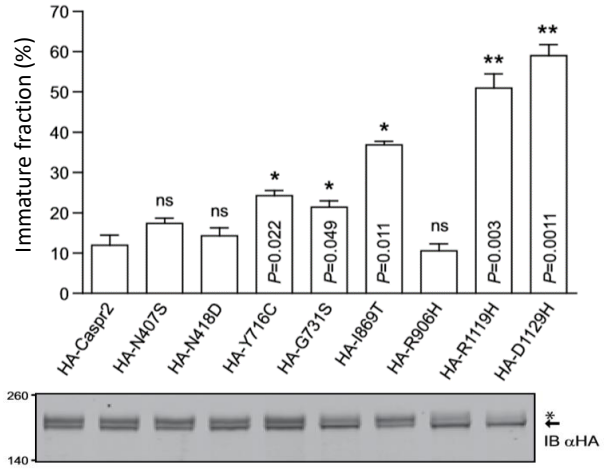

Figure 65: *CNTNAP2* variants expressed in COS7 cells. The protein results in 2 bands on the western blot, with the upper band representing the mature Caspr2 fraction (membrane-expressed) and the lower band representind the immature Caspr2 fraction (intracellular / ER-retained). The immature fraction of the protein (lower band / both bands) is displayed on the bar graph, with the representative blots of each variant underneath.

As the *CNTNAP2* variants present a continuum of ER-retention, we can imagine that they could lead to a continuum of functional effects on Caspr2 and displayed phenotypes, both *in vitro* and *in vivo*. This could contribute to inter-individual variability not only in ASD patients, but also in the general population. There have been numerous *CNTNAP2* variants identified in healthy people, along with all the variants identified in ASD patients. Thus, each variant may contribute to ASD-related phenotypes on a spectrum, contributing to a clinical phenotype only when extremely severe or when in combination with other known ASD risk factors.

6. *CNTNAP2* variants in other physiological conditions and neurological disorders?

My PhD work has shown that *CNTNAP2* variants such as I236S can affect Caspr2 function in the myelination process. Myelin defects have been associated with multiple conditions across the lifespan, including normal aging, degenerative (Alzheimer's disease) and demyelinating diseases such as multiple sclerosis (MS). One could question whether ER-retained *CNTNAP2* variants could influence these trajectories, notably remyelination in MS. One way to investigate this is by treating KI-I236S mice with Cuprizone, a neurotoxic agent which causes OL death and subsequent reversible demyelination. By subjecting mice to this treatment for a specified time frame and then removing the treatment and assessing re-myelination over time, we can observe if the re-myelination process recapitulates the naïve myelination process. We have, in fact, already begun a pilot study with KI-I236S female mice in the lab.

Also, myelin is known to be plastic throughout a lifetime. The formation of myelin in the CNS is a dynamic life-long process, and can be conceptually divided into two phases: an intrinsic phase, genetically predefined, which occurs prenatally and in early childhood, and follows a

chronological and topographical fixed sequence, as described in this manuscript; and an adaptive phase, which in contrast is modified by experience, occurring according to the need of neuronal networks, and thereby contributing to physiological brain function and behavior (Baraban, Mensch, and Lyons 2016; Monje 2018). Various experiences during the adaptive myelination phase can alter the plasticity of myelination in the brain; for example, several rodent studies revealed that motor learning triggers and requires the generation of newly-formed OLs and myelin sheaths (Xiao et al. 2016; McKenzie et al. 2014; J. Zheng et al. 2019). Conversely, some forms of sensory-motor deprivation such as social isolation result in down-regulation of myelin thickness in the prefrontal cortex and reduced social interaction, which can be normalized by social re-integration (Liu et al. 2012). It could be that ER-retained *CNTNAP2* variants also influence myelin plasticity during this adaptive phase of myelination. The team plans to investigate this possibility by assessing the effects of external factors such as exercise and social isolation in KI-I236S mice.

References

A

Abe, Namiko, Steven H. Borson, Michael J. Gambello, Fan Wang, and Valeria Cavalli. 2010. "Mammalian Target of Rapamycin (MTOR) Activation Increases Axonal Growth Capacity of Injured Peripheral Nerves." *The Journal of Biological Chemistry* 285 (36): 28034–43.

Aboitiz, F., A. B. Scheibel, R. S. Fisher, and E. Zaidel. 1992. "Fiber Composition of the Human Corpus Callosum." *Brain Research* 598 (1–2): 143–53.

Abrahams, B. S., D. Tentler, J. V. Perederiy, M. C. Oldham, G. Coppola, and D. H. Geschwind. 2007. "Genome-Wide Analyses of Human Perisylvian Cerebral Cortical Patterning." *Proceedings of the National Academy of Sciences of the United States of America* 104 (45): 17849–54.

Ahimsadasan, Nilah, Vamsi Reddy, Mahammed Z. Khan Suheb, and Anil Kumar. 2022. *Neuroanatomy, Dorsal Root Ganglion*. StatPearls Publishing.

Alarcón, M., A. L. Yonan, T. C. Gilliam, R. M. Cantor, and D. H. Geschwind. 2005. "Quantitative Genome Scan and Ordered-Subsets Analysis of Autism Endophenotypes Support Language QTLs." *Molecular Psychiatry* 10 (8): 747–57.

Alarcón, Maricela, Brett S. Abrahams, Jennifer L. Stone, Jacqueline A. Duvall, Julia V. Perederiy, Jamee M. Bomar, Jonathan Sebat, et al. 2008. "Linkage, Association, and Gene-Expression Analyses Identify CNTNAP2 as an Autism-Susceptibility Gene." *American Journal of Human Genetics* 82 (1): 150–59.

Alarcón, Maricela, Rita M. Cantor, Jianjun Liu, T. Conrad Gilliam, Daniel H. Geschwind, and Autism Genetic Research Exchange Consortium. 2002. "Evidence for a Language Quantitative Trait Locus on Chromosome 7q in Multiplex Autism Families." *American Journal of Human Genetics* 70 (1): 60–71.

Almeida, Rafael G., Tim Czopka, Charles Ffrench-Constant, and David A. Lyons. 2011. "Individual Axons Regulate the Myelinating Potential of Single Oligodendrocytes in Vivo." *Development* 138 (20): 4443–50.

American Psychiatric Association. 2013. *Diagnostic and Statistical Manual, Fifth Edition (DSM-5)*. American Psychiatric Publishing.

Anderson, Garret R., Timothy Galfin, Wei Xu, Jason Aoto, Robert C. Malenka, and Thomas C. Südhof. 2012. "Candidate Autism Gene Screen Identifies Critical Role for Cell-Adhesion Molecule CASPR2 in Dendritic Arborization and Spine Development." *Proceedings of the National Academy of Sciences of the United States of America* 109 (44): 18120–25.

Angelakos, Christopher C., Jennifer C. Tudor, Sarah L. Ferri, Thomas A. Jongens, and Ted Abel. 2019. "Home-Cage Hypoactivity in Mouse Genetic Models of Autism Spectrum Disorder." *Neurobiology of Learning and Memory* 165 (November): 107000.

Antoine, Michelle W., Tomer Langberg, Philipp Schnepel, and Daniel E. Feldman. 2019. "Increased Excitation-Inhibition Ratio Stabilizes Synapse and Circuit Excitability in Four Autism Mouse Models." *Neuron* 101 (4): 648-661.e4.

Arancibia-Carcamo, I. Lorena, and David Attwell. 2014. “The Node of Ranvier in CNS Pathology.” *Acta Neuropathologica* 128 (2): 161–75.

Arancibia-Cárcamo, I. Lorena, Marc C. Ford, Lee Cossell, Kinji Ishida, Koujiro Tohyama, and David Attwell. 2017. “Node of Ranvier Length as a Potential Regulator of Myelinated Axon Conduction Speed.” *ELife* 6 (January). https://doi.org/10.7554/eLife.23329.

Arking, Dan E., David J. Cutler, Camille W. Brune, Tanya M. Teslovich, Kristen West, Morna Ikeda, Alexis Rea, et al. 2008. “A Common Genetic Variant in the Neurexin Superfamily Member CNTNAP2 Increases Familial Risk of Autism.” *American Journal of Human Genetics* 82 (1): 160–64.

Aylward, E. H., N. J. Minshew, K. Field, B. F. Sparks, and N. Singh. 2002. “Effects of Age on Brain Volume and Head Circumference in Autism.” *Neurology* 59 (2): 175–83.

B

Bailey, A., A. Le Couteur, I. Gottesman, P. Bolton, E. Simonoff, E. Yuzda, and M. Rutter. 1995. “Autism as a Strongly Genetic Disorder: Evidence from a British Twin Study.” *Psychological Medicine* 25 (1): 63–77.

Bakkaloglu, Betul, Brian J. O’Roak, Angeliki Louvi, Abha R. Gupta, Jesse F. Abelson, Thomas M. Morgan, Katarzyna Chawarska, et al. 2008. “Molecular Cytogenetic Analysis and Resequencing of Contactin Associated Protein-like 2 in Autism Spectrum Disorders.” *American Journal of Human Genetics* 82 (1): 165–73.

Balasco, Luigi, Marco Pagani, Luca Pangrazzi, Gabriele Chelini, Francesca Viscido, Alessandra Georgette Ciancone Chama, Alberto Galbusera, Giovanni Provenzano, Alessandro Gozzi, and Yuri Bozzi. 2022. “Somatosensory Cortex Hyperconnectivity and Impaired Whisker-Dependent Responses in Cntnap2-/- Mice.” *Neurobiology of Disease* 169 (July): 105742.

Baraban, Marion, Sigrid Mensch, and David A. Lyons. 2016. “Adaptive Myelination from Fish to Man.” *Brain Research* 1641 (Pt A): 149–61.

Barateiro, Andreia, and Adelaide Fernandes. 2014. “Temporal Oligodendrocyte Lineage Progression: In Vitro Models of Proliferation, Differentiation and Myelination.” *Biochimica et Biophysica Acta* 1843 (9): 1917–29.

Barres, B. A., and M. C. Raff. 1993. “Proliferation of Oligodendrocyte Precursor Cells Depends on Electrical Activity in Axons.” *Nature* 361 (6409): 258–60.

Basbaum, Allan I., Diana M. Bautista, Grégory Scherrer, and David Julius. 2009. “Cellular and Molecular Mechanisms of Pain.” *Cell* 139 (2): 267–84.

Belin, Sophie, Kristen L. Zuloaga, and Yannick Poitelon. 2017. “Influence of Mechanical Stimuli on Schwann Cell Biology.” *Frontiers in Cellular Neuroscience* 11 (November): 347.

Bemben, Michael A., Seth L. Shipman, Roger A. Nicoll, and Katherine W. Roche. 2015. “The Cellular and Molecular Landscape of Neuroligins.” *Trends in Neurosciences* 38 (8): 496–505.

Ben Bashat, Dafna, Vered Kronfeld-Duenias, Ditza A. Zachor, Perla M. Ekstein, Talma Hendler, Ricardo Tarrasch, Ariela Even, Yonata Levy, and Liat Ben Sira. 2007. “Accelerated Maturation of

White Matter in Young Children with Autism: A High b Value DWI Study." *NeuroImage* 37 (1): 40–47.

Bercury, Kathryn K., and Wendy B. Macklin. 2015. "Dynamics and Mechanisms of CNS Myelination." *Developmental Cell* 32 (4): 447–58.

Bergles, D. E., J. D. Roberts, P. Somogyi, and C. E. Jahr. 2000. "Glutamatergic Synapses on Oligodendrocyte Precursor Cells in the Hippocampus." *Nature* 405 (6783): 187–91.

Bhat, M. A., J. C. Rios, Y. Lu, G. P. Garcia-Fresco, W. Ching, M. St Martin, J. Li, et al. 2001. "Axon-Glia Interactions and the Domain Organization of Myelinated Axons Requires Neurexin IV/Caspr/Paranodin." *Neuron* 30 (2): 369–83.

Binder, Matthew S., Dalton G. Jones, Samantha L. Hodges, and Joaquin N. Lugo. 2020. "NS-Pten Adult Knockout Mice Display Both Quantitative and Qualitative Changes in Urine-Induced Ultrasonic Vocalizations." *Behavioural Brain Research* 378 (January): 112189.

Bishop, Naomi, Azhari Aziz, and Christian Barth. 2014. "Phenotypic Variation in Autism Spectrum Disorder: Insights from Syndromic Forms of Autism." In *Comprehensive Guide to Autism*, edited by Vinood B. Patel, Victor R. Preedy, and Colin R. Martin, 1715–35. New York, NY: Springer New York.

Boedhoe, Premika S. W., Daan van Rooij, Martine Hoogman, Jos W. R. Twisk, Lianne Schmaal, Yoshinari Abe, Pino Alonso, et al. 2020. "Subcortical Brain Volume, Regional Cortical Thickness, and Cortical Surface Area Across Disorders: Findings From the ENIGMA ADHD, ASD, and OCD Working Groups." *The American Journal of Psychiatry* 177 (9): 834–43.

Bonilha, Leonardo, Fernando Cendes, Chris Rorden, Mark Eckert, Paulo Dalgalarrondo, Li Min Li, and Carlos E. Steiner. 2008. "Gray and White Matter Imbalance--Typical Structural Abnormality Underlying Classic Autism?" *Brain & Development* 30 (6): 396–401.

Boyle, M. E., E. O. Berglund, K. K. Murai, L. Weber, E. Peles, and B. Ranscht. 2001. "Contactin Orchestrates Assembly of the Septate-like Junctions at the Paranode in Myelinated Peripheral Nerve." *Neuron* 30 (2): 385–97.

Brandes, Nadav, Grant Goldman, Charlotte H. Wang, Chun Jimmie Ye, and Vasilis Ntranos. 2023. "Genome-Wide Prediction of Disease Variant Effects with a Deep Protein Language Model." *Nature Genetics*, August. https://doi.org/10.1038/s41588-023-01465-0.

Brinkmann, Bastian G., Amit Agarwal, Michael W. Sereda, Alistair N. Garratt, Thomas Müller, Hagen Wende, Ruth M. Stassart, et al. 2008. "Neuregulin-1/ErbB Signaling Serves Distinct Functions in Myelination of the Peripheral and Central Nervous System." *Neuron* 59 (4): 581–95.

Brunner, Daniela, Patricia Kabitzke, Dansha He, Kimberly Cox, Lucinda Thiede, Taleen Hanania, Emily Sabath, et al. 2015. "Comprehensive Analysis of the 16p11.2 Deletion and Null Cntnap2 Mouse Models of Autism Spectrum Disorder." *PloS One* 10 (8): e0134572.

Bujalka, Helena, Matthias Koenning, Stacey Jackson, Victoria M. Perreau, Bernard Pope, Curtis M. Hay, Stanlislaw Mitew, et al. 2013. "MYRF Is a Membrane-Associated Transcription Factor That Autoproteolytically Cleaves to Directly Activate Myelin Genes." *PLoS Biology* 11 (8): e1001625.

Butts, B. D., C. Houde, and H. Mehmet. 2008. “Maturation-Dependent Sensitivity of Oligodendrocyte Lineage Cells to Apoptosis: Implications for Normal Development and Disease.” *Cell Death and Differentiation* 15 (7): 1178–86.

C

Câmara, Joana, Zhen Wang, Cristina Nunes-Fonseca, Hana C. Friedman, Matthew Grove, Diane L. Sherman, Noboru H. Komiyama, et al. 2009. “Integrin-Mediated Axoglial Interactions Initiate Myelination in the Central Nervous System.” *The Journal of Cell Biology* 185 (4): 699–712.

Canali, Giorgia, Marta Garcia, Bruno Hivert, Delphine Pinatel, Aline Goullancourt, Ksenia Oguievetskaia, Margaux Saint-Martin, Jean-Antoine Girault, Catherine Faivre-Sarrailh, and Laurence Goutebroze. 2018. “Genetic Variants in Autism-Related CNTNAP2 Impair Axonal Growth of Cortical Neurons.” *Human Molecular Genetics* 27 (11): 1941–54.

Canali, Giorgia, and Laurence Goutebroze. 2018. “CNTNAP2 Heterozygous Missense Variants: Risk Factors for Autism Spectrum Disorder and/or Other Pathologies?” *Journal of Experimental Neuroscience*.

Carlin, Dan, Judith P. Golden, Amit Mogha, Vijay K. Samineni, Kelly R. Monk, Robert W. Gereau 4th, and Valeria Cavalli. 2018. “Deletion of Tsc2 in Nociceptors Reduces Target Innervation, Ion Channel Expression, and Sensitivity to Heat.” *ENeuro* 5 (2). https://doi.org/10.1523/ENEURO.0436-17.2018.

Castelnovo, Luca Franco, Veronica Bonalume, Simona Melfi, Marinella Ballabio, Deborah Colleoni, and Valerio Magnaghi. 2017. “Schwann Cell Development, Maturation and Regeneration: A Focus on Classic and Emerging Intracellular Signaling Pathways.” *Neural Regeneration Research* 12 (7): 1013–23.

Chang, Kae-Jiun, Stephanie A. Redmond, and Jonah R. Chan. 2016. “Remodeling Myelination: Implications for Mechanisms of Neural Plasticity.” *Nature Neuroscience* 19 (2): 190–97.

Chen, Jason A., Olga Peñagarikano, T. Grant Belgard, Vivek Swarup, and Daniel H. Geschwind. 2015. “The Emerging Picture of Autism Spectrum Disorder: Genetics and Pathology.” *Annual Review of Pathology* 10: 111–44.

Chen, Ning, Frank Koopmans, Aaron Gordon, Iryna Paliukhovich, Remco V. Klaassen, Roel C. van der Schors, Elior Peles, Matthijs Verhage, August B. Smit, and Ka Wan Li. 2015. “Interaction Proteomics of Canonical Caspr2 (CNTNAP2) Reveals the Presence of Two Caspr2 Isoforms with Overlapping Interactomes.” *Biochimica et Biophysica Acta* 1854 (7): 827–33.

Chen, Rong, Yun Jiao, and Edward H. Herskovits. 2011. “Structural MRI in Autism Spectrum Disorder.” *Pediatric Research* 69 (5 Pt 2): 63R-8R.

Chen, Ying, Heng Wu, Shuzong Wang, Hisami Koito, Jianrong Li, Feng Ye, Jenny Hoang, et al. 2009. “The Oligodendrocyte-Specific G Protein-Coupled Receptor GPR17 Is a Cell-Intrinsic Timer of Myelination.” *Nature Neuroscience* 12 (11): 1398–1406.

Choe, Katrina Y., Richard A. I. Bethlehem, Martin Safrin, Hongmei Dong, Elena Salman, Ying Li, Valery Grinevich, et al. 2022. “Oxytocin Normalizes Altered Circuit Connectivity for Social Rescue of the Cntnap2 Knockout Mouse.” *Neuron* 110 (5): 795-808.e6.

Choi, Yong-Jin, Alessia Di Nardo, Ioannis Kramvis, Lynsey Meikle, David J. Kwiatkowski, Mustafa Sahin, and Xi He. 2008. “Tuberous Sclerosis Complex Proteins Control Axon Formation.” *Genes & Development* 22 (18): 2485–95.

Cifuentes-Diaz, Carmen, Giorgia Canali, Marta Garcia, Mélanie Druart, Taylor Manett, Mythili Savariradjane, Camille Guillaume, Corentin Le Magueresse, and Laurence Goutebroze. 2023. “Differential Impacts of Cntnap2 Heterozygosity and Cntnap2 Null Homozygosity on Axon and Myelinated Fiber Development in Mouse.” *Frontiers in Neuroscience* 17. https://doi.org/10.3389/fnins.2023.1100121.

Cifuentes-Diaz, Carmen, Fabrice Chareyre, Marta Garcia, Jérôme Devaux, Michèle Carnaud, Grégoire Levasseur, Michiko Niwa-Kawakita, et al. 2011. “Protein 4.1B Contributes to the Organization of Peripheral Myelinated Axons.” *PloS One* 6 (9): e25043.

Colardo, Mayra, Marco Segatto, and Sabrina Di Bartolomeo. 2021. “Targeting RTK-PI3K-MTOR Axis in Gliomas: An Update.” *International Journal of Molecular Sciences* 22 (9). https://doi.org/10.3390/ijms22094899.

Courchet, Virginie, Amanda J. Roberts, Géraldine Meyer-Dilhet, Peggy Del Carmine, Tommy L. Lewis Jr, Franck Polleux, and Julien Courchet. 2018. “Haploinsufficiency of Autism Spectrum Disorder Candidate Gene NUAK1 Impairs Cortical Development and Behavior in Mice.” *Nature Communications* 9 (1): 4289.

Crawford, Latasha K., and Michael J. Caterina. 2020. “Functional Anatomy of the Sensory Nervous System: Updates From the Neuroscience Bench.” *Toxicologic Pathology* 48 (1): 174–89.

D

Dawes, John M., Greg A. Weir, Steven J. Middleton, Ryan Patel, Kim I. Chisholm, Philippa Pettingill, Liam J. Peck, et al. 2018. “Immune or Genetic-Mediated Disruption of CASPR2 Causes Pain Hypersensitivity Due to Enhanced Primary Afferent Excitability.” *Neuron* 97 (4): 806-822.e10.

Dawson, Matt S., Kevin Gordon-Fleet, Lingxin Yan, Vera Tardos, Huanying He, Kwong Mui, Smriti Nawani, et al. 2023. “Sexual Dimorphism in the Social Behaviour of Cntnap2-Null Mice Correlates with Disrupted Synaptic Connectivity and Increased Microglial Activity in the Anterior Cingulate Cortex.” *Communications Biology* 6 (1): 846.

De León Reyes, Noelia S., Lorena Bragg-Gonzalo, and Marta Nieto. 2020. “Development and Plasticity of the Corpus Callosum.” *Development* 147 (18). https://doi.org/10.1242/dev.189738.

Deemyad, Tara, Stephanie Puig, Andrew E. Papale, Hang Qi, Gregory M. LaRocca, Deepthi Aravind, Emma LaNoce, and Nathaniel N. Urban. 2022. “Lateralized Decrease of Parvalbumin+ Cells in the Somatosensory Cortex of ASD Models Is Correlated with Unilateral Tactile Hypersensitivity.” *Cerebral Cortex* 32 (3): 554–68.

Denisenko-Nehrbass, Natalia, Ksénia Oguievetskaia, Laurence Goutebroze, Thierry Galvez, Hisashi Yamakawa, Osamu Ohara, Michèle Carnaud, and Jean-Antoine Girault. 2003. “Protein 4.1B Associates with Both Caspr/Paranodin and Caspr2 at Paranodes and Juxtaparanodes of Myelinated Fibres.” *The European Journal of Neuroscience* 17 (2): 411–16.

Devlin, Bernie, and Stephen W. Scherer. 2012. “Genetic Architecture in Autism Spectrum Disorder.” *Current Opinion in Genetics & Development* 22 (3): 229–37.

Doldur-Balli, Fusun, Toshihiro Imamura, Olivia J. Veatch, Naihua N. Gong, Diane C. Lim, Michael P. Hart, Ted Abel, Matthew S. Kayser, Edward S. Brodkin, and Allan I. Pack. 2022. “Synaptic Dysfunction Connects Autism Spectrum Disorder and Sleep Disturbances: A Perspective from Studies in Model Organisms.” *Sleep Medicine Reviews* 62 (April): 101595.

Donahoo, Amber-Lee S., and Linda J. Richards. 2009. “Understanding the Mechanisms of Callosal Development through the Use of Transgenic Mouse Models.” *Seminars in Pediatric Neurology* 16 (3): 127–42.

Dougherty, Jose, Natasha Marrus, Susan E. Maloney, Benjamin Yip, Sven Sandin, Tychele N. Turner, Din Selmanovic, et al. 2022. “Can the ‘Female Protective Effect’ Liability Threshold Model Explain Sex Differences in Autism Spectrum Disorder?” *Neuron* 110 (20): 3243–62.

Dupree, J. L., J. A. Girault, and B. Popko. 1999. “Axo-Glial Interactions Regulate the Localization of Axonal Paranodal Proteins.” *The Journal of Cell Biology* 147 (6): 1145–52.

E

Ecker, Christine, John Suckling, Sean C. Deoni, Michael V. Lombardo, Ed T. Bullmore, Simon Baron-Cohen, Marco Catani, et al. 2012. “Brain Anatomy and Its Relationship to Behavior in Adults with Autism Spectrum Disorder: A Multicenter Magnetic Resonance Imaging Study.” *Archives of General Psychiatry* 69 (2): 195–209.

Elder, G. A., V. L. Friedrich Jr, and R. A. Lazzarini. 2001. “Schwann Cells and Oligodendrocytes Read Distinct Signals in Establishing Myelin Sheath Thickness.” *Journal of Neuroscience Research* 65 (6): 493–99.

Emery, Ben, Dritan Agalliu, John D. Cahoy, Trent A. Watkins, Jason C. Dugas, Sara B. Mulinyawe, Adilijan Ibrahim, Keith L. Ligon, David H. Rowitch, and Ben A. Barres. 2009. “Myelin Gene Regulatory Factor Is a Critical Transcriptional Regulator Required for CNS Myelination.” *Cell* 138 (1): 172–85.

Eshed-Eisenbach, Yael, and Elior Peles. 2013. “The Making of a Node: A Co-Production of Neurons and Glia.” *Current Opinion in Neurobiology* 23 (6): 1049–56.

F

Falivelli, Giulia, Antonella De Jaco, Flores Lietta Favaloro, Hyuck Kim, Jennifer Wilson, Noga Dubi, Mark H. Ellisman, Brett S. Abrahams, Palmer Taylor, and Davide Comoletti. 2012. “Inherited Genetic Variants in Autism-Related CNTNAP2 Show Perturbed Trafficking and ATF6 Activation.” *Human Molecular Genetics* 21 (21): 4761–73.

Fame, Ryann M., Jessica L. MacDonald, and Jeffrey D. Macklis. 2011. “Development, Specification, and Diversity of Callosal Projection Neurons.” *Trends in Neurosciences* 34 (1): 41–50.

Fancy, Stephen P. J., Sergio E. Baranzini, Chao Zhao, Dong-In Yuk, Karen-Amanda Irvine, Sovann Kaing, Nader Sanai, Robin J. M. Franklin, and David H. Rowitch. 2009. “Dysregulation of the Wnt Pathway Inhibits Timely Myelination and Remyelination in the Mammalian CNS.” *Genes & Development* 23 (13): 1571–85.

Fenlon, Laura R., Rodrigo Suarez, Zorana Lynton, and Linda J. Richards. 2021. “The Evolution, Formation and Connectivity of the Anterior Commissure.” *Seminars in Cell & Developmental Biology* 118 (October): 50–59.

Fernandes, Dominique, Sandra D. Santos, Ester Coutinho, Jessica L. Whitt, Nuno Beltrão, Tiago Rondão, M. Isabel Leite, Camilla Buckley, Hey-Kyoung Lee, and Ana Luísa Carvalho. 2019. “Disrupted AMPA Receptor Function upon Genetic- or Antibody-Mediated Loss of Autism-Associated CASPR2.” *Cerebral Cortex* 29 (12): 4919–31.

Fernandez, Bridget A., and Stephen W. Scherer. 2017. “Syndromic Autism Spectrum Disorders: Moving from a Clinically Defined to a Molecularly Defined Approach.” *Dialogues in Clinical Neuroscience* 19 (4): 353–71.

Folstein, S. E., and R. E. Mankoski. 2000. “Chromosome 7q: Where Autism Meets Language Disorder?” *American Journal of Human Genetics*.

Folstein, S., and M. Rutter. 1977. “Infantile Autism: A Genetic Study of 21 Twin Pairs.” *Journal of Child Psychology and Psychiatry, and Allied Disciplines* 18 (4): 297–321.

Foran, D. R., and A. C. Peterson. 1992. “Myelin Acquisition in the Central Nervous System of the Mouse Revealed by an MBP-Lac Z Transgene.” *The Journal of Neuroscience: The Official Journal of the Society for Neuroscience* 12 (12): 4890–97.

Freeman, Sean A., Anne Desmazières, Desdemona Fricker, Catherine Lubetzki, and Nathalie Sol-Foulon. 2016. “Mechanisms of Sodium Channel Clustering and Its Influence on Axonal Impulse Conduction.” *Cellular and Molecular Life Sciences: CMLS* 73 (4): 723–35.

Friedman, J. I., T. Vrijenhoek, S. Markx, I. M. Janssen, W. A. van der Vliet, B. H. W. Faas, N. V. Knoers, et al. 2008. “CNTNAP2 Gene Dosage Variation Is Associated with Schizophrenia and Epilepsy.” *Molecular Psychiatry* 13 (3): 261–66.

G

Galvez-Contreras, Alma Y., David Zarate-Lopez, Ana L. Torres-Chavez, and Oscar Gonzalez-Perez. 2020. “Role of Oligodendrocytes and Myelin in the Pathophysiology of Autism Spectrum Disorder.” *Brain Sciences* 10 (12). https://doi.org/10.3390/brainsci10120951.

Gao, Ruoqi, Colleen R. Zaccard, Lauren P. Shapiro, Leonardo E. Dionisio, Maria Dolores Martin-de-Saavedra, Nicolas H. Piguel, Christopher P. Pratt, Katherine E. Horan, and Peter Penzes. 2019. “The CNTNAP2-CASK Complex Modulates GluA1 Subcellular Distribution in Interneurons.” *Neuroscience Letters* 701 (May): 92–99.

Gegenhuber, B., M. V. Wu, R. Bronstein, and J. Tollkuhn. 2022. “Gene Regulation by Gonadal Hormone Receptors Underlies Brain Sex Differences.” *Nature* 606 (7912): 153–59.

Gendre, Thierry, Jean-Pascal Lefaucheur, Jérôme Devaux, and Alain Créange. 2021. “A Patient with Distal Lower Extremity Neuropathic Pain and Anti-Contactin-Associated Protein-2 Antibodies.” *Muscle & Nerve* 64 (3): E15–17.

Geren, B. B., and F. O. Schmitt. 1954. “THE STRUCTURE OF THE SCHWANN CELL AND ITS RELATION TO THE AXON IN CERTAIN INVERTEBRATE NERVE FIBERS.” *Proceedings of the National Academy of Sciences of the United States of America* 40 (9): 863–70.

Girault, Jessica B., and Joseph Piven. 2020. “The Neurodevelopment of Autism from Infancy Through Toddlerhood.” *Neuroimaging Clinics of North America* 30 (1): 97–114.

Glessner, Joseph T., Kai Wang, Guiqing Cai, Olena Korvatska, Cecilia E. Kim, Shawn Wood, Haitao Zhang, et al. 2009. “Autism Genome-Wide Copy Number Variation Reveals Ubiquitin and Neuronal Genes.” *Nature* 459 (7246): 569–73.

Glinton, Kevin E., and Sarah H. Elsea. 2019. “Untargeted Metabolomics for Autism Spectrum Disorders: Current Status and Future Directions.” *Frontiers in Psychiatry / Frontiers Research Foundation* 10 (September): 647.

Goel, Ayush. 2013. “6 Nerve Fibers.” *MedicoNotebook* (blog). January 2013. http://www.mediconotebook.com/2013/01/nerve-fibers.html.

Gordon, Aaron, Daniela Salomon, Noy Barak, Yefim Pen, Michael Tsoory, Tali Kimchi, and Elior Peles. 2016. “Expression of Cntnap2 (Caspr2) in Multiple Levels of Sensory Systems.” *Molecular and Cellular Neurosciences* 70 (January): 42–53.

Graciarena, Mariana, Araceli Seiffe, Brahim Nait-Oumesmar, and Amaicha M. Depino. 2018. “Hypomyelination and Oligodendroglial Alterations in a Mouse Model of Autism Spectrum Disorder.” *Frontiers in Cellular Neuroscience* 12: 517.

Gregor, Anne, Beate Albrecht, Ingrid Bader, Emilia K. Bijlsma, Arif B. Ekici, Hartmut Engels, Karl Hackmann, et al. 2011. “Expanding the Clinical Spectrum Associated with Defects in CNTNAP2 and NRXN1.” *BMC Medical Genetics* 12 (August): 106.

H

Hao, Han, Rosmaliza Ramli, Caixue Wang, Chao Liu, Shihab Shah, Pierce Mullen, Varinder Lall, et al. 2023. “Dorsal Root Ganglia Control Nociceptive Input to the Central Nervous System.” *PLoS Biology* 21 (1): e3001958.

Harding, Erika K., Samuel Wanchi Fung, and Robert P. Bonin. 2020. “Insights Into Spinal Dorsal Horn Circuit Function and Dysfunction Using Optical Approaches.” *Frontiers in Neural Circuits* 14 (June): 31.

Hivert, Bruno, Delphine Pinatel, Marilyne Labasque, Nicolas Tricaud, Laurence Goutebroze, and Catherine Faivre-Sarrailh. 2016. “Assembly of Juxtaparanodes in Myelinating DRG Culture: Differential Clustering of the Kv1/Caspr2 Complex and Scaffolding Protein 4.1B.” *Glia* 64 (5): 840–52.

Hofer, Sabine, Xiaoqing Wang, Volkert Roeloffs, and Jens Frahm. 2015. “Single-Shot T1 Mapping of the Corpus Callosum: A Rapid Characterization of Fiber Bundle Anatomy.” *Frontiers in Neuroanatomy* 9 (May): 57.

Horresh, Ido, Vered Bar, Joseph L. Kissil, and Elior Peles. 2010. “Organization of Myelinated Axons by Caspr and Caspr2 Requires the Cytoskeletal Adapter Protein 4.1B.” *The Journal of Neuroscience: The Official Journal of the Society for Neuroscience* 30 (7): 2480–89.

Horresh, Ido, Sebastian Poliak, Seth Grant, David Bredt, Matthew N. Rasband, and Elior Peles. 2008. “Multiple Molecular Interactions Determine the Clustering of Caspr2 and Kv1 Channels in Myelinated Axons.” *The Journal of Neuroscience: The Official Journal of the Society for Neuroscience* 28 (52): 14213–22.

Huang, Junting, Vinicius M. Gadotti, Lina Chen, Ivana A. Souza, Shuo Huang, Decheng Wang, Charu Ramakrishnan, Karl Deisseroth, Zizhen Zhang, and Gerald W. Zamponi. 2019. “A Neuronal Circuit for Activating Descending Modulation of Neuropathic Pain.” *Nature Neuroscience* 22 (10): 1659–68.

I

Inoki, Ken, Yong Li, Tianquan Zhu, Jun Wu, and Kun-Liang Guan. 2002. “TSC2 Is Phosphorylated and Inhibited by Akt and Suppresses MTOR Signalling.” *Nature Cell Biology* 4 (9): 648–57.

Isom, Lori L. 2002. “The Role of Sodium Channels in Cell Adhesion.” *Frontiers in Bioscience: A Journal and Virtual Library* 7 (January): 12–23.

J

Jang, Wooyoung Eric, Ji Hwan Park, Gaeun Park, Geul Bang, Chan Hyun Na, Jin Young Kim, Kwang-Youl Kim, et al. 2022. “Cntnap2-Dependent Molecular Networks in Autism Spectrum Disorder Revealed through an Integrative Multi-Omics Analysis.” *Molecular Psychiatry*, October. https://doi.org/10.1038/s41380-022-01822-1.

Jash, Sukanta, and Surendra Sharma. 2022. “Pathogenic Infections during Pregnancy and the Consequences for Fetal Brain Development.” *Pathogens* 11 (2). https://doi.org/10.3390/pathogens11020193.

Jessen, Kristján R., Rhona Mirsky, and Alison C. Lloyd. 2015. “Schwann Cells: Development and Role in Nerve Repair.” *Cold Spring Harbor Perspectives in Biology* 7 (7): a020487.

Jiménez-Díaz, Lydia, Sandrine M. Géranton, Gayle M. Passmore, J. Lianne Leith, Amy S. Fisher, Laura Berliocchi, Anantha K. Sivasubramaniam, Anne Sheasby, Bridget M. Lumb, and Stephen P. Hunt. 2008. “Local Translation in Primary Afferent Fibers Regulates Nociception.” *PloS One* 3 (4): e1961.

Jong, Job O. de, Ceyda Llapashtica, Matthieu Genestine, Kevin Strauss, Frank Provenzano, Yan Sun, Huixiang Zhu, et al. 2021. “Cortical Overgrowth in a Preclinical Forebrain Organoid Model of CNTNAP2-Associated Autism Spectrum Disorder.” *Nature Communications* 12 (1): 4087.

Joubert, Bastien, Florent Gobert, Laure Thomas, Margaux Saint-Martin, Virginie Desestret, Philippe Convers, Véronique Rogemond, et al. 2017. “Autoimmune Episodic Ataxia in Patients with Anti-CASPR2 Antibody-Associated Encephalitis.” *Neurology(R) Neuroimmunology & Neuroinflammation* 4 (4): e371.

Joubert, Bastien, Margaux Saint-Martin, Nelly Noraz, Géraldine Picard, Veronique Rogemond, François Ducray, Virginie Desestret, et al. 2016. “Characterization of a Subtype of Autoimmune Encephalitis With Anti-Contactin-Associated Protein-like 2 Antibodies in the Cerebrospinal Fluid, Prominent Limbic Symptoms, and Seizures.” *JAMA Neurology* 73 (9): 1115–24.

Jurgensen, Sofia, and Pablo E. Castillo. 2015. “Selective Dysregulation of Hippocampal Inhibition in the Mouse Lacking Autism Candidate Gene CNTNAP2.” *The Journal of Neuroscience: The Official Journal of the Society for Neuroscience* 35 (43): 14681–87.

Just, Marcel Adam, Vladimir L. Cherkassky, Timothy A. Keller, and Nancy J. Minshew. 2004. “Cortical Activation and Synchronization during Sentence Comprehension in High-Functioning Autism: Evidence of Underconnectivity.” *Brain: A Journal of Neurology* 127 (Pt 8): 1811–21.

K

Kaiser, Tobias, Harrison Mitchell Allen, Ohyoon Kwon, Boaz Barak, Jing Wang, Zhigang He, Minqing Jiang, and Guoping Feng. 2021. “MyelTracer: A Semi-Automated Software for Myelin g-Ratio Quantification.” *ENeuro* 8 (4). https://doi.org/10.1523/ENEURO.0558-20.2021.

Kang, Minkyung, and Yao Yao. 2022. “Laminin Regulates Oligodendrocyte Development and Myelination.” *Glia* 70 (3): 414–29.

Káradóttir, Ragnhildur, Pauline Cavelier, Linda H. Bergersen, and David Attwell. 2005. “NMDA Receptors Are Expressed in Oligodendrocytes and Activated in Ischaemia.” *Nature* 438 (7071): 1162–66.

Karayannis, T., E. Au, J. C. Patel, I. Kruglikov, S. Markx, R. Delorme, D. Héron, et al. 2014. “Cntnap4 Differentially Contributes to GABAergic and Dopaminergic Synaptic Transmission.” *Nature* 511 (7508): 236–40.

Kato, Daisuke, and Hiroaki Wake. 2019. “Activity-Dependent Myelination.” *Advances in Experimental Medicine and Biology* 1190: 43–51.

Kawamura, Atsuki, Yuta Katayama, Masaaki Nishiyama, Hirotaka Shoji, Kota Tokuoka, Yoshifumi Ueta, Mariko Miyata, et al. 2020. “Oligodendrocyte Dysfunction Due to Chd8 Mutation Gives Rise to Behavioral Deficits in Mice.” *Human Molecular Genetics* 29 (8): 1274–91.

Kessaris, Nicoletta, Matthew Fogarty, Palma Iannarelli, Matthew Grist, Michael Wegner, and William D. Richardson. 2006. “Competing Waves of Oligodendrocytes in the Forebrain and Postnatal Elimination of an Embryonic Lineage.” *Nature Neuroscience* 9 (2): 173–79.

Khan, Sheraz, Alexandre Gramfort, Nandita R. Shetty, Manfred G. Kitzbichler, Santosh Ganesan, Joseph M. Moran, Su Mei Lee, et al. 2013. “Local and Long-Range Functional Connectivity Is Reduced in Concert in Autism Spectrum Disorders.” *Proceedings of the National Academy of Sciences of the United States of America* 110 (8): 3107–12.

Khanbabaei, Maryam, Elizabeth Hughes, Jacob Ellegood, Lily R. Qiu, Raven Yip, Jenna Dobry, Kartikeya Murari, Jason P. Lerch, Jong M. Rho, and Ning Cheng. 2019. “Precocious Myelination in a Mouse Model of Autism.” *Translational Psychiatry* 9 (1): 251.

Kidd, Grahame J., Nobuhiko Ohno, and Bruce D. Trapp. 2013. “Chapter 5 - Biology of Schwann Cells.” In *Handbook of Clinical Neurology*, edited by Gérard Said and Christian Krarup, 115:55–79. Elsevier.

Kim, Ji-Woon, Kwanghoon Park, Ri Jin Kang, Edson Luck Gonzales, Hyun Ah Oh, Hana Seung, Mee Jung Ko, Jae Hoon Cheong, Chihye Chung, and Chan Young Shin. 2019. “Gene-Environment Interaction Counterbalances Social Impairment in Mouse Models of Autism.” *Scientific Reports* 9 (1): 11490.

Kim, Ji-Woon, Kwanghoon Park, Ri Jin Kang, Edson Luck T. Gonzales, Do Gyeong Kim, Hyun Ah Oh, Hana Seung, et al. 2019. “Pharmacological Modulation of AMPA Receptor Rescues Social Impairments in Animal Models of Autism.” *Neuropsychopharmacology: Official Publication of the American College of Neuropsychopharmacology* 44 (2): 314–23.

Kitada, Masaaki, and David H. Rowitch. 2006. “Transcription Factor Co-Expression Patterns Indicate Heterogeneity of Oligodendroglial Subpopulations in Adult Spinal Cord.” *Glia* 54 (1): 35–46.

Klibaite, Ugne, Mikhail Kislin, Jessica L. Verpeut, Silke Bergeler, Xiaoting Sun, Joshua W. Shaevitz, and Samuel S-H Wang. 2022. “Deep Phenotyping Reveals Movement Phenotypes in Mouse Neurodevelopmental Models.” *Molecular Autism* 13 (1): 12.

Klingler, Esther, Pierre-Marie Martin, Marta Garcia, Caroline Moreau-Fauvarque, Julien Falk, Fabrice Chareyre, Marco Giovannini, Alain Chédotal, Jean-Antoine Girault, and Laurence Goutebroze. 2015. “The Cytoskeleton-Associated Protein SCHIP1 Is Involved in Axon Guidance, and Is Required for Piriform Cortex and Anterior Commissure Development.” *Development* 142 (11): 2026–36.

Koenning, Matthias, Stacey Jackson, Curtis M. Hay, Clare Faux, Trevor J. Kilpatrick, Melanie Willingham, and Ben Emery. 2012. “Myelin Gene Regulatory Factor Is Required for Maintenance of Myelin and Mature Oligodendrocyte Identity in the Adult CNS.” *The Journal of Neuroscience: The Official Journal of the Society for Neuroscience* 32 (36): 12528–42.

Kwon, Chang-Hyuk, Bryan W. Luikart, Craig M. Powell, Jing Zhou, Sharon A. Matheny, Wei Zhang, Yanjiao Li, Suzanne J. Baker, and Luis F. Parada. 2006. “Pten Regulates Neuronal Arborization and Social Interaction in Mice.” *Neuron* 50 (3): 377–88.

L

LaMantia, A. S., and P. Rakic. 1990. “Axon Overproduction and Elimination in the Corpus Callosum of the Developing Rhesus Monkey.” *The Journal of Neuroscience: The Official Journal of the Society for Neuroscience* 10 (7): 2156–75.

Lamb, J. A., G. Barnby, E. Bonora, N. Sykes, E. Bacchelli, F. Blasi, E. Maestrini, et al. 2005. “Analysis of IMGSAC Autism Susceptibility Loci: Evidence for Sex Limited and Parent of Origin Specific Effects.” *Journal of Medical Genetics* 42 (2): 132–37.

Lauber, Emanuel, Federica Filice, and Beat Schwaller. 2018. “Dysregulation of Parvalbumin Expression in the Cntnap2-/- Mouse Model of Autism Spectrum Disorder.” *Frontiers in Molecular Neuroscience* 11 (August): 262.

Lazaro, Maria T., Jiannis Taxidis, Tristan Shuman, Iris Bachmutsky, Taruna Ikrar, Rommel Santos, G. Mark Marcello, et al. 2019. “Reduced Prefrontal Synaptic Connectivity and Disturbed Oscillatory Population Dynamics in the CNTNAP2 Model of Autism.” *Cell Reports* 27 (9): 2567-2578.e6.

Leblond, Claire S., Caroline Nava, Anne Polge, Julie Gauthier, Guillaume Huguet, Serge Lumbroso, Fabienne Giuliano, et al. 2014. “Meta-Analysis of SHANK Mutations in Autism Spectrum Disorders: A Gradient of Severity in Cognitive Impairments.” *PLoS Genetics* 10 (9): e1004580.

Lee, Seonok, Michelle K. Leach, Stephanie A. Redmond, S. Y. Christin Chong, Synthia H. Mellon, Samuel J. Tuck, Zhang-Qi Feng, Joseph M. Corey, and Jonah R. Chan. 2012. “A Culture System to Study Oligodendrocyte Myelination Processes Using Engineered Nanofibers.” *Nature Methods* 9 (9): 917–22.

Levitt, Pat, and Daniel B. Campbell. 2009. “The Genetic and Neurobiologic Compass Points toward Common Signaling Dysfunctions in Autism Spectrum Disorders.” *The Journal of Clinical Investigation* 119 (4): 747–54.

Leyva-Díaz, E., and G. López-Bendito. 2013. “In and out from the Cortex: Development of Major Forebrain Connections.” *Neuroscience* 254 (December): 26–44.

Li, Qun, Marcel Brus-Ramer, John H. Martin, and John W. McDonald. 2010. “Electrical Stimulation of the Medullary Pyramid Promotes Proliferation and Differentiation of Oligodendrocyte Progenitor Cells in the Corticospinal Tract of the Adult Rat.” *Neuroscience Letters* 479 (2): 128–33.

Liang, Zhuowen, Tao Lei, Shuang Wang, Zhuojing Luo, and Xueyu Hu. 2019. “A Simple Electrical Stimulation Cell Culture System on the Myelination of Dorsal Root Ganglia and Schwann Cells.” *BioTechniques* 67 (1): 11–15.

Lim, Lynette, Da Mi, Alfredo Llorca, and Oscar Marín. 2018. “Development and Functional Diversification of Cortical Interneurons.” *Neuron* 100 (2): 294–313.

Linke, Annika C., R. Joanne Jao Keehn, Ellyn B. Pueschel, Inna Fishman, and Ralph-Axel Müller. 2018. “Children with ASD Show Links between Aberrant Sound Processing, Social Symptoms, and Atypical Auditory Interhemispheric and Thalamocortical Functional Connectivity.” *Developmental Cognitive Neuroscience* 29 (January): 117–26.

Liska, Adam, Alice Bertero, Ryszard Gomolka, Mara Sabbioni, Alberto Galbusera, Noemi Barsotti, Stefano Panzeri, Maria Luisa Scattoni, Massimo Pasqualetti, and Alessandro Gozzi. 2018. “Homozygous Loss of Autism-Risk Gene CNTNAP2 Results in Reduced Local and Long-Range Prefrontal Functional Connectivity.” *Cerebral Cortex* 28 (4): 1141–53.

Liu, Jia, Karen Dietz, Jacqueline M. DeLoyht, Xiomara Pedre, Dipti Kelkar, Jasbir Kaur, Vincent Vialou, et al. 2012. “Impaired Adult Myelination in the Prefrontal Cortex of Socially Isolated Mice.” *Nature Neuroscience* 15 (12): 1621–23.

Lu, Ping, Fengpeng Wang, Shuixiu Zhou, Xiaohua Huang, Hao Sun, Yun-Wu Zhang, Yi Yao, and Honghua Zheng. 2021. “A Novel CNTNAP2 Mutation Results in Abnormal Neuronal E/I Balance.” *Frontiers in Neurology* 12 (October): 712773.

Lu, Zhuoyang, M. V. V. V. Sekhar Reddy, Jianfang Liu, Ana Kalichava, Jiankang Liu, Lei Zhang, Fang Chen, et al. 2016. “Molecular Architecture of Contactin-Associated Protein-like 2 (CNTNAP2) and Its Interaction with Contactin 2 (CNTN2).” *The Journal of Biological Chemistry* 291 (46): 24133–47.

Lyall, Kristen, Lisa Croen, Julie Daniels, M. Daniele Fallin, Christine Ladd-Acosta, Brian K. Lee, Bo Y. Park, et al. 2017. “The Changing Epidemiology of Autism Spectrum Disorders.” *Annual Review of Public Health* 38 (March): 81–102.

Lynn, Andrew C., Aarthi Padmanabhan, Daniel Simmonds, William Foran, Michael N. Hallquist, Beatriz Luna, and Kirsten O’Hearn. 2018. “Functional Connectivity Differences in Autism during Face and Car Recognition: Underconnectivity and Atypical Age-Related Changes.” *Developmental Science* 21 (1). https://doi.org/10.1111/desc.12508.

M

MacLusky, N. J., and F. Naftolin. 1981. “Sexual Differentiation of the Central Nervous System.” *Science* 211 (4488): 1294–1302.

Maenner, Matthew J., Zachary Warren, Ashley Robinson Williams, Esther Amoakohene, Amanda V. Bakian, Deborah A. Bilder, Maureen S. Durkin, et al. 2023. “Prevalence and Characteristics of Autism Spectrum Disorder Among Children Aged 8 Years - Autism and Developmental Disabilities Monitoring Network, 11 Sites, United States, 2020.” *Morbidity and Mortality Weekly Report. Surveillance Summaries* 72 (2): 1–14.

Marie, Corentine, Adrien Clavairoly, Magali Frah, Hatem Hmidan, Jun Yan, Chuntao Zhao, Juliette Van Steenwinckel, et al. 2018. “Oligodendrocyte Precursor Survival and Differentiation Requires Chromatin Remodeling by Chd7 and Chd8.” *Proceedings of the National Academy of Sciences of the United States of America* 115 (35): E8246–55.

Markram, Henry, Maria Toledo-Rodriguez, Yun Wang, Anirudh Gupta, Gilad Silberberg, and Caizhi Wu. 2004. “Interneurons of the Neocortical Inhibitory System.” *Nature Reviews. Neuroscience* 5 (10): 793–807.

Marques, Sueli, Amit Zeisel, Simone Codeluppi, David van Bruggen, Ana Mendanha Falcão, Lin Xiao, Huiliang Li, et al. 2016. “Oligodendrocyte Heterogeneity in the Mouse Juvenile and Adult Central Nervous System.” *Science* 352 (6291): 1326–29.

Martin, Pierre-Marie, Carmen Cifuentes-Diaz, Jérôme Devaux, Marta Garcia, Jocelyne Bureau, Sylvie Thomasseau, Esther Klingler, Jean-Antoine Girault, and Laurence Goutebroze. 2017. “Schwannomin-Interacting Protein 1 Isoform IQCJ-SCHIP1 Is a Multipartner Ankyrin- and Spectrin-Binding Protein Involved in the Organization of Nodes of Ranvier.” *The Journal of Biological Chemistry* 292 (6): 2441–56.

Martin-Lopez, Eduardo, Sarah J. Meller, and Charles A. Greer. 2018. “Development of Piriform Cortex Interhemispheric Connections via the Anterior Commissure: Progressive and Regressive Strategies.” *Brain Structure & Function* 223 (9): 4067–85.

McCarthy, Margaret M. 2008. “Estradiol and the Developing Brain.” *Physiological Reviews* 88 (1): 91–124.

McEwen, B. S. 1981. “Neural Gonadal Steroid Actions.” *Science* 211 (4488): 1303–11.

McKenzie, Ian A., David Ohayon, Huiliang Li, Joana Paes de Faria, Ben Emery, Koujiro Tohyama, and William D. Richardson. 2014. “Motor Skill Learning Requires Active Central Myelination.” *Science* 346 (6207): 318–22.

Menegoz, M., P. Gaspar, M. Le Bert, T. Galvez, F. Burgaya, C. Palfrey, P. Ezan, F. Arnos, and J. A. Girault. 1997. “Paranodin, a Glycoprotein of Neuronal Paranodal Membranes.” *Neuron* 19 (2): 319–31.

Milan, Marta, Chiara Balestrieri, Gabriele Alfarano, Sara Polletti, Elena Prosperini, Paola Nicoli, Paola Spaggiari, et al. 2020. “Pancreatic Cancer Cells Require the Transcription Factor MYRF to Maintain ER Homeostasis.” *Developmental Cell* 55 (4): 398-412.e7.

Mishra, Santosh K. 2022. “The Role of CNTNAP2 in Itch Sensation.” *The Journal of Investigative Dermatology* 142 (1): 251–53.

Modabbernia, Amirhossein, Eva Velthorst, and Abraham Reichenberg. 2017. “Environmental Risk Factors for Autism: An Evidence-Based Review of Systematic Reviews and Meta-Analyses.” *Molecular Autism* 8 (March): 13.

Monje, Michelle. 2018. “Myelin Plasticity and Nervous System Function.” *Annual Review of Neuroscience* 41 (July): 61–76.

Montalban, Enrica, Albert Giralt, Lieng Taing, Evelien H. S. Schut, Laura F. Supiot, Laia Castell, Yuki Nakamura, et al. 2022. “Translational Profiling of Mouse Dopaminoceptive Neurons Reveals Region-Specific Gene Expression, Exon Usage, and Striatal Prostaglandin E2 Modulatory Effects.” *Molecular Psychiatry* 27 (4): 2068–79.

Monteiro, Patricia, and Guoping Feng. 2017. “SHANK Proteins: Roles at the Synapse and in Autism Spectrum Disorder.” *Nature Reviews. Neuroscience* 18 (3): 147–57.

Muhle, Rebecca, Stephanie V. Trentacoste, and Isabelle Rapin. 2004. “The Genetics of Autism.” *Pediatrics* 113 (5): e472-86.

Mukhtar, Tanzila, and Verdon Taylor. 2018. “Untangling Cortical Complexity During Development.” *Journal of Experimental Neuroscience* 12 (March): 1179069518759332.

Muñiz-Castrillo, Sergio, Bastien Joubert, Mad-Hélénie Elsensohn, Anne-Laurie Pinto, Margaux Saint-Martin, Alberto Vogrig, Géraldine Picard, et al. 2020. “Anti-CASPR2 Clinical Phenotypes Correlate with HLA and Immunological Features.” *Journal of Neurology, Neurosurgery, and Psychiatry* 91 (10): 1076–84.

Murdoch, John D., Abha R. Gupta, Stephan J. Sanders, Michael F. Walker, John Keaney, Thomas V. Fernandez, Michael T. Murtha, et al. 2015. “No Evidence for Association of Autism with Rare

Heterozygous Point Mutations in Contactin-Associated Protein-Like 2 (CNTNAP2), or in Other Contactin-Associated Proteins or Contactins." *PLoS Genetics* 11 (1): e1004852.

N

Narita, Akira, Masato Nagai, Satoshi Mizuno, Soichi Ogishima, Gen Tamiya, Masao Ueki, Rieko Sakurai, et al. 2020. "Clustering by Phenotype and Genome-Wide Association Study in Autism." *Translational Psychiatry* 10 (1): 290.

Newville, Jessie, Lauren L. Jantzie, and Lee Anna Cunningham. 2017. "Embracing Oligodendrocyte Diversity in the Context of Perinatal Injury." *Neural Regeneration Research* 12 (10): 1575–85.

Nicolini, Chiara, and Margaret Fahnestock. 2018. "The Valproic Acid-Induced Rodent Model of Autism." *Experimental Neurology* 299 (Pt A): 217–27.

Nishiyama, Akiko, Takahiro Shimizu, Amin Sherafat, and William D. Richardson. 2021. "Life-Long Oligodendrocyte Development and Plasticity." *Seminars in Cell & Developmental Biology* 116 (August): 25–37.

O

O'Brien, John S., and E. Lois Sampson. 1965. "Lipid Composition of the Normal Human Brain: Gray Matter, White Matter, and Myelin*." *Journal of Lipid Research* 6 (4): 537–44.

Ogawa, Yasuhiro, Juan Oses-Prieto, Moon Young Kim, Ido Horresh, Elior Peles, Alma L. Burlingame, James S. Trimmer, Dies Meijer, and Matthew N. Rasband. 2010. "ADAM22, a Kv1 Channel-Interacting Protein, Recruits Membrane-Associated Guanylate Kinases to Juxtaparanodes of Myelinated Axons." *The Journal of Neuroscience: The Official Journal of the Society for Neuroscience* 30 (3): 1038–48.

Olsen, Abby L., Yongjie Lai, Josep Dalmau, Steven S. Scherer, and Eric Lancaster. 2015. "Caspr2 Autoantibodies Target Multiple Epitopes." *Neurology(R) Neuroimmunology & Neuroinflammation* 2 (4): e127.

O'Roak, Brian J., and Matthew W. State. 2008. "Autism Genetics: Strategies, Challenges, and Opportunities." *Autism Research: Official Journal of the International Society for Autism Research* 1 (1): 4–17.

P

Pagani, Marco, Noemi Barsotti, Alice Bertero, Stavros Trakoshis, Laura Ulysse, Andrea Locarno, Ieva Miseviciute, et al. 2021. "MTOR-Related Synaptic Pathology Causes Autism Spectrum Disorder-Associated Functional Hyperconnectivity." *Nature Communications* 12 (1): 6084.

Pagnamenta, Alistair T., Elena Bacchelli, Maretha V. de Jonge, Ghazala Mirza, Thomas S. Scerri, Fiorella Minopoli, Andreas Chiocchetti, et al. 2010. "Characterization of a Family with Rare Deletions in CNTNAP5 and DOCK4 Suggests Novel Risk Loci for Autism and Dyslexia." *Biological Psychiatry* 68 (4): 320–28.

Park, Kevin Kyungsuk, Kai Liu, Yang Hu, Patrice D. Smith, Chen Wang, Bin Cai, Bengang Xu, et al. 2008. “Promoting Axon Regeneration in the Adult CNS by Modulation of the PTEN/MTOR Pathway.” *Science* 322 (5903): 963–66.

Peñagarikano, Olga, Brett S. Abrahams, Edward I. Herman, Kellen D. Winden, Amos Gdalyahu, Hongmei Dong, Lisa I. Sonnenblick, et al. 2011. “Absence of CNTNAP2 Leads to Epilepsy, Neuronal Migration Abnormalities, and Core Autism-Related Deficits.” *Cell* 147 (1): 235–46.

Pereira, Jorge A., Frédéric Lebrun-Julien, and Ueli Suter. 2012. “Molecular Mechanisms Regulating Myelination in the Peripheral Nervous System.” *Trends in Neurosciences* 35 (2): 123–34.

Pinatel, Delphine, Bruno Hivert, José Boucraut, Margaux Saint-Martin, Véronique Rogemond, Lida Zoupi, Domna Karagogeos, Jérôme Honnorat, and Catherine Faivre-Sarrailh. 2015. “Inhibitory Axons Are Targeted in Hippocampal Cell Culture by Anti-Caspr2 Autoantibodies Associated with Limbic Encephalitis.” *Frontiers in Cellular Neuroscience* 9 (July): 265.

Pinto, Dalila, Alistair T. Pagnamenta, Lambertus Klei, Richard Anney, Daniele Merico, Regina Regan, Judith Conroy, et al. 2010. “Functional Impact of Global Rare Copy Number Variation in Autism Spectrum Disorders.” *Nature* 466 (7304): 368–72.

Podbielska, Maria, Naren L. Banik, Ewa Kurowska, and Edward L. Hogan. 2013. “Myelin Recovery in Multiple Sclerosis: The Challenge of Remyelination.” *Brain Sciences* 3 (3): 1282–1324.

Poliak, S., L. Gollan, R. Martinez, A. Custer, S. Einheber, J. L. Salzer, J. S. Trimmer, P. Shrager, and E. Peles. 1999. “Caspr2, a New Member of the Neurexin Superfamily, Is Localized at the Juxtaparanodes of Myelinated Axons and Associates with K+ Channels.” *Neuron* 24 (4): 1037–47.

Poliak, S., L. Gollan, D. Salomon, E. O. Berglund, R. Ohara, B. Ranscht, and E. Peles. 2001. “Localization of Caspr2 in Myelinated Nerves Depends on Axon-Glia Interactions and the Generation of Barriers along the Axon.” *The Journal of Neuroscience: The Official Journal of the Society for Neuroscience* 21 (19): 7568–75.

Poliak, Sebastian, and Elior Peles. 2003. “The Local Differentiation of Myelinated Axons at Nodes of Ranvier.” *Nature Reviews. Neuroscience* 4 (12): 968–80.

Poliak, Sebastian, Daniela Salomon, Hadas Elhanany, Helena Sabanay, Brent Kiernan, Larysa Pevny, Colin L. Stewart, et al. 2003. “Juxtaparanodal Clustering of Shaker-like K+ Channels in Myelinated Axons Depends on Caspr2 and TAG-1.” *The Journal of Cell Biology* 162 (6): 1149–60.

Poot, Martin. 2015. “Connecting the CNTNAP2 Networks with Neurodevelopmental Disorders.” *Molecular Syndromology* 6 (1): 7–22.

Poot, Martin, Vera Beyer, Ira Schwaab, Natalja Damatova, Ruben Van’t Slot, Jo Prothero, Sue E. Holder, and Thomas Haaf. 2010. “Disruption of CNTNAP2 and Additional Structural Genome Changes in a Boy with Speech Delay and Autism Spectrum Disorder.” *Neurogenetics* 11 (1): 81–89.

Porreca, Frank, Michael H. Ossipov, and G. F. Gebhart. 2002. “Chronic Pain and Medullary Descending Facilitation.” *Trends in Neurosciences* 25 (6): 319–25.

Price, Theodore J., Md Harunor Rashid, Magali Millecamps, Raul Sanoja, Jose M. Entrena, and Fernando Cervero. 2007. “Decreased Nociceptive Sensitization in Mice Lacking the Fragile X Mental Retardation Protein: Role of MGluR1/5 and MTOR.” *The Journal of Neuroscience: The Official Journal of the Society for Neuroscience* 27 (51): 13958–67.

Q

Qiu, Shuang, Yingjia Qiu, Yan Li, and Xianling Cong. 2022. “Genetics of Autism Spectrum Disorder: An Umbrella Review of Systematic Reviews and Meta-Analyses.” *Translational Psychiatry* 12 (1): 249.

R

Rafiee, Faranak, Roya Rezvani Habibabadi, Mina Motaghi, David M. Yousem, and Ilyssa J. Yousem. 2022. “Brain MRI in Autism Spectrum Disorder: Narrative Review and Recent Advances.” *Journal of Magnetic Resonance Imaging: JMRI* 55 (6): 1613–24.

Ramanathan, Sudarshini, Mandy Tseng, Alexander J. Davies, Christopher E. Uy, Sofija Paneva, Victor C. Mgbachi, Sophia Michael, et al. 2021. “Leucine-Rich Glioma-Inactivated 1 versus Contactin-Associated Protein-like 2 Antibody Neuropathic Pain: Clinical and Biological Comparisons.” *Annals of Neurology* 90 (4): 683–90.

Ramesh, Vijaya. 2004. “Merlin and the ERM Proteins in Schwann Cells, Neurons and Growth Cones.” *Nature Reviews. Neuroscience* 5 (6): 462–70.

Rasband, M. N., E. Peles, J. S. Trimmer, S. R. Levinson, S. E. Lux, and P. Shrager. 1999. “Dependence of Nodal Sodium Channel Clustering on Paranodal Axoglial Contact in the Developing CNS.” *The Journal of Neuroscience: The Official Journal of the Society for Neuroscience* 19 (17): 7516–28.

Rasband, Matthew N., and Elior Peles. 2015. “The Nodes of Ranvier: Molecular Assembly and Maintenance.” *Cold Spring Harbor Perspectives in Biology* 8 (3): a020495.

———. 2021. “Mechanisms of Node of Ranvier Assembly.” *Nature Reviews. Neuroscience* 22 (1): 7–20.

Raybaud, Charles. 2010. “The Corpus Callosum, the Other Great Forebrain Commissures, and the Septum Pellucidum: Anatomy, Development, and Malformation.” *Neuroradiology* 52 (6): 447–77.

Ren, Tianbo, Aurora Anderson, Wei-Bin Shen, Hao Huang, Celine Plachez, Jiangyang Zhang, Susumu Mori, Stephen L. Kinsman, and Linda J. Richards. 2006. “Imaging, Anatomical, and Molecular Analysis of Callosal Formation in the Developing Human Fetal Brain.” *The Anatomical Record. Part A, Discoveries in Molecular, Cellular, and Evolutionary Biology* 288 (2): 191–204.

Richards, L. J., C. Plachez, and T. Ren. 2004. “Mechanisms Regulating the Development of the Corpus Callosum and Its Agenesis in Mouse and Human.” *Clinical Genetics* 66 (4): 276–89.

Rodier, P. M., J. L. Ingram, B. Tisdale, S. Nelson, and J. Romano. 1996. “Embryological Origin for Autism: Developmental Anomalies of the Cranial Nerve Motor Nuclei.” *The Journal of Comparative Neurology* 370 (2): 247–61.

Rodrigues, Carlos Hm, Douglas Ev Pires, and David B. Ascher. 2018. “DynaMut: Predicting the Impact of Mutations on Protein Conformation, Flexibility and Stability.” *Nucleic Acids Research* 46 (W1): W350–55.

Roohi, J., C. Montagna, D. H. Tegay, L. E. Palmer, C. DeVincent, J. C. Pomeroy, S. L. Christian, N. Nowak, and E. Hatchwell. 2009. “Disruption of Contactin 4 in Three Subjects with Autism Spectrum Disorder.” *Journal of Medical Genetics* 46 (3): 176–82.

Rubio-Marrero, Eva N., Gabriele Vincelli, Cy M. Jeffries, Tanvir R. Shaikh, Irene S. Pakos, Fanomezana M. Ranaivoson, Sventja von Daake, et al. 2016. “Structural Characterization of the Extracellular Domain of CASPR2 and Insights into Its Association with the Novel Ligand Contactin1.” *The Journal of Biological Chemistry* 291 (11): 5788–5802.

Rudy, Bernardo, Gordon Fishell, Soohyun Lee, and Jens Hjerling-Leffler. 2011. “Three Groups of Interneurons Account for Nearly 100% of Neocortical GABAergic Neurons.” *Developmental Neurobiology* 71 (1): 45–61.

Rylaarsdam, Lauren, and Alicia Guemez-Gamboa. 2019. “Genetic Causes and Modifiers of Autism Spectrum Disorder.” *Frontiers in Cellular Neuroscience* 13 (August): 385.

S

Saifetiarova, Julia, Xi Liu, Anna M. Taylor, Jie Li, and Manzoor A. Bhat. 2017. “Axonal Domain Disorganization in Caspr1 and Caspr2 Mutant Myelinated Axons Affects Neuromuscular Junction Integrity, Leading to Muscle Atrophy.” *Journal of Neuroscience Research* 95 (7): 1373–90.

Saint-Martin, Margaux, Bastien Joubert, Véronique Pellier-Monnin, Olivier Pascual, Nelly Noraz, and Jérôme Honnorat. 2018. “Contactin-Associated Protein-like 2, a Protein of the Neurexin Family Involved in Several Human Diseases.” *The European Journal of Neuroscience* 48 (3): 1906–23.

Sampath, Srirangan, Shambu Bhat, Simone Gupta, Ashley O’Connor, Andrew B. West, Dan E. Arking, and Aravinda Chakravarti. 2013. “Defining the Contribution of CNTNAP2 to Autism Susceptibility.” *PloS One* 8 (10): e77906.

Sanders, Stephan J., Michael T. Murtha, Abha R. Gupta, John D. Murdoch, Melanie J. Raubeson, A. Jeremy Willsey, A. Gulhan Ercan-Sencicek, et al. 2012. “De Novo Mutations Revealed by Whole-Exome Sequencing Are Strongly Associated with Autism.” *Nature* 485 (7397): 237–41.

Savvaki, Maria, Theofanis Panagiotaropoulos, Antonis Stamatakis, Irene Sargiannidou, Pinelopi Karatzioula, Kazutada Watanabe, Fotini Stylianopoulou, Domna Karagogeos, and Kleopas A. Kleopa. 2008. “Impairment of Learning and Memory in TAG-1 Deficient Mice Associated with Shorter CNS Internodes and Disrupted Juxtaparanodes.” *Molecular and Cellular Neurosciences* 39 (3): 478–90.

Schaaf, Christian P., and Huda Y. Zoghbi. 2011. “Solving the Autism Puzzle a Few Pieces at a Time.” *Neuron*.

Schanen, N. Carolyn. 2006. “Epigenetics of Autism Spectrum Disorders.” *Human Molecular Genetics* 15 Spec No 2 (October): R138-50.

Scott, Kaela E., Rajkamalpreet S. Mann, Ashley L. Schormans, Susanne Schmid, and Brian L. Allman. 2022. “Hyperexcitable and Immature-like Neuronal Activity in the Auditory Cortex of Adult Rats Lacking the Language-Linked CNTNAP2 Gene.” *Cerebral Cortex* 32 (21): 4797–4817.

Scott, Ricardo, Alberto Sánchez-Aguilera, Kim van Elst, Lynette Lim, Nathalie Dehorter, Sung Eun Bae, Giorgia Bartolini, et al. 2019. “Loss of Cntnap2 Causes Axonal Excitability Deficits, Developmental Delay in Cortical Myelination, and Abnormal Stereotyped Motor Behavior.” *Cerebral Cortex* 29 (2): 586–97.

Shangguan, Yafei, Xin Xu, Baigalimaa Ganbat, Yun Li, Wei Wang, Yong Yang, Xi Lu, Chao Du, Xin Tian, and Xuefeng Wang. 2018. “CNTNAP4 Impacts Epilepsy Through GABAA Receptors Regulation: Evidence From Temporal Lobe Epilepsy Patients and Mouse Models.” *Cerebral Cortex* 28 (10): 3491–3504.

Sharma, Samata R., Xenia Gonda, and Frank I. Tarazi. 2018. “Autism Spectrum Disorder: Classification, Diagnosis and Therapy.” *Pharmacology & Therapeutics* 190 (October): 91–104.

Shiota, Yuka, Tetsu Hirosawa, Yuko Yoshimura, Sanae Tanaka, Chiaki Hasegawa, Sumie Iwasaki, Kyung-Min An, et al. 2021. “A Common Variant of CNTNAP2 Is Associated with Sub-Threshold Autistic Traits and Intellectual Disability.” *PloS One* 16 (12): e0260548.

Simons, Mikael, and David A. Lyons. 2013. “Axonal Selection and Myelin Sheath Generation in the Central Nervous System.” *Current Opinion in Cell Biology* 25 (4): 512–19.

Smith, David I., Yu Zhu, Sarah McAvoy, and Robert Kuhn. 2006. “Common Fragile Sites, Extremely Large Genes, Neural Development and Cancer.” *Cancer Letters* 232 (1): 48–57.

Snaidero, Nicolas, Wiebke Möbius, Tim Czopka, Liesbeth H. P. Hekking, Cliff Mathisen, Dick Verkleij, Sandra Goebbels, et al. 2014. “Myelin Membrane Wrapping of CNS Axons by PI(3,4,5)P3-Dependent Polarized Growth at the Inner Tongue.” *Cell* 156 (1–2): 277–90.

Sobottka, Bettina, Urs Ziegler, Andres Kaech, Burkhard Becher, and Norbert Goebels. 2011. “CNS Live Imaging Reveals a New Mechanism of Myelination: The Liquid Croissant Model.” *Glia* 59 (12): 1841–49.

Strauss, Kevin A., Erik G. Puffenberger, Matthew J. Huentelman, Steven Gottlieb, Seth E. Dobrin, Jennifer M. Parod, Dietrich A. Stephan, and D. Holmes Morton. 2006. “Recessive Symptomatic Focal Epilepsy and Mutant Contactin-Associated Protein-like 2.” *The New England Journal of Medicine* 354 (13): 1370–77.

Suárez, Rodrigo, Ilan Gobius, and Linda J. Richards. 2014. “Evolution and Development of Interhemispheric Connections in the Vertebrate Forebrain.” *Frontiers in Human Neuroscience* 8 (July): 497.

Supekar, Kaustubh, Lucina Q. Uddin, Amirah Khouzam, Jennifer Phillips, William D. Gaillard, Lauren E. Kenworthy, Benjamin E. Yerys, Chandan J. Vaidya, and Vinod Menon. 2013. “Brain Hyperconnectivity in Children with Autism and Its Links to Social Deficits.” *Cell Reports* 5 (3): 738–47.

T

Tartaglione, Anna Maria, Sara Schiavi, Gemma Calamandrei, and Viviana Trezza. 2019. “Prenatal Valproate in Rodents as a Tool to Understand the Neural Underpinnings of Social Dysfunctions in Autism Spectrum Disorder.” *Neuropharmacology* 159 (November): 107477.

Taveggia, Carla, George Zanazzi, Ashley Petrylak, Hiroko Yano, Jack Rosenbluth, Steven Einheber, Xiaorong Xu, et al. 2005. “Neuregulin-1 Type III Determines the Ensheathment Fate of Axons.” *Neuron* 47 (5): 681–94.

Tierney, Adrienne L., and Charles A. Nelson 3rd. 2009. “Brain Development and the Role of Experience in the Early Years.” *Zero to Three* 30 (2): 9–13.

Toma, Claudio, Kerrie D. Pierce, Alex D. Shaw, Anna Heath, Philip B. Mitchell, Peter R. Schofield, and Janice M. Fullerton. 2018. “Comprehensive Cross-Disorder Analyses of CNTNAP2 Suggest It Is Unlikely to Be a Primary Risk Gene for Psychiatric Disorders.” *PLoS Genetics* 14 (12): e1007535.

Tong, Da-Li, Rui-Guo Chen, Yu-Lan Lu, Wei-Ke Li, Yue-Fang Zhang, Jun-Kai Lin, Ling-Jie He, et al. 2019. “The Critical Role of ASD-Related Gene CNTNAP3 in Regulating Synaptic Development and Social Behavior in Mice.” *Neurobiology of Disease* 130 (October): 104486.

Torre-Fuentes, L., L. Moreno-Jiménez, V. Pytel, J. A. Matías-Guiu, U. Gómez-Pinedo, and J. Matías-Guiu. 2020. “Experimental Models of Demyelination and Remyelination.” *Neurología (English Edition)* 35 (1): 32.

Townsend, Leah B., and Spencer L. Smith. 2017. “Genotype- and Sex-Dependent Effects of Altered Cntnap2 Expression on the Function of Visual Cortical Areas.” *Journal of Neurodevelopmental Disorders* 9 (January): 2.

Traka, Maria, Jeffrey L. Dupree, Brian Popko, and Domna Karagogeos. 2002. “The Neuronal Adhesion Protein TAG-1 Is Expressed by Schwann Cells and Oligodendrocytes and Is Localized to the Juxtaparanodal Region of Myelinated Fibers.” *The Journal of Neuroscience: The Official Journal of the Society for Neuroscience* 22 (8): 3016–24.

Traka, Maria, Laurence Goutebroze, Natalia Denisenko, Maria Bessa, Artemisia Nifli, Sophia Havaki, Yoichiro Iwakura, et al. 2003. “Association of TAG-1 with Caspr2 Is Essential for the Molecular Organization of Juxtaparanodal Regions of Myelinated Fibers.” *The Journal of Cell Biology* 162 (6): 1161–72.

Travers, Brittany G., Nagesh Adluru, Chad Ennis, Do P. M. Tromp, Dan Destiche, Sam Doran, Erin D. Bigler, Nicholas Lange, Janet E. Lainhart, and Andrew L. Alexander. 2012. “Diffusion Tensor Imaging in Autism Spectrum Disorder: A Review.” *Autism Research: Official Journal of the International Society for Autism Research* 5 (5): 289–313.

U

U.S. Department of Health & Human Services. 2022. “What Is Autism Spectrum Disorder?” Centers for Disease Control and Prevention. December 9, 2022. https://www.cdc.gov/ncbddd/autism/facts.html.

Usoskin, Dmitry, Alessandro Furlan, Saiful Islam, Hind Abdo, Peter Lönnerberg, Daohua Lou, Jens Hjerling-Leffler, et al. 2015. “Unbiased Classification of Sensory Neuron Types by Large-Scale Single-Cell RNA Sequencing.” *Nature Neuroscience* 18 (1): 145–53.

Utzschneider, D., J. Kocsis, and M. Devor. 1992. “Mutual Excitation among Dorsal Root Ganglion Neurons in the Rat.” *Neuroscience Letters* 146 (1): 53–56.

V

Varea, Olga, Maria Dolores Martin-de-Saavedra, Katherine J. Kopeikina, Britta Schürmann, Hunter J. Fleming, Jessica M. Fawcett-Patel, Anthony Bach, et al. 2015. “Synaptic Abnormalities and Cytoplasmic Glutamate Receptor Aggregates in Contactin Associated Protein-like 2/Caspr2 Knockout Neurons.” *Proceedings of the National Academy of Sciences of the United States of America* 112 (19): 6176–81.

Verkerk, Annemieke J. M. H., Carol A. Mathews, Marijke Joosse, Bert H. J. Eussen, Peter Heutink, Ben A. Oostra, and Tourette Syndrome Association International Consortium for Genetics. 2003. “CNTNAP2 Is Disrupted in a Family with Gilles de La Tourette Syndrome and Obsessive Compulsive Disorder.” *Genomics* 82 (1): 1–9.

Vicari, Stefano, Eleonora Napoli, Viviana Cordeddu, Deny Menghini, Viola Alesi, Sara Loddo, Antonio Novelli, and Marco Tartaglia. 2019. “Copy Number Variants in Autism Spectrum Disorders.” *Progress in Neuro-Psychopharmacology & Biological Psychiatry* 92 (June): 421–27.

Vogt, Daniel, Kathleen K. A. Cho, Samantha M. Shelton, Anirban Paul, Z. Josh Huang, Vikaas S. Sohal, and John L. R. Rubenstein. 2018. “Mouse Cntnap2 and Human CNTNAP2 ASD Alleles Cell Autonomously Regulate PV+ Cortical Interneurons.” *Cerebral Cortex* 28 (11): 3868–79.

W

Wake, Hiroaki, Philip R. Lee, and R. Douglas Fields. 2011. “Control of Local Protein Synthesis and Initial Events in Myelination by Action Potentials.” *Science* 333 (6049): 1647–51.

Waxman, S. G., and T. J. Sims. 1984. “Specificity in Central Myelination: Evidence for Local Regulation of Myelin Thickness.” *Brain Research* 292 (1): 179–85.

Wen, Zhu, Tian-Lin Cheng, Gai-Zhi Li, Shi-Bang Sun, Shun-Ying Yu, Yi Zhang, Ya-Song Du, and Zilong Qiu. 2017. “Identification of Autism-Related MECP2 Mutations by Whole-Exome Sequencing and Functional Validation.” *Molecular Autism* 8 (August): 43.

Werner, Emily, Geraldine Dawson, Jeffrey Munson, and Julie Osterling. 2005. “Variation in Early Developmental Course in Autism and Its Relation with Behavioral Outcome at 3-4 Years of Age.” *Journal of Autism and Developmental Disorders* 35 (3): 337–50.

Wiel, Laurens, Coos Baakman, Daan Gilissen, Joris A. Veltman, Gerrit Vriend, and Christian Gilissen. 2019. “MetaDome: Pathogenicity Analysis of Genetic Variants through Aggregation of Homologous Human Protein Domains.” *Human Mutation* 40 (8): 1030–38.

Winden, Kellen D., Darius Ebrahimi-Fakhari, and Mustafa Sahin. 2018. “Abnormal MTOR Activation in Autism.” *Annual Review of Neuroscience* 41 (July): 1–23.

Witelson, S. F. 1989. “Hand and Sex Differences in the Isthmus and Genu of the Human Corpus Callosum. A Postmortem Morphological Study.” *Brain: A Journal of Neurology* 112 (Pt 3) (June): 799–835.

Wolff, Jason J., Guido Gerig, John D. Lewis, Takahiro Soda, Martin A. Styner, Clement Vachet, Kelly N. Botteron, et al. 2015. “Altered Corpus Callosum Morphology Associated with Autism over the First 2 Years of Life.” *Brain: A Journal of Neurology* 138 (Pt 7): 2046–58.

Woodbury-Smith, Marc, and Stephen W. Scherer. 2018. “Progress in the Genetics of Autism Spectrum Disorder.” *Developmental Medicine and Child Neurology* 60 (5): 445–51.

X

Xiao, Lin, David Ohayon, Ian A. McKenzie, Alexander Sinclair-Wilson, Jordan L. Wright, Alexander D. Fudge, Ben Emery, Huiliang Li, and William D. Richardson. 2016. “Rapid Production of New Oligodendrocytes Is Required in the Earliest Stages of Motor-Skill Learning.” *Nature Neuroscience* 19 (9): 1210–17.

Xing, Xiaoliang, Kunyang Wu, Yufan Dong, Yimei Zhou, Jing Zhang, Fang Jiang, Wang-Ping Hu, and Jia-Da Li. 2020. “Hyperactive Akt-MTOR Pathway as a Therapeutic Target for Pain Hypersensitivity in Cntnap2-Deficient Mice.” *Neuropharmacology* 165 (March): 107816.

Xing, Xiaoliang, Jing Zhang, Kunyang Wu, Beibei Cao, Xianfeng Li, Fang Jiang, Zhengmao Hu, Kun Xia, and Jia-Da Li. 2019. “Suppression of Akt-MTOR Pathway Rescued the Social Behavior in Cntnap2-Deficient Mice.” *Scientific Reports* 9 (1): 3041.

Xu, Guifeng, Lane Strathearn, Buyun Liu, Binrang Yang, and Wei Bao. 2018. “Twenty-Year Trends in Diagnosed Attention-Deficit/Hyperactivity Disorder Among US Children and Adolescents, 1997-2016.” *JAMA Network Open* 1 (4): e181471.

Y

Yang, Qun, Peng Huang, Chen Li, Peng Fang, Ningxia Zhao, Jie Nan, Bingzhao Wang, Wei Gao, and Long-Biao Cui. 2018. “Mapping Alterations of Gray Matter Volume and White Matter Integrity in Children with Autism Spectrum Disorder: Evidence from FMRI Findings.” *Neuroreport* 29 (14): 1188–92.

Z

Zeidán-Chuliá, Fares, Ben-Hur Neves de Oliveira, Manuel F. Casanova, Emily L. Casanova, Mami Noda, Alla B. Salmina, and Alexei Verkhratsky. 2016. “Up-Regulation of Oligodendrocyte Lineage Markers in the Cerebellum of Autistic Patients: Evidence from Network Analysis of Gene Expression.” *Molecular Neurobiology* 53 (6): 4019–25.

Zerbi, Valerio, Giovanna D. Ielacqua, Marija Markicevic, Matthias Georg Haberl, Mark H. Ellisman, Arjun A-Bhaskaran, Andreas Frick, Markus Rudin, and Nicole Wenderoth. 2018. “Dysfunctional Autism Risk Genes Cause Circuit-Specific Connectivity Deficits With Distinct Developmental Trajectories.” *Cerebral Cortex* 28 (7): 2495–2506.

Zhang, Jie, Daniel J. Cavanaugh, Michael I. Nemenov, and Allan I. Basbaum. 2013. “The Modality-Specific Contribution of Peptidergic and Non-Peptidergic Nociceptors Is Manifest at the Level of Dorsal Horn Nociresponsive Neurons.” *The Journal of Physiology* 591 (4): 1097–1110.

Zhang, Zaiqi, Zhiyong Yao, Kunyang Wu, Ti Zhang, Chaoqun Xing, and Xiao-Liang Xing. 2021. “Resveratrol Rescued the Pain Related Hypersensitivity for Cntnap2-Deficient Mice.” *European Journal of Pharmacology* 891 (January): 173704.

Zhao, Yilu, Li Yang, Gaolang Gong, Qingjiu Cao, and Jing Liu. 2022. “Identify Aberrant White Matter Microstructure in ASD, ADHD and Other Neurodevelopmental Disorders: A Meta-Analysis of Diffusion Tensor Imaging Studies.” *Progress in Neuro-Psychopharmacology & Biological Psychiatry* 113 (March): 110477.

Zheng, Alice, Kaela E. Scott, Ashley L. Schormans, Rajkamalpreet Mann, Brian L. Allman, and Susanne Schmid. 2023. “Differences in Startle and Prepulse Inhibition in Contactin-Associated Protein-like 2 Knock-out Rats Are Associated with Sex-Specific Alterations in Brainstem Neural Activity.” *Neuroscience* 513 (January): 96–110.

Zheng, Jian, Xuan Sun, Chaolin Ma, Bao-Ming Li, and Fei Luo. 2019. “Voluntary Wheel Running Promotes Myelination in the Motor Cortex through Wnt Signaling in Mice.” *Molecular Brain* 12 (1): 85.

Zhou, Yang, Tobias Kaiser, Patrícia Monteiro, Xiangyu Zhang, Marie S. Van der Goes, Dongqing Wang, Boaz Barak, et al. 2016. “Mice with Shank3 Mutations Associated with ASD and Schizophrenia Display Both Shared and Distinct Defects.” *Neuron* 89 (1): 147–62.

Zonouzi, Marzieh, Joseph Scafidi, Peijun Li, Brian McEllin, Jorge Edwards, Jeffrey L. Dupree, Lloyd Harvey, et al. 2015. “GABAergic Regulation of Cerebellar NG2 Cell Development Is Altered in Perinatal White Matter Injury.” *Nature Neuroscience* 18 (5): 674–82.

Zweier, Christiane, Eiko K. de Jong, Markus Zweier, Alfredo Orrico, Lilian B. Ousager, Amanda L. Collins, Emilia K. Bijlsma, et al. 2009. “CNTNAP2 and NRXN1 Are Mutated in Autosomal-Recessive Pitt-Hopkins-like Mental Retardation and Determine the Level of a Common Synaptic Protein in Drosophila.” *American Journal of Human Genetics* 85 (5): 655–66.

Annex

frontiers | Frontiers in Neuroscience

TYPE Original Research
PUBLISHED 30 January 2023
DOI 10.3389/fnins.2023.1100121

OPEN ACCESS

EDITED BY
Subashika Govindan,
DBT/Wellcome Trust India Alliance, India

REVIEWED BY
Ricardo Scott,
University of Alicante, Spain
Dies Meijer,
The University of Edinburgh, United Kingdom

*CORRESPONDENCE
Laurence Goutebroze
✉ laurence.goutebroze@inserm.fr

†PRESENT ADDRESS
Mélanie Druart,
Department of Psychiatry,
Physiology and Neuroscience, New York
University Grossman School of Medicine,
New York, NY, United States

‡These authors have contributed equally to this work

SPECIALTY SECTION
This article was submitted to
Translational Neuroscience,
a section of the journal
Frontiers in Neuroscience

RECEIVED 16 November 2022
ACCEPTED 09 January 2023
PUBLISHED 30 January 2023

CITATION
Cifuentes-Diaz C, Canali G, Garcia M, Druart M, Manett T, Savariradjane M, Guillaume C, Le Magueresse C and Goutebroze L (2023) Differential impacts of *Cntnap2* heterozygosity and *Cntnap2* null homozygosity on axon and myelinated fiber development in mouse. *Front. Neurosci.* 17:1100121. doi: 10.3389/fnins.2023.1100121

Differential impacts of *Cntnap2* heterozygosity and *Cntnap2* null homozygosity on axon and myelinated fiber development in mouse

Carmen Cifuentes-Diaz[1,2,3‡], Giorgia Canali[1,2,3‡], Marta Garcia[1,2,3], Mélanie Druart[1,2,3†], Taylor Manett[1,2,3], Mythili Savariradjane[1,2,3], Camille Guillaume[1,2,3], Corentin Le Magueresse[1,2,3] and Laurence Goutebroze[1,2,3*]

[1]Inserm, Unité Mixte de Recherche (UMR)-S 1270, Paris, France, [2]Faculté des Sciences et Ingénierie, Sorbonne University, Paris, France, [3]Institut du Fer à Moulin, Paris, France

Over the last decade, a large variety of alterations of the *Contactin Associated Protein 2 (CNTNAP2)* gene, encoding Caspr2, have been identified in several neuronal disorders, including neurodevelopmental disorders and peripheral neuropathies. Some of these alterations are homozygous but most are heterozygous, and one of the current challenges is to estimate to what extent they could affect the functions of Caspr2 and contribute to the development of these pathologies. Notably, it is not known whether the disruption of a single *CNTNAP2* allele could be sufficient to perturb the functions of Caspr2. To get insights into this issue, we questioned whether *Cntnap2* heterozygosity and *Cntnap2* null homozygosity in mice could both impact, either similarly or differentially, some specific functions of Caspr2 during development and in adulthood. We focused on yet poorly explored functions of Caspr2 in axon development and myelination, and performed a morphological study from embryonic day E17.5 to adulthood of two major brain interhemispheric myelinated tracts, the anterior commissure (AC) and the corpus callosum (CC), comparing wild-type (WT), *Cntnap2*$^{-/-}$ and *Cntnap2*$^{+/-}$ mice. We also looked for myelinated fiber abnormalities in the sciatic nerves of mutant mice. Our work revealed that Caspr2 controls the morphology of the CC and AC throughout development, axon diameter at early developmental stages, cortical neuron intrinsic excitability at the onset of myelination, and axon diameter and myelin thickness at later developmental stages. Changes in axon diameter, myelin thickness and node of Ranvier morphology were also detected in the sciatic nerves of the mutant mice. Importantly, most of the parameters analyzed were affected in *Cntnap2*$^{+/-}$ mice, either specifically, more severely, or oppositely as compared to *Cntnap2*$^{-/-}$ mice. In addition, *Cntnap2*$^{+/-}$ mice, but not *Cntnap2*$^{-/-}$ mice, showed motor/coordination deficits in the grid-walking test. Thus, our observations show that both *Cntnap2* heterozygosity and *Cntnap2* null homozygosity impact axon and central and

peripheral myelinated fiber development, but in a differential manner. This is a first step indicating that *CNTNAP2* alterations could lead to a multiplicity of phenotypes in humans, and raising the need to evaluate the impact of *Cntnap2* heterozygosity on the other neurodevelopmental functions of Caspr2.

KEYWORDS

Caspr2, corpus callosum, anterior commissure, sciatic nerve, axon diameter, myelin thickness, node of Ranvier, neuronal activity

Introduction

The *Contactin Associated Protein 2* gene (*CNTNAP2*), encoding the neuronal cell-adhesion transmembrane glycoprotein Caspr2, has gained prominence over the last decade in the field of neurological disabilities. A duplication of exon 4 of *CNTNAP2* was identified in two sisters suffering from Charcot–Marie–Tooth type 2, a peripheral motor and sensory neuropathy (Hoyer et al., 2015). Additionally, an increasing number of *CNTNAP2* alterations have been reported in patients with various neurodevelopmental disorders, including autism spectrum disorders (ASD), schizophrenia, intellectual disability, obsessive compulsive disorder, Pitt-Hopkins-like syndrome, attention deficit hyperactivity disorder, Gilles de la Tourette syndrome and cortical dysplasia focal epilepsy (Rodenas-Cuadrado et al., 2014; Poot, 2015, 2017; Saint-Martin et al., 2018). The genetic alterations identified in these disorders comprise a large diversity ranging from complex genomic rearrangements, homozygous and compound-heterozygous deletions and mutations, homozygous truncating non-sense mutations or deletions, and a large number of heterozygous missense variants found mainly in ASD patients. Currently, one of the major challenges is to estimate to what extent *CNTNAP2* alterations could affect the molecular and cellular functions of Caspr2, and therefore contribute to the development of the pathologies.

Caspr2 was initially identified as a component of the juxtaparanodal domains (juxtaparanodes) of the nodes of Ranvier in mature myelinated neurons, both in the central (CNS) and peripheral (PNS) nervous system (Poliak et al., 1999). Within the juxtaparanodes, Caspr2 is involved in the organization of specific axo-glial contacts, forming complexes with the cell-adhesion molecule Contactin2/TAG-1. These complexes are required for the clustering of the *Shaker*-type Kv1 (Kv1.1 and Kv1.2) channels (Poliak et al., 2003; Traka et al., 2003; Scott et al., 2017). Since Caspr2's identification, several studies conducted in *Cntnap2*$^{-/-}$ (KO) mice revealed that Caspr2 also plays critical roles in contributing to neuronal network formation during brain development, notably in neuronal migration (Penagarikano et al., 2011), dendritic arborization (Anderson et al., 2012; Gao et al., 2018), spine formation and maintenance (Gdalyahu et al., 2015; Varea et al., 2015; Lazaro et al., 2019), and synapse development and function (Anderson et al., 2012; Pinatel et al., 2015; Varea et al., 2015; Fernandes et al., 2019; Gao et al., 2019). Electrophysiological and imaging approaches further demonstrated that Caspr2 contributes to local and long-range brain connectivity (Penagarikano et al., 2011; Scott et al., 2017; Liska et al., 2018; Vogt et al., 2018; Zerbi et al., 2018; Antoine et al., 2019). Moreover, behavioral studies showed deficits in KO mice, some of which replicate clinical ASD phenotypes and are rescued by normalizing altered circuit connectivity (Penagarikano et al., 2011; Brunner et al., 2015; Scott et al., 2017; Choe et al., 2022). These data revealed mechanisms through which some *CNTNAP2* alterations may contribute to the development of neurological pathologies in humans.

However, studies in KO mice do not accurately replicate the genetic situations in patients and are not sufficient to fully explore the potential impact of the multiple *CNTNAP2* alterations identified thus far. Most of the genetic alterations are heterozygous and it is currently not known whether disruption of a single *CNTNAP2* allele could be sufficient to perturb the functions of Caspr2. Our recent observations indicate that some Caspr2 functions could be modulated by the level of the protein and affected by some ASD missense variants in a *Cntnap2*$^{+/-}$ (HET) background (Canali et al., 2018). We showed that Caspr2 plays a dose-dependent function in cortical neuron axon growth *in vitro*, and that certain variants impinge Caspr2 cell adhesive properties and display loss of function, while others lead to protein retention in the endoplasmic reticulum and display a dominant-negative effect through oligomerization with wild-type (WT) Caspr2. Vogt et al. (2018) also found that HET fast-spiking PV^{+} cortical interneurons exhibit an intermediate electrophysiological phenotype between WT and KO interneurons. Nevertheless, whether or not the level of Caspr2 could more broadly modulate its functions remains to be determined.

In this study, we addressed this question, focusing on poorly explored functions of Caspr2 in axon development and myelination *in vivo*, whose disturbances could contribute to the development of both peripheral and central neurological disabilities. We performed a morphological study from embryonic day E17.5 to adulthood of two major brain interhemispheric myelinated tracts, the anterior commissure (AC) and the corpus callosum (CC), comparing WT, *Cntnap2* HET and KO mice. We also characterized myelinated fiber abnormalities in the sciatic nerves of mutant mice. Overall, our observations indicate that the level of Caspr2 modulates the development and organization of myelinated fibers both in the CNS and in the PNS.

Materials and methods

Animals

Contactin Associated Protein 2 (Cntnap2) mutant mice, previously described (Poliak et al., 2003), were obtained from the Jackson Laboratory and maintained in a C57BL/6J background. They were group-housed with *ad libitum* access to food and water and a 12–12 h light–dark cycle (light phase onset at 7 a.m.). For staging of embryos, the day of vaginal plug was considered E0.5.

Tissue processing

For brain morphology analyses, E17.5 embryos were rapidly decapitated. Pups (P2, P7), juvenile (P30), and adult (P90) mice were deeply anesthetized by intraperitoneal injection of ketamine (100 mg/kg) and xylazine (10 mg/kg) and transcardially perfused with 4% paraformaldehyde (PFA) in 0.12 M phosphate buffer pH 7.4. Brains were fixed (embryos) or post-fixed (P2, P7, P30, P90) overnight (O/N) at 4°C in 4% PFA. Embryonic, P2 and P7 brains were washed in sodium phosphate buffered saline (PBS), embedded in 75 g/l gelatin and 100 g/l sucrose in PBS or in 15 g/l agarose and 20 g/l sucrose in PBS, and serial coronal (E17.5, P2, P7, 60 μm-thick) and sagittal (E17.5, 60 μm-thick; P7, 45 μm-thick) sections were obtained using a vibratome (Leica, France). Thirty-five μm-thick serial sagittal sections of P30 and P90 brains embedded in 35 g/l agarose and 80 g/l sucrose in PBS were obtained similarly. Forty μm-thick serial coronal sections of P30 and P90 brains and 500 μm-thick horizontal sections of P90 brains were performed without inclusion. All floating sections were conserved at 4°C in PBS with 1 g/l sodium azide until use.

For sciatic nerve immunostainings, 2-month-old mice were perfused as described above, sciatic nerves were dissected, fibers were teased apart on slides to yield single fiber preparations, air-dried and kept at −20°C.

Immunostainings

For morphological analysis of the CC and AC, brain sections of E17.5, P2 and P7 animals were incubated in a permeabilization/saturation solution (PS1: PBS, 5 ml/l Triton X-100, 100 ml/l normal goat serum) for 1 h at room temperature (RT) and then O/N at 4°C (72 h for P7) with the anti-L1CAM antibody (Millipore, rat clone 324, #MAB5272, 1:400) diluted in PS1. Sections were then washed three times for 10 min in PBS/5 ml/l Triton X-100 (WS1) and incubated for 2 h at RT with adequate fluorophore-conjugated-secondary antibodies (Molecular Probes, Invitrogen, Waltham, MA, USA) diluted in PS1. For brain sections of P30 and P90 animals, permeabilization and saturation were performed in PBS supplemented with 2 g/l porcine skin gelatin and 2.5 ml/l Triton X-100 (PS2 solution), before incubation O/N at 4°C with the anti-NF-M antibody (Sigma, mouse clone NN18, #N5264, 1:300) diluted in PS2. The following day, sections were washed three times for 10 min in PBS/2.5 ml/l Triton X-100 (WS2) and incubated for 2 h at RT with secondary antibodies diluted in PS2. For all ages, after secondary antibody incubation, sections were washed three times for 10 min in WS1 (E17.5, P2, P7) or WS2 (P30, P90), and nuclei were stained for 10 min with Hoechst before mounting with Fluoromount-G medium (Invitrogen, Waltham, MA, USA). For neuron counting in the cortex, E17.5 sections were incubated with the anti-L1CAM antibody (1:750) together with the anti-Satb2 (Abcam, Cambridge, UK, mouse clone SATBA4B10, #ab51502, 1:750) and the anti-Ctip2 (Abcam, Cambridge, UK, rabbit #ab28448, 1:500) antibodies diluted in PS1.

Immunofluorescent staining of sciatic nerves was performed as described previously (Martin et al., 2017). Briefly, slides were treated with 0.1 M glycine for 30 min at RT or with methanol 50%/acetone 50% for 20 min at −20°C, pre-incubated for 1 h at room temperature in PS2, before incubation with primary antibodies diluted in PS2 overnight at 4°C (K_v1.2 α subunit, mouse clone K67/25 #75-075, NeuroMab, 1:400; F3, goat #AF904, R&D Systems, 1:400; NrCAM, rabbit #ab24344, Abcam, Cambridge, UK, 1:300; TAG-1, goat #AF4439, R&D Systems, 1:500; Caspr (L51, 1:500) and Caspr2 (191, 1:400) previously described) (Menegoz et al., 1997; Denisenko-Nehrbass et al., 2003). After washing with PBS, coverslips were incubated for 2 h at room temperature with secondary antibodies diluted in PS2, washed again with PBS, and mounted with Fluoromount-G medium.

Image acquisition and analysis

Images of immunostained brain sections or phase-contrast images were acquired using a macroscope MVX10 (Olympus, Tokyo, Japan). Thickness and area measurements were performed using the ImageJ software, for six mice/genotype/condition, except for AC area at E17.5 (four embryos/genotype). CC and cortex thicknesses were measured on one coronal section per brain per animal for E17.5 and P2 stages and three consecutive sections per animal for P90. Measurements were performed independently on both hemispheres and averaged; the measures were further averaged between the three consecutive sections for P90. Anterior branch (ACa) thickness at P90 was measured independently on both hemispheres on one horizontal section per brain per animal, and averaged. Measurements of CC and AC areas were performed on three consecutive sagittal sections per animal at all ages, and averaged.

For quantification of Satb2- or Ctip2-positive neurons at E17.5, images were acquired using a Leica SP5 confocal laser-scanning microscope (Leica microsystems, Watzlar, Germany, Z stack 1 μm, 25 stacks, 40× immersion objective) at the level of the somatosensory cortex of both hemispheres for two successive medial coronal sections per animal (n = 4 animals/genotype). The density of Satb2- or Ctip2-positive neurons was estimated using the Imaris software (Bitplane, Zurick, CH). To do so, images were cropped to exclude the region corresponding to the intermediate zone and the subplate layer, using L1CAM immunostaining to delineate these regions. The average volume of Satb2- and Ctip2-positive nuclei was calculated by averaging the volumes of 15 isolated nuclei. Masks were built to obtain the total volumes occupied by Satb2- and Ctip2-positive nuclei, respectively, excluding objects with a volume lower than the smallest volume out of the 15 used for averaging. The density of Satb2- or Ctip2-positive neurons was then calculated by dividing these total volumes by the average nucleus volume (Hoechst staining).

Images of stained sciatic nerve fibers were acquired using a Zeiss Celldiscoverer 7 imaging system for quantification analyzes, and a STELLARIS 5 confocal laser-scanning microscope (Leica Microsystems, Watzlar, Germany) to acquire representative images. Measurements of node length and node axonal diameter were performed manually on NrCAM stainings using the ImageJ software (3 mice/genotype, 81 nodes/mouse).

Electron microscopy

For ultrastructural studies of the CC and the AC, P7 animals (3 pups/genotype) were deeply anesthetized by intraperitoneal injection of ketamine (100 mg/kg) and xylazine (10 mg/kg), and transcardially perfused with 4% PFA (EMS) and 2.5% glutaraldehyde

(Microm Microtech, G003) in phosphate buffer 0.1 M pH 7.4. Brains were removed and post-fixed in the same fixative solution O/N at 4°C. P30 animals (3 mice/genotype) were anesthetized as above and transcardially perfused with 3% glutaraldehyde in Milloning's phosphate buffer 0.1 M pH 7.4. Brains were removed and immediately processed. For the two ages, 1 mm-thick brain sagittal sections were produced and post-fixed for 1 h at 4°C in fresh fixative solution, washed once with phosphate buffer 0.1 M pH 7.4 (P7) or Milloning's phosphate buffer 0.1 M (P30), and three times for 10 min with Palade buffer. Samples were then incubated in 2% osmium tetroxide in Palade buffer for 1 h at RT, rinsed in Palade buffer for 3 min and three times for 3 min in distilled water, dehydrated in a series of ethanol baths, and flat embedded in epoxy resin (EPON 812, Polysciences). After polymerization, 0.5 μm-thick semi-thin sections stained with toluidine blue to locate the CC and the AC. Then, blocks containing the CC and the AC were cut in 50 nm-thick ultrathin sections using an ultramicrotome (Ultracut E, Leica). Sections were examined with a Philips CM100 electron microscope and digital images acquired with a CCD camera (Gatan Orius). Diameters were calculated from areas measured manually using the Image J software (P7, ACa/ACp 300 axons/pup, CC 360 axons/pup; P30, ACa/ACp 147 myelinated fibers/mouse, CC 150 myelinated fibers/mouse). The percentage of myelinated fibers was determined by counting the numbers of unmyelinated and myelinated axons on 18 photos at magnification 9700×. The percentage of myelinated axons containing mitochondria was measured on six photos at magnification 2500×.

For ultrastructural analyses of peripheral myelinated fibers, the sciatic nerves were fixed *in situ* for ∼1 min with 3% glutaraldehyde in Milloning's phosphate buffer 0.1 M pH 7.4, dissected out, placed in fixative O/N at 4°C, rinsed in PB, post-fixed in 2% osmium tetroxide in PB, dehydrated in an ascending series of ethanol, and embedded in epoxy resin. The global morphology of the nerves was evaluated on 0.5 μm-thick semi-thin transversal sections stained with toluidine blue and visualized with a DM6000 Leica microscope. Morphometric analyzes were performed on ultra-thin sections (50 nm) and examined as above (4 mice/genotype, 47 myelinated fibers/mouse).

Brain lysate preparation and immunoblotting

To analyze protein levels, brains (six mice/genotype/age) were lysed in RIPA buffer containing proteases inhibitors and immunoblotting was performed as previously described (Canali et al., 2018). Briefly, equal amounts of proteins (40 μg) were loaded on NuPAGE 8–12% Bis-Tris gels (Thermo Fisher Scientific, Waltham, MA, USA) and transferred to 0.45 μm Nitrocellulose membranes. Membranes were blocked with 50 g/l non-fat dry milk in Tris-Buffered Saline solution/0.1 ml/l Tween 20 for 1 h at RT, incubated with primary antibodies in the same solution for 2 h at RT or O/N at 4°C, 1 h at RT with appropriate IRDye-conjugated secondary antibodies, and imaged and quantified using Odyssey Imaging System (LiCOR Biosciences, Lincolm, NE, USA). The commercial antibodies were from the following sources: anti-MBP, Serotec, rat clone 82–87, #MCA409S, 1:250; anti-PLP, Novus Biochemicals, rabbit, #NBP1-87781, 1:1000; anti-MAG, Zymed, rabbit, #34–6200, 1:1000; anti-GAPDH, Millipore, chicken, #AB2302, 1:5000. The anti-TAG-1 antibody has been described previously (Traka et al., 2003). The anti-Caspr2 was the same as the one used for immunostainings.

RT-qPCR experiments

For mRNA expression analysis, total mRNA was extracted from brains (six mice/genotype/age) using the TRIzol™ Reagent (Invitrogen, Waltham, MA, USA) following the manufacturer's recommendations. Reverse transcription was performed with the SuperScript II reverse transcriptase (Invitrogen, Waltham, MA, USA, #18064-022) and random primers, and qPCR in a Stratagene™ Mx3005P qPCR instrument (Agilent Technologies, Santa Clara, CA, USA) using the Brilliant II SYBR® Green QPCR Master Mix (Agilent Technologies, Santa Clara, CA, USA, #600828). The MxPro QPCR Software (Agilent Technologies, Santa Clara, CA, USA) was used to perform expression analyses. The expression level of *Cntnap2* mRNA was normalized to *Psap* mRNA level. Primers for *Cntnap2* were designed on two 5′ exons: primer sense 5′CAGCGCTCTCGCTCTGGATT (accession number NM_001004357, nucleotides 261–280), primer anti-sense 5′CCCCAGCACCTCCTCGTTTATT (nucleotides 425–446), amplified DNA fragment 186 bp. Primers for *Psap* were the following: primer sense 5′CTGGTGTCAGAACATGGAGACTG (accession number NM_001146120, nucleotides 1708–1730), primer anti-sense 5′TGACTTCTGCAGCTGGGAAA (nucleotides 1781–1800), amplified DNA fragment 93 bp.

Electrophysiology

Acute slice preparation

A total of 250 μm-thick coronal slices of the somatosensory cortex were prepared from brains of KO, HET, and WT littermates aged P10–P12. Acute coronal slices were cut using a vibroslicer (HM 650 V, Microm) in ice-cold artificial cerebrospinal fluid (ACSF) containing the following (in mM): 125 NaCl, 2.5 KCl, 25 glucose, 25 NaHCO3, 1.25 NaH2PO4, 2 CaCl2, and 1 MgCl2, continuously bubbled with 95% O_2–5% CO_2. Slices were incubated in ACSF at 32°C for 20 min and then at room temperature (20–25°C). For patch-clamp recordings, slices were transferred to the recording chamber where they were continuously superfused with ACSF (30–32°C).

Patch-clamp

Patch-clamp pipettes (4–6 Mohm resistance) were prepared from borosilicate glass (BF150-86-10; Harvard Apparatus, Holliston, MA, USA) using a DMZ pipette puller (Zeitz). Patch-clamp recordings were performed using an EPC-10 amplifier (HEKA Elecktronik GmbH, Reutlingen, Germany) with the following intracellular solution (in mM): 105 K-gluconate, 10 HEPES, 10 phosphocreatine-Na, 4 ATP-Na2, 30 KCl (pH 7.25, adjusted with KOH). Intrinsic excitability was measured in current-clamp using depolarizing current steps of increasing amplitude (0–500 pA, 500 ms) at an interstimulus interval of 6 s, from a cell potential set to −70 mV, in the presence of SR95531 hydrobromide (Gabazine, 10 μm, Hello Bio) to block $GABA_A$ receptor-mediated synaptic transmission, 6-cyano-7-nitroquinoxaline-2,3-dione (CNQX, 10 μm, Biotrend, Köln, Germany) to block AMPA receptor-mediated synaptic transmission and D-2-amino-5-phosphonopentanoic acid (D-APV, 50 μm, Hello Bio) to block NMDA receptor-mediated synaptic transmission.

Data acquisition and analysis

Stimulus delivery and data acquisition were performed using the Patchmaster software (HEKA Elecktronik GmbH, Reutlingen, Germany). The junction potential (−5 mV) was left uncorrected. Signals were sampled at 20 kHz and filtered at 4 kHz. Offline analysis was performed using Igor Pro (WaveMetrics).

Grid-walking test

Coordination between forelimbs and hind limbs and accurate limb placement were examined by assessing the ability to walk on metal grid bars with 1.5 cm gaps on the bottom of a 30 × 20 × 20 cm box (8–9 6-month-old males/genotype). The performance of each animal was analyzed by counting and averaging the number of errors in foot placement/total number of steps, during 2-min sessions, once a day, for three consecutive days. On the day before data collection, each mouse was allowed to walk on the grid for 2 min.

Statistical analysis

Statistical analyses were performed with the GraphPad Prism 9 Software (GraphPad Software, San Diego, CA, USA). Results are provided as mean ± SEM or median ± quartile (Violin plot, medium smoothing). The normality of the samples was tested using the Shapiro–Wilk test. When the variables followed a normal distribution, statistical analyses were carried out using the unpaired *t*-test to compare 2 genotypes and the one-way ANOVA test to compare the three genotypes, followed by a Tukey's multiple comparisons test. When the variables did not follow a normal distribution, the Mann–Whitney test was used to compare two genotypes and the Kruskal–Wallis test to compare the three genotypes, followed by a Dunn's multiple comparisons test. The thicknesses of the CC measured on coronal section and the firings of cortical neurons were compared between genotypes using Two-way RM ANOVA tests, followed by a Tukey's multiple comparisons test or a Sidak *post-hoc* test. Statistical analyses to compare the distributions of two quantitative variables were carried out using the Kolmogorov–Smirnov test. Linear regression analyzes were performed after checking the correlations between the variables (Pearson coefficient). The significance was established at a P-value < 0.05.

Results

Caspr2 level modulates CC morphology during development

The CC is the most prominent white matter structure in the brain, formed by ∼80% of axons coming from neocortical neurons in layers II/III and ∼20% of axons coming from cortical neurons in layer V (Ku and Torii, 2020). A potential implication of Caspr2 in the development of this tract was suggested by our previous *in vitro* study showing a role for Caspr2 in axon growth of embryonic neocortical neurons (Canali et al., 2018). The morphology of the CC was first examined in WT, HET and KO mice at postnatal day P90 on brain coronal sections selected at Bregma +1.1, +0.55, and 0, and on mid-brain sagittal sections. Brain slices were immunostained with antibodies directed against the neurofilament subunit NF-M, which is expressed in commissural axons at late stages of development. From this point onward in the manuscript, the analyses were performed by comparing the three genotypes to investigate dose-dependent effects, but also by comparing HET and KO mice individually to WT mice to reveal potential effects of *Cntnap2* heterozygosity and/or null homozygosity, which would not be revealed by three-genotype comparisons. Main statistical results were reported on figures in black for three-genotype comparisons, and in color for individual comparisons to WT conditions when the difference was significant (HET, orange; KO, blue; all statistical analyses reported in **Supplementary Table 1**). When measuring the thickness of the CC in different positions from the brain midline to the lateral parts of coronal brain sections (**Figure 1B**, inset), we did not detect significant differences when comparing the three genotypes at the three Bregma levels, but a significant decrease in KO mice as compared to WT mice when comparing the two at Bregma + 0.50 (**Figures 1A, B**; data not shown for brain sections at Bregma +1.1 and 0). Decreased thickness was particularly pronounced at the midline of the brain (**Figure 1C**). Immunostainings of mid-sagittal sections consistently showed a decrease of CC area in KO mice as compared to WT and HET mice, as well as a decreased minimum caliper as compared to WT mice (**Figures 1D–G**). In HET mice, none of the morphometric parameters were significantly different from those in WT mice.

Decreased CC thickness and area in adult KO mice were likely not due to a major decrease in the number of axons forming this tract since a previous study showed a normal distribution of the neocortical neurons projecting their axon through the CC in these mice (Scott et al., 2017). We attempted to find the temporal origin of the phenotype by characterizing the morphology of the CC through development. In mice, E15 pioneering axons from the cingulate cortex are the first axons forming the CC to reach the midline, followed later by neocortical projections at around E17.5 (Suarez et al., 2014). The formation of the CC continues after birth, until some axons begin to be myelinated by oligodendrocytes (OLs) (Suarez et al., 2014). The first myelinated sheaths are observable at P11 and a rapid phase of myelination occurs between P14 and P45 (Sturrock, 1980). We characterized CC morphology at P30 when myelination is ongoing, at P7 before the onset of myelination, at an early stage of axon development (E17.5), and at an intermediate developmental stage (P2). Morphometric analyzes were performed on mid-sagittal sections at P30 and P7, and on coronal sections at P2 and E17.5 because the structure of the CC at these stages did not allow measuring its area with confidence on sagittal sections. At P7, P2, and E17.5, brain sections were immunostained with antibodies directed against the cell-adhesion molecule L1CAM, which is widely expressed in commissural axons at embryonic and early post-natal developmental stages. The observations at P30 were comparable to those at P90, with a decrease in CC area and minimum and maximum calipers in KO mice as compared to WT (**Figure 2A**). In contrast, no difference was observed between the three genotypes either at P7 (**Figure 2B**) or at P2 (**Figures 2C–E**). Moreover, the thickness of the CC was remarkably increased in both HET and KO embryos at E17.5 as compared to WT embryos, with no significant difference between HET and KO embryos (**Figures 2F, G**). CC thickness at the brain midline was significantly increased in HET embryos as compared to WT embryos (**Figure 2H**). This increase was likely not due to an increased number of axons, since neither the thickness of the cortex nor the

10.3389/fnins.2023.1100121

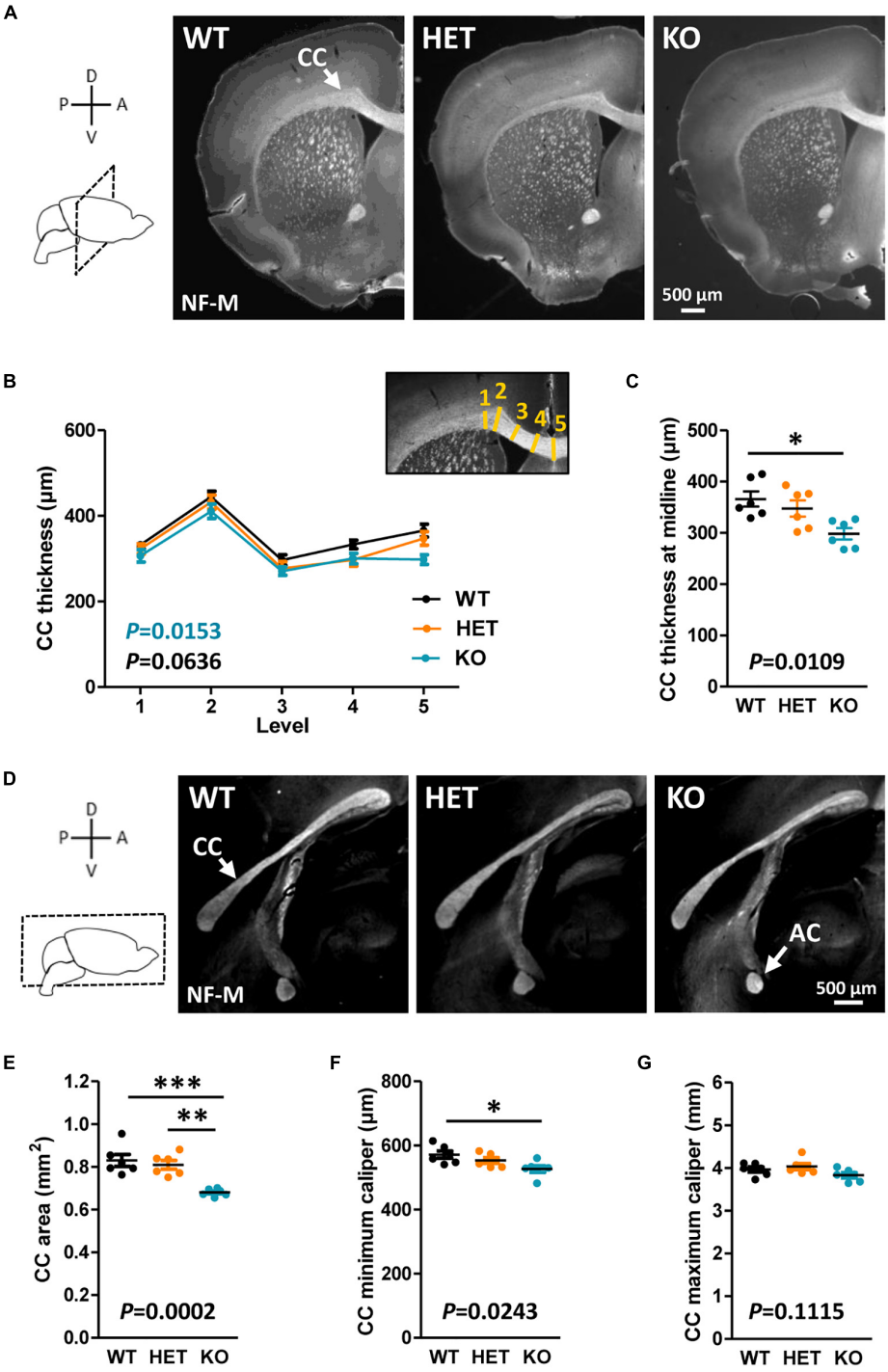

FIGURE 1
Corpus callosum (CC) morphology in adult mice. Representative images of brain coronal sections (Bregma + 0.50) of wild-type (WT), HET, and KO P90 mice showing CC immunostained with anti-NF-M antibodies **(A)**. CC thickness measured at different levels on coronal sections **(B)**; inset, schematic representation of the levels (yellow lines) where CC thickness measurements were performed. CC thickness at the midline of the brains **(C)**. Representative images of mid-sagittal brain sections of WT, HET, and KO P90 mice, showing the CC and the AC immunostained with anti-NF-M antibodies **(D)**. CC area **(E)**, minimum caliper **(F)**, and maximum caliper **(G)** measured on mid-sagittal brain sections. **(B,C,E–G)** Six animals/genotype, **(B)** average of measurements on both hemispheres on three consecutive sections/animal, **(C,E–G)** average of measurements on three consecutive sections/animal. Statistical tests: **(B)** Two-way RM ANOVA test; **(C,E–G)** Unpaired *t*-test to compare HET or KO mice to WT mice, and one-way ANOVA test to compare the three genotypes; $^{*}P < 0.05$, $^{**}P < 0.01$, $^{***}P < 0.001$.

densities of callosal Ctip2^{+} and Satb2^{+} projecting neurons in the cortex were different between the three genotypes (Supplementary Figure 1). These observations demonstrate that the level of Caspr2 modulates the morphology of the CC during development, with a remarkable "switch" at P7, immediately before the onset of myelination. Furthermore, they strongly suggested that Caspr2 could play previously unidentified functions in axon development and/or myelination.

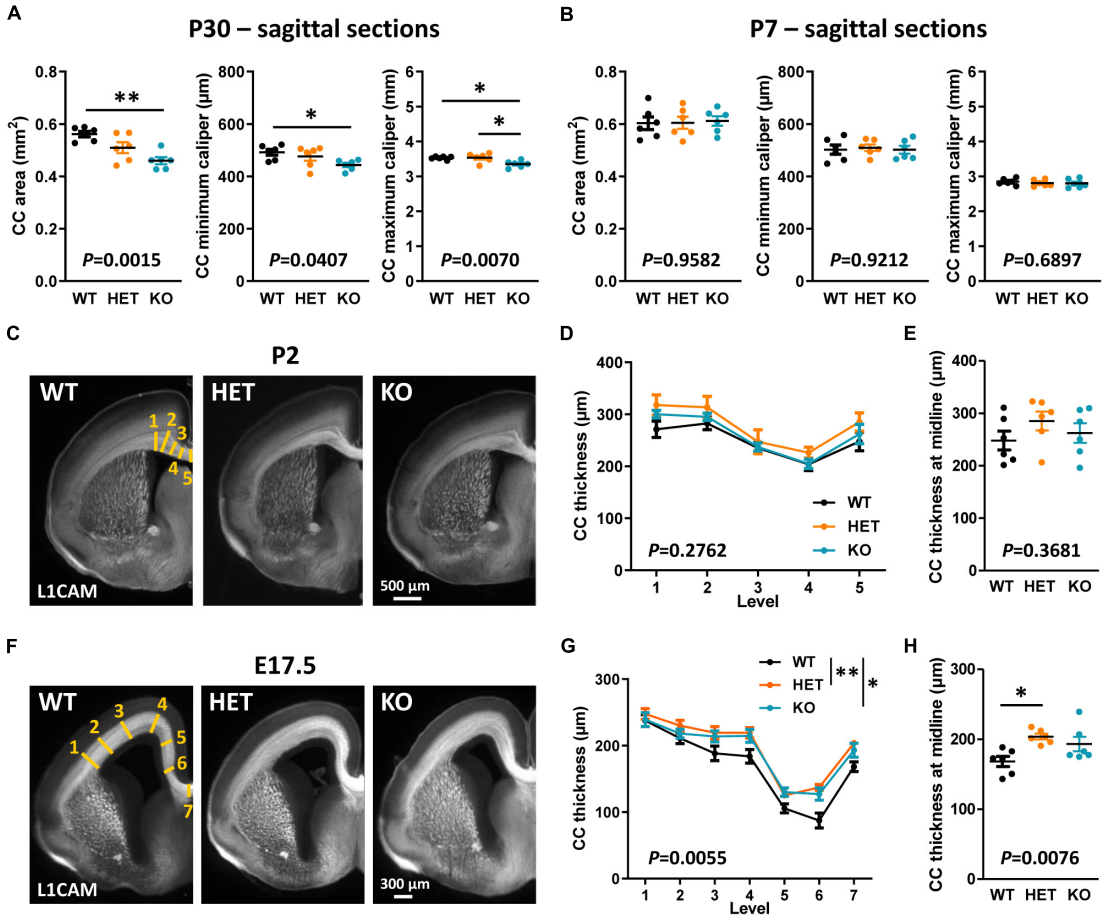

FIGURE 2
Corpus callosum (CC) morphology during development. CC area, minimum caliper, and maximum caliper measured on mid-sagittal brain sections of wild-type (WT), HET, and KO P30 mice **(A)** and P7 pups **(B)**. Representative images of brain coronal sections of WT, HET, and KO P2 pups **(C)** and E17.5 embryos **(F)** showing CC immunostained with anti-L1-CAM antibodies; the levels where CC thickness measurements were performed are schematized on the images of WT mice (yellow lines). CC thickness measured on coronal sections of P2 pups **(D)** and E17.5 embryos **(G)** at the levels indicated in panels **(C,F)**. CC thickness at the midline of the brains of P2 pups **(E)** and E17.5 embryos **(H)**. **(A,B,D,E,G,H)** Six animals/genotype, **(A,B)** average of measurements on three consecutive sections/animal, **(D,G)** average of measurements on both hemispheres on one section/animal, **(E,H)** measurements on one section/animal. Statistical tests: Unpaired *t*-test **(A,B,E)** or Mann–Whitney test **(H)** to compare HET or KO mice to WT mice, and one-way ANOVA test **(A,B,E)** or Kruskal–Wallis test **(H)** to compare the three genotypes; **(D,G)** Two-way RM ANOVA test followed by a Tukey's multiple comparisons test **(G)**; $*P < 0.05$, $**P < 0.01$.

Caspr2 level modulates AC morphology during development

The AC is formed by two main branches, contacting each other at the midline of the brain (Figure 3A). The ACa is composed mainly of axons from the anterior piriform cortex and the anterior olfactory nucleus, whereas the posterior branch (ACp) is composed mostly of axons from the posterior piriform cortex and the amygdala. We assumed that Caspr2 could contribute to the development and organization of this tract because *Cntnap2* expression was previously detected in the piriform cortex (Penagarikano et al., 2011; Gordon et al., 2016). As the AC follows a developmental timeline comparable to that of the CC in mice (Martin-Lopez et al., 2018), we characterized its morphology at the same developmental stages–P90, P30, P7, and E17.5. Phase-contrast images of 500 µm-thick horizontal brain sections did not reveal gross morphological defects in adult mutant mice (Figure 3A). However, we detected an increased thickness of the ACa in HET mice as compared to WT and KO mice, while the thickness tended to be decreased in KO mice, although not significantly different from that in WT mice (Figures 3A, B). This tendency turned out to be significant when considering the area of the whole AC on mid-sagittal sections (Figures 1D, 3D), suggesting that both the ACa and the ACp were thinner in KO mice as compared to WT mice. The area of the AC in KO mice appeared also significantly smaller than in HET mice. The AC area in HET mice was not significantly different from that in WT mice, but showed a strong tendency to increase (unpaired *t*-test, $P = 0.0571$), which was consistent with the increased thickness of the ACa. Results following a similar trend were observed in juvenile mice at P30 (Figures 3C, E). In contrast, no major differences were observed between the three genotypes in P7 pups (Figures 3C, F). In addition, the AC area was significantly increased in KO mice as compared to WT and HET mice in E17.5 embryos (Figures 3C, G). These data demonstrated that the level of Caspr2 also modulates the morphology of the AC during development, with a switch immediately before the onset of myelination as for the CC. They also suggested that Caspr2 could display functions in axon development and/or myelination extended to several myelinated tracts.

10.3389/fnins.2023.1100121

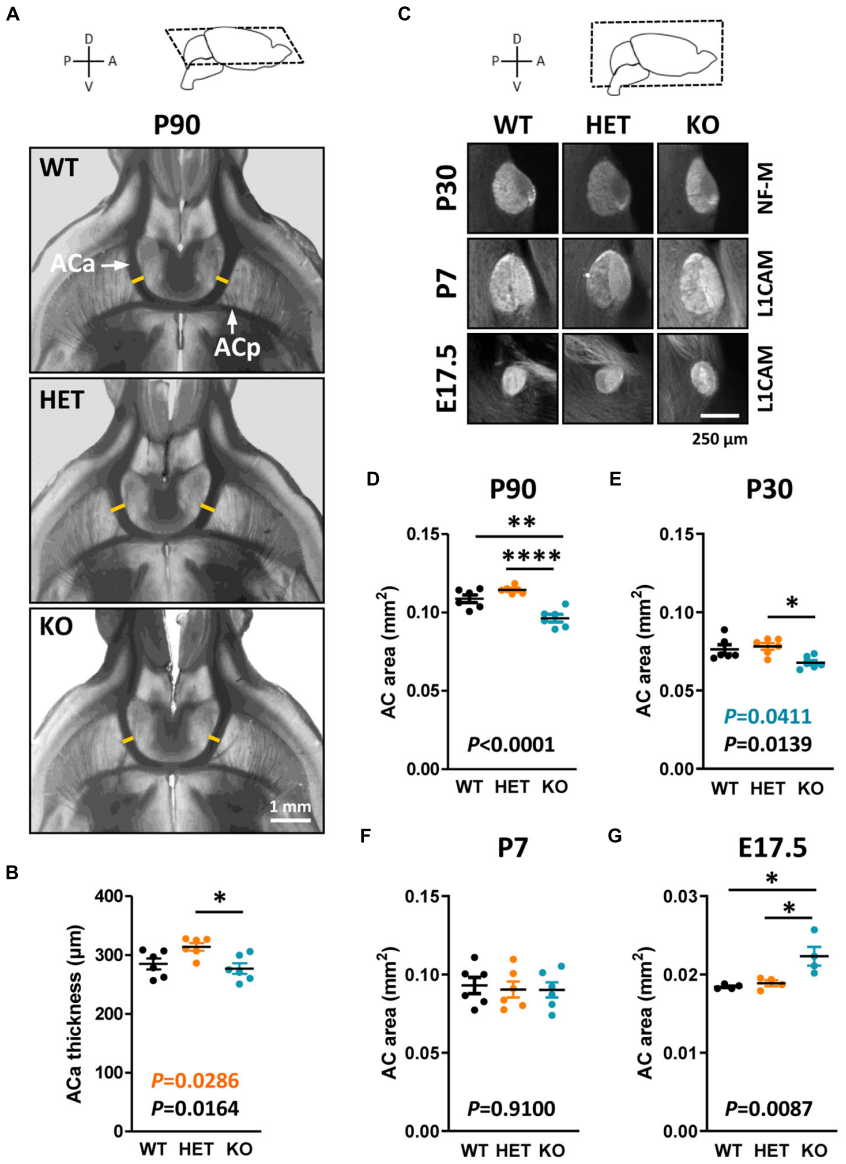

FIGURE 3
Anterior commissure (AC) morphology during development and at adulthood. Representative phase-contrast images of horizontal brain sections of wild-type (WT), HET, and KO P90 mice, showing the two branches of the AC **(A)**; yellow lines, levels where the thickness of the anterior branch (ACa) was measured. ACa thickness measured on horizontal brain sections of P90 mice **(B)**. Representative images of mid-sagittal brain sections of WT, HET, and KO mice at P30, P7, and E17.5, showing AC immunostained with anti-NF-M (P30) or L1CAM (P7, E17.5) antibodies **(C)**. AC area measured on mid-sagittal brain sections of P90 **(D)** and P30 **(E)** mice, P7 pups **(F)**, and E17.5 embryos **(G)**. **(B,D–F)** Six animals/genotype, **(G)** four animals/genotype, **(B)** average of measurements on both hemispheres on one section/animal, **(D–G)** average of measurements on three consecutive sections/animal. Statistical tests: Unpaired *t*-test **(B,D,F,G)** or Mann–Whitney test **(E)** to compare HET or KO mice to WT mice, and one-way ANOVA test **(B,D,F,G)** or Kruskal–Wallis test **(E)** to compare the three genotypes; $*P < 0.05$, $**P < 0.01$, $****P < 0.0001$.

Caspr2 level modulates axon diameter and myelin thickness of CC myelinated fibers in P30 mice

To further investigate the potential functions of Caspr2 in axon development and myelination, we first evaluated the timeline of overall myelination in HET and KO mice at four developmental stages from the onset of myelination (P10) to adulthood, by quantifying the levels of myelin proteins in whole brain extracts. Immunoblots showed a significant decrease of MBP, PLP, and MAG levels in KO mice at P30 as compared to WT mice, but not in P10, P15, and P90 mice (**Supplementary Figures 2A–C**), suggesting a potential widespread myelination delay in KO mice at P30. No alterations of myelin protein levels were detectable in HET mice, regardless of the developmental stage. We then performed tissue microdissection to compare myelin protein levels in the CC and the neocortex of P30 mice. Immunoblots revealed a significant decrease of MBP and MAG levels in the neocortex of KO mice as compared to WT mice (**Supplementary Figures 2D, E**), which was consistent with a delay of myelination previously reported in the neocortex of KO mice at P21 (Scott et al., 2017). However, no alteration of myelin protein level was detected in the CC of KO mice, in agreement with two previous studies showing similar MBP-immunoreactivity of the CC on brain coronal sections of WT and KO mice (Scott et al., 2017;

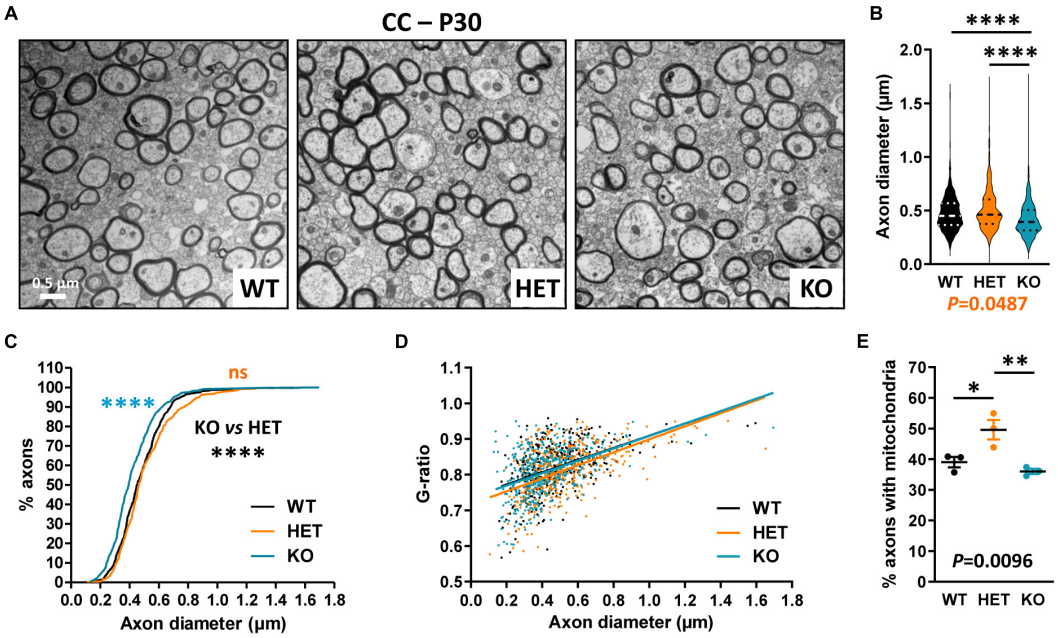

FIGURE 4
Ultrastructural abnormalities of corpus callosum (CC) myelinated fibers in P30 mice. Electron micrographs of transversal sections of the CC at brain midline, from wild-type (WT), HET, and KO P30 mice **(A)**. Axonal diameters of CC myelinated fibers **(B)**. Cumulative frequency distribution of axonal diameters (in %) **(C)**. Scatter plot graph displaying G-ratios of individual myelinated axons as a function of the respective axon diameters, and linear regression of the G-ratio measurements for each genotype **(D)**. Percentage of myelinated axons containing mitochondria **(E)**. **(B–D)** 450 myelinated fibers/genotype, 3 mice/genotype, 150 myelinated fibers/mouse; **(E)** 3 mice/genotype, % of mitochondria counted on ∼2000 axons/mouse. Statistical tests: **(B)** Mann–Whitney test to compare HET or KO mice to WT mice, and Kruskal–Wallis test to compare the three genotypes; **(C)** Kolmogorov–Smirnov test for pairwise comparisons; **(D)** Linear regression (WT R^2 = 0.2102, HET R^2 = 0.2871, KO R^2 = 0.1959) for pairwise comparisons, HET vs. WT elevation $P < 0.0001$, HET vs. KO elevation $P = 0.0005$; **(E)** Unpaired *t*-test to compare HET or KO mice to WT mice, and one-way ANOVA test to compare the three genotypes; $*P < 0.05$, $**P < 0.01$, $****P < 0.0001$; ns, non-significant.

Liska et al., 2018). No alteration of myelin protein level was detected in the CC of HET mice either.

We further evaluated CC myelination in P30 mice at the ultrastructural level by measuring myelinated fiber and axon diameters, to subsequently calculate the G-ratio, which is the ratio of axon diameter to fiber diameter whose variations can reveal myelin thickness defects. Transversal sections were observed at ∼Bregma + 0.02, in dorsal projection of the AC. We detected a significant decrease in axon diameters in KO mice as compared both to WT and HET (**Figures 4A–C**), which was consistent with previous observations at Bregma −2.46 (Zerbi et al., 2018). No difference between KO and WT mice was detectable when plotting the G-ratios as a function of axon diameters, indicating absence of major myelination changes in KO mice (**Figure 4D**). No significant difference was observed either in the % of myelinated fibers between KO and WT mice (WT 16.5 ± 0.6775, KO 13.84 ± 2.594, unpaired *t*-test $P = 0.3775$, three mice/genotype), thus confirming that P30 KO mice do not present major myelination defects of the CC. In contrast, the % of myelinated fibers appeared significantly decreased in HET mice when compared to WT mice (WT 16.5 ± 0.6775, HET 8.747 ± 1.709, unpaired *t*-test $P = 0.0135$, three mice/genotype). In parallel, axon diameters were slightly decreased as compared to WT mice (**Figures 4B, C**). A significant difference was also detectable between WT and HET mice when plotting the G-ratios as a function of axon diameters (**Figure 4D**). The mean G-ratio was consistently decreased in HET mice as compared to WT mice, reflecting hypermyelination (WT 0.8200 ± 0.003069, HET 0.8099 ± 0.003189, Mann–Whitney test $P = 0.0271$, 450 fibers/genotype, three mice/genotype, 150 fibers/mouse). Interestingly, we also noticed a significant increase in the % of myelinated axons containing mitochondria in HET mice as compared to WT and KO mice (**Figure 4E**). Thus, our observations showed alterations of myelinated fibers in the CC of P30 HET mice which were not suspected by myelin protein level analyses, perhaps because the hypermyelination was masked by the decrease in the myelinated fiber number. Overall, axon diameter and myelin thickness modifications observed in mutant mice confirm the assumption that Caspr2 could play roles in axon development and/or myelination, which could be modulated by the protein level.

Caspr2 level modulates axon diameter and myelin thickness of AC myelinated fibers in P30 mice

We further evaluated whether Caspr2 could also display functions in axon development and/or myelination in the AC, searching similar axonal and/or myelination defects in mutant mice at P30. Ultrastructural analyses of the ACa and the ACp were performed separately, since the two branches are distinguishable on mid-brain transversal sections (**Figures 5A, F**, insets). No significant difference in the % of myelinated fibers was observed between the three genotypes, either in the ACa (WT 18.2 ± 1.554, HET 21.24 ± 0.611, KO 13.4 ± 3.022, one-way ANOVA test $P = 0.0818$, three mice/genotype) or in the ACp (WT 11.8 ± 1.02, HET 9.716 ± 0.7453, KO, 7.655 ± 0.8618, Kruskal–Wallis test $P = 0.0857$,

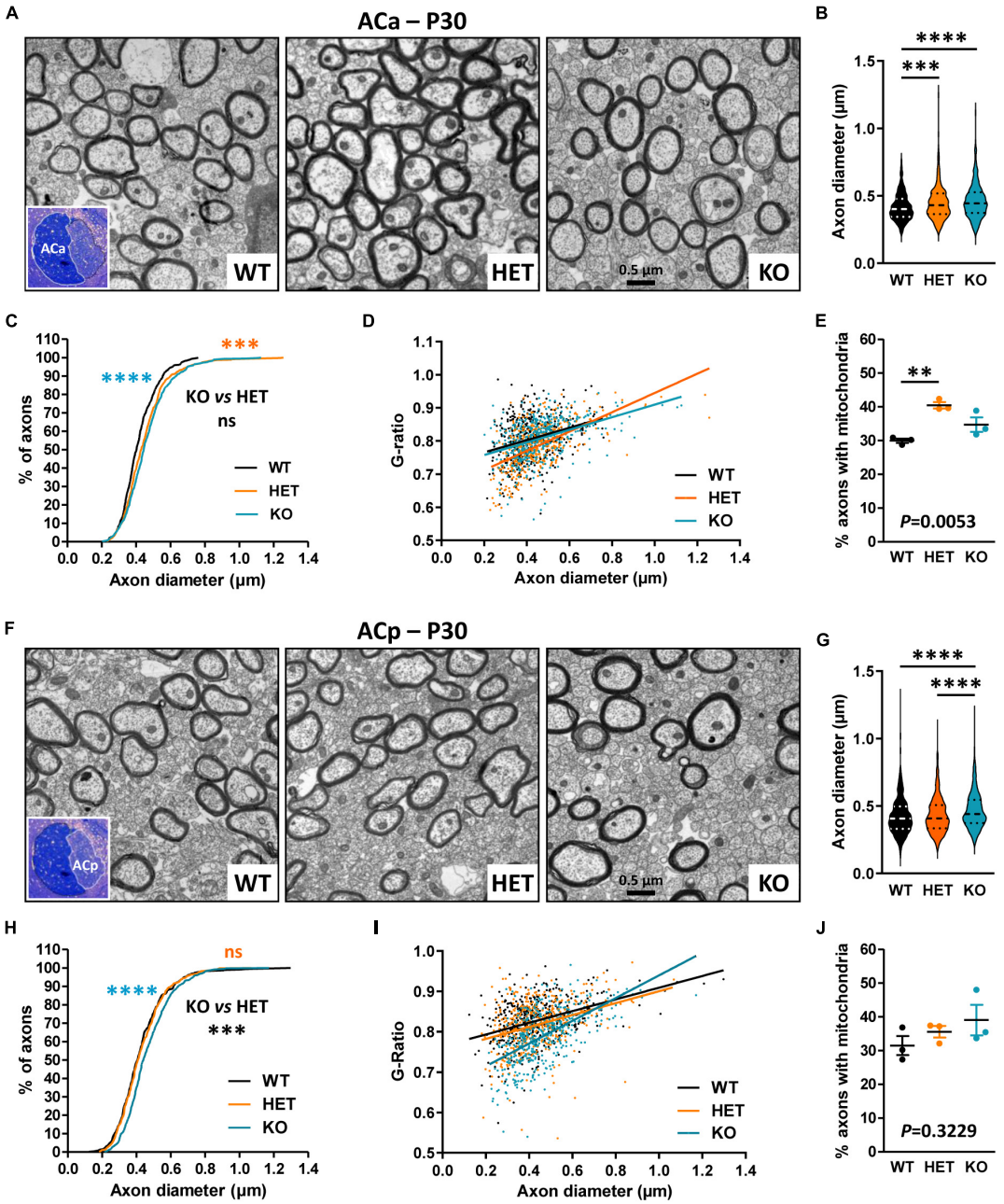

FIGURE 5
Ultrastructural abnormalities of anterior branch (ACa) and posterior branch (ACp) myelinated fibers in P30 mice. Electron micrographs of transversal sections of the ACa **(A)** and ACp **(F)** at brain midline, from wild-type (WT), HET, and KO P30 mice; insets, semi-thin transversal sections of the AC stained with toluidine blue, showing the ACa and the ACp. Axonal diameters of ACa **(B)** and ACp **(G)** myelinated fibers. Cumulative frequency distribution of axonal diameters (in %) of ACa **(C)** and ACp **(H)** myelinated fibers. Scatter plot graphs displaying G-ratios of individual myelinated axons as a function of the respective axon diameters, and the linear regression of the G-ratio measurements for each genotype, for the ACa **(D)** and the ACp **(I)**. Percentage of myelinated axons containing mitochondria in the ACa **(E)** and the ACp **(J)**. **(B–D,G–I)** 441 myelinated fibers/genotype, 3 mice/genotype, 147 myelinated fibers/mouse; **(E)** 3 mice/genotype, % of mitochondria counted on ∼2000 axons/mouse; **(J)** 3 mice/genotype, % of mitochondria counted on ∼1000 axons/mouse. Statistical tests: **(B,G)** Mann–Whitney test to compare HET or KO mice to WT mice, and Kruskal–Wallis test to compare the three genotypes; **(C,H)** Kolmogorov–Smirnov test for pairwise comparisons; **(D)** Linear regression (WT R^2 = 0.08121, HET R^2 = 0.3458, KO R^2 = 0.1727) for pairwise comparisons, HET vs. WT slope P = 0.0024, HET vs. KO slope P = 0.0003; **(I)** Linear regression (WT R^2 = 0.1589, HET R^2 = 0.1062, KO R^2 = 0.3420) for pairwise comparisons, HET vs. WT elevation P = 0.0047, KO vs. WT slope $P < 0.0001$, HET vs. KO slope $P < 0.0001$; **(E,J)** Unpaired t-test **(E)** or Mann–Whitney test **(J)** to compare HET or KO mice to WT mice, and one-way ANOVA test **(E)** or Kruskal–Wallis test **(J)** to compare the three genotypes; $^{**}P < 0.01$, $^{***}P < 0.001$, $^{****}P < 0.0001$; ns, non-significant.

three mice/genotype). In contrast, we detected modifications in axon diameters and myelination, which were remarkably different between the ACa and the ACp. While axon diameters of the ACa were significantly increased in both HET and KO mice as compared to WT mice, with an intermediate phenotype in HET mice (Figures 5B, C), axon diameters of the ACp were increased in KO mice only (Figures 5G, H). Additionally, plotting of the G-ratios as a function of axon diameters revealed a significant difference between HET mice

and WT and KO mice for the ACa (Figure 5D), while both HET and KO mice were significantly different from WT mice for the ACp (Figure 5I). These observations were consistent with decreases of the mean G-ratios, demonstrating hypermyelination of ACa fibers in HET mice (WT 0.8060 ± 0.003146, HET 0.7854 ± 0.003246, KO 0.8077 ± 0.002936, Kruskal–Wallis test $P < 0.0001$, HET vs. WT $P < 0.0001$, HET vs. KO $P < 0.0001$, 441 fibers/genotype, 3 mice/genotype, 147 fibers/mouse), and of ACp fibers in both HET and KO mice, with an intermediate phenotype in HET mice (WT 0.8264 ± 0.005555, HET 0.8167 ± 0.002880, KO 0.7899 ± 0.003097, Kruskal–Wallis test $P < 0.0001$, KO vs. WT $P < 0.0001$, KO vs. HET $P < 0.0001$, HET vs. WT $P = 0.0169$, 441 fibers/genotype, 3 mice/genotype, 147 fibers/mouse). The % of myelinated axons of the ACa containing mitochondria was also significantly higher in HET mice than in WT (Figure 5E), while no difference was observed between the three genotypes for the ACp (Figure 5J). Altogether these data reinforce the assumption that Caspr2 could display functions in axon development and/or myelination of several myelinated tracts. In addition, they suggest that the underlying mechanisms may be different, depending on myelinated fiber type, and may therefore be differentially affected by variations in Caspr2 level.

Caspr2 level modulates axon diameter and neuronal activity before and at the onset of myelination

Myelination in the CNS relies on a complex sequence of cellular events, which includes proliferation and migration of oligodendrocyte precursor cells (OPCs) in white matter tracts, recognition of target axons, and axon-glia signaling, differentiation of OPCs into mature myelinating OLs, axonal ensheathment, and myelin compaction. This sequence is controlled by intrinsic factors that are responsive to extracellular cues, including signaling molecules released by neurons or glial cells and cell-surface expressed proteins, and by neuronal activity, which regulates OPC proliferation and survival potentiating OL differentiation, and drives the extent of myelin formation (Stassart et al., 2018; de Faria et al., 2019). The changes in the morphology of the CC and AC in mutant mice at P7 suggested that Caspr2 could regulate some neuronal parameters immediately before and/or at the onset of myelination, which could control axo-glial cross-talk and, later, axon diameter and myelin thickness. To evaluate this hypothesis, we first compared the diameter of the axons between WT, HET, and KO pups at P7. Ultrastructural analyses did not reveal significant axon diameter difference between the three genotypes for the ACp (Figures 6A, C, F), but a slight decrease of axon diameters of the ACa in KO pups as compared to WT and HET pups (Figures 6A, B, E). In addition, axon diameters of the CC were significantly increased in HET pups as compared to WT and KO pups, and decreased in KO pups as compared to WT pups (Figures 6A, D, G).

Following this observation, we explored whether Caspr2 could regulate the intrinsic excitability of layers III cortical neurons which project their axons in the CC at the onset of myelination, i.e., the propensity of neurons to fire action potentials when subjected to an input current. We measured the firing frequency of action potentials in response to 500 ms depolarizing current steps from a membrane potential of −70 mV, in the presence of blockers of synaptic activity. We found that intrinsic excitability was significantly increased in HET and KO neurons as compared to WT neurons (Figures 7A, B), while the resting membrane potential was unchanged (Figure 7C). The intrinsic excitability did not significantly differ between HET and KO mice. These results may, at least in part, reflect a role of Caspr2 at the axon initial segment, the site of initiation of action potentials, since Caspr2 has been detected in the axon initial segment of both pyramidal cells of human temporal neocortex (Inda et al., 2006) and rat hippocampal neurons in culture (Ogawa et al., 2008). Altogether our observations suggest that decreased Caspr2 dosage may indirectly control myelination through activity-dependent mechanisms, and by regulating axon diameter.

Caspr2 levels are downregulated in HET mouse brain before the onset of myelination

The impacts of *Cntnap2* heterozygosity on myelinated tract morphology, axon diameter, myelin thickness, and neuronal activity, either specific, opposite, or stronger than those of *Cntnap2* null homozygosity, led us to question Caspr2 levels in HET mice at different stages from E17.5 to adulthood. These levels were expected to be ∼50% relative to levels in WT brains. Immunoblots on whole brain extracts showed that this was the case at P15, P30, and P90, but not earlier during development (Figures 8A, B). Caspr2 levels were indeed reduced to ∼35% at E17.5, P2, P7, and P10, and significantly different from those in P90 HET mice. RT-qPCR experiments showed that this reduction may not be due to a decrease in gene expression (Figure 8C). *Cntnap2* mRNA level at P10 was actually increased and higher than that at P30 (unpaired *t*-test, $P = 0.0564$, six mice/genotype), indicating a need for cells to increase the level of Caspr2 around this developmental stage.

Decreased levels of cell-surface expressed proteins can be due to increased turnover and degradation, reflecting potential modifications in their interactions with their partners. We investigated this possibility, postulating that TAG-1 could be a partner of Caspr2 not only at juxtaparanodes of mature myelinated axons but also throughout development. Immunoblots on whole brain extracts of KO mice supported this assumption, showing that TAG-1 levels in these mice started to decrease from P2, to reach ∼33–42% decrease from P7 to P15, and ∼90% decrease at P30 and P90, as compared to WT mice (Figures 8A, D). In contrast, TAG-1 levels were not significantly affected in HET mice, except at P30. This indicates that the association of Caspr2 and TAG-1 are mostly preserved in HET mice and that the mechanisms which regulate Caspr2 levels at early developmental stages are probably independent of TAG-1. However, these data also suggest that the differential phenotypes observed in HET and KO could be partly due to the fact that the functions of TAG-1 are preserved in HET mice while they are highly perturbed in KO mice.

Caspr2 level also modulates the organization of myelinated fibers in peripheral nerves

The identification of a *CNTNAP2* genetic alteration in Charcot–Marie–Tooth patients led us to finally question whether *Cntnap2*

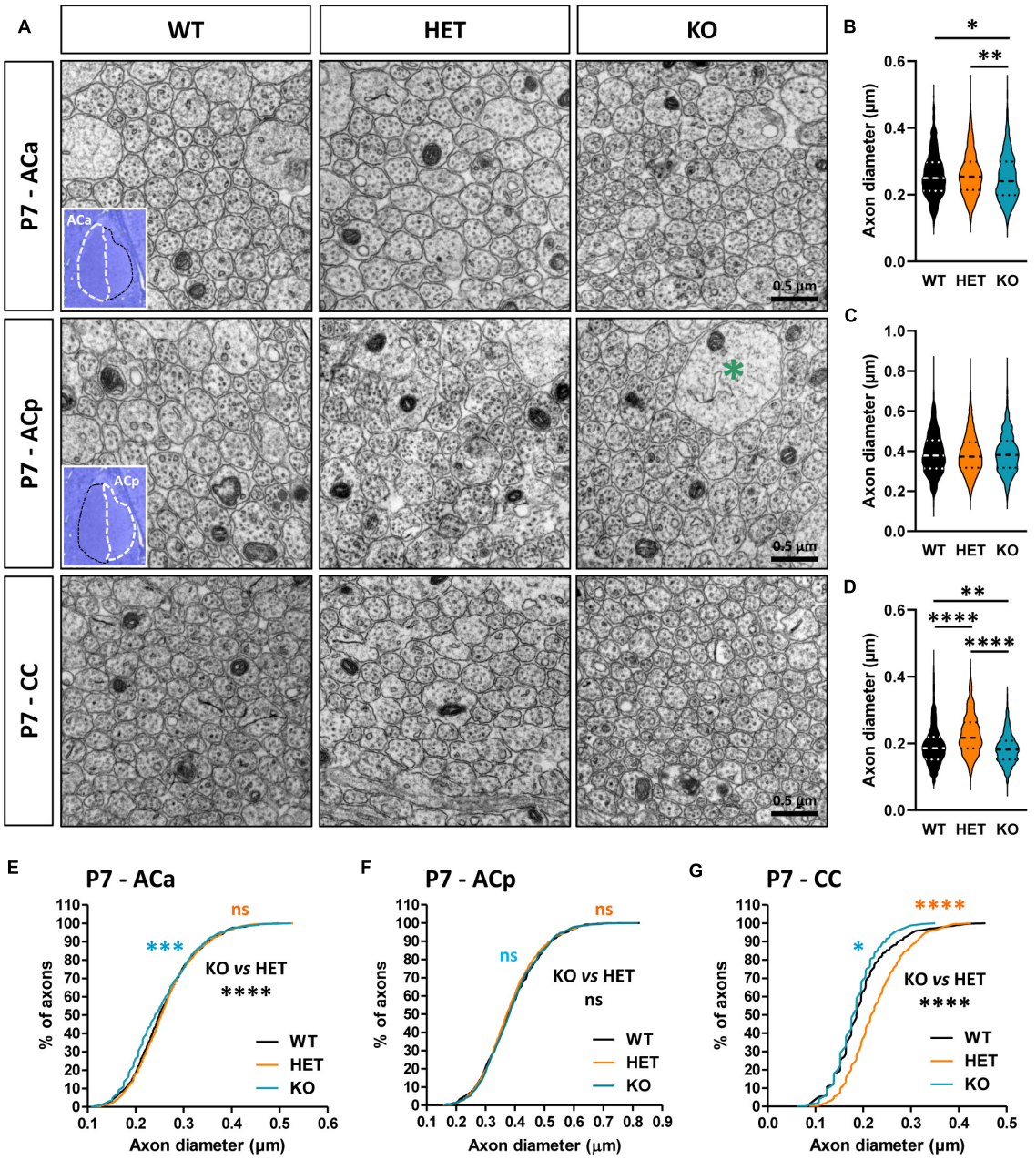

FIGURE 6
Anterior commissure (AC) and corpus callosum (CC) axon diameter abnormalities in P7 pups. Electron micrographs of transversal sections of the anterior branch (ACa), posterior branch (ACp), and CC at brain midline, from wild-type (WT), HET, and KO P7 pups; insets, semi-thin transversal sections of the AC stained with toluidine blue, showing the ACa and the ACp; the green asterisk indicates a growth cone **(A)**. Axonal diameters of the ACa **(B)**, ACp **(C)**, and CC **(D)**. Cumulative frequency distribution of axonal diameters (in %) of the ACa **(E)**, ACp **(F)**, and CC **(G)**. **(B,C,E,F)** 900 axons/genotype, 3 pups/genotype, 300 axons/pup; **(D,G)** 1080 axons/genotype, 3 pups/genotype, 360 axons/pup. Statistical tests: **(B–D)** Mann–Whitney test to compare HET or KO mice to WT mice, and Kruskal–Wallis test to compare the three genotypes; **(E–G)** Kolmogorov–Smirov test for pairwise comparisons; $^{*}P < 0.05$, $^{**}P < 0.01$, $^{***}P < 0.001$, $^{****}P < 0.0001$; ns, non-significant.

heterozygosity and null homozygosity could also perturb the organization of peripheral myelinated fibers in adult mice. Semi-thin transversal sections of sciatic nerves stained with toluidine blue did not reveal any major difference in the global morphology of the nerves between adult WT, HET, and KO mice, nor in the total number of axons (data not shown). The structure of the myelin appeared normal both in HET and KO mice (Figure 9A). A previous study reported comparable values of axon diameters and G-ratios in the sciatic nerves of WT and KO adult mice (Poliak et al., 2003). We re-evaluated these data by focusing our ultrastructural analysis on large caliber motor fibers only. We found that the axonal diameters were increased in HET and KO mice as compared to WT mice, with an intermediate phenotype in HET mice (Figure 9B). When plotting the G-ratios as a function of axon diameter, we did not detect any difference between KO and WT mice, but a significant difference between HET and WT mice (Figure 9C). The mean G-ratio was consistently increased in HET mice as compared to WT mice, reflecting hypomyelination (WT 0.6948 ± 0.003826,

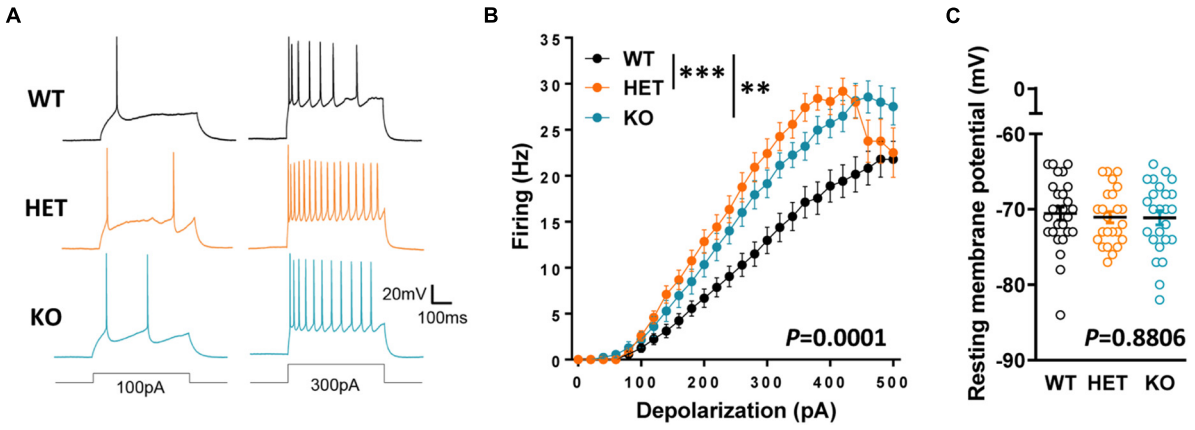

FIGURE 7
Intrinsic excitability in cortical pyramidal cells from P10–P12 pups. Sample spike trains evoked by a 100-pA (left) or a 300-pA somatic current injection (right) in a WT (top), HET (middle) and KO (bottom) neuron **(A)**. Mean f-i curve for WT (n = 27 cells from three mice), HET (n = 24 cells from three mice), and KO (n = 27 cells from three mice) **(B)**. Resting membrane potential of the recorded neurons **(C)**. Statistical tests: **(B)** Two-way RM ANOVA followed by Sidak's *post-hoc* test; **(C)** One-way ANOVA to compare the three genotypes; $^{**}P < 0.01$, $^{***}P < 0.001$.

HET 0.7244 ± 0.004060, Mann–Whitney test $P < 0.0001$, 141 fibers/genotype, 4 mice/genotype, 47 fibers/mouse). Furthermore, fluorescent immunolabelings on teased myelinated fibers confirmed a drastic reduction of TAG-1 and Kv1.2 channel enrichment in the juxtaparanodes of KO mice (**Figure 9D**), as previously described (Poliak et al., 2003), but did not reveal obvious modification in the enrichment of Caspr2, TAG-1, and Kv1.2 in HET mice (proteins detected in more than 90% of the juxtaparanodes). The levels of TAG-1 and Kv1.2 in nerve extracts were not affected either in HET mice as compared to WT mice (data not shown). However, a morphometric analysis showed an unexpected decrease in the length of the nodes (labeled for NrCAM) in both HET and KO mice, with an intermediate phenotype for HET mice (**Figures 9E, F**), while no difference was observed for the axonal diameters of the nodes (WT 2.640 ± 0.045 μm, HET 2.535 ± 0.036 μm, KO 2.677 ± 0.054 μm, Kruskal–Wallis test $P = 0.5342$, three mice/genotype). We questioned whether defects in sciatic nerve organization could lead to motor and coordination deficits in a grid-walking test. Interestingly, adult HET mice made significantly more slips than WT and KO mice during the 2 min of the test (**Figure 9G**). Altogether these observations demonstrate that Caspr2 level also modulates the organization of mature peripheral myelinated fibers, with potential functional consequences in HET mice.

Discussion

A large variety of homozygous and heterozygous genetic alterations of the *CNTNAP2* gene have been identified in several neuronal disorders (Rodenas-Cuadrado et al., 2014; Hoyer et al., 2015; Poot, 2015, 2017; Saint-Martin et al., 2018). However, the impact of these mutations on Caspr2 functions remains unknown. To better elucidate this issue, we questioned whether *Cntnap2* heterozygosity and *Cntnap2* null homozygosity could impact, either similarly or differentially, some specific functions of Caspr2 during development and in adulthood. Our study indicates that Caspr2 levels influence the gross morphology of both CC and AC, as well as axon diameter at early developmental stages, cortical neuronal activity at the onset of myelination, and axon diameter, myelin thickness and nodal length at later developmental stages (**Figure 10**). Our observations also highlight Caspr2 functions in axon development and myelination, through which the protein could contribute to normal neuronal network connectivity.

Two previous studies proposed that some functions of Caspr2 in the CNS could be modulated by the level of the protein (Canali et al., 2018; Vogt et al., 2018). Our study reinforces this assumption and further shows that *Cntnap2* heterozygosity and *Cntnap2* null homozygosity lead to complex phenotypes in myelinated fibers. Among all the parameters that we quantified, some present an intermediate phenotype in HET mice as compared to WT and KO mice, some show an opposite phenotype in HET and KO mice, some others are affected in HET or KO mice only, while few tend to be more severely affected in HET mice than in KO mice (**Figure 10**). The diversity of the phenotypes does not only illustrate differences between HET and KO mice, but also demonstrates that *Cntnap2* heterozygosity and *Cntnap2* null homozygosity impact different types of myelinated fibers differentially. This diversity may be due to the complexity of the mechanisms involved in the bi-directional axo-glial signaling regulating axon and myelin dimensions (which might be disparately affected by the level of protein), and to differences in the molecular mechanisms in which Caspr2 could be implicated from one axon to another. Our observations suggest that these mechanisms could involve the protein TAG-1, which is expressed in both CC and AC axons during development (Kastriti et al., 2019). Caspr2 could also very likely be associated with one or more additional partners among the numerous membranous proteins differentially expressed in CC and AC axons.

According to our observations, Caspr2 could intervene at several time points during the myelination process in the CNS. A handful of elements points to potential roles at the onset of myelination. This includes the switch in morphologies of the CC and AC observed at P7 in mutant pups. Also, as aforementioned, myelination in the CNS relies on a complex sequence of cellular events, which is controlled by OLs intrinsic factors but is also modulated by extrinsic factors, including neuronal activity (Stassart et al., 2018; de Faria et al., 2019). We observed increased neuronal activities in layer

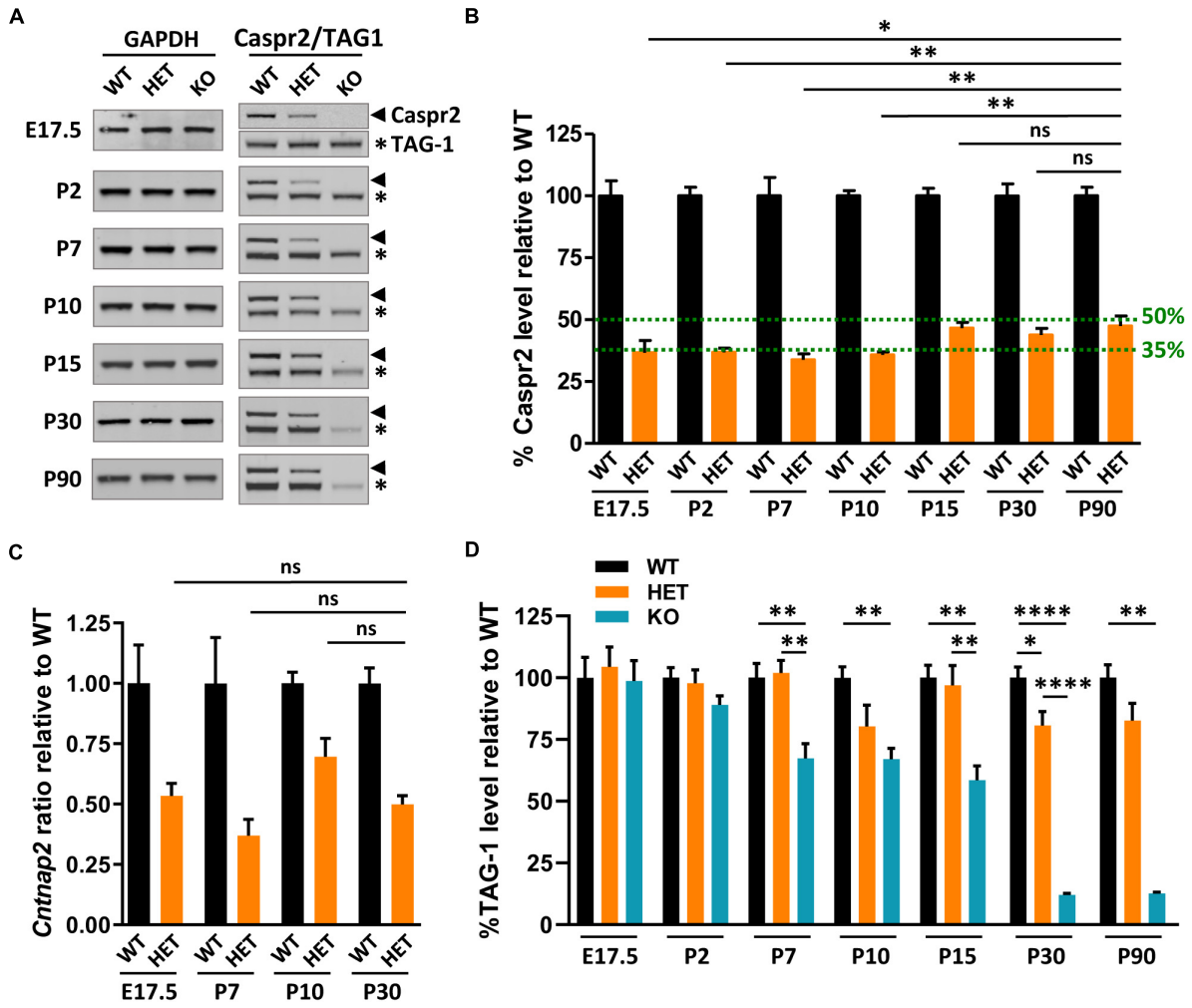

FIGURE 8
Caspr2, TAG-1, and *Cntnap2* mRNA levels in mouse brains during development. Representative immunoblots showing Caspr2, TAG-1, and GAPDH levels in brain lysates of wild-type (WT), HET, and KO mice at different developmental stages and at adulthood **(A)**. Levels of Caspr2 normalized to GAPDH levels and relative to mean WT (in %) **(B)**. Levels of *Cntnap2* mRNAs normalized to the *Psap* gene and relative to mean WT (ratio) in brain of WT, HET, and KO mice at E17.5, P7, P10, and P30 **(C)**. Levels of TAG-1 normalized to GAPDH levels and relative to mean WT (in %) **(D)**. **(B–D)** Six animals/genotype/age. Statistical tests: **(B)** Mann–Whitney test to compare Caspr2 levels in HET mice at stages E17.5, P2, P7, P10, P15, or P30, to Caspr2 level in HET mice at P90. **(C)** Unpaired *t*-test to compare *Cntnap2* mRNA levels in HET mice at stages E17.5, P7, or P10, to *Cntnap2* mRNA level in HET mice at P30. **(D)** One-way ANOVA test or Kruskal–Wallis test to compare the three genotypes at different ages; $*P < 0.05$, $**P < 0.01$, $****P < 0.0001$; ns, non-significant.

III cortical neurons in mutant pups at P10–P12, supporting the possibility that Caspr2 might participate in the cross-talk between the axons of the CC and the OLs at these stages, and possibly later in myelin sheath growth. Caspr2 is involved in the formation and stabilization of neuronal synapses, and in the trafficking of the GluA1 subunits of the AMPA receptors (Gdalyahu et al., 2015; Varea et al., 2015). Of interest, myelination is thought to be modulated by the establishment of axon-oligodendroglial cell synapses and synaptic-like interactions, which respond to the electrical activity of those axons (Bergles and Richardson, 2015). The OPCs display expression of ionotropic neurotransmitter receptors and receive direct glutamatergic and GABAergic synaptic inputs from unmyelinated or partially myelinated axons. In addition, myelin sheath growth involves the establishment of specialized synaptic-like micro-domains at the axon-myelin interface and is regulated by the activity-dependent vesicular release of neurotransmitters along axons (Mensch et al., 2015; Hughes and Appel, 2019). Thus it is possible that Caspr2 plays functions at axon/OLs connections, and possibly also in OL differentiation since single-cell RNA sequencing experiments indicate that Caspr2 is expressed in OLs at different differentiation stages (Marques et al., 2016).

The wrapping of OLs around the axons and the extension of myelin along its length are intrinsically regulated, but modulated by the diameter of the axon they wrap (Stassart et al., 2018). Our data showing axon diameter modifications in the CC and the ACa at P7 indicate that Caspr2 likely contributes to the regulation of the axon diameters of unmyelinated axons before and at the onset of myelination. When considering a single axon, its diameter depends on the axonal cytoskeleton, which is made up of neurofilaments, microtubules, deep dynamic actin trails, and a submembranous actin-spectrin network–which is composed of actin rings regularly spaced by spectrin tetramers (Costa and Sousa, 2021). This membrane periodic skeleton (MPS) can organize transmembrane cell adhesion molecules along neurites and has been shown to regulate multiple aspects of neuronal physiology, including axon diameter, axon-axon interactions, axonal

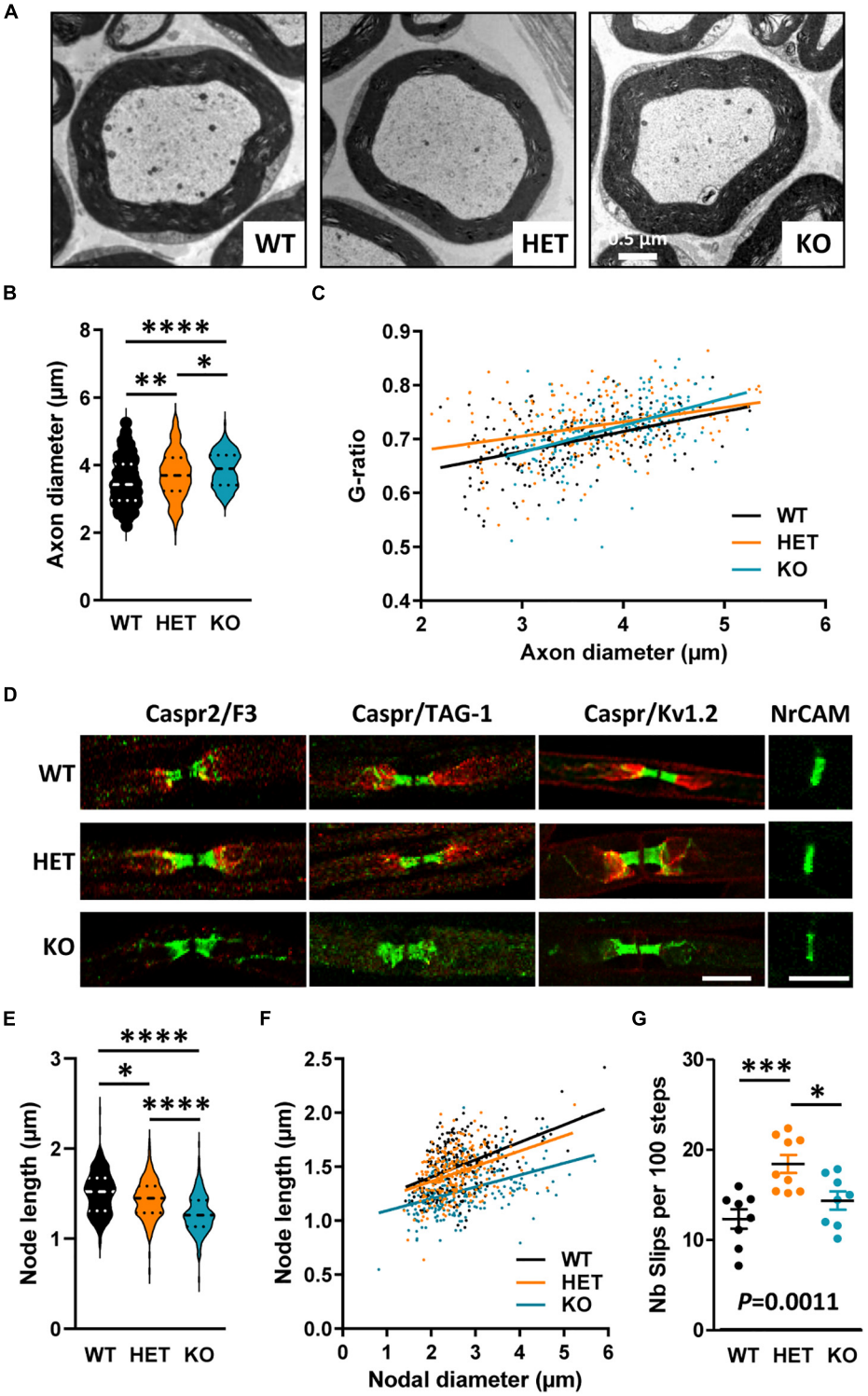

FIGURE 9
Myelinated fiber abnormalities in sciatic nerves of adult mice. Electron micrographs of transversal sections of the sciatic nerve of wild-type (WT), HET, and KO adult mice, showing a single myelinated fiber for each genotype **(A)**. Axonal diameters of myelinated fibers **(B)**. Scatter plot graph displaying G-ratios of individual myelinated axons as a function of the respective axon diameters, and the linear regression of the G-ratio measurements for each genotype **(C)**. Representative confocal images of immunostainings of sciatic nerves fibers from WT, HET, and KO adult mice, for nodal (NrCAM), paranodal (Caspr, F3), and juxtaparanodal (Caspr2, TAG-1, Kv1.2) proteins **(D)**. Length of the nodes measured on NrCAM immunostainings **(E)**. Scatter plot graph displaying length of individual node as a function of the respective nodal diameters, and the linear regression of the node length measurements for each genotype **(F)**. Number of slips per 100 steps made by WT, HET, and KO adult males during the grid-walking test **(G)**. **(B,C)** 141 myelinated fibers/genotype, 4 mice/genotype, 47 myelinated fibers/mouse, **(E,F)** 243 nodes/genotype, 3 mice/genotype, 81 nodes/mouse, **(G)** 8–9 mice/genotype. Statistical tests: **(B,E)** Kruskal–Wallis test to compare the three genotypes; **(C)** Linear regression (WT R^2 = 0.2093, HET R^2 = 0.1143, KO R^2 = 0.2022) for pairwise comparisons, HET vs. WT elevation $P < 0.0001$, HET vs. KO slope $P = 0.019$; **(F)** Linear regression (WT R^2 = 0.2295, HET R^2 = 0.1368, KO R^2 = 0.1935) for pairwise comparisons, HET vs. WT elevation $P = 0.0052$, KO vs. WT slope $P = 0.0315$, HET vs. KO elevation $P < 0.0001$; **(G)** one-way ANOVA test to compare the three genotypes; $^*P < 0.05$, $^{**}P < 0.01$, $^{***}P < 0.001$, $^{****}P < 0.0001$. Bar scales, 10 µm **(E)**.

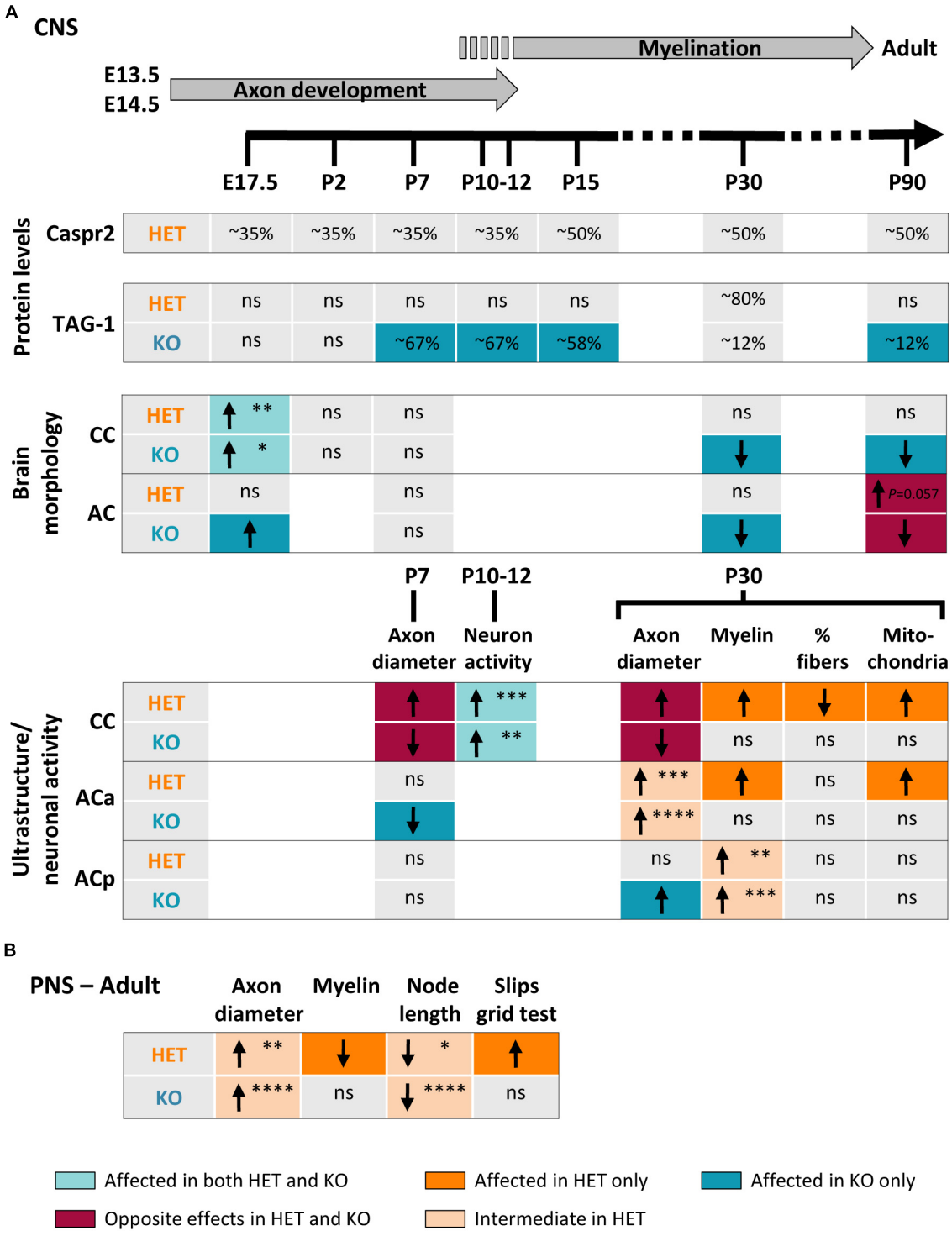

FIGURE 10
Summary of changes observed in HET and KO mice as compared to wild-type (WT) mice. Changes observed in the brain during development and in adulthood **(A)**. Upper part, timeline of axonal development and myelination in mouse. Changes observed in the sciatic nerves and in the grid test performance **(B)**. Arrows indicate increase (↑) or decrease (↓) in the parameters; ns, non-significant changes. The colors of the boxes underline the nature of the differences between HET and KO (color code at the bottom of the figure). The *P*-values are indicated when HET mice present an intermediate phenotype or tend to be more affected than KO mice (*$P < 0.05$, **$P < 0.01$, ***$P < 0.001$, ****$P < 0.0001$). Corpus callosum (CC) E17.5, *P*-values for coronal sections; posterior branch (ACp) myelin P30, *P*-values for G-ratios.

transport, and microtubule stability (Zhou et al., 2022). We previously showed that Caspr2 presents the capacity to interact with actin/spectrin-associated proteins of the 4.1 family (Denisenko-Nehrbass et al., 2003). So, it is tempting to speculate that Caspr2 could participate in the regulation of axon diameter by interacting with the MPS through a 4.1 protein, although it cannot be excluded that Caspr2 could also regulate neurofilament and/or microtubule organization.

Morphological modifications at the ultrastructural levels undoubtedly contribute to the alterations of the gross morphology of the CC and the ACa observed in HET and KO mice during development and at adulthood, but no strict correlation can be established. This is probably due to the fact that, at late development stages, myelinated axons represent only a small percentage of all the axons composing the tracts. In addition, at all developmental stages, the morphology of the tracts may not be dependent on axon diameters only, but also on the compaction of unmyelinated axons. A close observation of the electron micrographs of the CC and AC at P7 seems to show that the organization of the contacts between the axons could be different between WT, HET, and KO conditions (see **Figure 6A**, compare for example ACa WT and KO), suggesting that Caspr2 could also participate in the regulation of axon-axon contacts. Dedicated image analyses and *in vitro* cellular approaches will have to be developed to investigate this hypothesis. We didn't analyze the ultrastructure of the CC and AC at E17.5 because their morphology was not sufficiently well-defined to ensure confident measurements. However, it is very likely that the enlargement of the tracts at this stage is also due to an increase in axon diameter and/or modifications in axon-axon contacts, possibly combined with perturbations in the mechanisms guiding growing axons across the midline at early embryonic stages (Nishikimi et al., 2013; Suarez et al., 2014; Fenlon et al., 2021).

The changes in the morphology of the CC and ACa in HET and KO mice during development are interesting with regard to the neurodevelopmental disorders in which *CNTNAP2* alterations have been identified, notably ASD. This disorder is characterized by atypical brain connectivity associated with neural alterations in white matter production and myelination in diverse brain regions (Galvez-Contreras et al., 2020). Numerous structural MRI studies indicate that transient CC overgrowth could be among the earliest neural signatures of ASD in young toddlers (Wolff et al., 2015; Fingher et al., 2017), while disproportionally small CCs relative to overall brain size are among the most replicated imaging findings in older patients (Frazier and Hardan, 2009). We intriguingly observed a similar trend, with an increased thickness in HET and KO embryos at E17.5 and a decreased thickness in KO juvenile and adult mice. Beyond that, our observations support the possibility that the *CNTNAP2* alterations could contribute broadly to myelin defects in ASD patients. Of interest, performing an integrative multi-omics analysis, Jang et al. (2022) recently identified *Cntnap2*-associated ASD networks and found a downregulation in the prefrontal cortex of KO mice of proteins implicated in the formation of the myelin sheath, axon growth, and axonal transport. These data are in line with our current observations and support the role of Caspr2 in axon growth that we described previously (Canali et al., 2018). In addition, they strongly suggest that the increased percentages of myelinated axons containing mitochondria that we observed in the CC and ACa of HET mice could reflect defects in axonal transport.

Finally, we showed that the level of Caspr2 also modulates the organization of peripheral myelinated fibers in adult mice. *Cntnap2* heterozygosity and *Cntnap2* null homozygosity impact the diameter of the axons, the G-ratio, and the length of the nodes differentially. The increase in axon diameters that we observed, notably in KO mice, was not previously reported (Poliak et al., 1999), either because only the diameters of the large-caliber fibers are increased, or because the phenotype was masked in previous morphometric analyses performed on fibers of wide range calibers. The decrease in the nodal length was not previously detected either, although a decreased tendency in the nodal length-to-axonal diameter ratio was reported in KO mice as compared to WT mice (Gordon et al., 2014). When calculating this ratio with our data, it turns out that the decrease measured in KO mice is significant (WT 0.596 ± 0.008, KO 0.510 ± 0.008, Mann–Whitney test $P < 0.0001$), probably because we analyzed a larger number of nodes. Similar to our observations in central myelinated fibers, these abnormalities reveal that Caspr2 plays previously unidentified functions in the development of peripheral myelinated fibers as well. These functions might be similar but also distinct from those in the CNS, since there are substantial differences between the PNS and CNS in the intrinsic and extrinsic signals that dictate axonal ensheathment, myelin thickness, and the formation of the nodes of Ranvier (Nave and Werner, 2014; Salzer, 2015; Rasband and Peles, 2021). Of great interest, we observed that the perturbations of the peripheral functions of Caspr2 have functional consequences in HET mice which present motor and coordination deficits, suggesting that such perturbations in humans could lead to the development of peripheral neuropathies, especially non-demyelinating Charcot–Marie–Tooth disease type 2.

Conclusion

In conclusion, our study demonstrates that both *Cntnap2* heterozygosity and *Cntnap2* null homozygosity impact axon and myelinated fiber development both in the CNS and the PNS, but in a differential manner. It is a first step indicating that *CNTNAP2* alterations may lead to multiple phenotypes. Further experiments will have to be developed to evaluate the consequences on functional connectivity, especially for HET mice. Another challenge will be understanding how a decrease in Caspr2 level in HET mice on one side, and a total absence of the protein in KO mice on the other side, can eventually lead to different or opposite effects. This will require the characterization of the molecular and cellular mechanisms in which Caspr2 is implicated during axon development and myelination. The switch in the level of Caspr2 in whole brain extracts of HET mice from ∼35% at early developmental stages to ∼50% at later development stages, when compared to WT, supports the possibility that Caspr2 plays major functions before and at the onset of myelination. However, it is unlikely that this switch could be attributed to the functions of Caspr2 in axon and myelin development only. On the contrary, it strongly suggests that *Cntnap2* heterozygosity probably impacts the developmental functions of the protein more broadly. Active phases of dendritic spine formation and synapse development occur from the second week of post-natal development (Farhy-Tselnicker and Allen, 2018). Therefore, our study raises the need to evaluate the impact of *Cntnap2* heterozygosity on the functions of Caspr2 in these processes as well, to further assess the possible consequences of *CNTNAP2* alterations in neurodevelopmental disorders. It would also be of great interest to conduct similar studies for other members of the Contactin Associated Protein family, which have also been associated with neurodevelopmental disorders such as ASD, especially Caspr3/*CNTNAP3* (Vaags et al., 2012; Turner et al., 2017), Caspr4/*CNTNAP4* (Wang et al., 2010; O'Roak et al., 2012; Costa et al., 2022), and Caspr5/*CNTNAP5* (Pagnamenta et al., 2010; Aleo et al., 2020; Ludington et al., 2020). Little is known about the functions of these three proteins compared to Caspr2. However, Caspr3 and Caspr4 have been implicated in synapse formation and/or

transmission. Very interestingly Caspr4 was shown to act in a gene dose-dependent manner in the structural maturation of interneuron synapses (Karayannis et al., 2014; Shangguan et al., 2018; Tong et al., 2019), suggesting that the modulation of the biological functions by protein levels could be a common feature to the Contactin Associated Proteins.

Data availability statement

The original contributions presented in this study are included in the article/**Supplementary material**, further inquiries can be directed to the corresponding author.

Ethics statement

This animal study was reviewed and approved by French Ministry of Higher Education, Research and Innovation (Institute agreement D750522; project agreements APAFlS#5496-2016051915l48075 v8 and APAFIS#31520-2021051709364077 v3).

Author contributions

CC-D was responsible for the preparation of the samples for electron microscopy and for image acquisition, before performing measurements with GC and MS. GC, CG, and LG performed the brain sections and immunostainings to characterize brain morphology. GC and LG were responsible for the conception or design of the work and carried out the measurements. MG and LG performed the other experiments: sciatic nerve teasing and immunostaining and image acquisition and quantification. GC performed Ctip2$^+$ and Satb2$^+$ immunostainings and image acquisition and quantification. MD performed electrophysiological recordings. TM performed RT-qPCR experiments. LG performed immunoblots on brain and sciatic extracts and grid-walking test and drafted the work. GC, MG, MD, CL, and LG analyzed the data. All the authors approved the final version of the manuscript.

Funding

Our salaries and lab were supported by Centre National de la Recherche Scientifique (CNRS), Sorbonne University, Institut National de la Santé et de la Recherche Médicale (Inserm), the French Ministry of Higher Education, Research and Innovation (Ph.D. fellowship GC and MD), the Fondation pour la sclérose en plaques (ARSEP, grant and Ph.D. fellowship GC), the Fédération pour la Recherche sur la Cerveau (FRC, grant), and the Fondation pour la Recherche Médicale (FRM, Ph.D. fellowship TM). The tissue imaging platform at the Institut du Fer à Moulin was supported in part by the Région Ile-de-France and the FRC Rotary. The team was associated during the period of this work with the BioPsy Labex project and the Ecole des Neurosciences de Paris Ile-de-France network.

Acknowledgments

We thank all members of the lab for their comments and discussions. We are grateful to all the members of the animal facility and of the cellular and tissue imaging platforms for animal care and assistance with microscope. We also thank G. Martinez Lorenzana for help in electron microscopy experiments.

Conflict of interest

The authors declare that the research was conducted in the absence of any commercial or financial relationships that could be construed as a potential conflict of interest.

Publisher's note

Supplementary material

The Supplementary Material for this article can be found online at: https://www.frontiersin.org/articles/10.3389/fnins.2023.1100121/full#supplementary-material

SUPPLEMENTARY FIGURE 1
Density of callosal projecting neurons in the somatosensory cortex and cortex thickness of E17.5 embryos. Representative images (stacks of 10 confocal images) of the somatosensory cortex (coronal sections) of wild-type (WT), HET, and KO E17.5 embryos immunostained with antibodies directed against Satb2 (green), Ctip2 (red), and L1CAM (white) **(A)**; IZ, intermediate zone; SPL, subplate layer; CP, cortical plate; MZ, marginal zone. Density of Satb2-positive **(B)** and Ctip2-positive **(C)** cells in the somatosensory cortex. Cortex thickness measured at the same levels as corpus callosum (CC) thickness (**Figure 2G**, levels 1 to 5) **(D)**. **(B,C)** Four animals/genotype, average of measurements on both hemispheres/animal, 25 confocal 1 μm-stacks/hemisphere; **(D)** Six animals/genotype, average of measurements on both hemispheres on one section/animal. Statistical tests: **(B,C)** One-way ANOVA; **(D)** Two-way RM ANOVA.

SUPPLEMENTARY FIGURE 2
Myelin protein levels in brain extracts. Representative immunoblots showing MBP, MAG, PLP, and GAPDH levels in brain extracts of wild-type (WT), HET, and KO mice at P30 and P90 **(A)**. Levels of MBP normalized to GAPDH levels and relative to mean WT (in %) in brain extracts of mice at P10, P15, P30, and P90 **(B)**. Levels of PLP and MAG normalized to GAPDH levels and relative to mean WT (in %) in brain extracts of mice at P30 and P90 **(C)**. Representative immunoblots showing MBP, MAG, and GAPDH levels in extracts from the neocortex and the corpus callosum (CC) of WT, HET, and KO mice at P30 **(D)**. Levels of MBP and MAG normalized to GAPDH levels and relative to mean WT (in %) in extracts from the neocortex and the CC of mice at P30 **(E)**. **(A,D)** Molecular mass markers positions are shown in kDa on the left of the panels. **(B,C,E)** 6 animals/genotype/age. Statistical tests: Unpaired *t*-test (**E**, CC-P30 MAG, Neocortex-P30 MBP and MAG) or Mann–Whitney test (**B**,**E**, CC-P30 MBP) to compare HET or KO mice to WT mice, and one-way ANOVA test (**B**, P10, P30 and P90; **E**, CC-P30 MAG, Neocortex-P30 MBP and MAG) or Kruskal–Wallis test (**A**, P15; **B**,**E**, CC-P30 MBP) to compare the three genotypes; $^*P < 0.05$, $^{**}P < 0.01$.

SUPPLEMENTARY TABLE 1
Statistical tests and results (*P*-values for genotype effect).

References

Aleo, S., Milani, D., Pansa, A., Marchisio, P., Guerneri, S., and Silipigni, R. (2020). Autism spectrum disorder and intellectual disability in an inherited 2q14.3 microdeletion involving CNTNAP5. *Am. J. Med. Genet. A* 182, 3071–3073. doi: 10.1002/ajmg.a.61881

Anderson, G. R., Galfin, T., Xu, W., Aoto, J., Malenka, R. C., and Sudhof, T. C. (2012). Candidate autism gene screen identifies critical role for cell-adhesion molecule CASPR2 in dendritic arborization and spine development. *Proc. Natl. Acad. Sci. U.S.A.* 109, 18120–18125. doi: 10.1073/pnas.1216398109

Antoine, M. W., Langberg, T., Schnepel, P., and Feldman, D. E. (2019). Increased excitation-inhibition ratio stabilizes synapse and circuit excitability in four autism mouse models. *Neuron* 101, 648.e4–661.e4. doi: 10.1016/j.neuron.2018.12.026

Bergles, D. E., and Richardson, W. D. (2015). Oligodendrocyte development and plasticity. *Cold Spring Harb. Perspect. Biol.* 8:a020453. doi: 10.1101/cshperspect.a020453

Brunner, D., Kabitzke, P., He, D., Cox, K., Thiede, L., Hanania, T., et al. (2015). Comprehensive analysis of the 16p11.2 deletion and null cntnap2 mouse models of autism spectrum disorder. *PLoS One* 10:e0134572. doi: 10.1371/journal.pone.0134572

Canali, G., Garcia, M., Hivert, B., Pinatel, D., Goullancourt, A., Oguievetskaia, K., et al. (2018). Genetic variants in autism-related CNTNAP2 impair axonal growth of cortical neurons. *Hum. Mol. Genet.* 27, 1941–1954. doi: 10.1093/hmg/ddy102

Choe, K. Y., Bethlehem, R. A. I., Safrin, M., Dong, H., Salman, E., Li, Y., et al. (2022). Oxytocin normalizes altered circuit connectivity for social rescue of the Cntnap2 knockout mouse. *Neuron* 110, 795.e6–808.e6. doi: 10.1016/j.neuron.2021.11.031

Costa, A. R., and Sousa, M. M. (2021). The role of the membrane-associated periodic skeleton in axons. *Cell Mol. Life Sci.* 78, 5371–5379. doi: 10.1007/s00018-021-03867-x

Costa, C. I. S., da Silva Montenegro, E. M., Zarrei, M., de Sa Moreira, E., Silva, I. M. W., de Oliveira Scliar, M., et al. (2022). Copy number variations in a Brazilian cohort with autism spectrum disorders highlight the contribution of cell adhesion genes. *Clin. Genet.* 101, 134–141. doi: 10.1111/cge.14072

de Faria, O. Jr., Gonsalvez, D. G., Nicholson, M., and Xiao, J. (2019). Activity-dependent central nervous system myelination throughout life. *J. Neurochem.* 148, 447–461. doi: 10.1111/jnc.14592

Denisenko-Nehrbass, N., Oguievetskaia, K., Goutebroze, L., Galvez, T., Yamakawa, H., Ohara, O., et al. (2003). Protein 4.1B associates with both Caspr/paranodin and Caspr2 at paranodes and juxtaparanodes of myelinated fibres. *Eur. J. Neurosci.* 17, 411–416. doi: 10.1046/j.1460-9568.2003.02441.x

Farhy-Tselnicker, I., and Allen, N. J. (2018). Astrocytes, neurons, synapses: a tripartite view on cortical circuit development. *Neural Dev.* 13:7. doi: 10.1186/s13064-018-0104-y

Fenlon, L. R., Suarez, R., Lynton, Z., and Richards, L. J. (2021). The evolution, formation and connectivity of the anterior commissure. *Semin. Cell Dev. Biol.* 118, 50–59. doi: 10.1016/j.semcdb.2021.04.009

Fernandes, D., Santos, S. D., Coutinho, E., Whitt, J. L., Beltrao, N., Rondao, T., et al. (2019). Disrupted AMPA receptor function upon genetic- or antibody-mediated loss of autism-associated CASPR2. *Cereb. Cortex* 29, 4919–4931. doi: 10.1093/cercor/bhz032

Fingher, N., Dinstein, I., Ben-Shachar, M., Haar, S., Dale, A. M., Eyler, L., et al. (2017). Toddlers later diagnosed with autism exhibit multiple structural abnormalities in temporal corpus callosum fibers. *Cortex* 97, 291–305. doi: 10.1016/j.cortex.2016.12.024

Frazier, T. W., and Hardan, A. Y. (2009). A meta-analysis of the corpus callosum in autism. *Biol. Psychiatry* 66, 935–941. doi: 10.1016/j.biopsych.2009.07.022

Galvez-Contreras, A. Y., Zarate-Lopez, D., Torres-Chavez, A. L., and Gonzalez-Perez, O. (2020). Role of Oligodendrocytes and myelin in the pathophysiology of autism spectrum disorder. *Brain Sci.* 10:951. doi: 10.3390/brainsci10120951

Gao, R., Piguel, N. H., Melendez-Zaidi, A. E., Martin-de-Saavedra, M. D., Yoon, S., Forrest, M. P., et al. (2018). CNTNAP2 stabilizes interneuron dendritic arbors through CASK. *Mol. Psychiatry* 23, 1832–1850. doi: 10.1038/s41380-018-0027-3

Gao, R., Zaccard, C. R., Shapiro, L. P., Dionisio, L. E., Martin-de-Saavedra, M. D., Piguel, N. H., et al. (2019). The CNTNAP2-CASK complex modulates GluA1 subcellular distribution in interneurons. *Neurosci. Lett.* 701, 92–99. doi: 10.1016/j.neulet.2019.02.025

Gdalyahu, A., Lazaro, M., Penagarikano, O., Golshani, P., Trachtenberg, J. T., and Geschwind, D. H. (2015). The autism related protein contactin-associated protein-like 2 (CNTNAP2) stabilizes new spines: an *in vivo* mouse study. *PLoS One* 10:e0125633. doi: 10.1371/journal.pone.0125633

Gordon, A., Adamsky, K., Vainshtein, A., Frechter, S., Dupree, J. L., Rosenbluth, J., et al. (2014). Caspr and caspr2 are required for both radial and longitudinal organization of myelinated axons. *J. Neurosci.* 34, 14820–14826. doi: 10.1523/JNEUROSCI.3369-14.2014

Gordon, A., Salomon, D., Barak, N., Pen, Y., Tsoory, M., Kimchi, T., et al. (2016). Expression of Cntnap2 (Caspr2) in multiple levels of sensory systems. *Mol. Cell. Neurosci.* 70, 42–53. doi: 10.1016/j.mcn.2015.11.012

Hoyer, H., Braathen, G. J., Eek, A. K., Nordang, G. B., Skjelbred, C. F., and Russell, M. B. (2015). Copy number variations in a population-based study of Charcot-Marie-Tooth disease. *BioMed. Res. Int.* 2015:960404. doi: 10.1155/2015/960404

Hughes, A. N., and Appel, B. (2019). Oligodendrocytes express synaptic proteins that modulate myelin sheath formation. *Nat. Commun.* 10:4125. doi: 10.1038/s41467-019-12059-y

Inda, M. C., DeFelipe, J., and Munoz, A. (2006). Voltage-gated ion channels in the axon initial segment of human cortical pyramidal cells and their relationship with chandelier cells. *Proc. Natl. Acad. Sci. U.S.A.* 103, 2920–2925. doi: 10.1073/pnas.0511197103

Jang, W. E., Park, J. H., Park, G., Bang, G., Na, C. H., Kim, J. Y., et al. (2022). Cntnap2-dependent molecular networks in autism spectrum disorder revealed through an integrative multi-omics analysis. *Mol. Psychiatry* [Epub ahead of print]. doi: 10.1038/s41380-022-01822-1

Karayannis, T., Au, E., Patel, J. C., Kruglikov, I., Markx, S., Delorme, R., et al. (2014). Cntnap4 differentially contributes to GABAergic and dopaminergic synaptic transmission. *Nature* 511, 236–240. doi: 10.1038/nature13248

Kastriti, M. E., Stratigi, A., Mariatos, D., Theodosiou, M., Savvaki, M., Kavkova, M., et al. (2019). Ablation of CNTN2+ pyramidal neurons during development results in defects in neocortical size and axonal tract formation. *Front. Cell. Neurosci.* 13:454. doi: 10.3389/fncel.2019.00454

Ku, R. Y., and Torii, M. (2020). New molecular players in the development of callosal projections. *Cells* 10:29. doi: 10.3390/cells10010029

Lazaro, M. T., Taxidis, J., Shuman, T., Bachmutsky, I., Ikrar, T., Santos, R., et al. (2019). Reduced prefrontal synaptic connectivity and disturbed oscillatory population dynamics in the CNTNAP2 model of Autism. *Cell Rep.* 27, 2567.e6–2578.e6. doi: 10.1016/j.celrep.2019.05.006

Liska, A., Bertero, A., Gomolka, R., Sabbioni, M., Galbusera, A., Barsotti, N., et al. (2018). Homozygous loss of autism-risk gene CNTNAP2 results in reduced local and long-range prefrontal functional connectivity. *Cereb. Cortex* 28, 1141–1153. doi: 10.1093/cercor/bhx022

Ludington, E. G., Yu, S., Bae, H. A., and Barnett, C. P. (2020). Novel de novo 2q14.3 deletion disrupting CNTNAP5 in a girl with intellectual impairment, thin corpus callosum, and microcephaly. *Am. J. Med. Genet. A* 182, 1824–1828. doi: 10.1002/ajmg.a.61592

Marques, S., Zeisel, A., Codeluppi, S., van Bruggen, D., Mendanha Falcao, A., Xiao, L., et al. (2016). Oligodendrocyte heterogeneity in the mouse juvenile and adult central nervous system. *Science* 352, 1326–1329. doi: 10.1126/science.aaf6463

Martin, P. M., Cifuentes-Diaz, C., Devaux, J., Garcia, M., Bureau, J., Thomasseau, S., et al. (2017). Schwannomin-interacting protein 1 isoform IQCJ-SCHIP1 is a multipartner ankyrin- and spectrin-binding protein involved in the organization of nodes of Ranvier. *J. Biol. Chem.* 292, 2441–2456. doi: 10.1074/jbc.M116.758029

Martin-Lopez, E., Meller, S. J., and Greer, C. A. (2018). Development of piriform cortex interhemispheric connections via the anterior commissure: progressive and regressive strategies. *Brain Struct. Funct.* 223, 4067–4085. doi: 10.1007/s00429-018-1741-y

Menegoz, M., Gaspar, P., Le Bert, M., Galvez, T., Burgaya, F., Palfrey, C., et al. (1997). Paranodin, a glycoprotein of neuronal paranodal membranes. *Neuron* 19, 319–331. doi: 10.1016/s0896-6273(00)80942-3

Mensch, S., Baraban, M., Almeida, R., Czopka, T., Ausborn, J., El Manira, A., et al. (2015). Synaptic vesicle release regulates myelin sheath number of individual oligodendrocytes in vivo. *Nat. Neurosci.* 18, 628–630. doi: 10.1038/nn.3991

Nave, K. A., and Werner, H. B. (2014). Myelination of the nervous system: mechanisms and functions. *Annu. Rev. Cell Dev. Biol.* 30, 503–533. doi: 10.1146/annurev-cellbio-100913-013101

Nishikimi, M., Oishi, K., and Nakajima, K. (2013). Axon guidance mechanisms for establishment of callosal connections. *Neural Plast.* 2013:149060. doi: 10.1155/2013/149060

Ogawa, Y., Horresh, I., Trimmer, J. S., Bredt, D. S., Peles, E., and Rasband, M. N. (2008). Postsynaptic density-93 clusters Kv1 channels at axon initial segments independently of Caspr2. *J. Neurosci.* 28, 5731–5739. doi: 10.1523/JNEUROSCI.4431-07.2008

O'Roak, B. J., Vives, L., Girirajan, S., Karakoc, E., Krumm, N., Coe, B. P., et al. (2012). Sporadic autism exomes reveal a highly interconnected protein network of de novo mutations. *Nature* 485, 246–250. doi: 10.1038/nature10989

Pagnamenta, A. T., Bacchelli, E., de Jonge, M. V., Mirza, G., Scerri, T. S., Minopoli, F., et al. (2010). Characterization of a family with rare deletions in CNTNAP5 and DOCK4 suggests novel risk loci for autism and dyslexia. *Biol. Psychiatry* 68, 320–328. doi: 10.1016/j.biopsych.2010.02.002

Penagarikano, O., Abrahams, B. S., Herman, E. I., Winden, K. D., Gdalyahu, A., Dong, H., et al. (2011). Absence of CNTNAP2 leads to epilepsy, neuronal migration abnormalities, and core autism-related deficits. *Cell* 147, 235–246. doi: 10.1016/j.cell.2011.08.040

Pinatel, D., Hivert, B., Boucraut, J., Saint-Martin, M., Rogemond, V., Zoupi, L., et al. (2015). Inhibitory axons are targeted in hippocampal cell culture by anti-Caspr2 autoantibodies associated with limbic encephalitis. *Front. Cell. Neurosci.* 9:265. doi: 10.3389/fncel.2015.00265

Poliak, S., Gollan, L., Martinez, R., Custer, A., Einheber, S., Salzer, J. L., et al. (1999). Caspr2, a new member of the neurexin superfamily, is localized at the juxtaparanodes of myelinated axons and associates with K+ channels. *Neuron* 24, 1037–1047. doi: 10.1016/s0896-6273(00)81049-1

Poliak, S., Salomon, D., Elhanany, H., Sabanay, H., Kiernan, B., Pevny, L., et al. (2003). Juxtaparanodal clustering of Shaker-like K+ channels in myelinated axons depends on Caspr2 and TAG-1. *J. Cell Biol.* 162, 1149–1160. doi: 10.1083/jcb.200305018

Poot, M. (2015). Connecting the CNTNAP2 networks with neurodevelopmental disorders. *Mol. Syndromol.* 6, 7–22. doi: 10.1159/000371594

Poot, M. (2017). Intragenic CNTNAP2 deletions: a bridge too far? *Mol. Syndromol.* 8, 118–130. doi: 10.1159/000456021

Rasband, M. N., and Peles, E. (2021). Mechanisms of node of Ranvier assembly. *Nat. Rev. Neurosci.* 22, 7–20. doi: 10.1038/s41583-020-00406-8

Rodenas-Cuadrado, P., Ho, J., and Vernes, S. C. (2014). Shining a light on CNTNAP2: complex functions to complex disorders. *Eur. J. Hum. Genet.* 22, 171–178. doi: 10.1038/ejhg.2013.100

Saint-Martin, M., Joubert, B., Pellier-Monnin, V., Pascual, O., Noraz, N., and Honnorat, J. (2018). Contactin-associated protein-like 2, a protein of the neurexin family involved in several human diseases. *Eur. J. Neurosci.* 48, 1906–1923. doi: 10.1111/ejn.14081

Salzer, J. L. (2015). Schwann cell myelination. *Cold Spring Harb. Perspect. Biol.* 7:a020529. doi: 10.1101/cshperspect.a020529

Scott, R., Sanchez-Aguilera, A., van Elst, K., Lim, L., Dehorter, N., Bae, S. E., et al. (2017). Loss of Cntnap2 causes axonal excitability deficits, developmental delay in cortical myelination, and abnormal stereotyped motor behavior. *Cereb. Cortex* 29, 1–12. doi: 10.1093/cercor/bhx341

Shangguan, Y., Xu, X., Ganbat, B., Li, Y., Wang, W., Yang, Y., et al. (2018). CNTNAP4 impacts epilepsy through GABAA receptors regulation: evidence from temporal lobe epilepsy patients and mouse models. *Cereb. Cortex* 28, 3491–3504. doi: 10.1093/cercor/bhx215

Stassart, R. M., Mobius, W., Nave, K. A., and Edgar, J. M. (2018). The axon-myelin unit in development and degenerative disease. *Front. Neurosci.* 12:467. doi: 10.3389/fnins.2018.00467

Sturrock, R. R. (1980). Myelination of the mouse corpus callosum. *Neuropathol. Appl. Neurobiol.* 6, 415–420. doi: 10.1111/j.1365-2990.1980.tb00219.x

Suarez, R., Gobius, I., and Richards, L. J. (2014). Evolution and development of interhemispheric connections in the vertebrate forebrain. *Front. Hum. Neurosci.* 8:497. doi: 10.3389/fnhum.2014.00497

Tong, D. L., Chen, R. G., Lu, Y. L., Li, W. K., Zhang, Y. F., Lin, J. K., et al. (2019). The critical role of ASD-related gene CNTNAP3 in regulating synaptic development and social behavior in mice. *Neurobiol. Dis.* 130:104486. doi: 10.1016/j.nbd.2019.104486

Traka, M., Goutebroze, L., Denisenko, N., Bessa, M., Nifli, A., Havaki, S., et al. (2003). Association of TAG-1 with Caspr2 is essential for the molecular organization of juxtaparanodal regions of myelinated fibers. *J. Cell Biol.* 162, 1161–1172.

Turner, T. N., Coe, B. P., Dickel, D. E., Hoekzema, K., Nelson, B. J., Zody, M. C., et al. (2017). Genomic patterns of de novo mutation in simplex autism. *Cell* 171, 710.e2–722.e2. doi: 10.1016/j.cell.2017.08.047

Vaags, A. K., Lionel, A. C., Sato, D., Goodenberger, M., Stein, Q. P., Curran, S., et al. (2012). Rare deletions at the neurexin 3 locus in autism spectrum disorder. *Am. J. Hum. Genet.* 90, 133–141. doi: 10.1016/j.ajhg.2011.11.025

Varea, O., Martin-de-Saavedra, M. D., Kopeikina, K. J., Schurmann, B., Fleming, H. J., Fawcett-Patel, J. M., et al. (2015). Synaptic abnormalities and cytoplasmic glutamate receptor aggregates in contactin associated protein-like 2/Caspr2 knockout neurons. *Proc. Natl. Acad. Sci. U.S.A.* 112, 6176–6181. doi: 10.1073/pnas.1423205112

Vogt, D., Cho, K. K. A., Shelton, S. M., Paul, A., Huang, Z. J., Sohal, V. S., et al. (2018). Mouse Cntnap2 and human CNTNAP2 ASD alleles cell autonomously regulate PV+ cortical interneurons. *Cereb. Cortex* 28, 3868–3879. doi: 10.1093/cercor/bhx248

Wang, L. S., Hranilovic, D., Wang, K., Lindquist, I. E., Yurcaba, L., Petkovic, Z. B., et al. (2010). Population-based study of genetic variation in individuals with autism spectrum disorders from Croatia. *BMC Med. Genet.* 11:134. doi: 10.1186/1471-2350-11-134

Wolff, J. J., Gerig, G., Lewis, J. D., Soda, T., Styner, M. A., Vachet, C., et al. (2015). Altered corpus callosum morphology associated with autism over the first 2 years of life. *Brain* 138, 2046–2058. doi: 10.1093/brain/awv118

Zerbi, V., Ielacqua, G. D., Markicevic, M., Haberl, M. G., Ellisman, M. H., A-Bhaskaran, A., et al. (2018). Dysfunctional autism risk genes cause circuit-specific connectivity deficits with distinct developmental trajectories. *Cereb. Cortex* 28, 2495–2506. doi: 10.1093/cercor/bhy046

Zhou, R., Han, B., Nowak, R., Lu, Y., Heller, E., Xia, C., et al. (2022). Proteomic and functional analyses of the periodic membrane skeleton in neurons. *Nat. Commun.* 13:3196. doi: 10.1038/s41467-022-30720-x